Sr-Nd-Hf-Pb ISOTOPE AND TRACE ELEMENT GEOCHEMISTRY OF THE NATKUSIAK FORMATION CONTINENTAL FLOOD BASALTS OF THE NEOPROTEROZOIC FRANKLIN LARGE IGNEOUS PROVINCE, VICTORIA ISLAND, CANADA

By

TRENT ARTHUR DELL'ORO

B.Sc., Rutgers the State University of New Jersey, 2010

A THESIS SUBMITTED IN PARTIAL FULLFILMENT OF

THE REQUIREMENTS FOR THE DEGREE OF

MASTER OF SCIENCE

in

THE FACULTY OF GRADUATE STUDIES

(GEOLOGICAL SCIENCES)

THE UNIVERSITY OF BRITISH COLUMBIA
(Vancouver)

October 2012

ABSTRACT

The Neoproterozoic (ca. 723 Ma) Franklin large igneous province (LIP) located on Victoria Island, Arctic Canada, consists of the Natkusiak Formation continental flood basalts and a sill-dominated feeder system exposed in the Minto Inlier. The Franklin LIP is temporally linked with the breakup of Laurentia from Siberia and the Sturtian glaciation or "Snowball Earth". Recent mapping shows that the Natkusiak Formation, preserved in two lobes (northern and southern), has a thin basal unit, ~50 m thick, followed by two ~500 m thick cycles (1 and 2) of basaltic sheet-flows. Sr-Nd-Pb-Hf isotopic compositions, major element oxides, and trace element concentrations of the Natkusiak basalts allow for the characterization of mantle source components and the extent of crustal contamination. Four geochemical groups (southern low- and high-Ti basalts; northern low- and high-Ti basalts) are defined. The basal basalts (low-Ti, 1.0-1.2 wt.% TiO_2) are distinguished from the overlying cycle 1 and 2 basalts (high-Ti, 1.2-1.8 wt.% TiO_2). The high-Ti basalts are characterized by a narrow range in $^{87}Sr/^{86}Sr_i$ (0.7027-0.7045), high ε_{Ndi} and ε_{Hfi}, and relatively low $^{206}Pb/^{204}Pb_i$, $^{207}Pb/^{204}Pb_i$, and $^{208}Pb/^{204}Pb_i$ compared to the low-Ti basalts ($^{87}Sr/^{86}Sr_i$ = 0.7033-0.7057). The northern (low- and high-Ti) basalts are isotopically distinct from the southern (low- and high-Ti) basalts with lower ε_{Ndi} values for a given $^{87}Sr/^{86}Sr_i$. The chemistry of the coeval Franklin intrusions mainly overlaps that of the northern basalts and they show only limited isotopic correlation with the southern basalts, which indicates that the southern basalts were fed from a separate feeder system. Significant major and trace element and isotopic differences between the low- and high-Ti basalts are inconsistent with the effects of crustal contamination and are related to different mantle source compositions, with a garnet-bearing source for the low-Ti basalts and a spinel-bearing source for the high-Ti basalts. A shift in mantle source region, likely reflected by an episode of syn-volcanic extension, occurred after the emplacement of the low-Ti basalts, which represent the earliest volcanic products of the Franklin LIP.

PREFACE

All research, trace element and isotopic analytical work was carried out by the author (with the exception of 5 samples analyzed in 2008) and with the help of the PCIGR staff. My supervisors James S. Scoates, Dominique Weis, and Jean Bédard provided research advice and ideas, helped interpret data, thoroughly edited the thesis, and provided financial support. Financial support for the Geo-mapping for Energy and Minerals (G.E.M.) project and the affiliated M.Sc. thesis presented here was provided by the Geological Survey of Canada (GSC), Earth Sciences Sector (ESS) of Natural Resources Canada (NRCan), and NSERC Discovery Grants to Dominique Weis and James Scoates. A version of Chapter 2 will be submitted as a manuscript to a scientific journal.

CHAPTER 2
Sr-Nd-Hf-Pb Isotope and Trace Element Geochemistry of the Natkusiak Basalts, Franklin Large Igneous Province (Victoria Island, Canada)
Authors: Trent Dell'Oro, Dominique Weis, James S. Scoates, Jean Bédard

TABLE OF CONTENTS

LIST OF TABLES

LIST OF FIGURES

ACKNOWLEDGEMENTS

CHAPTER 1

CONTINENTAL FLOOD BASALTS AND INTRODUCTION TO THE FRANKLIN LARGE IGNEOUS PROVINCE

1.1 INTRODUCTION AND SCIENTIFIC RATIONAL

Large igneous provinces (LIP) are massive and rapid emplacements of predominantly mafic (Fe- and Mg-rich) intrusive and extrusive rocks, distinct from normal seafloor spreading and subduction-related magmatism, with areal extents >0.1 Mkm^2 and igneous volumes >0.1 Mkm^3 (Mahoney & Coffin, 1997; Sheth, 2007; Bryan & Ernst, 2008) (Fig. 1.1). Large igneous province is an all-inclusive term that covers flood basalts, continental flood basalts, volcanic rifted margins, oceanic plateaux, and aseismic ridges that have intraplate tectonic settings or geochemical affinities (DePaolo & Weis, 2007; Bryan & Ernst, 2008). LIP typically have maximum lifespans of ~50 Ma, and are characterized by igneous pulse(s) of short duration (1-5 Ma), during which a large proportion (>75%) of the total igneous volume is emplaced (Lin & Keken, 2005; Sheth, 2007; Bryan & Ernst, 2008). LIP are the largest melting events to occur on Earth (Fig. 1.1) and likely form the dominant type of magmatism on other terrestrial planets and moons in our solar system (Head & Coffin, 1997).

The research reported in this thesis is a field and geochemical study of the Natkusiak Formation flood basalts located on Victoria Island, Northwest Territories, Canada, that form part of the Franklin large igneous province (Fig. 1.2) This project is a component of a larger Geological Survey of Canada (GSC) effort with a principal objective to identify the potential for energy and mineral resources in the Arctic and provide geological maps for private sector exploration companies. The Franklin LIP is one of the less well-studied LIP in the world due to its remote location in the Arctic. The Sr-Nd-Hf-Pb isotopic and trace element geochemical research presented here on the Natkusiak basalts is a partner study to the M.Sc. thesis of Charlie Beard (Beard, 2012, Bristol University) on the geochemistry of the Franklin sills and to the M.Sc. thesis of Nicole Williamson (Carleton University) on the stratigraphy and physical
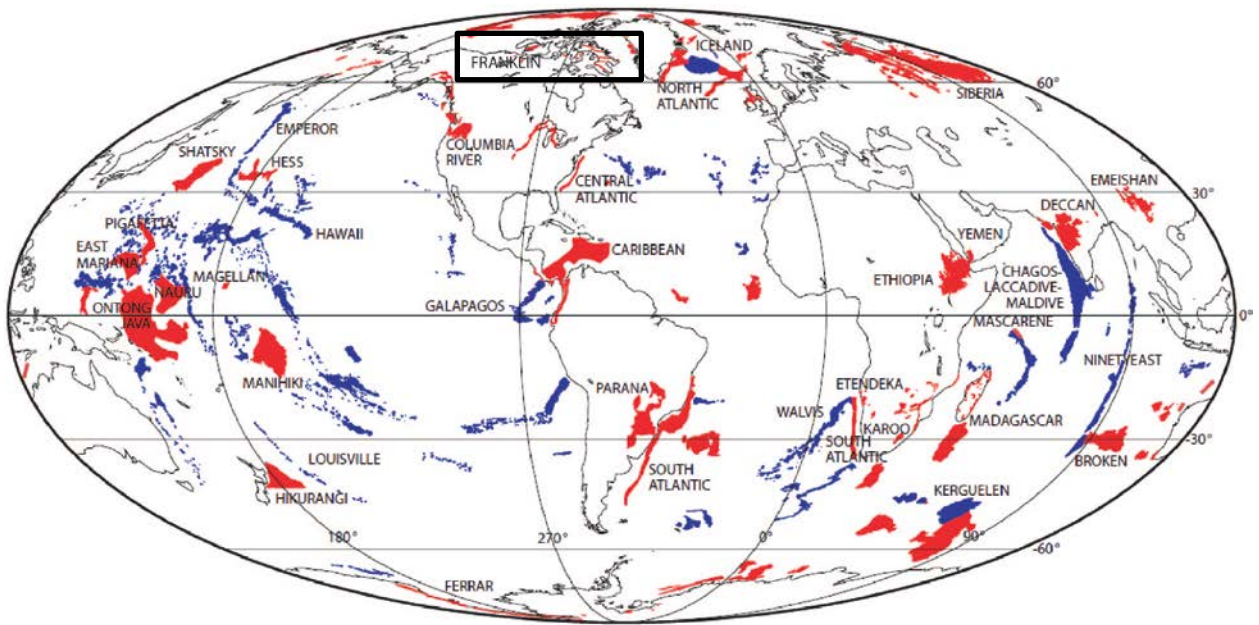
Figure 1.1 Global distribution of large igneous provinces on Earth. Transient LIP ("plume head") in red and persistent LIP ("plume tail") in blue. Franklin LIP highlighted with black rectangle, flood basalt exposure is colored red. Map modified from Figure 1 by Coffin et al. (2006).

Figure 1.2 Regional map of the Franklin large igneous province in the Arctic. The map shows the Natkusiak basalts on Victoria Island (VI) in black, the Coronation sills of the Amundsen Basin, the Franklin sill (green) and dike (red) complex on Victoria Island, and the Neoproterozoic dike swarms found on Banks and Baffin Islands, Brock Inlier, and western Greenland. The red star indicates the proposed Franklin plume center. Figure from Buchan et al., (2010) GSC Open File 5985.

volcanology of the lower part of the Natkusiak Formation. The present study provides a geochemical framework for the evolution of these continental basaltic magmas and a characterization of the source components involved in their genesis. The results will allow for geochemical correlations to be made on a larger scale that may support mineral exploration initiatives in the future.

Geochemical research on flood basalts is one important way we gain information on the processes by which basaltic magmas form from mantle plumes, ascend, and erupt onto the surface of the Earth. The primary goal of this study is to establish the geochemical signature of the Natkusiak basalts and to evaluate the source and potential contamination history as the magmas traversed through the crust. The research is based on the determination of radiogenic isotope compositions (Rb-Sr, Sm-Nd, Lu-Hf, and Pb-Pb) of the Natkusiak basalts and integration with major element oxide and trace element concentrations. Radiogenic isotopes are a very powerful tool in identifying mantle source components, as isotope ratios do not change during crystallization and may provide the geochemical "fingerprint" of the primary magma. Work in this project focused on the basal 140 m of the Natkusiak volcanic section (from the contact with the underlying Kuujjua sandstone), as it provides a rare opportunity to examine the onset of continental flood basalt volcanism in a stratigraphic and geochemical context.

In the following sections, the geological significance of large igneous provinces and continental flood basalts worldwide are outlined. LIP are found in many regions on Earth in both oceanic and continental settings (Fig. 1.1) and are thought to have had significant impacts on global climate as well as the biosphere (e.g., mass extinction events). The geological background and previous studies conducted on the Franklin LIP will also be addressed to provide context to the work reported in this thesis.

1.2 LARGE IGNEOUS PROVINCES AND CONTINENTAL FLOOD BASALTS

1.2.1 Large Igneous Provinces

Large igneous provinces on the Earth's surface are thought to be related to large mantle plumes that rise through the mantle to the base of the lithosphere from a thermal boundary layer in the planet (i.e., core-mantle boundary) due to thermal or compositional buoyancy (Campbell & Griffiths, 1990; Carlson, 1991; Jellinek & Manga, 2004; Montelli et al., 2004). Intraplate flood basalt volcanism marks the initial breach in the crust in response to the rising mantle plume and partial melting in the plume head. Large volumes of mafic magma (10^5-10^7 km^3) are extruded onto the surface as a result, typically over a very short period of time (Morgan, 1971; Morgan, 1972; Richards et al., 1989; Ernst et al., 2005). The emplacement of flood basalts onto the surface may occur in short intervals (10^5-10^6 years) or significantly longer periods (10^7-10^8 years) of time (Coffin et al., 2006). In either case, enormous volumes of magma may erupt onto the surface as a result of extensive partial melting in the plume head (Morgan, 1971; Morgan, 1972; Richards et al., 1989; Ernst et al., 2005, Herzberg & Gazel, 2009). This brief stage of eruption typifies the transient phase (high-rate) of LIP volcanism (Kerguelen Plateau, Siberian and Deccan Traps, e.g., Sharma, 1997; Neal et al., 2002; Jay & Widdowson, 2008) and may continue for several millions of years (Duncan & Richards, 1991; Coffin et al., 2006; Sheth, 2007). The persistent (low-rate) stage or post-flood basalt volcanism is thought to be the result of the ascending conduit tail of the plume partially melting beneath the lithosphere (Hawaii, e.g., Ballmer et al., 2012). As the plume's conduit tail may extend several hundred km into the mantle (to the original thermal boundary layer itself), the majority of existing LIP on Earth remain active in the persistent phase of volcanism (e.g., Iceland hotspot and the North Atlantic igneous province; Reunion hotspot and Deccan Traps; Galapagos hotspot and Caribbean Plateau; Richards et al., 1989; Campbell & Griffiths, 1990; Sharma, 1997; Jellinek & Manga, 2004; Hoernle et al., 2004).

1.2.2 Large igneous provinces and environmental consequences

Large igneous provinces have been associated with major geologic events ranging from mass extinctions to continental break-up. The eruption of LIP has the potential to significantly affect the composition of the atmosphere and oceans by releasing large amounts of gas (CO_2 and SO_2) and aerosols (Pollack et al., 1976; Coffin & Eldholm, 1994; Self et al., 2005; Sobolev et al., 2011). Volcanic cooling caused by the backscatter and absorption of the Sun's radiation by aerosols and SO_2 has been proposed to be responsible for several extinction events. However, the most compelling evidence is for a climatic warming scenario, because the vast amounts of CO_2 and methane (strong greenhouse gases) released would cause significant warming and climatic shifts (Saunders, 2005; Wignall, 2005; Sobolev et al., 2011). The most important example is the eruption of the Siberian Traps at ~250 Ma (Permian-Triassic boundary), which coincides with the largest mass extinction event observed in the geological record where 96% of all marine and 70% of all terrestrial vertebrate species became extinct (Coffin & Eldholm, 1994; Sharma, 1997; Coffin et al., 2006; Saunders, 2005). The Central Atlantic Magmatic Province (CAMP) is another important volcanism-extinction-related event at ~200 Ma, marked by the end-Triassic mass extinction (Deenen et al., 2010; Whiteside et al., 2010). The eruption of the Deccan Traps at ~65 Ma coincides with the Maastrichtian warm pulse and may have substantially weakened the biosphere in conjunction with the contemporaneous Chicxulub meteorite impact (Courtillot et al., 1986; Wignall, 2005; Courtillot et al., 2010; Schulte et al., 2010). The combined effects of both may have led to the end-Cretaceous mass extinction.

The end of the Proterozoic Eon (2500 to 542 Ma) was marked by several major events in Earth's history including the eruption and emplacement of the Franklin LIP (ca. 723 Ma). Great environmental and biological change occurred during this period, as well as the formation of the supercontinent Rodinia from about 1000 to 800 Ma and its eventual break-up and reassembly

7

into a different configuration by ~550 Ma (Heaman et al. 1992; Hoffman et al., 1998; Hyde et al., 2000; Pisarevsky et al., 2008; MacDonald et al., 2010). The greatest ice age event to have ever occurred on Earth (Snowball Earth) occurred during the Neoproterozoic era. The discovery of Neoproterozoic ice sheet extension to sea level near the equator provides the strongest evidence of a global glaciation or a "Snowball" Earth during this time period (Hoffman et al., 1998; Hoffman & Schrag, 2002). The earliest major phase of glaciation and ice advance occurred from 760 to 700 Ma (Hyde et al., 2000). The Franklin igneous event has been tentatively linked with the environmental shifts of this time period (MacDonald et al., 2010). A volcanic tuff (volcanic exposure in the Ogilvie Mountains, Yukon) is interbedded with Neoproterozoic Sturtian glacial deposits and has been dated by the U-Pb zircon method at 716.5 ± 0.24 Ma, and interpreted to be synchronous with the age of the Franklin LIP (MacDonald et al., 2010). Erosion and weathering of the low-latitude (~10 degrees) Franklin basalts may have facilitated the drawdown of atmospheric CO_2 and sequestration in the oceans, thus making the climate more susceptible to cooling and glaciation (MacDonald et al., 2010).

1.2.3 Flood Basalts

Flood basalts are considered to be the surface expression of a partially melted mantle plume (Herzberg, 2011). They form enormous, laterally extensive (several hundred km) and thick (about a km on average) volcanic constructs of mantle-derived basaltic lava flows typically erupted from a surface fissure (White & McKenzie, 1995; Foulger, 2007; Sheth, 2007). Flood basalts are generally tholeiitic in composition with MgO = 5-12 wt. %, SiO_2 = 45-56 wt. %, and total alkalis (Na_2O + K_2O) = 2-5 wt. % (Le Bas, 2000). At the scale of individual basaltic units, flood basalts generally show remarkable homogeneity in mineralogy and chemical composition, however, at the regional-scale flood basalts show significant compositional variation both

temporally and spatially (White and McKenzie, 1995; Jerram & Widdowson, 2005; Bryan & Ernst, 2008).

Geochemical studies have recognized multiple magma types in single flood basalt provinces (e.g., Albarède, 1992; Arndt et al., 1997; Marsh et al., 2001; Pik et al., 2006; Greene et al., 2008; Greene et al., 2009; Søager & Holm, 2011; Zhang et al., 2012). A common feature is the presence of both low-Ti (typically <1.5 wt. % TiO_2) and high-Ti (typically >1.5 wt. % TiO_2) magma types within a single province. Low-Ti basalts are commonly found in the initial lava flows of flood basalt provinces, and they are thought to represent partial contamination of plume-derived melt with either the subcontinental lithospheric mantle and/or continental crust (e.g., Hergt et al., 1991; Carlson, 1991; Arndt & Christensen, 1992; Gallagher & Hawkesworth, 1992; Arndt et al., 1993; Wooden et al., 1993; Griselin, et al., 1997; Greene et al., 2008; Greene et al., 2009; Keays & Lightfoot, 2010). The high-Ti basalts typically erupt after the low-Ti basalts and are considered to represent plume-derived magmas (Pik et al., 1999; Xiao et al., 2004; Greene et al., 2009).

Wide variations in incompatible trace element concentrations and isotopic compositions are observed in flood basalt provinces worldwide. These variations are typically independent of MgO contents (a tracer of extent of partial melting and fractional crystallization, e.g., Herzberg, 2011) and thus reflect variable enrichment of the different mantle source components (e.g., Campbell & Griffiths, 1990; Millet et al., 2008; Chakrabarti et al., 2009; Said & Kerrich, 2009; Søager & Holm, 2011). Flood basalts are found in both oceanic and continental plate settings. However, continental flood basalts are typically characterized by distinctive trace element contents such as negative Nb and Ta anomalies relative to other incompatible elements, and radiogenic Sr isotope and unradiogenic Nd and Hf isotope compositions, similar to continental crust and/or lithospheric mantle rocks (DePaolo, 1981; Perry et al., 1987; Carlson, 1991; Arndt & Christensen, 1992; Pik et al., 1999; Beccaluva et al., 2009; Jackson & Carlson, 2011). These

9

geochemical signatures found in continental flood basalts likely result from processes that only occur beneath continental crust, as they are noticeably absent in oceanic settings. The incorporation of crustal and lithospheric material would occur due to thermal erosion of the lithosphere after impact of the plume head and/or during the transit of magma through continental crust (e.g., Arndt & Christensen, 1992; Pik et al., 1999; Frey et al., 2002; Ridley & Richards, 2010).

1.2.4 Onset and emplacement of continental flood basalts

The initial lavas of continental flood basalt volcanism commonly erupt onto active sedimentary environments as in the case of Parana-Etendeka and Deccan (Peate, 1997; Jerram & Widdowson, 2005). For example, the Parana-Etendeka region was an expansive aeolian desert prior to the onset of flood basalt volcanism. The earliest lavas erupted onto and interacted with an active aeolian-driven sand sea and resulted in extremely well-preserved sedimentary features such as 100-m-high sand dunes (Jerram et al., 2000). The Coppermine flood basalts of the Mackenzie igneous event (ca. 1.27 Ga) erupted onto an active sedimentary system and preserve red fluvial sandstones in between basalt flows (Griselin et al., 1997). Field observations during the present study suggest that the Natkusiak basalts on Victoria Island erupted onto a wet and active sedimentary system. The Natkusiak basalts are underlain by fluvial sandstone, and they preserve pillows in some locations and thin lenses of interbedded sandstone in the lowermost flows (<16 m above the Kuujjua sandstone contact).

The largest continental flood basalt provinces consist of millions of cubic kilometers of tholeiitic basalt erupted over time intervals as short as a million years. The construction of continental flood basalt provinces typically begins with limited basaltic lava eruptions, which may be preceded by small volumes of more exotic lava types such as carbonatites or lamprophyres as a result of sublithospheric mantle melting (Jerram & Widdowson, 2005; Jay &

Widdowson, 2008). The immense outpourings of tholeiitic basalt that typically follow the initial basal eruptions form the transient phase of the LIP and constitute the majority of eruptive activity where most of the flood basalt province is constructed (Coffin & Eldholm, 1994; Jerram & Widdowson, 2005).

Continental flood basalts are predominantly emplaced as inflated compound pahoehoe flow fields via prolonged, episodic eruptions (Self et al., 1997; Thordarson & Self, 1998; Anderson et al., 1999). The sheet flows of the Kilauea Volcano, Hawaii, have formed exclusively by continuous lava injection and inflation mechanisms (Walker, 1991; Hon et al., 1994). Pahoehoe lobes, toes, and pillows act as liquid-filled balloons held up by a partially-cooled viscoelastic skin of lava that forms on the outer surface. The viscoelastic behavior of the skin both supports the sheet flow and also acts to constrain the inflation rate during the emplacement process (Self et al., 1997; Anderson et al., 1999). If the rate of inflation is too high the skin will burst, fresh lava will escape from the rupture and a new pillow, lobe, or toe will form from the original flow. The sequential emplacement of inflationary lavas produces the sheet-like or planar geometry observed at the actively growing Kilauea and Mauna Loa flow fields in Hawaii. Hon et al. (1994) and Self et al. (1997) suggest inflation as the principal mechanism of emplacement of continental flood basalts rather than nearly instantaneous emplacement of "floods" of lava. Many of these features are documented in lava fields of other continental flood basalts (Deccan and Columbia River; e.g., Self et al., 1998; Jay & Widdowson, 2008). A shift from sheet flow eruptions to more explosive volcanic activity (i.e., phreatomagmatic volcanism) is a consequence of water-magma interaction (Jolley & Widdowson, 2005; McClintock & White, 2006). Inundation of the volcanic province is more likely to occur in rift-related settings and since continental flood basalts are closely related to rifting and continental break-up, a shift to explosive volcanism may occur during the life-span of

continental flood basalt provinces (North Atlantic Igneous Province, e.g., Egger & Brückl, 2006).

Continental flood basalts are closely related with continental breakup. One of the most recent eruptions of continental flood basalts on Earth, the Ethiopian Traps at ~30 Ma, erupted prior to rifting of the Arabian Peninsula and African continent (Kieffer et al., 2004; Chakrabarti et al., 2009; Keir et al., 2011). The formation of the Parana-Etendeka magmatic province (138 to 125 Ma) preceded the opening of the South Atlantic Ocean and formation of the North Atlantic Volcanic Province (62 to 60 Ma) preceded the opening of the North Atlantic Ocean (Dalziel et al., 2000; Hawkesworth et al., 2000). The eruption of the Franklin Natkusiak basalts preceded the rifting and extension that led to the breakup of the Laurentian Supercontinent and the opening of the Neoproterozoic Palaeo-Asian Ocean (600 Ma) (Li et al., 2008; Pisarevsky et al., 2008).

1.2.5 Isotope geochemistry of continental flood basalts

Radiogenic isotope compilations provide a powerful tool in the study of the mantle source of flood basalts and they are essential when studying the influence of crustal contamination and defining mantle end-member components (Zindler & Hart, 1986; Sun & McDonough, 1989; Kerr et al., 1995; Arndt et al., 1997; Zhu, 2007; Albaréde, 2009). Unlike major and trace elemental abundances, isotopic abundances of Sr, Nd, Hf, and Pb are not fractionated during magma genesis (e.g., partial melting, fractional crystallization). Their radiogenic-to-stable isotope ratios (e.g., $^{87}Sr/^{86}Sr$) are only subject to the calculable rate of change over time due to radioactive decay of the parent nuclides (e.g., $^{87}Rb \rightarrow {}^{87}Sr$) (Zindler et al., 1982; White, 1985; Sun & McDonough, 1989; Hofmann, 2003; Farmer, 2003). Thus, the back-calculated $^{87}Sr/^{86}Sr$ ratio (i.e., initial ratio) of a volcanic rock directly reflects the time-averaged ratio of its mantle source (Tatsumoto, 1965; Hofmann, 2003).

Isotopic analyses of continental flood basalts worldwide demonstrate heterogeneity in the composition of the Earth's mantle (Fig. 1.3) (Rampone & Hoffman, 2012). The combined Sr, Nd, Hf, and Pb isotopic compositions of mantle-derived rocks define a finite number of geochemical reservoirs in the mantle. These reservoirs result from differentiation and recycling processes in the Earth that continuously produce crust, and enriched and depleted geochemical reservoirs such as depleted-mantle (DM), HIMU (high μ = high $^{238}U/^{204}Pb$), FOZO (FOcus ZOne), and enriched-mantle I and II (EM I and EM II) (e.g., White, 1985; Zindler & Hart, 1986; Sun & McDonough, 1989; Hofmann, 1997; Stracke et al., 2005; Tatsumi, 2005; Zhu, 2007; Willbold & Stracke, 2010). For example, back-calculated (to 723 Ma, the age of the Franklin LIP in this study) isotopic ratios show a wide variation in continental flood basalts due to the mixing of various components (e.g., mantle, lithosphere, crust). The Deccan Traps and the North Atlantic igneous province (NAP) show large variations in Sr-Nd-Pb isotopic space with values that extend into EM II and EM I components, respectively (Fig. 1.3). The Siberian Traps also deviate from the FOZO or "common" component and extend towards both EM I and EM II endmembers. Similarly, the Karoo province basalts plot between both EM I and EM II. Flood basalts from Ethiopia and Wrangellia (technically an accreted ocean plateau) show more
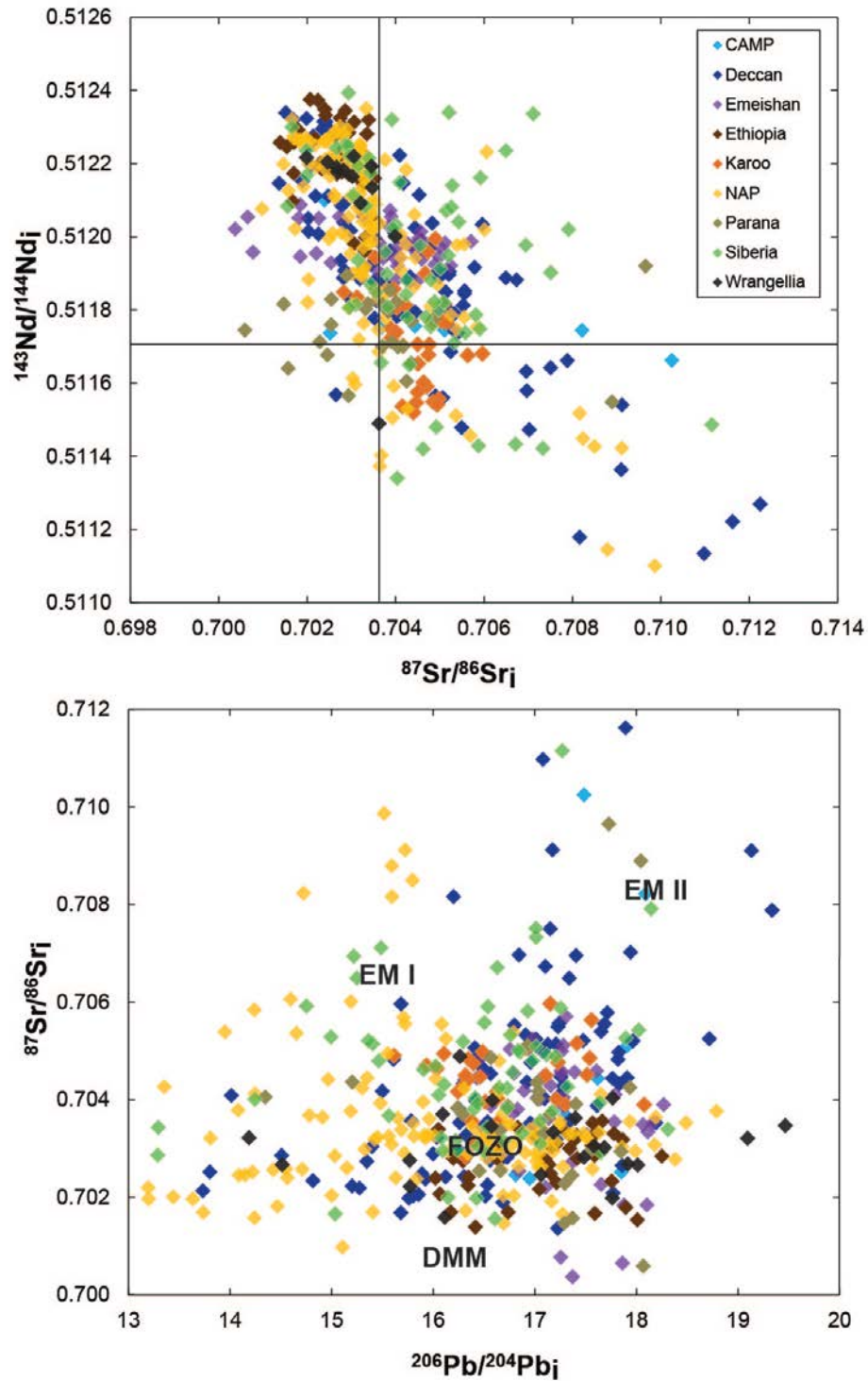
Figure 1.3 Diagrams of $^{143}Nd/^{144}Nd_i$ versus $^{87}Sr/^{86}Sr_i$ and $^{87}Sr/^{86}Sr_i$ versus $^{206}Pb/^{204}Pb_i$ for select continental flood basalts worldwide (calculated to 723 Ma the age of Franklin LIP). The horizontal line is Bulk Earth composition of $^{143}Nd/^{144}Nd_i$, and the vertical line is $^{87}Sr/^{86}Sr_i$ Bulk Earth composition. End-member compositions (DMM = Depleted MORB mantle; EMI = enriched mantle 1; EMII = enriched mantle 2; FOZO = FOcus ZOne) are from Zindler & Hart (1986) and Hart et al. (1992). Data from the GEOROC database compilation (http://www.georoc.mpch-mainz.gwdg.de). CAMP = Central Atlantic magmatic province, NAP = North Atlantic igneous province.

14

restricted isotopic compositions than other continental flood basalts with minimal enriched

component. Some authors have proposed that the FOZO (Common "C" or PREvalent Mantle

"PREMA") component may be the located in the lower mantle at the core-mantle boundary itself

and that the addition of EM and HIMU components to lower mantle-derived plumes result in the

ubiquitous divergence from FOZO in ocean island basalts and continental flood basalts

worldwide (Hart et al., 1992; Willbold & Stracke, 2010).

1.3 THE FRANKLIN LARGE IGNEOUS PROVINCE

1.3.1 Geological Background

The Neoproterozoic Franklin large igneous province includes a system of dikes, sills, and

continental flood basalts in the northern Canadian Arctic Platform (Heaman et al., 1992;

Pehrsson et al., 1999). The Franklin LIP is comprised of several intrusive igneous members,

including the Coronation sills of the Amundsen Basin, the Franklin sill complex on Victoria

Island, and Neoproterozoic dike swarms found on Banks and Baffin Islands, Brock Inlier, and

western Greenland (Fig. 1.2) (Heaman et al., 1992; Pehrsson et al., 1999; Shellnutt et al., 2004).

The Natkusiak basalts, found on Victoria Island, are the only known surface expression of the

Neoproterozoic Franklin magmatic province in North America (Fig. 1.4) (Fahrig et al., 1971).

The Franklin intrusions are hosted within the Neoproterozoic Shaler Supergroup located

in the Minto Inlier on Victoria Island (Heaman et al., 1992; McDonald et al., 2010; Jones et al.,

2010; Bédard et al., 2012 a). The Shaler Supergroup represents a succession of shallow-water

marine sedimentary rock that was deposited in an intracontinental basin of Rodinia during the

Proterozoic (Rainbird et al., 1993; Hofmann & Rainbird, 1994). The dominant rock types include

limestone, dolostone, sandstone, and lesser shales and evaporites (Fig. 1.5 A and B), which are

intruded by the gabbroic sills and overlain by the Natkusiak basalts. The Franklin sills are

located directly below the Natkusiak basalts with the uppermost sill exposed only a few tens of

meters stratigraphically below the basalts, and some intrusions transgress through the basal basalts. The sills are prevalent all throughout the Shaler Supergroup and range in thickness from 2-120 m, typically extending for ~20 km or more along strike with minimal change in thickness; they constitute the majority of the exposed feeder system (Baragar, 1976; Jefferson et al., 1994; Bédard et al., 2012a). Sedimentological field observations on Victoria Island indicate syn-depositional uplift of the crust immediately prior to the emplacement of the Franklin sills and their extrusive equivalents (Rainbird et al., 1993). This evidence supports a mantle plume model as the most applicable hypothesis for the emplacement of the Franklin LIP.

The Natkusiak basalts are preserved in two lobes in the Minto Inlier with a maximum preserved thickness of 1100 meters in the northeast (Baragar, 1976; Jefferson, 1985; Dostal et al., 1986). The Natkusiak basalts lie unconformably on top of the Kilian Formation in the northeast (northern lobe), and conformably on top of the Kuujjua Formation in the southwest (southern lobe) of Minto Inlier (Fig 1.5 C), with local occurrences of lenses of sandstone and pepperites in basal lavas, as well as fluidal sedimentary structures in the Kuujjua Formation (Rainbird et al., 1993). The Natkusiak Formation is included in the Shaler Supergroup because of its conformable contact with the Kuujjua Formation in the southwest, with rare interbeds of sandstone and basalt in the first few meters. Most flows are subaerial basalts; however, pillows and polygonal fractures are found in the lowermost flows and suggest early subaqueous extrusions, perhaps into lakes or rivers. The lowermost unit of the Natkusiak Formation is a thin amygdaloidal basal unit that consists of lava flows, pillow basalts (Fig.1.5 D & E), and volcaniclastic deposits. The basal unit (40-50 m thick) is then followed by two series of blocky fine-crystalline sheet flows (Fig.1.5 F) that represent two volcanic fractionation cycles (cycle 1: ~285 m, and cycle 2: ~450 m thick) (Dostal et al., 1986). Native copper occurrences are found
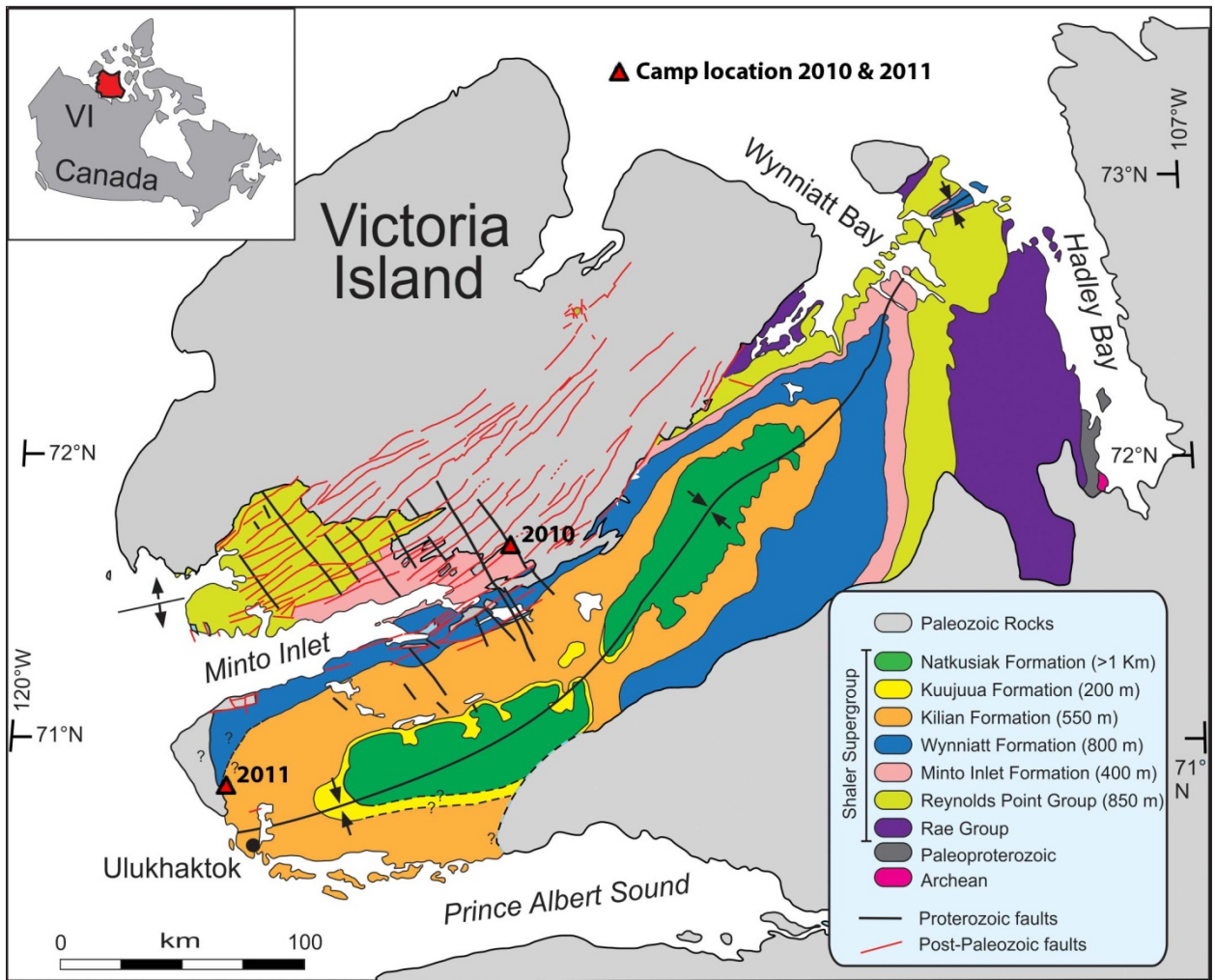
Figure 1.4 Regional geological map of Victoria Island. Natkusiak basalts are shown in green. GSC camp locations for 2010 and 2011 field seasons are indicated with red triangles. Modified from Figure 1 by Bédard et al. (2012a).

throughout the formation and are commonly associated with disseminated prehnite and pumpellyite in highly vesicular flows and scoria deposits. Economic-grade copper deposits have not yet been found, however, the existence several large sheets of native copper in vein and fracture systems in the northern lobe prompted a few exploration ventures by mining companies in the late 1960s (Baragar, 1976; Jefferson et al., 1985).

1.3.2 Previous work

The first comprehensive field study of the Natkusiak basalts was carried out and presented by Baragar (1976). His study consisted of five weeks in the field on Victoria Island, where he observed and documented the volcanic stratigraphy in the thick northern lobe (1100 m) of the Natkusiak Formation (Fig. 1.6). Subaerial sheet flow units were found with exceptionally amygdule-rich bases and tops, and minor sediment interbeds in the lowermost basaltic flow units. Some basalts were noted as being especially plagioclase-phyric, and rare native copper occurrences were also reported by Baragar (1976). The Natkusiak Formation was later subdivided into seven regionally mappable members by Jefferson et al. (1985) and include: the Basal, Pyroclastic, Lower massive, Lower recessive, Middle massive, Upper recessive, and Upper massive units (Fig. 1.6). This informal subdivision of volcanic stratigraphy was prompted by the need to consider the copper occurrences of the basalts in a stratigraphic context. The first geochemical study of the Natkusiak basalts was carried out by Dostal et al. (1986). They analyzed 18 dolerite and basalt samples collected by Baragar (1976) for major and trace elements and found that the basalts demonstrate geochemical characteristics typical of continental tholeiites variably contaminated with a crustal component. The next major geochemical study of the basalts was conducted by Dupuy et al. (1995) on 10 basalt and sill samples from Dostal et al. (1986) that were analyzed for Sr, Nd, and Pb isotope compositions by the TIMS (thermal
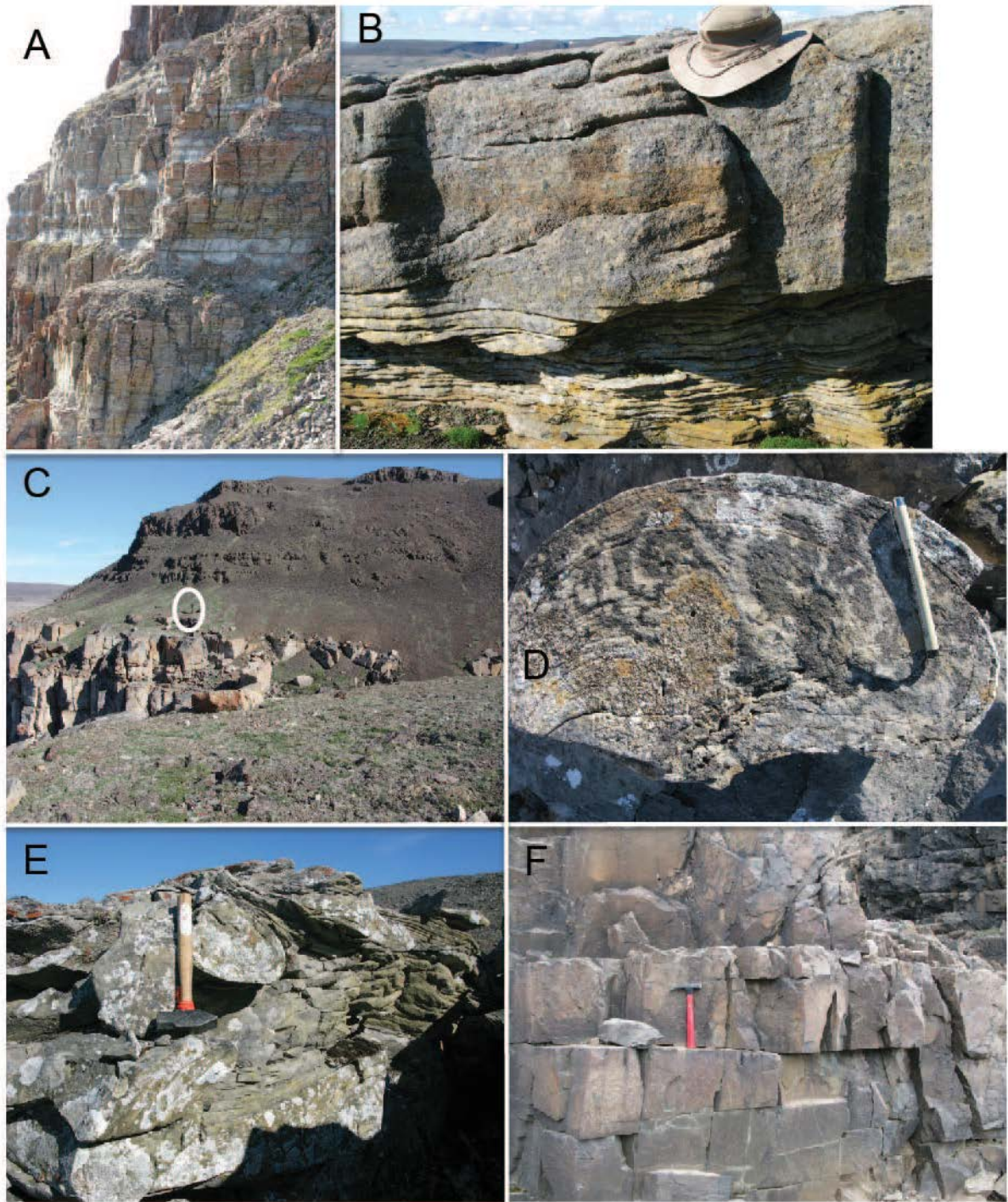
Figure 1.5 Photographs of basement rocks and Natkusiak basalts on Victoria Island. **A)** Jago Bay Formation of the Shaler Supergroup, consisting of shallow water carbonates and interbedded silt stones. Scale = 7 m top to bottom. **B)** Kuujjua Formation, a mature quartz sandstone with large decimeter-sized crossbedding. Hat for scale. **C)** Contact between Kuujjua Formation (light-colored rocks) and Natkusiak Formation (dark-colored rocks) in the southern lobe. Person circled for scale. **D)** Pillow basalt with recognizable rind, located in the basal unit of the Natkusiak Formation. Pen for scale. **E)** Well-formed pillow basalts overlying flattened pillows and lobate basalt structures. Rock hammer for scale. **F)** Fine-grained basalt with blocky fractures from Cycle 1. Rock hammer for scale.
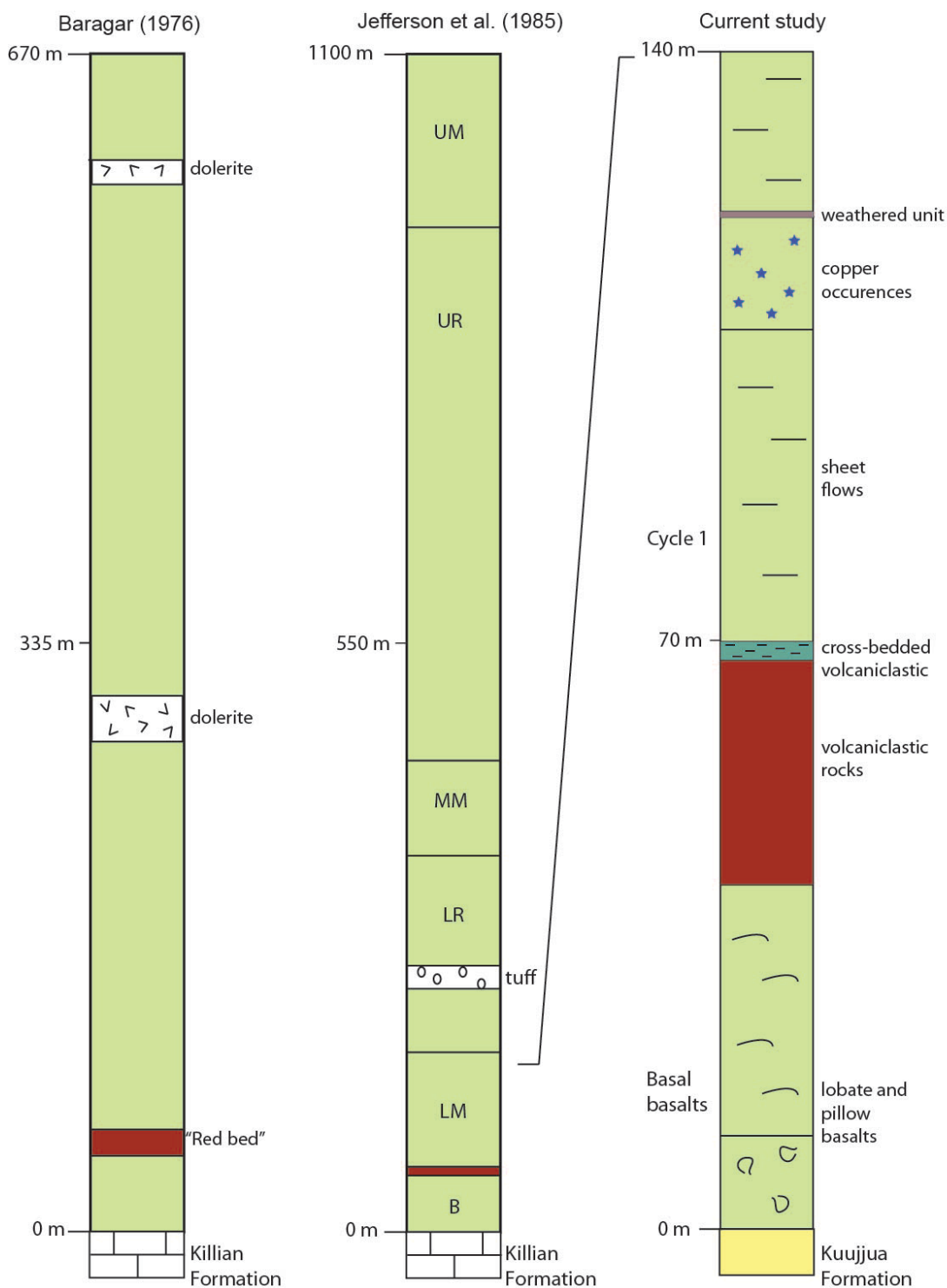
Figure 1.6 Volcanic stratigraphy of the Natkusiak basalts. Modified from Baragar (1976), Jefferson et al. (1985), and the new field observations from the current study modified from Nicole Williamson (M.Sc. thesis work, personal communication). Baragar (1976) and Jefferson et al. (1985) sections are from the northern lobe, the "current study" section is representative of the volcanic stratigraphy of the southern lobe. For Jefferson et al. (1985) B = Basal, LM = Lower massive, LR = Lower recessive, MM = Middle massive, UR = Upper recessive, and UM = Upper massive units.

ionization mass spectrometry) method. They found variations in incompatible trace elements and isotopic ratios that they linked to various mantle and crustal components involved in the genesis of the basalts.

1.4 FIELD TECHNIQUES

All fieldwork was conducted and sponsored by the Geologic Survey of Canada (GSC) as part of an Earth Sciences Sector (ESS) Natural Resources Canada (NRCan) Geo-Mapping for Energy and Minerals (GEM) project on Victoria Island, Northwest Territories, Canada. The overarching goal of the project was to provide maps and thematic studies of central-northern Victoria Island for private sector exploration companies. The Victoria Island GEM project, of which this thesis is a part of, was led by Jean Bédard (GSC-Québec, Igneous stratigraphy, sills, geochemistry and metal potential), Robert Rainbird (GSC-Ottawa, Proterozoic stratigraphy, provenance and mineral potential), and Keith Dewing (GSC-Calgary, Paleozoic stratigraphy).

Preliminary fieldwork was conducted on Victoria Island in the summer of 2008 by Jean Bédard. The main fieldwork and mapping was successfully completed during the summer months of 2010 (June 18th to August 10th) and 2011 (June 19th to August 2nd) with a full field crew of ~16 to 25 at a time. Outcrop exposure on Victoria Island is excellent and requires work near exceedingly beautiful arctic lakes (Fig. 1.7 A). The GSC field camp itself was based in different locations each season with major infrastructure (Fig. 1.7 B) including helicopter support. Two to three helicopters were in operation during each field season to assist teams of two to four in daily assignments. Fieldwork included mapping and sample collection of Paleozoic / Proterozoic strata and the Proterozoic Natkusiak basalts with the utilization of ArcGIS geographical technology and software accompanied by hand-held Getac® data entry units. Traverses for field teams were planned in base camp beforehand and were aimed primarily for the completion of the mapping assignment through the Minto Inlier and for the completion of

individual research projects (e.g., current thesis). In 2010, the base camp was located ~15 km

ENE of the easternmost end of Minto Inlet, whereas the 2011 camp was located just ~10 km

NNW of the town of Ulukhaktok (Fig. 1.4).

Victoria Island is the only known location of extrusive igneous rocks of the Franklin

large igneous province. Pertinent fieldwork included the geochemical sample collection of the

Natkusiak Formation at four separate locations; two sections in the southern lobe and two in the

northern lobe (Fig. 1.8). These sections were chosen on the basis of outcrop exposure,

accessibility, and regional location to maximize the degree of spatial extent of sampled sections

across the formation. The northernmost exposure of the northern lobe was traversed and sampled

in the summer of 2008 by Jean Bédard, complemented by samples from the GSC archive

collected by WRA Baragar and reanalyzed by ICP-MS. The remaining three sections were

sampled in 2010 and 2011, chiefly by Trent Dell'Oro (author) and Nicole Williamson (Carleton

University). Samples from 2008 include five northern basalts, which are supplemented by two

samples from Baragar (1976) that were reanalyzed for isotopic, and trace element geochemistry.

Collectively, these seven samples represent the northernmost section and are termed the

Northern Section (Fig. 1.8). Samples from 2010 include 24 basalt samples (i.e., central section)

processed for trace, rare earth element, and isotopic (Sr, Nd, Hf, Pb) geochemistry. Samples

collected in 2011 include 16 samples for trace element analysis, of which 8 were analyzed for

isotopic (Sr, Nd, Hf, Pb) compositions. The 16 samples collected in 2011 represent two separate

sections termed the western section (Fig. 1.7 C) of the southern lobe, and the eastern section

(Fig. 1.7 D) of the northern lobe (Fig. 1.8).

Sampled sections were chosen on the basis of geographic position and on the degree of

basalt exposure; typical sections were exposed as steep cliff faces (Fig. 1. E). Samples were

22
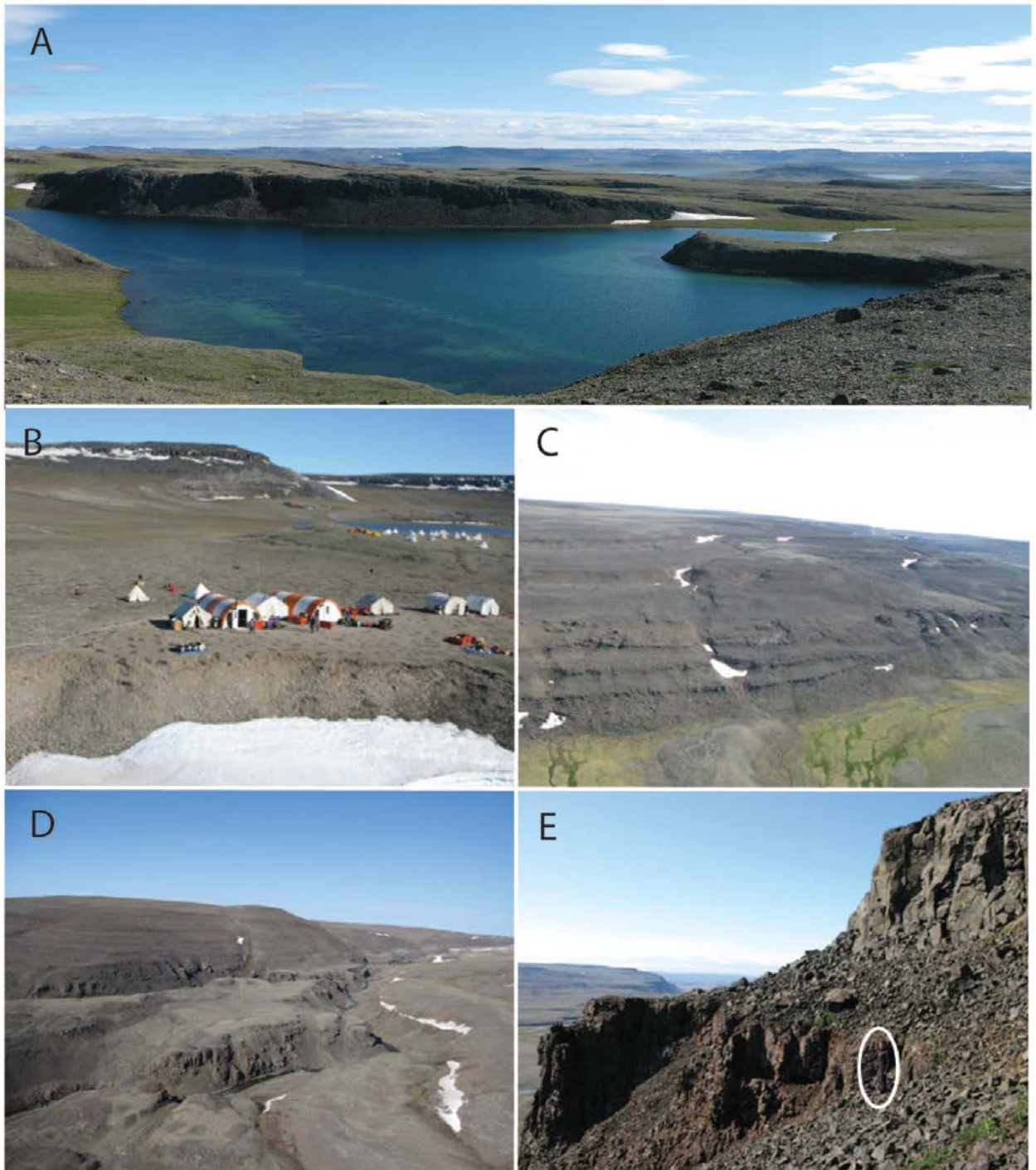
Figure 1.7 Photographs of outcrop and general field conditions on Victoria Island. **A)** Photograph of a gabbroic sill showing typical exposures on Victoria Island. Sill exposure across from lake is approximately 13 m thick (lake edge to top). **B)** Photograph of the 2011 base camp located ~10 km NNW of Ulukhaktok (looking ESE). People for scale. **C)** Aerial photograph of the Eastern Section (looking NE) located on the Northern Lobe. Basalt outcrop from the grassy field to the top of the hill is ~80 m in height. **D)** Aerial photograph of the Western Section (looking NW) located on the southern lobe. Outcrop exposure is ~40 m from river to the hilltop. **E)** Typical outcrop exposure in the Natkusiak Formation, with a person circled for scale.
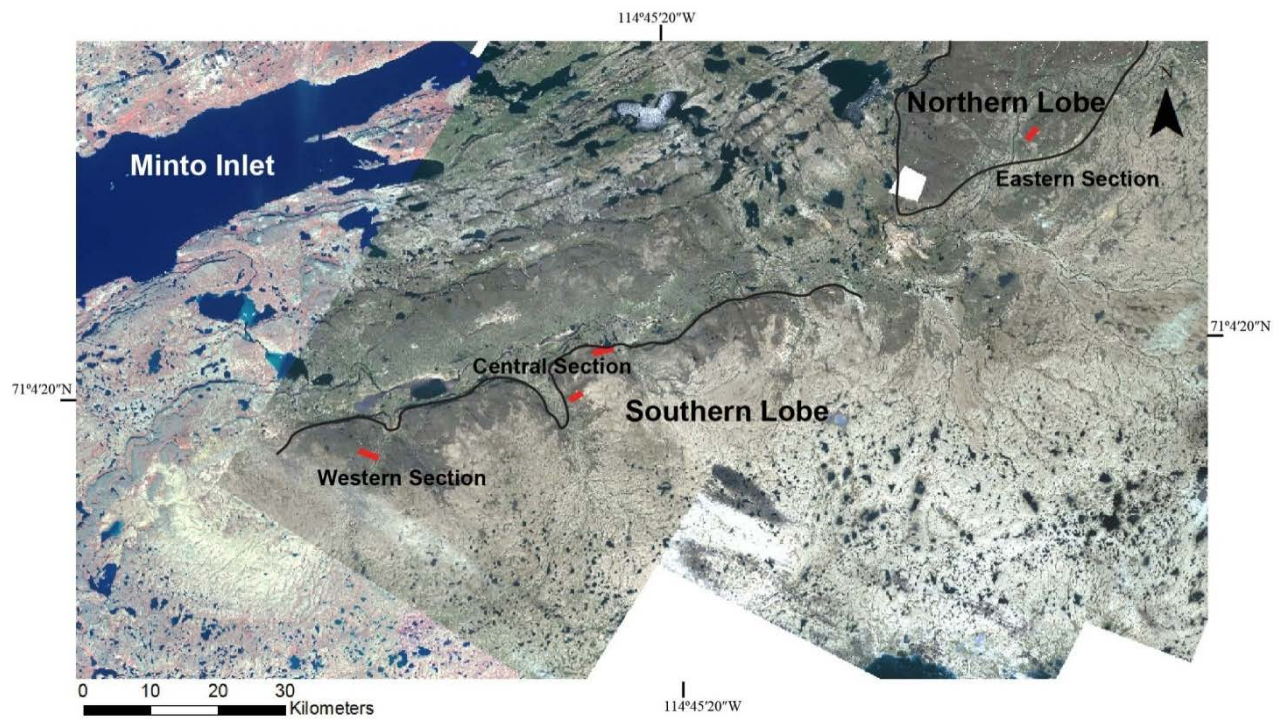
Figure 1.8 Satellite image of the Natkusiak Formation with sampled sections labeled and highlighted in red. Spot image, NASA 2009, mosaic, resolution 10 meters.

collected on the basis of freshness and spatial variation in the field. Samples with the least amount of amygdules were preferentially selected to minimize alteration. Our observed volcanic stratigraphy of the southern lobe of the Natkusiak Formation matches very closely to that of Jefferson et al. (1985), with only minor discrepancies. During the course of mapping facies of the Natkusiak Formation, a well-preserved vent complex was found at the eastern section, with multiple conduit necks protruding through volcanic stratigraphy (Fig.1.9 A and B) and spatter flow tops (Fig. 1.9 C). Pyroclastic deposits were discovered proximal to the conduit neck intrusions, including unconsolidated scoria deposits (Fig. 1.9 D) and elongate 10-15 cm football-shaped volcanic bombs. Both vent systems were sampled for geochemistry and petrographic analysis; the geochemical samples were processed and are archived at The University of British Columbia (UBC).

1.5 THESIS OVERVIEW

This thesis comprises an isotopic and trace element geochemical study of the Natkusiak basalts presented in Chapter 2. The main objective of this study was (1) to establish source components involved in the genesis of the lavas including mantle and crustal involvement, (2) to facilitate correlation with other igneous bodies of the Franklin LIP (sills and dikes), and (3) to integrate the geochemistry of the Franklin LIP with that of other LIP worldwide. Preliminary results of this work have been presented at the American Geophysical Union (AGU) Fall 2011 meeting (Bédard et al., 2011b), and Goldschmidt 2012 (Bédard et al., 2012b) international conferences by Jean Bédard (GSC, Quebec), the GSC project coordinator.

In Chapter 2, the field observations and major element, Sr-Nd-Hf-Pb isotope, trace element geochemistry of the Natkusiak Formation are presented. The distinguishing geochemical characteristics of the basaltic units are identified and a new geochemical classification of the
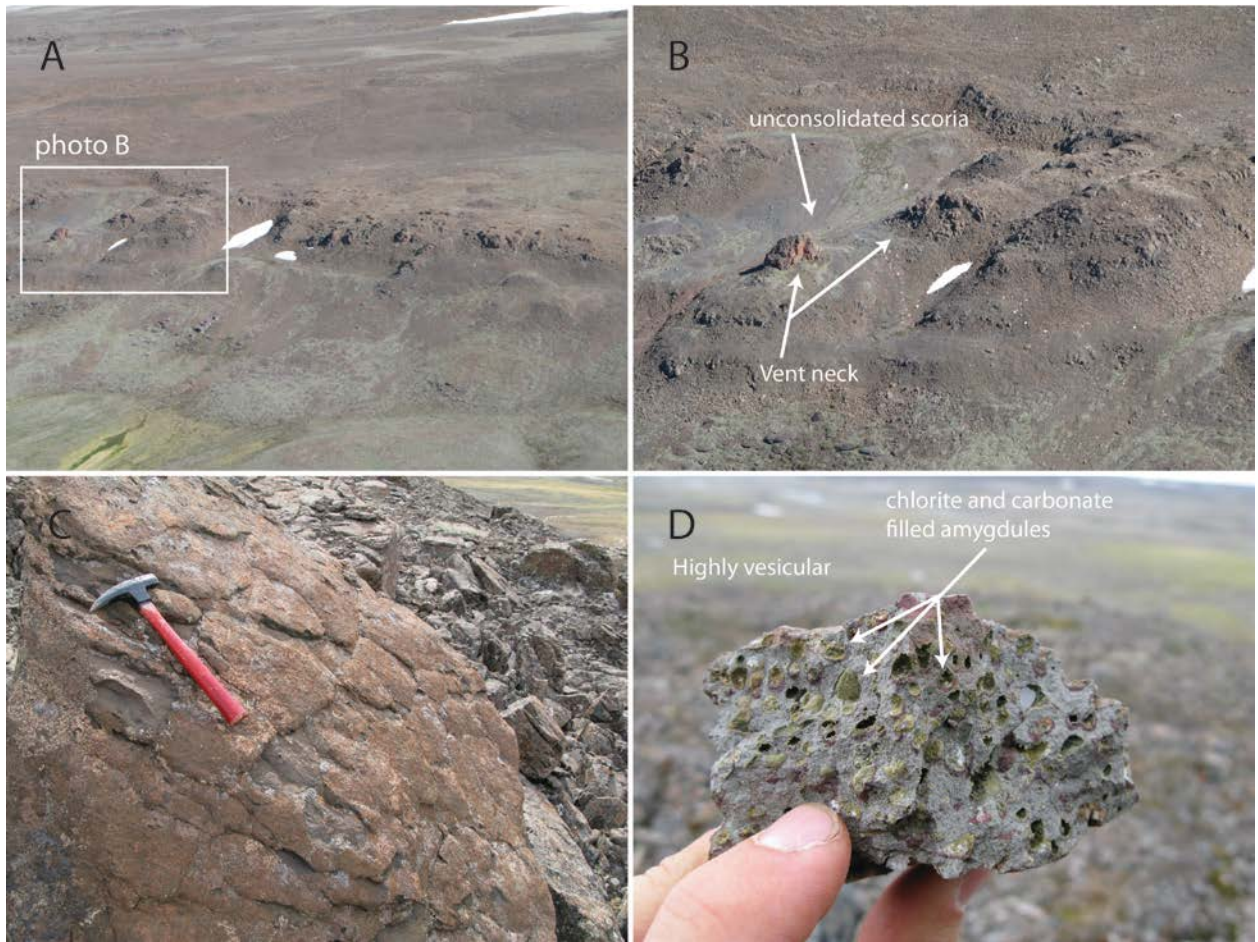
Figure 1.9 Photographs of the vent complex found at the eastern section. **A)** Aerial photograph of the eastern section with a preserved vent complex, cycle 1 sheet flows. Scale, approximately 80 m across. **B**) Close-up of the conduit neck of the vent complex from photograph A, unconsolidated scoria deposits, spatter flow tops, and football-shaped volcanic bombs are found proximal (tens of meters) from the conduit necks. Scale, approximately 30 m across. **C)** Spatter texture flow top. Hammer for scale. **D)** Highly-vesicular, unconsolidated scoria. Amygdules are filled with chlorite and calcite. Finger for scale.

Natkusiak flood basalt formation is recognized, the high- and low-Ti basalt groups. The extent of crustal contamination is addressed and an origin of the two geochemical basalt groups is proposed. Linkages between the Franklin intrusive rocks and the overlying Natkusiak Formation flood basalts are made utilizing Sr-Nd-Hf-Pb isotopes. Chapter 3 summarizes and concludes the study presented here.

Appendix A comprises a petrographic catalogue of all basalt samples processed for thin section (n = 47). The catalogue includes a petrographic description of mineralogy with modal abundances in volume percent and representative photomicrographs and scanned thin sections. Appendix B summarizes a microbeam study on the chlorite-filled amygdules in the Natkusiak basalts. The study was carried out as a project for the course EOSC 521 "Microbeam and Diffraction Methods for the Characterization of Minerals and Materials" with Dr. Mati Raudsepp to document the secondary alteration phases present and to define relative temperatures of precipitation of chlorite. Alteration phases were initially identified using a conventional optical microscope, with further alteration characterization and mineral identification carried out on a Phillips XL-30 Scanning electron Microscope (SEM) and on a CAMECA SX100 electron-probe micro-analyzer. Chlorite in the amygdules was targeted for microprobe analysis to apply a chlorite-smectite geothermometer method. Appendix C comprises a reconnaissance study of crystal size distribution (CSD) results from a project in the course EOSC 530 "Advanced Igneous Petrology" with Dr. James S. Scoates. Four basalt samples were selected for the application of quantitative textural analysis to determine the size distribution of plagioclase grains; results are reported in Appendix C. Appendix D is a full reference list of the isotopic compositions from the GEOROC database compilation (http://www.georoc.mpch-mainz.gwdg.de) used in this study.

CHAPTER 2

Sr-Nd-Hf-Pb ISOTOPE AND TRACE ELEMENT GEOCHEMISTRY OF THE NATKUSIAK BASALTS, FRANKLIN LARGE IGNEOUS PROVINCE (VICTORIA ISLAND, CANADA)

2.1 INTRODUCTION

Continental flood basalt volcanism is generally associated with rifting and extension (e.g., Kempton et al., 2000; Schlische et al., 2002; Kieffer et al. 2004; Pisarevsky et al., 2008; Meyer et al., 2009). During extension, the geochemical signature of the flood basalts typically evolves towards that of oceanic basalts (i.e., oceanic island basalts (OIB) and mid-ocean ridge basalts (MORB)), which is consistent with the increased involvement of an asthenospheric mantle source (e.g., Cox & Hawkesworth, 1984; Lightfoot et al., 1990; Hofmann, 2003; Xiao et al., 2004; Zhu, 2007; White, 2010; Shellnut & Jahn, 2011). The earliest erupted basalts in continental flood basalt provinces tend to show more contamination (i.e., higher LREE/HREE, elevated $^{87}Sr/^{86}Sr$, low ε_{Nd} and ε_{Hf} values, and more radiogenic Pb isotope ratios) than the more asthenospheric mantle-derived basalts that erupt in the latter stages of "transient" flood basalt volcanism and continue into the "persistent stage" of hotspot volcanism (Herzberg & Gazel, 2009; White, 2010). The geochemical variations observed in the early stages of continental flood basalt volcanism indicate that the initial stages of magma genesis include contributions from various sources (i.e., plume, lithospheric mantle, and upper and lower continental crust). Large igneous provinces (LIP), including continental flood basalts, have been linked to mantle plumes (e.g., Richards et al., 1989; Campbell & Griffiths, 1990; Carlson, 1991; Jellinek & Manga, 2004; Montelli et al., 2004; DePaolo & Weis, 2007; Herzberg & Gazel, 2009), although, the relative contribution of mantle and crustal sources in continental flood basalts is still a matter of much debate (e.g., Lightfoot et al., 1990; Arndt & Christensen, 1992; Peng et al., 1994; Greene et al., 2008).

This study focuses on the Sr-Nd-Hf-Pb isotope and trace element geochemistry of the Neoproterozoic Natkusiak Formation flood basalts of the Franklin large igneous province located on Victoria Island, Canada. The Franklin magmatic event is associated with plume-related uplift and rifting that eventually led to the breakup of the Laurentian Supercontinent and the opening of

the Neoproterozoic Palaeo-Asian Ocean (Rainbird, 1993; Pelechaty, 1996; Rainbird & Freitas, 1997; Li et al., 2008; Pisarevsky et al., 2008).The basalt exposures on Victoria Island are especially relevant to the study of LIP, as the earliest erupted flood basalts are well-preserved and accessible at the surface. The goal of this study is to assess the geochemical variation (radiogenic isotope and incompatible trace element) of the Franklin large igneous province and to constrain the mantle source(s) and extent of crustal contamination. Additionally, geochemical linkages with the underlying feeder system are made through an isotopic comparison of the results from the Franklin intrusive rocks (Beard, 2012). The combined analysis of trace elements and Sr-Nd-Hf-Pb isotope systems of flood basalts provide a powerful tool for the determination and characterization of mantle heterogeneities, source components, and contaminants involved in continental flood basalt genesis (e.g., Zindler & Hart, 1986; White, 1985; Albarede, 1992; Tejada et al., 2004; Stracke et al., 2005; Zhu, 2007). In a previous isotopic study of the Franklin magmatic province, Dupuy et al. (1995) provide a two-component mixing model based on trace element concentrations and Sr-Nd-Pb isotope compositions of 10 samples from the northern lobe of the Franklin LIP. They propose that the Natkusiak basalts were generated by the melting of a depleted subcontinental lithospheric source that was contaminated by crust prior to emplacement. The present study uses a significantly larger sample set from across the entire exposed Natkusiak Formation and provides evidence for the involvement of multiple geochemical components based on Sr-Nd-Hf-Pb and trace element geochemistry with relatively minor contribution from continental crust.

2.2 GEOLOGICAL BACKGROUND

2.2.1 Geological setting of Victoria Island

The Neoproterozoic Franklin large igneous province includes a system of dikes, sills, and continental flood basalts in the northern Canadian Shield, which was emplaced at ca. 723 Ma

(Heaman et al., 1992; Pehrsson et al., 1999; Shellnutt et al., 2004) (Fig. 2.1). The Franklin LIP on Victoria Island is dominated by the Natkusiak basalts and the coeval Franklin sill intrusive system (Fig. 2.1) (Bédard et al., 2012a). The deep basement rock of Victoria Island comprises granitoid Archean rocks of the Slave Province (2.6-2.4 Ga) and is exposed on the eastern-half of the island (Kolebaba et al., 2003). The crust has a thickness of 37.3 km in the northwesternmost part of the craton, subjacent to Victoria Island (Bank et al., 2000; Davis et al., 2003). On Victoria Island, the Archean rocks are overlain by the Neoproterozoic Shaler Supergroup that represents a succession of shallow-water continental and marine sedimentary rocks that were deposited in an intracontinental basin of Rodinia during the Proterozoic (~850 to 635 Ma) (Thorsteinsson & Tozer, 1962; Rainbird,1993, Hofmann & Rainbird, 1994, Macdonald et al., 2010). The dominant rock types include limestone, dolostone, sandstone, and lesser shales and evaporites that were intruded by the gabbroic Franklin sills and dikes (Heaman et al., 1992; McDonald et al., 2010; Jones et al., 2010; Bédard et al., 2011b). The Franklin sills are prevalent throughout the Shaler Supergroup and range in thickness from 2-120 m and typically extend for ~20 km or more along strike with minimal change in thickness (Baragar 1976; Jefferson et al., 1994; Bédard et al., 2012a). The Neoproterozoic sedimentary and igneous rocks are unconformably overlain by a Paleozoic sedimentary sequence ranging in age from Cambrian to Devonian. The Paleozoic rocks are mainly clastic sedimentary at the base and shift up-section to a carbonate-dominated sequence (Thorsteinsson & Tozer, 1962; Durbano et al, 2010). The Natkusiak basalts are well exposed in the Minto Inlier on Victoria Island due to post-depositional erosion.
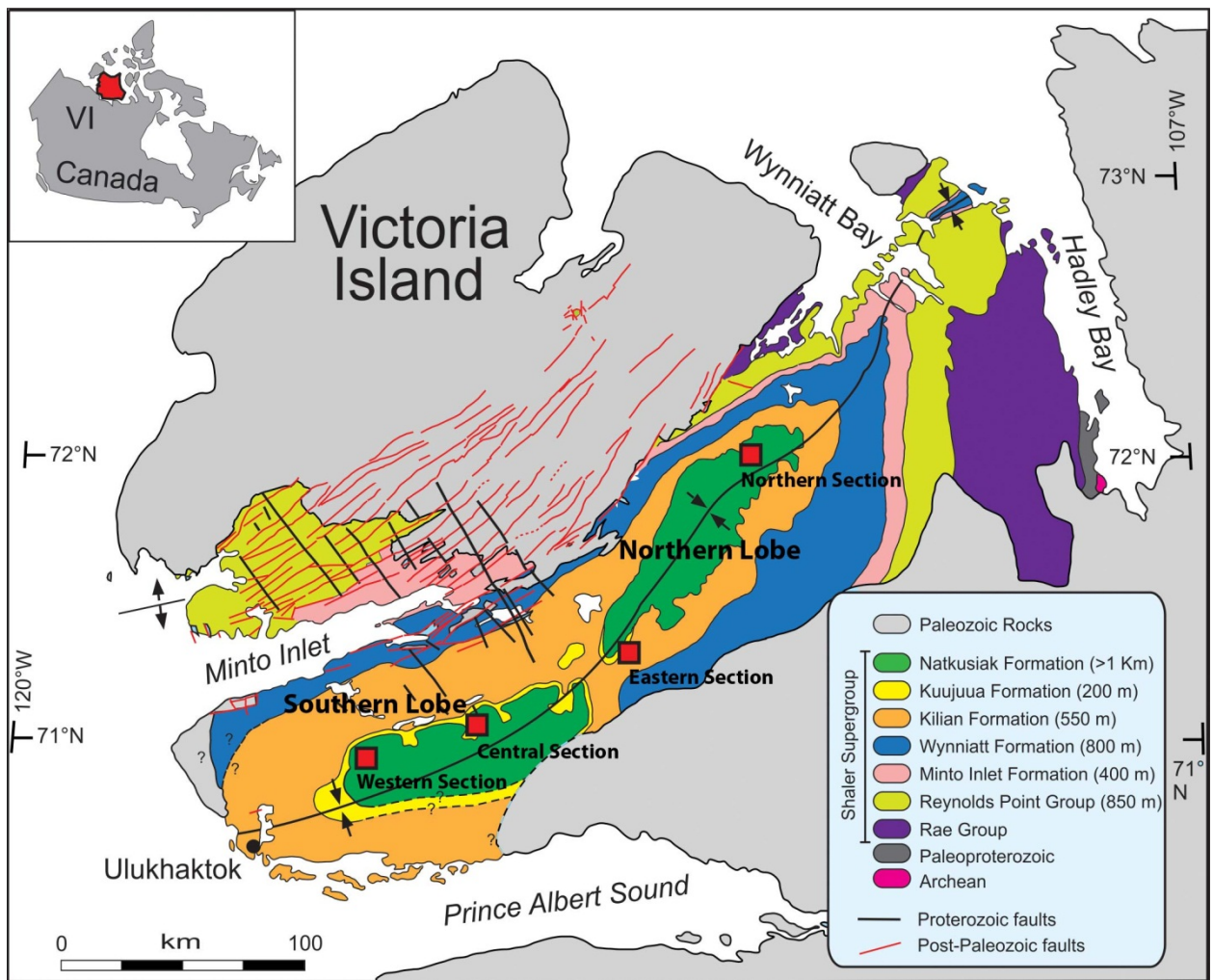
Figure 2.1 Regional geological map of Victoria Island. Natkusiak basalts are shown in green. Volcanic sections sampled during this study are labeled and indicated with red squares. Modified from Figure 1 by Bédard et al. (2012a).

2.2.2 The Natkusiak basalts

The Shaler Supergroup is capped by the Natkusiak Formation that is preserved in two lobes in the northeast and southwest regions of the Minto Inlier, Victoria Island, and referred to as the northern and southern lobes, respectively (Fig. 2.1). Each lobe is about 100 km long and 10-30 km wide (Baragar, 1976). The Natkusiak basalts lie unconformably on top of the Kilian Formation in the northeast, and conformably on top of the Kuujjua Formation in the southwest of Minto Inlier. Locally, there are occurrences of lenses of sandstone and pepperites in basal lavas of the southern lobe as well as fluidal sedimentary structures in the Kuujjua Formation (Rainbird et al., 1993). The basalts reach a maximum preserved thickness of 1100 m in the center of the northern lobe, but only 140 m are preserved in the southern lobe (Fig. 2.2). The basalts may be divided into three volcanological units, the basal unit and the two overlying cycles of sheet flows (cycle 1 and cycle 2). Only basal and cycle 1 basalts are exposed in the southwest, while the northern lobe preserves the basal, cycle 1, and cycle 2 units. The thin basal unit (up to 70 m thick) is characterized by brown-green rubbly basalt flows with local hyaloclastites, pepperites, and pillow basalts (Jefferson, 1985; Bédard et al., 2011b; Williamson et al., 2012). Pipe vesicles are common at the base of individual flows and the tops are commonly rubbly and highly amygdaloidal. A shift in eruptive style between the basal basalts and cycles 1 and 2 is marked by a maroon-colored volcaniclastic unit that contains matrix-supported conglomerates (interpreted as lahars or damburst deposits) that fill palaeovalleys (Bédard et al., 2012b; Williamson et al., 2012). The lower portion of the volcaniclastic unit is dominated by an unsorted matrix with no systematic size grading, whereas the upper ~5 m is characterized by cross-bedding and a greenish-brown color. The volcaniclastic unit is thicker in the northwest (> 100 m), and pinches out the southeast of the southern lobe. The overlying sheet flows are characterized by fine-grained massive basalt flows with fewer amygdules and range up to a few tens of meters in thickness. The sheet flow basalts are blue-green to grey on a fresh surface and weather green to

orange-brown. Large columnar-jointed (0.5-1 m diameter) units result in spectacular cliffs; 'a'a

and pāhoehoe flow-tops and are rarely preserved throughout. Previous geochemical studies of

the Natkusiak basalts include Baragar (1976), Baragar & Loveridge (1982), Dostal et al. (1986),

and Dupuy et al. (1995).

There is a noticeable gap in the stratigraphy between 40 and 70 m due to the lack of

outcrop exposure. Field observations indicate a shift in eruptive style between the basal basalts

and the cycle 1 sheet flows in the southern lobe. Evidence of this transition is preserved in the

volcanic stratigraphy as interbedded basalt flows and volcaniclastic beds, which may indicate a

shift to more explosive volcanism for a period of time immediately following the emplacement

of the basal basalts and prior to the emplacement of the overlying cycle 1 and 2 sheet flows.

2.3 STRATIGRAPHIC SECTIONS AND SAMPLES

The samples analyzed in this study were collected with a rock-hammer at four separate

locations of the Natkusiak Formation (see Chapter 1 Field Techniques for more details). These

locations are termed the central, eastern, western, and northern sections (Fig. 2.3). The seven

northern samples are from the ~1100 m volcanic pile of the northern lobe; two are from Baragar

(1976) and five were collected by Jean Bédard in summer 2008. The samples collected at the

central (24 samples; Fig. 2.4), eastern (n = 9), and western (n = 7) sections are from volcanic

exposures no thicker than ~140 m. All samples (total of 47) are subaerial basalts that are

dominantly composed of plagioclase, clinopyroxene, and opaque minerals (predominantly

titanomagnetite) with minor plagioclase- and clinopyroxene-phyric basalts. Alteration of the

Natkusiak basalts is manifested through replacement of plagioclase by clay minerals and

clinopyroxene by chlorite. Vesicles and veins are filled with secondary chlorite, calcite, and

quartz in variable proportions (amygdules up to 35 vol. %). A few relict olivine grains are found

in the northern basalts; however, the southern basalts are noticeably devoid of either relict or
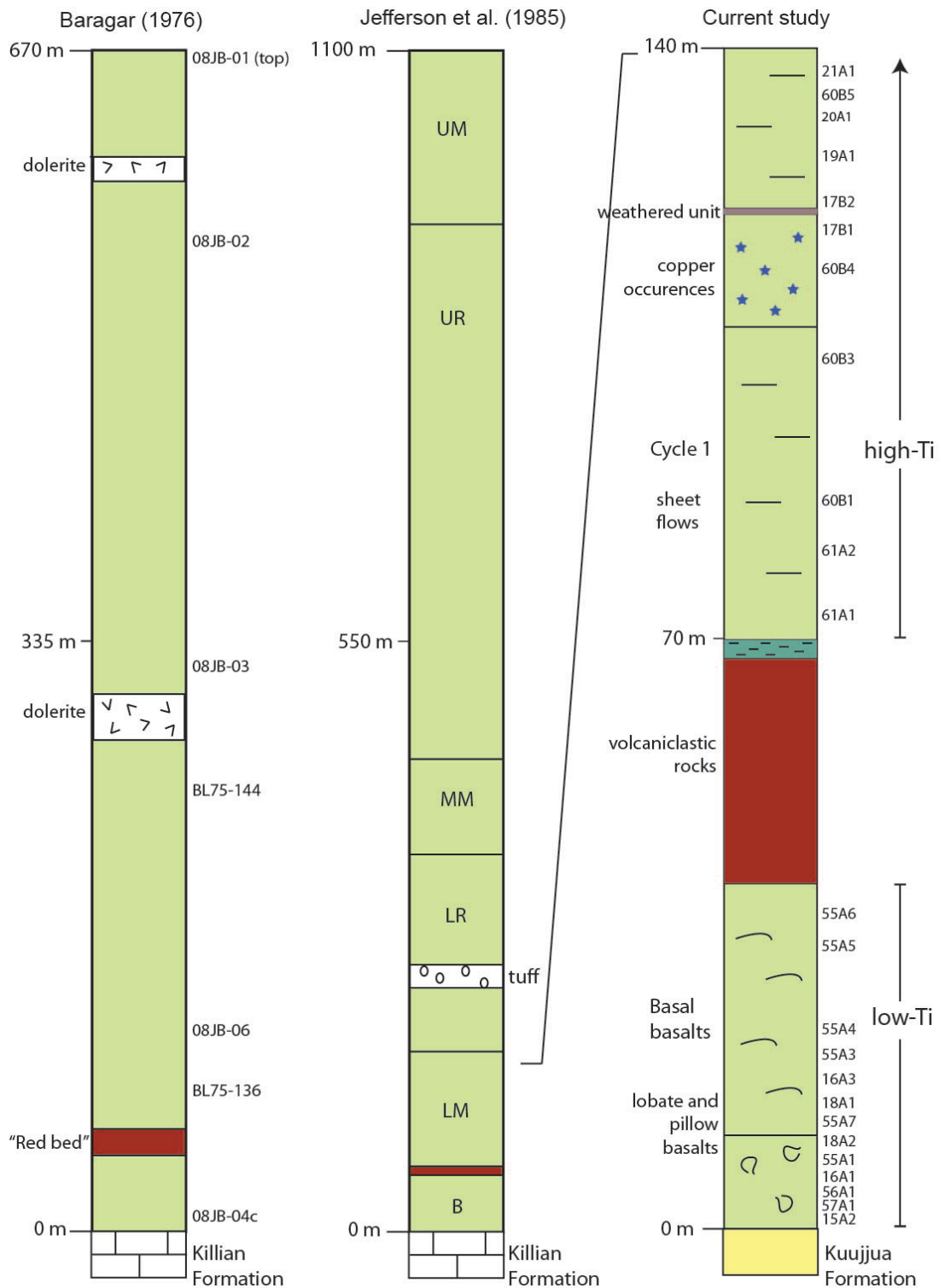
Figure 2.2 Volcanic stratigraphy of the Natkusiak basalts. Stratigraphic sections modified from Baragar (1976), Jefferson et al. (1985), and the new field observations from the current study of Nicole Williamson (M.Sc. thesis work, Carleton University, personal communication). Baragar (1976) and Jefferson et al. (1985) sections are from the northern lobe, the "current study" section is representative of the volcanic stratigraphy of the southern lobe. Sample locations are indicated. For Jefferson et al. (1985) B = Basal, LM = Lower massive, LR = Lower recessive, MM = Middle massive, UR = Upper recessive, and UM = Upper massive units.

primary olivine and commonly contain subophitic clinopyroxene. Table 2.1 provides a summary

of the petrographic observations (further characterization is provided in Appendix A) and

includes sample, section, and group name of each sample, as well as phenocryst proportions,

dominant igneous textures, and relevant sample notes.

Due to the age (723 Ma) and extent of alteration of the Natkusiak basalts, it was

necessary to minimize any chemical disturbance imparted during subsequent hydrothermal

alteration (see Appendix B for discussion of chlorite alteration) (e.g., Hart et al., 1974;

Hawkesworth & Morrison, 1978; Verma, 1992; White et al., 2003). To remove the secondary

effects from alteration and contamination in the Natkusiak basalts, a sample-by-sample acid-

leaching procedure, following the protocol in Weis et al. (2005), was implemented prior to

dissolution and analysis. The acid-leaching method has proven to be an effective and essential

step in sample processing for the isotopic analysis of basalts (Weis et al, 2005; Nobre Silva et al.,

2009; Hanano et al., 2009; Nobre Silva et al., 2010).

2.4 ANALYTICAL TECHNIQUES

2.4.1 Laboratory and chemical techniques

Samples collected during the summers of 2010 and 2011 were processed at the Pacific

Centre for Isotopic and Geochemical Research (PCIGR), University of British Columbia,

Canada. All geochemical samples were first washed in tap-water to remove dirt and cut with a

diamond-embedded tile-saw to remove weathered/altered surfaces. Samples with sufficient

volume were processed into thin sections or polished thin sections (Vancouver Petrographics

Ltd.). A complete petrographic catalogue of the sample suite is included in Appendix A and

includes primary mineral abundance (by estimation of total surface area percentage), amygdule-
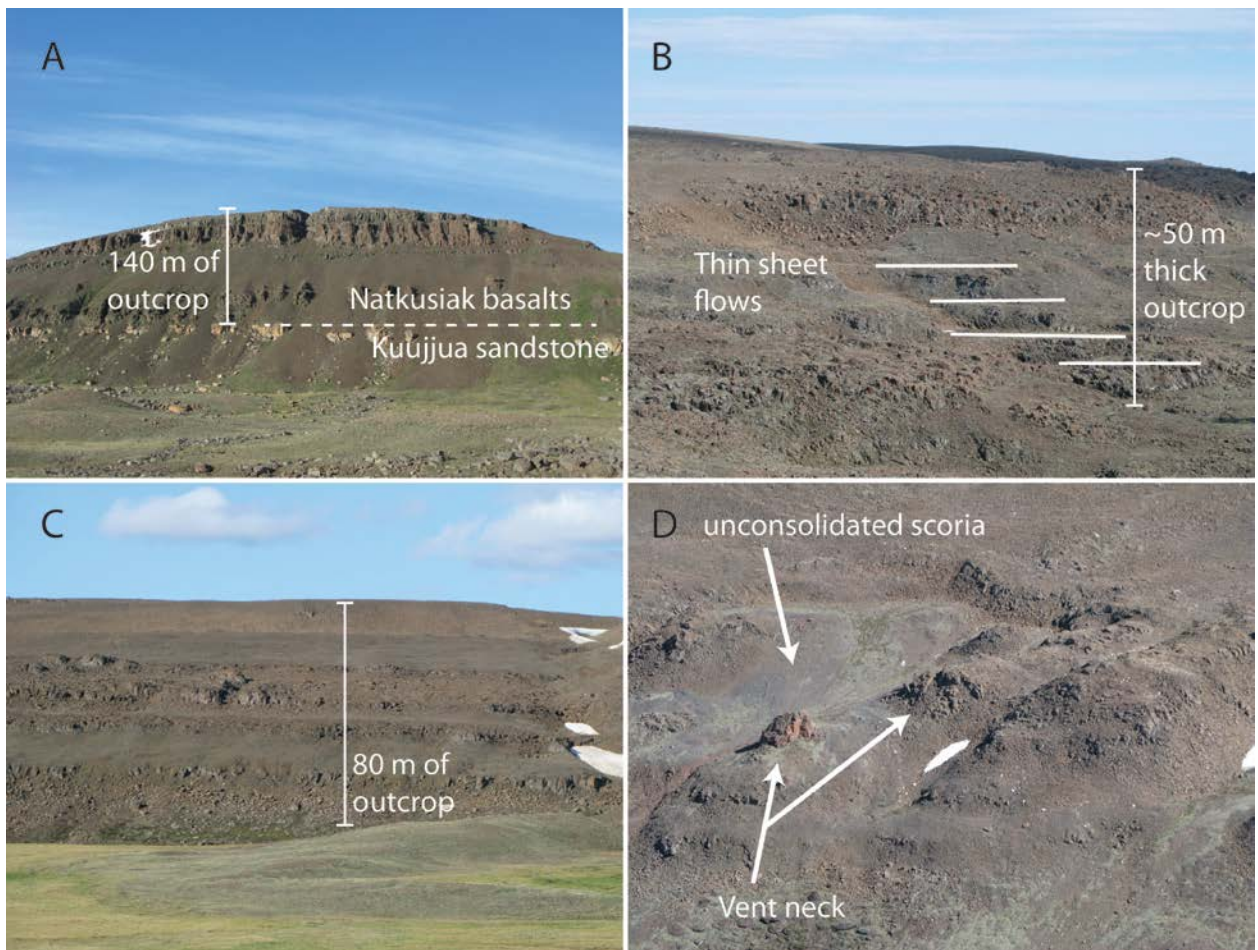
Figure 2.3 Photographs of the Natkusiak basalt sections sampled during this study. **A)** The central section with the Kuujjua sandstone contact exposed, basal and cycle 1 basalts are preserved here. Scale indicated on photo, looking ENE. **B)** Western section with thin, decameter-sized sheet flows in cycle 1. Scale indicated in photo, looking NNW. **C)** Eastern section with thin sheet flows (similar to western section), cycle 1 preserved here. Scale indicated in photo, looking NE. **D)** Volcanic vent complex found at the eastern section with a feeder neck preserved and unconsolidated scoria deposits proximal to the conduit neck. Looking NE.
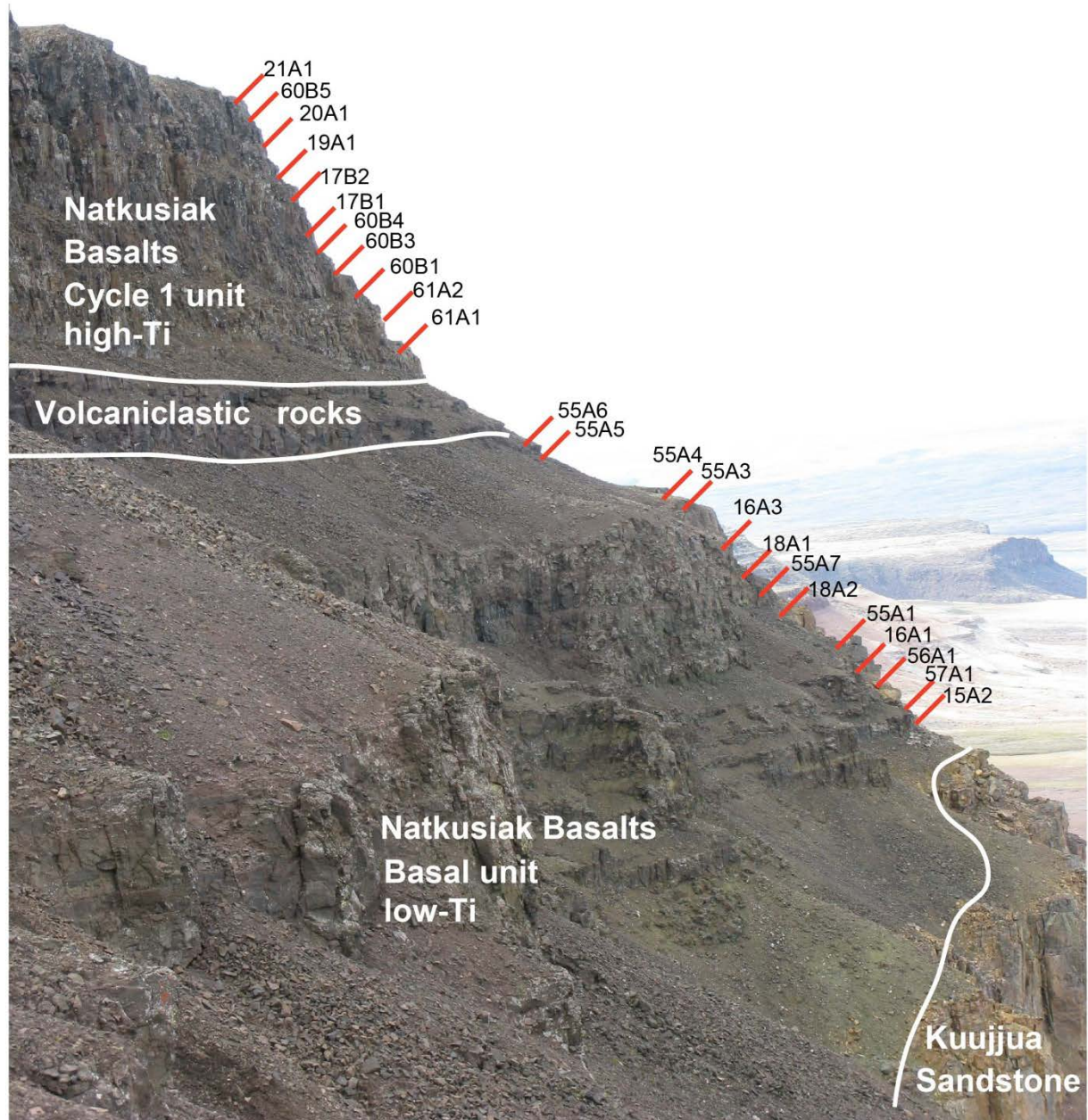
Figure 2.4 Photograph of the central section with marked locations of geochemical samples collected during the summer of 2010. The central section represents the most complete and well-preserved section in the southern lobe, and is the only section sampled and measured from the contact between the Kuujjua sandstone and Natkusiak Formation. The entire basalt section measures 140 m starting from the white line of the Kuujjua sandstone contact and ending at the top of the cliff. All sample numbers prefaced by '10RATTD'. Looking WSW.

Table 2.1: Summary of petrographic characteristics and phenocryst proportions of the Natkusiak basalts, Victoria Island, Canada

Sample	Section	Unit	Texture	Phenocrsyt Vol. %	Plag.	Cpx.	Amyg.	Notes
08JB01	Northern	Cycle 2	intergranular				10	
08JB02	Northern	Cycle 2	amygdaloidal				13	
08JB03	Northern	Cycle 2	subophitic				14	Relict olivine
08JB04C	Northern	Basal	intergranular				16	Relict olivine, high $^{87}Sr/^{86}Sr$
08JB06	Northern	Cycle 1	intergranular				2	
10RATTD15A2	Central	Basal	subophitic				17	Plag glomerocrysts
10RATTD16A1	Central	Basal	amygdaloidal, altered				28	Strong alteration , high $^{87}Sr/^{86}Sr$
10RATTD16A2	Central	Basal	amygdaloidal			2	35	Strong alteration
10RATTD16A3	Central	Basal	amygdaloidal			5	25	Strong alteration
10RATTD17B1	Central	Cycle 1	intergranular				<1	Very fine-grained
10RATTD17B2	Central	Cycle 1	intergranular				<1	Very fine-grained
10RATTD18A1	Central	Basal	amygdaloidal			3	25	Strong alteration, high $^{87}Sr/^{86}Sr$
10RATTD18A2	Central	Basal	amygdaloidal		2	6	24	Strong alteration, high $^{87}Sr/^{86}Sr$
10RATTD19A1	Central	Cycle 1	intergranular				<1	
10RATTD20A1	Central	Cycle 1	intergranular				<1	
10RATTD21A1	Central	Cycle 1	intergranular				<1	
10RATTD55A1	Central	Basal	subophitic				22	
10RATTD55A2	Central	Basal	amygdaloidal				32	Strong alteration
10RATTD55A3	Central	Basal	subophitic, amygdaloidal				15	
10RATTD55A4	Central	Basal	subophitic, amygdaloidal				10	
10RATTD55A5	Central	Basal	porphyritic			11	10	High $^{87}Sr/^{86}Sr$
10RATTD55A6	Central	Basal	intergranular			2	12	High Sr concentration, and $^{87}Sr/^{86}Sr$
10RATTD56A1	Central	Basal	subophitic				15	
10RATTD57A1	Central	Basal	subophitic				13	
10RATTD60B1	Central	Cycle 1	intergranular				<1	Very fine-grained
10RATTD60B3	Central	Cycle 1	intergranular				<1	Very fine-grained
10RATTD60B4	Central	Cycle 1	subophitic				<1	High Sr concentration
10RATTD60B5	Central	Cycle 1	intergranular				<1	
10RATTD61A1	Central	Cycle 1	intergranular				<1	
10RATTD61A2	Central	Cycle 1	glomeroporphyritic		8	4	<1	Circular chalcedony nodules
11RATTD43B	Eastern	Cycle 1	intergranular				10	
11RATTD43C	Eastern	Cycle 1	intergranular				8	High Sr concentration
11RATTD72B	Eastern	Cycle 1	intergranular				9	High Sr concentration, and $^{87}Sr/^{86}Sr$
11RATTD72C	Eastern	Cycle 1	intergranular				10	High Sr concentration, and $^{87}Sr/^{86}Sr$
11RATTD72D	Eastern	Cycle 1	intergranular				7	
11RATTD72E	Eastern	Cycle 1	intergranular				14	
11RATTD72F	Eastern	Cycle 1	intergranular, porphyritic			6	7	
11RATTD72G	Eastern	Cycle 1	glomeroporphyritic		9	5	<1	Clots of coarse-grained cpx/plag
11RATTD73A	Eastern	Cycle 1	intergranular			3	15	
11RATTD129A	Western	Cycle 1	coarse grained				10	Very coarse-grained
11RATTD129B	Western	Cycle 1	glomeroporphyritic		18	6	5	
11RATTD129C	Western	Cycle 1	subophitic				20	
11RATTD129D	Western	Cycle 1	subophitic				20	
11RATTD129E	Western	Cycle 1	intergranular				<1	
11RATTD129F	Western	Cycle 1	intergranular				12	
11RATTD129G	Western	Cycle 1	intergranular				8	

* See Appendix A for complete petrographic characterization of samples.

volume percent, textures, mineral morphology, optical properties, and alteration. Samples were then chosen for geochemical analyses on the basis of relative alteration. Select samples were then crushed to centimeter-size fraction with a Rocklabs® hydraulic crusher equipped with Tungsten-Carbide plates to minimize contamination (e.g., percussion method). Samples were powdered to micron-size fraction (grain size <100 µm) using a Fritsch® Pulverisette planetary mill with agate jars and balls cleaned with quartz sand between samples. Sample pulverization in agate reduces the chance of sample contamination by metals (e.g., Nb, Ta) that are introduced through traditional shatter-box methods.

Major element analyses of the whole rock powders from the 2010 field season (n = 24) were performed at the INRS-ETE laboratories in Quebec City by inductively coupled plasma-atomic emission spectrometry (ICP-AES). Measurements were calibrated against USGS reference materials BCR-2 and BHVO-2. Samples from the 2011 field season (n = 16) were analyzed for major elements at Carleton University by fused-disc X-ray fluorescence spectrometry (XRF) and calibrated using BCR-2 reference material. All isotope and trace element analyses were conducted at the PCIGR. All chemical digestion and separation were carried out in Class 1000 clean laboratories, sample handling was carried out within Class 100 laminar flow hoods, and mass spectrometric analyses were carried out in Class 10,000 clean laboratories. Reagents used for leaching, dissolution, and separation were sub-boiled or quartz-distilled and all dilutions were made using 18.2 MΩ · cm de-ionized water, and labware was acid-washed prior to use.

Leaching and digestion for purification of Sr, Nd, Hf, and Pb for column chemistry began by weighing 300-400 mg of sample powder into 15 mL screw-top Savillex® beakers. The acid-leaching technique implemented in this study follows that of Weis et al. (2005), and is detailed by Nobre Silva et al. (2009). Samples were acid-leached with 10 mL of 6M HCl in an ultra-sonic bath for 20 minutes; this process brought the temperature near to ~50ºC. The leachate solution

was then immediately removed from the beakers, and this procedure was repeated until the leachate solution appeared transparent and pale yellow to colorless. At this point, the same procedure was repeated twice more using 18.2 MΩ · cm de-ionized water to remove any trace of remaining HCl acid. The leached rock powders were then dried to completion on a hot-plate at 120ºC and weighed after cooling to room temperature. The least altered samples required a minimum of five acid-leaching steps before rinsing was commenced and the most altered samples required nine acid-leaching steps before transparent leachate solution, free of fine-sized particles, was obtained.

Leached samples were digested in 15 mL screw-top Savillex® beakers using a 1:10 mixture of concentrated HNO_3 and HF acids. Beakers containing sample solutions were then heated on a hotplate at 120ºC for 48 hours; afterwards, the samples were ultrasonicated for ~20 minutes to ensure complete digestion. The samples were then dried down to completion and re-digested in 10 mL of 6M HCl acid for 24 hours. The samples were dried down again to completion for Sr, Nd, Hf, and Pb separation. The sequential chromatographic purification methods described in Weis et al. (2006) were used to separate Sr, Nd, Hf, and Pb from a single digested solution for each sample analyzed. Sample digestion for trace element and rare earth element (REE) concentration analysis followed the same method, without any preliminary acid-leaching steps.

2.4.2 Mass spectrometry

Whole rock samples analyzed for element concentrations were measured on an ELEMENT 2 (Thermo Finnigan) high resolution inductively-coupled plasma mass-spectrometer (ICP-MS) and on an Agilent 7700 Quadrupole ICP-MS at the PCIGR. Fully digested samples were diluted 5000 times in HNO_3 for analysis on the ELEMENT 2 and on the Agilent. Solutions analyzed on the ELEMENT 2 were spiked with Indium (10 ppb) as an internal standard.

ELEMENT 2 results were corrected for background and according to the BCR2 reference material run in-between every eight samples normalized to the published BCR-2 values (Raczek et al., 2001). The Agilent was run in both normal-mode and He-mode to reduce oxide interferences. Results from the Agilent were corrected for oxide interferences and according to several internal standards (Be, Re, Se, In) for mass correction during instrumental drift.

All Sr and a portion of Nd isotope ratios were measured on a TRITON Thermo Finnigan thermal ionization mass-spectrometer (TIMS) in static mode with relay rotation on single Ta filaments (for Sr) and double filaments Re-Ta (for Nd). Standard materials SRM987 and LaJolla were measured at least 3-4 times every 21 measurements for Sr and Nd isotopes, respectively. Sr and Nd analyses were normalized on the basis of the average of the standards SRM987 $^{87}Sr/^{86}Sr$ = 0.710252 ± 0.000018 (n = 17) and LaJolla $^{143}Nd/^{144}Nd$ = 0.511854 ± 0.000011 (n = 4), relative to the values of $^{87}Sr/^{86}Sr$ = 0.710248 and $^{143}Nd/^{144}Nd$ = 0.511858 (Weis et al., 2006). Nd isotope ratios measured on the Nu Plasma multiple collector inductively coupled plasma mass-spectrometer (MC-ICP-MS) were run under dry plasma conditions using a membrane desolvator (DSN) for sample introduction. The Rennes standard was run between every two samples and normalized on the basis of the average recorded Rennes value ($^{143}Nd/^{144}Nd$ = 0.511980 ± 0.000003, n = 27), relative to a $^{143}Nd/^{144}Nd$ value of 0.511972 (Weis et al., 2006).

Pb and Hf isotope ratios were measured on a Nu Plasma (MC-ICP-MS) under dry plasma conditions using a membrane desolvator (DSN) for sample introduction following the analytical procedures described by Weis et al. (2006, 2007). The configuration for Pb analyses allows for the collection of Pb and Tl together; Tl is used to monitor instrumental mass discrimination. The NBS981 standard (absolute average: $^{208}Pb/^{204}Pb$ = 36.0834 ± 0.0014, $^{207}Pb/^{204}Pb$ = 15.2363 ± 0.0005, $^{206}Pb/^{204}Pb$ = 16.6555 ± 0.0005, n = 58) was run between every two samples and the results were normalized to $^{208}Pb/^{204}Pb$ = 36.7219, $^{207}Pb/^{204}Pb$ = 15.4963, and $^{206}Pb/^{204}Pb$ = 16.9405 (Galer and Abouchami, 1998). Fractionation-corrected samples were further corrected

42

using the sample standard bracketing method. Hf isotopic ratios were analyzed on the Nu Plasma

MC-ICP-MS by similar methods to that of Pb isotopes, however mass fractionation for Hf was

internally monitored and corrected with the naturally existing ratio $^{179}Hf/^{177}Hf = 0.7325$ (Patchett

and Tatsumoto, 1984). Standard ULB-JMC 475 was run every two samples and results were

normalized on the basis of the average ULB-JMC 475 $^{176}Hf/^{177}Hf = 0.282170 \pm 0.000003$ (n =

37) relative to $^{176}Hf/^{177}Hf$ ratio of 0.28216 (Weis et al., 2007).

2.5 RESULTS

2.5.1 Major element oxides and trace element concentrations

The major and trace element contents of the Natkusiak basalts are reported in Table 2.2.

The Natkusiak basalts (6.2-10.9 wt.% MgO, 44.8-50.8 wt.% SiO_2) are characterized as tholeiitic

to transitional basalts on a total alkalis versus silica diagram after Le Bas et al. (1986) (Fig. 2.5).

Most compositions plot within the tholeiitic field; however, a group of samples lie along the

tholeiitic-alkalic divide and five samples have distinctly higher total-alkalis and LOI due to

element mobilization during alteration (Table 2.3). The Natkusiak basalts can be subdivided into

three distinct stratigraphic units (*basal*, *cycle 1*, and *cycle 2 basalts)*. These three stratigraphic

units correspond to two geochemical groups based on TiO_2 content (*low-Ti and high-Ti basalts*).

The basal basalts correspond to the low-Ti group and the overlying cycle 1 and 2 basalts

correspond to the high-Ti group.TiO_2 contents are lower and more restricted in the basal (low-Ti)

basalts (1.00-1.18 wt. % TiO_2), whereas the cycle 1 and 2 (high-Ti) basalts (1.24-1.83 wt. %

TiO_2) contain higher, and more variable values of TiO_2 (Fig. 2.6). Al_2O_3 contents range from

Table 2.2: Major element oxides (wt. %) and trace element concentrations (ppm) in whole rock samples of the Natkusiak basalts

Sample	10RATTD15A2	10RATTD16A1	10RATTD16A3	10RATTD17B1	10RATTD17B2	10RATTD18A1
Rock type	Basalt	Basalt	Basalt	Basalt	Basalt	Basalt
Location	Central Section	Central Section	Central Section	Central Section	Central Section	Central Section
Unit	Basal	Basal	Basal	Cycle 1	Cycle 1	Basal
Group	low-Ti	low-Ti	low-Ti	high-Ti	high-Ti	low-Ti
Lat.	71.13792441	71.13776941	71.13776941	71.13775274	71.13775274	71.13782774
Long.	-115.0271136	-115.0331752	-115.0331752	-115.0342936	-115.0342936	-115.0320269
Major elements (wt.%)						
SiO_2	46.67	38.58	47.45	48.26	48.61	43.98
TiO_2	1.00	0.95	1.08	1.39	1.40	0.98
Al_2O_3	14.05	14.24	14.24	14.16	14.21	13.53
Fe_2O_3	10.58	8.57	11.25	13.47	13.57	11.05
MnO	0.17	0.17	0.15	0.21	0.22	0.18
MgO	7.93	5.76	7.71	7.20	7.34	6.77
CaO	13.00	14.67	5.97	11.57	11.36	8.46
Na_2O	1.42	1.41	2.03	2.00	2.02	1.91
K_2O	0.32	2.67	3.41	0.15	0.15	3.77
P_2O_5	0.06	0.06	0.07	0.09	0.09	0.06
Total	100.20	99.80	100.20	100.20	100.40	100.00
LOI	4.80	13.70	6.70	1.50	1.30	9.10
Mg#	0.59	0.61	0.57	0.51	0.51	0.54
Trace elements (ppm)						
Cs	0.279	1.77	0.849	0.055	0.047	0.756
Rb	5.0	27.7	21.7	0.64	0.73	25.4
Ba	64.4	183	202	54.3	56.3	207
Th	1.01	0.99	1.12	0.79	0.82	1.00
U	0.254	0.255	0.277	0.192	0.192	0.247
Cr	427	381	299	174	176	287
Ni	139	111	113	115	117	107
Sc	41	39	42	39	38	39
Nb	4.98	4.80	5.64	3.96	3.98	4.95
Ta	0.30	0.29	0.35	0.24	0.25	0.30
La	5.69	5.90	6.12	5.62	5.54	6.06
Ce	14.5	14.6	15.5	15.3	15.2	14.9
Pb	1.06	2.73	2.48	1.20	1.21	2.78
Pr	1.86	1.94	2.01	2.14	2.14	1.91
Nd	8.57	8.95	9.11	10.4	10.6	8.76
Sr	123	147	106	149	151	125
Sm	2.43	2.57	2.57	3.19	3.22	2.41
Zr	54.9	53.4	62.6	75.6	76.4	54.5
Hf	1.55	1.46	1.72	2.18	2.21	1.51
Eu	0.81	0.88	0.87	1.11	1.11	0.84
Gd	2.90	3.03	3.03	3.90	3.94	2.85
Tb	0.510	0.497	0.519	0.686	0.681	0.497
Dy	3.15	3.25	3.30	4.27	4.09	3.11
Ho	0.664	0.691	0.685	0.829	0.865	0.661
Y	19.7	20.3	20.7	25.3	25.7	19.0
Er	1.88	1.84	1.95	2.31	2.35	1.84
Yb	1.74	1.77	1.84	2.20	2.22	1.65
Lu	0.260	0.254	0.265	0.299	0.318	0.233

Mg# = (MgO/40.311) / [(MgO/40.311) + (FeO/70.846)]. Major element oxide abundances of 10RAT- and 08JB- samples were determined at INRS-ETE laboratories in Quebec City by inductively coupled plasma – atomic emission spectrometry (ICP–AES) and calibrated against USGS reference materials BCR-2 and BHVO-2. Major element oxide abundances of 11RAT- and BL- samples were determined at Carleton University by fused-disc X-ray fluorescence spectrometry (XRF), and calibrated using BCR-2 reference material. All trace element abundances were determined by ICP-MS at the PCIGR. Fe_2O_3 is total Fe. The average values of reference materials BCR-2 and BHVO-2 (major elements INRS labs, trace elements PCIGR) are included in the table. Published values of BCR-2 and BHVO-2 are from Raczek et al. (2001).

Table 2.2 continued

Sample	10RATTD18A2	10RATTD19A1	Rep-19A1	Dup-19A1	10RATTD20A1	10RATTD21A1
Rock type	Basalt	Basalt			Basalt	Basalt
Location	Central Section	Central Section			Central Section	Central Section
Unit	Basal	Cycle 1			Cycle 1	Cycle 1
Group	low-Ti	high-Ti			high-Ti	high-Ti
Lat.	71.13782774	71.13899775			71.13867441	71.13793941
Long.	-115.0320269	-115.0515069			-115.0469019	-115.0391436

Major elements (wt.%)

SiO_2	45.53	48.25			48.17	48.49
TiO_2	1.05	1.35			1.38	1.35
Al_2O_3	14.77	14.15			13.99	14.12
Fe_2O_3	11.40	13.53			13.38	13.02
MnO	0.11	0.19			0.20	0.17
MgO	8.85	7.06			7.00	7.00
CaO	6.02	11.77			11.48	11.47
Na_2O	2.95	1.87			1.96	1.79
K_2O	1.00	0.11			0.27	0.13
P_2O_5	0.06	0.09			0.09	0.09
Total	100.10	100.80			100.40	101.10
LOI	8.20	2.30			2.40	3.30
Mg#	0.60	0.50			0.51	0.51

Trace elements (ppm)

Cs	0.451	0.416	0.410	0.148	0.084	0.067
Rb	12.3	1.53	1.50	0.934	4.8	2.23
Ba	111	40.8	41.9	38.6	58.1	25.0
Th	1.09	0.775	0.80	0.73	0.808	0.788
U	0.298	0.187	0.192	0.188	0.192	0.195
Cr	370	179	197	195	173	178
Ni	126	124	120	116	127	121
Sc	41	38	38	30	38	38
Nb	5.40	3.83	3.87	3.83	3.96	3.89
Ta	0.33	0.24	0.24	0.25	0.24	0.24
La	6.25	5.47	5.50	5.44	5.55	5.25
Ce	15.7	15.0	15.0	14.8	15.2	14.7
Pb	2.71	0.80	0.84	0.80	1.23	1.41
Pr	1.92	2.09	2.11	2.10	2.12	2.03
Nd	8.89	10.1	10.3	10.0	10.4	10.3
Sr	123	151	149	139	137	135
Sm	2.35	3.12	3.10	3.02	3.20	3.10
Zr	57.8	74.2	73.6	73.7	75.9	73.9
Hf	1.66	2.11	1.84	2.14	2.13	2.07
Eu	0.82	1.06	1.14	1.11	1.09	1.09
Gd	2.61	3.86	3.89	3.68	3.74	3.94
Tb	0.473	0.670	0.659	0.673	0.684	0.670
Dy	2.87	4.12	3.91	4.18	4.12	4.24
Ho	0.562	0.854	0.781	0.808	0.810	0.844
Y	17.1	24.5	24.7	23.6	25.1	25.3
Er	1.62	2.38	2.37	2.26	2.31	2.33
Yb	1.52	2.18	2.14	2.04	2.10	2.19
Lu	0.237	0.311	0.271	0.299	0.309	0.301

Table 2.2 continued

Sample	10RATTD55A1	10RATTD55A3	Rep-55A3	Dup-55A3	10RATTD55A4	10RATTD55A5
Rock type	Basalt	Basalt			Basalt	Basalt
Location	Central Section	Central Section			Central Section	Central Section
Unit	Basal	Basal			Basal	Basal
Group	low-Ti	low-Ti			low-Ti	low-Ti
Lat.	71.06605777	71.06605777			71.06605777	71.06605777
Long.	-115.2098336	-115.2098336			-115.2098336	-115.2098336

Major elements (wt.%)

SiO_2	46.59	47.22			47.84	47.35
TiO_2	0.97	0.99			1.13	0.98
Al_2O_3	14.49	14.39			14.35	14.11
Fe_2O_3	10.99	11.61			10.83	11.07
MnO	0.22	0.19			0.16	0.22
MgO	9.20	8.22			7.72	7.93
CaO	9.74	12.18			11.62	7.04
Na_2O	1.22	1.37			1.54	0.80
K_2O	0.89	0.24			0.56	6.24
P_2O_5	0.06	0.06			0.08	0.06
Total	100.30	100.80			100.20	100.30
LOI	5.70	4.10			4.20	4.30
Mg#	0.62	0.58			0.58	0.58

Trace elements (ppm)

Cs	0.428	0.124	0.124	0.045	0.202	0.739
Rb	12.5	2.82	2.72	1.03	8.82	45.6
Ba	66.4	45.4	45.4	38.6	101	180
Th	1.07	1.01	1.01	0.477	1.45	1.00
U	0.274	0.245	0.236	0.251	0.359	0.247
Cr	372	392	443	416	301	416
Ni	138	123	123	123	110	134
Sc	39	40	40	20	45	40
Nb	5.07	4.96	4.83	5.04	7.09	4.88
Ta	0.32	0.30	0.29	0.30	0.43	0.30
La	5.46	5.73	5.54	4.94	7.57	5.47
Ce	13.8	13.9	13.31	12.43	19.0	13.3
Pb	1.32	1.17	1.15	1.25	1.73	1.40
Pr	1.73	1.84	1.85	1.62	2.46	1.83
Nd	8.44	8.50	8.28	7.74	11.5	8.18
Sr	121	124	124	91	143	1046
Sm	2.34	2.34	2.30	2.16	3.17	2.32
Zr	54.9	54.8	56.4	31.3	76.2	55.8
Hf	1.51	1.55	1.64	0.790	2.15	1.42
Eu	0.80	0.80	0.84	0.76	1.07	0.81
Gd	2.71	2.78	2.84	2.37	3.75	2.82
Tb	0.496	0.471	0.509	0.426	0.645	0.492
Dy	2.93	3.11	3.14	2.91	4.10	3.10
Ho	0.630	0.580	0.637	0.540	0.808	0.676
Y	18.3	17.3	16.8	13.3	23.3	16.9
Er	1.68	1.86	1.74	1.64	2.52	1.82
Yb	1.71	1.67	1.62	1.52	2.20	1.66
Lu	0.240	0.242	0.252	0.226	0.342	0.265

Table 2.2 continued

Sample	10RATTD55A6	Dup-55A6	10RATTD55A7	10RATTD56A1	10RATTD57A1	10RATTD60B1
Rock type	Basalt		Basalt	Basalt	Basalt	Basalt
Location	Central Section		Central Section	Central Section	Central Section	Central Section
Unit	Basal		Basal	Basal	Basal	Cycle 1
Group	low-Ti		low-Ti	low-Ti	low-Ti	high-Ti
Lat.	71.06605777		71.06605777	71.06415277	71.06492777	71.06984444
Long.	-115.2098336		-115.2098336	-115.2090803	-115.2099469	-115.2104719

Major elements (wt.%)

SiO_2	48.50		46.05	45.99	47.04	49.44
TiO_2	0.97		1.03	1.02	0.97	1.43
Al_2O_3	14.73		15.05	14.51	14.60	14.57
Fe_2O_3	11.49		10.78	11.20	11.08	13.97
MnO	0.17		0.21	0.13	0.14	0.28
MgO	8.02		9.54	10.27	8.90	7.87
CaO	7.25		9.83	8.81	11.07	10.38
Na_2O	3.23		1.53	1.44	1.31	2.32
K_2O	2.00		1.03	0.74	0.83	0.85
P_2O_5	0.07		0.07	0.06	0.06	0.10
Total	100.40		102.60	100.50	101.20	102.90
LOI	3.80		7.30	6.00	5.00	1.60
Mg#	0.58		0.63	0.64	0.61	0.52

Trace elements (ppm)

Cs	0.297	0.037	0.492	0.302	0.418	0.048
Rb	34.2	6.94	14.0	11.6	13.5	11.8
Ba	337	280	61.3	73.6	96.1	71.8
Th	0.992	0.569	1.19	1.06	0.933	0.773
U	0.222	0.224	0.303	0.296	0.220	0.174
Cr	386	409	362	326	379	176
Ni	141	147	128	108	144	121
Sc	38	11	42	39	38	37
Nb	4.85	5.066	5.55	5.05	4.47	3.80
Ta	0.29	0.31	0.35	0.31	0.27	0.24
La	5.41	4.85	6.76	5.56	4.84	5.33
Ce	13.1	12.1	15.7	14.2	11.9	14.2
Pb	0.95	0.93	1.07	1.17	1.51	2.24
Pr	1.74	1.59	1.96	1.81	1.67	1.96
Nd	8.13	7.63	9.11	8.43	7.31	9.97
Sr	303	200	114	111	122	141
Sm	2.28	2.09	2.47	2.36	2.06	3.00
Zr	54.3	53.3	60.3	54.9	50.9	73.0
Hf	1.63	1.57	1.70	1.62	1.47	2.02
Eu	0.83	0.75	0.86	0.76	0.70	1.05
Gd	2.75	2.37	2.83	2.80	2.58	3.60
Tb	0.475	0.403	0.511	0.484	0.461	0.618
Dy	2.88	2.57	3.13	2.99	2.75	3.94
Ho	0.591	0.521	0.633	0.618	0.578	0.741
Y	16.9	13.5	19.1	18.5	15.0	21.9
Er	1.77	1.56	1.84	1.75	1.59	2.34
Yb	1.66	1.42	1.84	1.72	1.56	1.95
Lu	0.254	0.199	0.255	0.257	0.237	0.304

Table 2.2 continued

Sample	10RATTD60B3	10RATTD60B4	10RATTD60B5	10RATTD61A1	10RATTD61A2	11RATTD43B1
Rock type	Basalt	Basalt	Basalt	Basalt	Basalt	Basalt
Location	Central Section	Central Section	Central Section	Central Section	Central Section	Eastern section
Unit	Cycle 1	Cycle 1	Cycle 1	Cycle 1	Cycle 1	Cycle 1
Group	high-Ti	high-Ti	high-Ti	high-Ti	high-Ti	high-Ti
Lat.	71.06984444	71.06984444	71.06984444	71.06597443	71.06597443	71.40511914
Long.	-115.2104719	-115.2104719	-115.2104719	-115.1873636	-115.1873636	-113.2906738

Major elements (wt.%)

SiO_2	48.12	49.27	48.47	48.35	47.79	48.17
TiO_2	1.37	1.34	1.26	1.80	1.67	1.29
Al_2O_3	14.11	13.93	14.44	14.10	14.39	13.97
Fe_2O_3	13.20	13.39	12.87	14.56	13.39	13.21
MnO	0.18	0.22	0.20	0.22	0.28	0.20
MgO	7.71	7.65	7.65	6.73	6.54	7.48
CaO	9.63	7.80	11.84	10.38	10.93	8.66
Na_2O	2.40	3.61	1.92	2.45	2.01	3.25
K_2O	0.66	0.73	0.19	0.40	0.16	0.42
P_2O_5	0.09	0.08	0.09	0.12	0.11	0.10
Total	100.50	101.20	100.30	100.90	100.10	96.88
LOI	2.90	3.00	1.20	1.60	2.60	3.10
Mg#	0.53	0.53	0.54	0.47	0.49	0.53

Trace elements (ppm)

Cs	0.166	0.430	0.032	0.188	0.030	0.128
Rb	8.9	15.4	2.6	8.1	2.3	3.3
Ba	44.9	136	40.8	61.4	44.2	52.6
Th	0.775	0.756	0.856	0.711	0.948	0.825
U	0.181	0.186	0.194	0.186	0.246	0.180
Cr	175	193	173	138	232	159
Ni	114	121	111	85	100	107
Sc	37	39	39	39	35	35
Nb	3.82	3.83	3.98	4.88	5.09	3.87
Ta	0.25	0.24	0.24	0.30	0.31	0.24
La	5.34	5.18	5.33	7.09	6.18	5.38
Ce	14.1	13.9	14.2	17.0	17.0	14.5
Pb	1.29	1.87	1.01	2.41	5.05	1.44
Pr	2.02	1.94	2.00	2.48	2.48	1.98
Nd	9.97	10.1	9.75	12.4	12.3	9.75
Sr	144	332	145	147	158	151
Sm	3.01	3.08	2.94	3.80	3.76	2.95
Zr	73.4	74.0	73.9	97.0	97.6	72.0
Hf	2.02	2.14	2.08	2.81	2.76	2.32
Eu	1.02	1.08	1.01	1.31	1.26	1.01
Gd	3.71	3.75	3.57	4.81	4.51	3.66
Tb	0.649	0.615	0.647	0.834	0.749	0.641
Dy	4.01	4.12	3.84	4.88	4.66	4.02
Ho	0.769	0.753	0.791	1.01	0.954	0.848
Y	22.3	22.9	21.8	27.6	26.0	23.0
Er	2.29	2.25	2.23	2.87	2.62	2.29
Yb	2.07	2.20	2.05	2.50	2.25	2.19
Lu	0.293	0.323	0.285	0.353	0.332	0.301

Table 2.2 continued

Sample	Rep-43B1	11RATTD43C1	11RATTD72B1	11RATTD72C1	11RATTD72D1	11RATTD72E1
Rock type	Basalt	Basalt	Basalt	Basalt	Basalt	Basalt
Location	Eastern section	Eastern section	Eastern section	Eastern section	Eastern section	Eastern section
Unit		Cycle 1	Cycle 1	Cycle 1	Cycle 1	Cycle 1
Group		high-Ti	high-Ti	high-Ti	high-Ti	high-Ti
Lat.		71.40511914	71.39530413	71.39530413	71.39530413	71.39530413
Long.		-113.2906738	-113.2536238	-113.2536238	-113.2536238	-113.2536238

Major elements (wt.%)

SiO_2		48.42	48.42	48.35	49.28	47.39
TiO_2		1.26	1.26	1.29	1.56	1.50
Al_2O_3		13.83	13.96	14.04	13.36	13.32
Fe_2O_3		12.68	12.73	13.07	13.77	13.67
MnO		0.21	0.19	0.20	0.22	0.19
MgO		7.84	7.56	7.61	6.65	6.10
CaO		9.15	9.48	8.64	9.30	8.90
Na_2O		3.17	3.13	3.34	2.70	3.87
K_2O		0.55	0.57	0.42	0.58	0.06
P_2O_5		0.10	0.10	0.11	0.13	0.12
Total		97.32	97.53	97.20	97.66	95.22
LOI		2.60	2.50	2.60	1.90	4.30
Mg#		0.55	0.54	0.53	0.49	0.47

Trace elements (ppm)

Cs	0.123	0.224	0.400	0.528	0.208	0.022
Rb	3.3	8.0	10.3	8.0	12.9	1.1
Ba	52.8	78.4	86.1	139	92.2	11.0
Th	0.869	0.843	0.836	0.857	1.13	1.00
U	0.180	0.190	0.190	0.199	0.258	0.239
Cr	167	162	172	165	140	146
Ni	107	114	112	109	99	99
Sc	35	36	38			35
Nb	3.85	3.87	3.80	4.11	5.70	5.20
Ta	0.24	0.24	0.23	0.25	0.33	0.36
La	5.33	5.35	5.39	5.82	7.71	6.81
Ce	14.3	14.2	14.2	14.1	18.5	17.9
Pb	1.49	1.70	1.93	1.98	1.98	2.32
Pr	1.99	2.05	1.95	2.06	2.67	2.51
Nd	9.97	9.55	9.60	10.1	12.9	11.6
Sr	140	272	322	319	178	41
Sm	2.95	2.89	2.83	3.02	3.75	3.45
Zr	70.4	72.9	70.7	76.2	96.4	86.7
Hf	2.00	2.14	2.10	2.09	2.60	2.61
Eu	0.99	1.04	1.01	1.09	1.31	1.15
Gd	3.74	3.78	3.82	3.80	4.54	4.51
Tb	0.611	0.628	0.659	0.636	0.759	0.758
Dy	3.81	4.02	3.98	3.99	4.76	4.81
Ho	0.804	0.779	0.794	0.813	0.953	0.932
Y	23.2	22.5	22.2	22.9	27.3	26.4
Er	2.22	2.25	2.42	2.30	2.74	2.80
Yb	1.96	2.05	2.23	2.05	2.48	2.56
Lu	0.308	0.299	0.313	0.309	0.359	0.378

Table 2.2 continued

Sample	11RATTD72F1	11RATTD72G1	11RATTD73A1	Rep-73A1	11RATTD129A1	Rep-129A1
Rock type	Basalt	Basalt	Basalt	Basalt	Basalt	Basalt
Location	Eastern section	Eastern section	Eastern section	Eastern section	Western section	Western section
Unit	Cycle 1	Cycle 1	Cycle 1		Cycle 1	
Group	high-Ti	high-Ti	high-Ti		high-Ti	
Lat.	71.39530413	71.39530413	71.3939008		70.97802124	
Long.	-113.2536238	-113.2536238	-113.2478472		-116.0516218	

Major elements (wt.%)

SiO_2	48.15	49.30	48.41		48.38	
TiO_2	1.29	1.42	1.52		1.47	
Al_2O_3	13.95	13.78	13.49		14.90	
Fe_2O_3	12.41	13.61	14.08		12.82	
MnO	0.21	0.23	0.21		0.19	
MgO	7.93	6.70	6.82		6.37	
CaO	10.45	11.47	7.89		10.98	
Na_2O	2.62	2.12	3.50		1.99	
K_2O	0.49	0.31	0.84		0.44	
P_2O_5	0.10	0.12	0.13		0.12	
Total	97.75	99.16	97.01		97.77	
LOI	2.20	0.50	3.00		1.80	
Mg#	0.56	0.49	0.49		0.49	

Trace elements (ppm)

Cs	0.142	0.092	0.421	0.391	0.166	0.169
Rb	11.7	7.22	21.9	21.9	10.0	10.0
Ba	81.4	56.2	122	121	47.7	48.4
Th	0.761	0.799	1.17	1.07	0.806	0.806
U	0.168	0.189	0.272	0.255	0.205	0.214
Cr	225	130	143	148	121	123
Ni	112	103	100	101	80	78
Sc		34	35	35	30	30
Nb	3.90	4.08	5.26	5.19	4.04	4.04
Ta	0.23	0.25	0.33	0.32	0.27	0.26
La	4.97	5.37	7.08	7.05	5.15	5.12
Ce	12.6	14.8	18.3	18.4	14.7	14.5
Pb	2.03	1.75	2.66	2.52	1.31	1.38
Pr	1.90	2.14	2.58	2.50	2.08	2.06
Nd	9.53	10.3	13.2	12.1	11.0	10.9
Sr	162	130	203	201	143	138
Sm	2.95	3.20	3.83	3.53	3.39	3.33
Zr	76.1	80.7	88.3	87.7	84.0	82.2
Hf	2.13	2.29	2.66	2.56	2.44	2.28
Eu	1.07	1.10	1.18	1.19	1.16	1.12
Gd	3.79	4.44	4.77	4.47	4.28	3.99
Tb	0.640	0.699	0.772	0.713	0.706	0.658
Dy	4.04	4.63	4.92	4.54	4.37	4.01
Ho	0.815	0.891	0.931	0.934	0.868	0.851
Y	22.9	25.5	26.8	26.6	24.3	24.7
Er	2.33	2.67	2.91	2.81	2.66	2.24
Yb	2.13	2.50	2.56	2.47	2.26	1.96
Lu	0.306	0.329	0.370	0.377	0.302	0.294

Table 2.2 continued

Sample	11RATTD129B1	11RATTD129C1	11RATTD129D1	11RATTD129E1	11RATTD129F1	11RATTD129G1
Rock type	Basalt	Basalt	Basalt	Basalt	Basalt	Basalt
Location	Western section	Western section	Western section	Western section	Western section	Western section
Unit	Cycle 1	Cycle 1	Cycle 1	Cycle 1	Cycle 1	Cycle 1
Group	high-Ti	high-Ti	high-Ti	high-Ti	high-Ti	high-Ti
Lat.	70.97802124	70.97802124	70.97802124	70.97802124	70.97802124	70.97802124
Long.	-116.0516218	-116.0516218	-116.0516218	-116.0516218	-116.0516218	-116.0516218

Major elements (wt.%)

SiO_2	48.74	47.58	47.33	48.55	48.66	48.14
TiO_2	1.61	1.30	1.32	1.27	1.21	1.29
Al_2O_3	14.41	13.73	13.72	13.97	13.68	14.12
Fe_2O_3	13.99	13.12	13.44	12.82	12.87	12.47
MnO	0.21	0.19	0.18	0.18	0.21	0.24
MgO	6.13	7.21	7.69	7.71	7.57	7.50
CaO	10.91	9.85	8.92	11.19	10.85	11.71
Na_2O	2.01	3.25	3.26	1.80	1.67	1.83
K_2O	0.27	0.15	0.18	0.44	0.25	0.30
P_2O_5	0.13	0.10	0.11	0.10	0.10	0.10
Total	98.53	96.59	96.27	98.14	97.17	97.82
LOI	0.80	3.20	3.80	1.40	4.20	2.20
Mg#	0.46	0.52	0.53	0.54	0.53	0.54

Trace elements (ppm)

Cs	0.196	0.439	0.309	0.095	0.168	0.098
Rb	7.4	1.3	2.5	7.9	5.5	4.8
Ba	45.4	21.8	29.5	59.3	52.5	53.2
Th	0.859	0.702	0.716	0.818	0.804	0.821
U	0.224	0.172	0.170	0.193	0.186	0.198
Cr	115	176	190	158	161	158
Ni	81	124	111	108	113	109
Sc		33	35	35		34
Nb	4.57	3.48	3.48	3.89	3.88	3.80
Ta	0.27	0.22	0.22	0.23	0.22	0.23
La	5.89	5.05	4.67	5.54	4.97	4.78
Ce	15.2	13.4	12.9	14.4	12.6	13.4
Pb	1.51	1.42	1.40	1.72	1.10	1.23
Pr	2.35	1.86	1.87	2.04	1.89	1.92
Nd	12.0	9.34	9.27	9.63	9.31	9.51
Sr	158	189	181	137	135	133
Sm	3.69	2.85	2.87	2.95	2.79	2.85
Zr	96.5	67.2	69.4	70.3	71.6	70.3
Hf	2.63	1.88	1.99	2.13	1.96	2.05
Eu	1.33	0.96	0.96	1.03	1.02	0.95
Gd	4.57	3.71	3.65	3.61	3.54	3.82
Tb	0.753	0.583	0.631	0.625	0.590	0.632
Dy	4.67	3.69	3.79	3.63	3.69	3.89
Ho	0.925	0.765	0.785	0.784	0.751	0.791
Y	26.3	22.5	22.6	23.2	21.4	22.6
Er	2.61	2.20	2.24	2.17	2.12	2.16
Yb	2.28	1.98	2.05	1.95	1.96	2.08
Lu	0.326	0.315	0.295	0.282	0.285	0.306

Table 2.2 continued

Sample	08JB-01	08JB-02	08JB-03	08JB-04C1	08JB-06	BL75 136
Rock type	Basalt	Basalt	Basalt	Basalt	Basalt	Basalt
Location	Northern section	Northern section	Northern section	Northern section	Northern section	Northern section
Unit	Cycle 2	Cycle 2	Cycle 2	Basal	Cycle 1	Cycle 1
Group	high-Ti	high-Ti	high-Ti	high-Ti	high-Ti	high-Ti
Lat.	71.863594	71.869431	71.870078	71.984648	71.984692	71.83611111
Long.	-112.428987	-112.380935	-112.374445	-112.216366	-112.212283	-112.194444

Major elements (wt.%)

SiO_2	48.96	46.85	47.80	48.40	49.31	49.79
TiO_2	1.69	1.79	1.38	1.03	1.26	1.55
Al_2O_3	13.44	13.90	13.79	13.42	14.37	13.87
Fe_2O_3	14.67	14.78	12.88	11.84	12.85	13.91
MnO	0.21	0.21	0.21	0.15	0.20	0.20
MgO	6.63	7.42	6.85	9.66	7.83	6.82
CaO	10.86	10.08	12.10	11.28	11.53	8.19
Na_2O	2.53	2.58	2.63	1.77	2.24	2.81
K_2O	0.17	0.19	0.14	0.19	0.18	1.62
P_2O_5	0.12	0.11	0.10	0.08	0.09	0.10
Total	101.00	100.00	101.00	101.00	101.00	100.74
LOI	1.42	2.37	2.63	2.70	1.20	1.65
Mg#	0.47	0.50	0.51	0.61	0.54	0.49

Trace elements (ppm)

Cs	0.070	1.97	0.734	0.911	0.902	0.312
Rb	2.3	2.5	2.0	1.9	1.9	67.4
Ba	36.3	47.9	46.8	76.8	49.6	635
Th	0.565	0.574	0.641	1.61	0.704	0.959
U	0.160	0.164	0.175	0.335	0.146	0.194
Cr	75	197	210	576	149	133
Ni	86	115	78	157	138	111
Sc	38	40	37	43	42	40
Nb	4.79	4.74	3.99	4.24	3.84	5.03
Ta	0.29	0.29	0.25	0.26	0.23	0.35
La	5.02	5.26	4.47	7.03	4.82	6.95
Ce	14.5	14.4	12.9	17.2	12.8	17.4
Pb	0.99	2.80	1.32	3.06	1.16	1.97
Pr	2.24	2.23	1.96	2.27	1.88	2.40
Nd	12.0	11.6	10.1	10.7	9.63	12.0
Sr	158	170	168	132	134	202
Sm	3.73	3.63	3.16	2.84	2.99	3.39
Zr	89.7	89.3	75.1	68.7	72.2	92.8
Hf	2.63	2.62	2.28	2.04	2.12	2.65
Eu	1.30	1.30	1.09	0.98	1.04	1.17
Gd	4.36	4.18	3.49	3.12	3.59	4.20
Tb	0.753	0.752	0.645	0.557	0.642	0.672
Dy	4.72	4.72	4.10	3.44	3.95	4.47
Ho	0.917	0.838	0.782	0.651	0.806	0.776
Y	26.4	26.0	23.0	19.9	23.4	25.8
Er	2.63	2.48	2.08	1.74	2.20	2.59
Yb	2.21	2.22	1.91	1.75	2.11	2.26
Lu	0.334	0.314	0.276	0.263	0.319	0.342

Table 2.2 continued

Sample	BL75 144	BCR-2	BHVO-2	BCR-2	BHVO-2
Rock type	Basalt	Basalt	Basalt	Published	Published
Location	Northern section				
Unit	Cycle 1				
Group	high-Ti				
Lat.					
Long.					

Major elements (wt.%)

SiO_2	49.38	54.18	49.97	53.74	49.45
TiO_2	1.63	2.26	2.73	2.26	2.73
Al_2O_3	14.13	13.52	13.63	13.28	13.38
Fe_2O_3	14.27	13.72	12.23	13.65	12.23
MnO	0.19	0.19	0.16	0.19	0.17
MgO	6.36	3.59	7.30	3.56	7.23
CaO	10.10	7.26	10.96	7.14	11.45
Na_2O	2.31	3.09	2.15	3.08	2.14
K_2O	0.32	1.80	0.50	1.78	0.51
P_2O_5	0.10	0.36	0.26	0.31	0.22
Total	100.54	100.23	100.11		
LOI	1.61	0.00	0.00		
Mg#	0.47				

Trace elements (ppm)

|					
Cs	0.286	1.10	0.087		
Rb	2.5	46.9	8.9	46.9	9.8
Ba	55.5	677	130	677	130
Th	0.995	5.67	1.18		
U	0.216	1.678	0.430		
Cr	141	16	328	18	329
Ni	86	11	123	18	119
Sc	39		29	33	32
Nb	4.43	12.6	19.4	13	18
Ta	0.31	0.74	1.14	0.74	1.40
La	6.00	24.9	15.4	25	15
Ce	16.1	52.9	38.6	53	38
Pb	2.89	10.9	1.85		
Pr	2.42	6.68	5.29		
Nd	12.7	28.6	25.3	28.7	25
Sr	149	340	393	340	389
Sm	3.83	6.55	6.20	6.6	6.2
Zr	95.5	184	171	184	172
Hf	2.77	4.87	4.29	4.9	4.1
Eu	1.32	1.95	2.04		
Gd	4.91	6.72	6.19	6.75	6.3
Tb	0.769	1.063	0.930	1.07	0.90
Dy	5.15	6.37	5.27		
Ho	0.904	1.27	0.953	1.28	1.04
Y	29.4	37.0	28.3	37	26
Er	2.91	3.65	2.52		
Yb	2.51	3.37	1.94	3.38	2
Lu	0.377	0.502	0.267	0.503	0.280
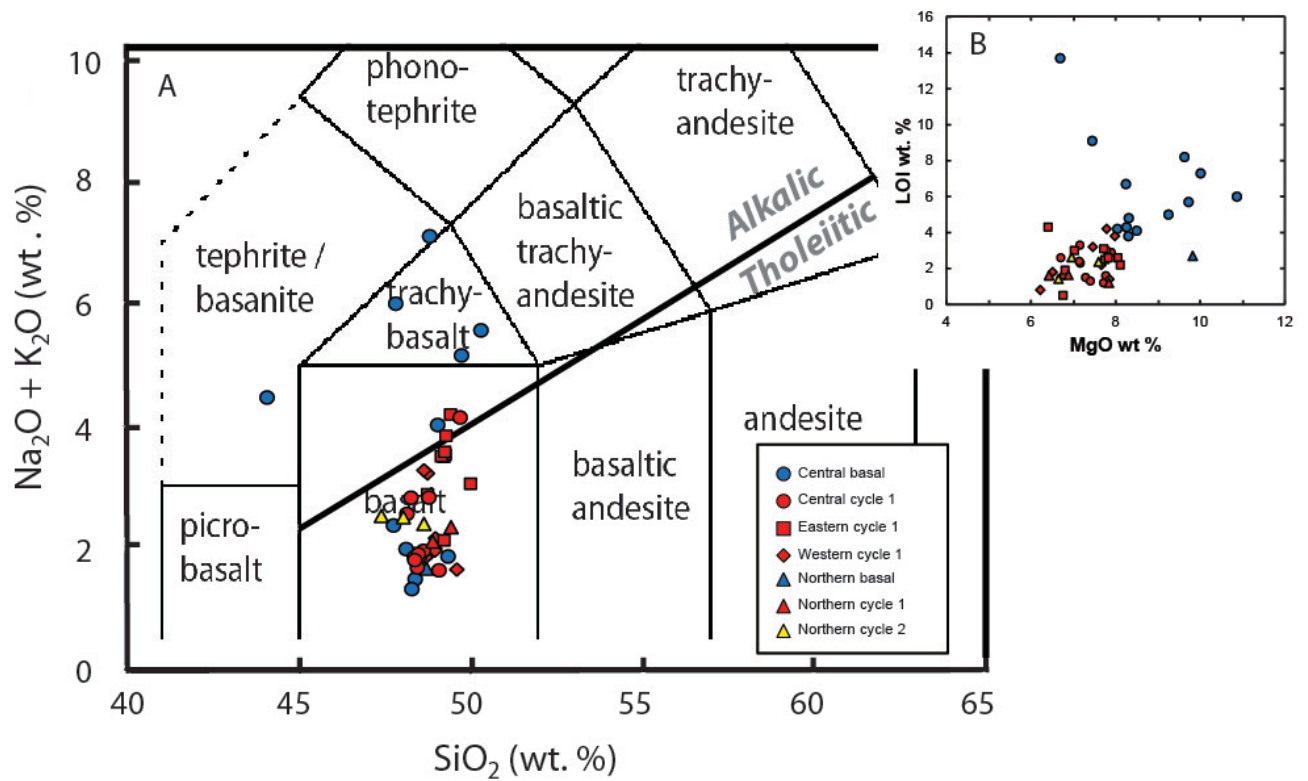
Figure 2.5 Anhydrous-corrected total alkalis versus silica and loss-on-ignition (LOI) diagrams. The Natkusiak basalts range from tholeiitic to transitional basalts. The five samples from the central section that lie in the alkalic field are strongly altered. Total alkalis versus silica (TAS) classification diagram after Le Bas et al. (1986).The tholeiitic-alkalic dividing line is from MacDonald & Katsura (1964).

Table 2.3: Summary of altered basalt samples from the Natkusiak Formation

Sample	*amyg. vol. %	LOI wt.%	Na_2O+K_2O wt.%	*wt.% rem. post-leaching	Sr (ppm)	$^{87}Sr/^{86}Sr_i$
10RAT TD16A1	28	13.7	4.74	30	147	0.707059
10RAT TD16A3	25	6.7	5.82	40	106	0.705080
10RAT TD18A1	25	9.1	6.25	25	125	0.706280
10RAT TD18A2	24	8.2	4.30	36	123	0.706365
10RAT TD55A5	10	4.3	7.33	35	1046	0.707908
10RAT TD55A6	15	3.8	5.41	33	303	0.706482
10RAT TD60B4	15	3.0	4.42	45	332	0.706052
11RAT TD72B	18	2.5	3.80	36	322	0.706606
11RAT TD72C	21	2.6	3.87	51	319	0.706266

* Amygdule volume percent indicated in the second column. Remaining wt. % of sample after HCl-acid-leaching procedure in the fifth column.
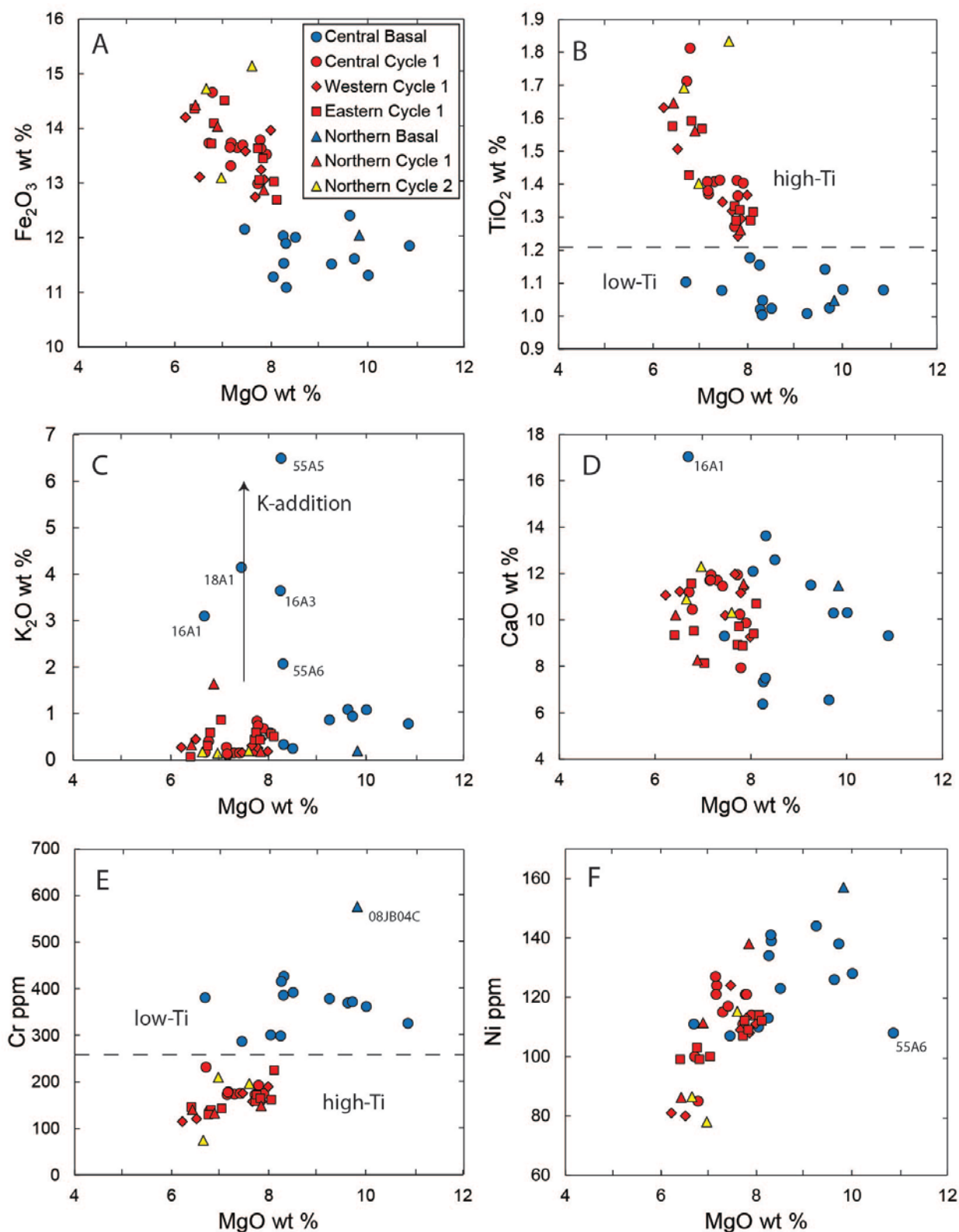
Figure 2.6 MgO variation diagrams of selected anhydrous-corrected major element oxides and compatible trace elements for the Natkusiak basalts. Fe_2O_3 is total Fe measured. The two geochemical groups (low and high-Ti) are indicated with the dashed line.

13.5 wt.% in the high-Ti basalts to 16.1 wt. % in the low-Ti basalts, and CaO contents range from 6.4 to 17.0 wt. % throughout. The basal (low-Ti) basalts are more altered with distinctly higher LOI (Fig. 2.5) and contain higher MgO (6.7-10.9 wt. %) on average than cycle 1 and 2 (high-Ti) basalts (6.2-8.1 wt. %) (Fig. 2.6).

The compatible elements Ni (78-157 ppm), Sc (11-45 ppm), and Cr (75-576 ppm) show large variations and are moderately correlated with MgO content (Fig. 2.6) reflecting the combined effects of olivine and clinopyroxene fractionation (Herzberg & Gazel, 2009; Herzberg, 2011). Ni and Cr concentrations are higher in the low-Ti basalts (107-157 ppm Ni and 287-576 ppm Cr) than in the high-Ti basalts (78-138 ppm Ni and 75-232 ppm Cr). Abundances of incompatible elements are variable throughout the sample suite, and show systematic differences between the two chemical groups. The high-Ti basalts show higher Sm (2.8-3.8 ppm), Hf (1.9-2.8 ppm) and Zr (67-97 ppm) than the low-Ti basalts (2.1-3.1 ppm Sm, 1.4-2.0 ppm Hf, and 51-76 ppm Zr). Highly incompatible elements (e.g., U, Th) are more abundant in the low-Ti basalts than they are in the overlying high-Ti basalts. The high field strength elements (Nb, Ta, Zr, Hf, Ti) form linear trends in binary diagrams and also distinguish the low-Ti basalts from the high-Ti basalts (Fig. 2.7). Plots of Nb vs. Zr, Th vs. La, Nd vs. La, and U vs. La show distinct geochemical groups indicating derivation from different sources. The large ion lithophile elements such as Rb (0.6-67 ppm), Ba (10-634 ppm), and Cs (0.02-1.97 ppm) are highly variable and show evidence of mobilization during alteration throughout the sample suite, especially in the basal unit basalts.

Chondrite-normalized rare earth element (REE) patterns of the Natkusiak basalts (Fig. 2.8) are light REE-enriched with La values up to 7.7 ppm (~32x chondrite) and show a minor negative or no Eu anomaly. The basal (low-Ti) basalts are characterized by steeper slopes ((La/Yb): 3.1-4.1) compared to both (high-Ti) cycle 1 ((La/Yb): 2.3-3.1) and cycle 2 ((La/Yb):
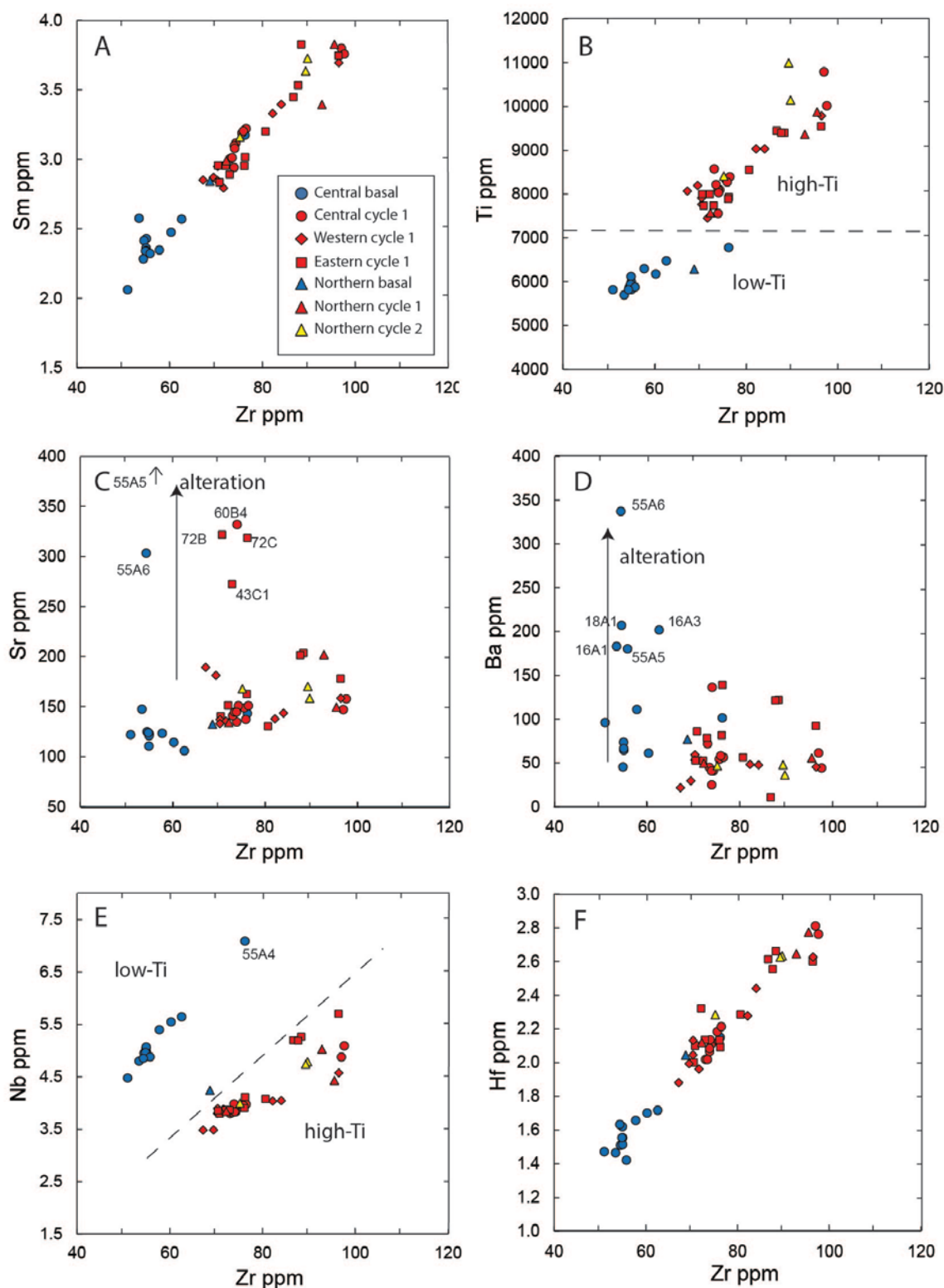
Figure 2.7 Trace element-element binary diagrams (in ppm) for the Natkusiak basalts. High-Ti and low-Ti basalts form distinct groups and correlations in various diagrams. Dashed lines are separate the different types of basalt. Zr and La are least affected by alteration. Samples 10RAT TD55A6, 10RAT TD60B4, 11RAT TD43C, 11RAT TD72B, and 11RAT TD72C have elevated Sr concentrations due to alteration. Alteration trends are indicated with a black arrow.
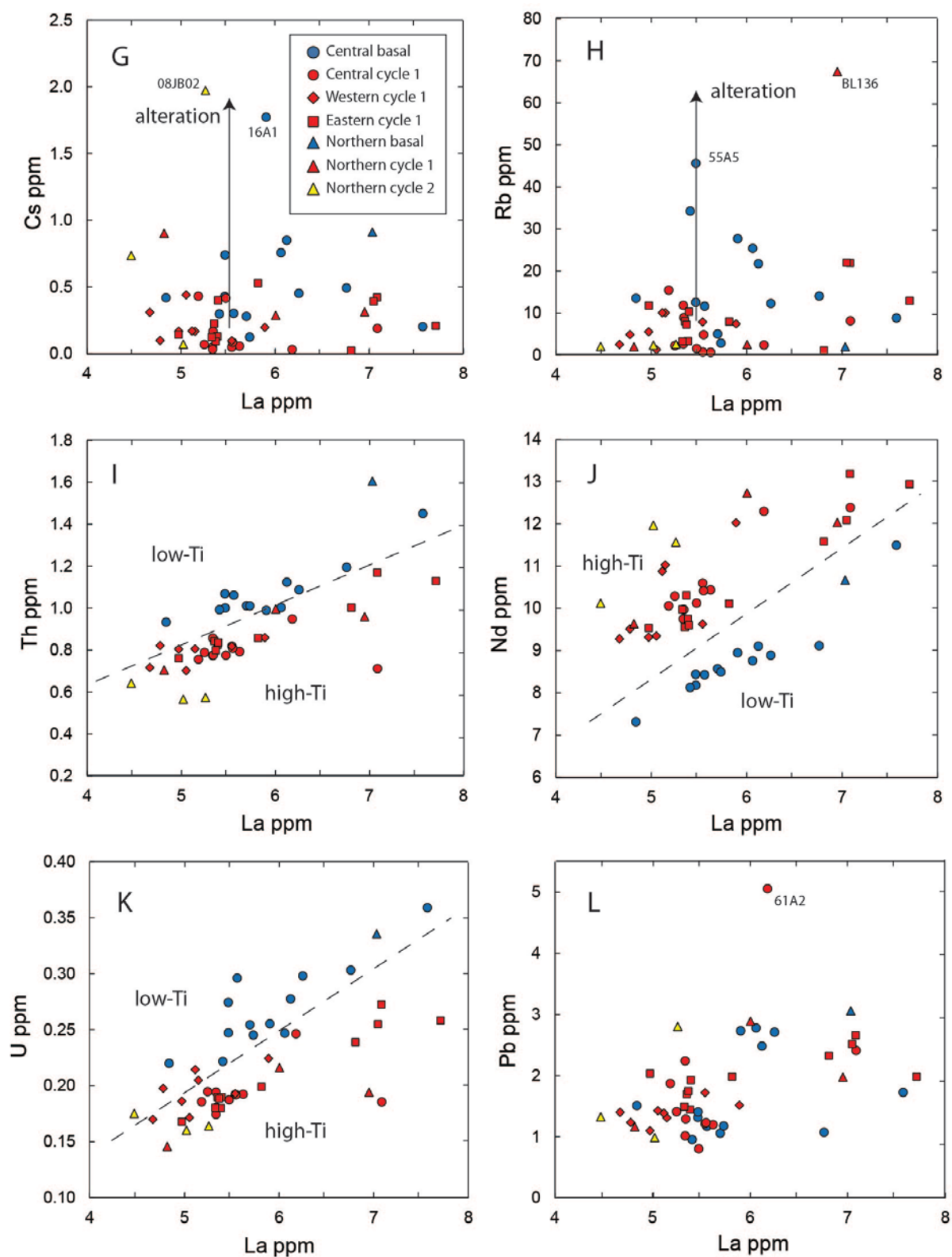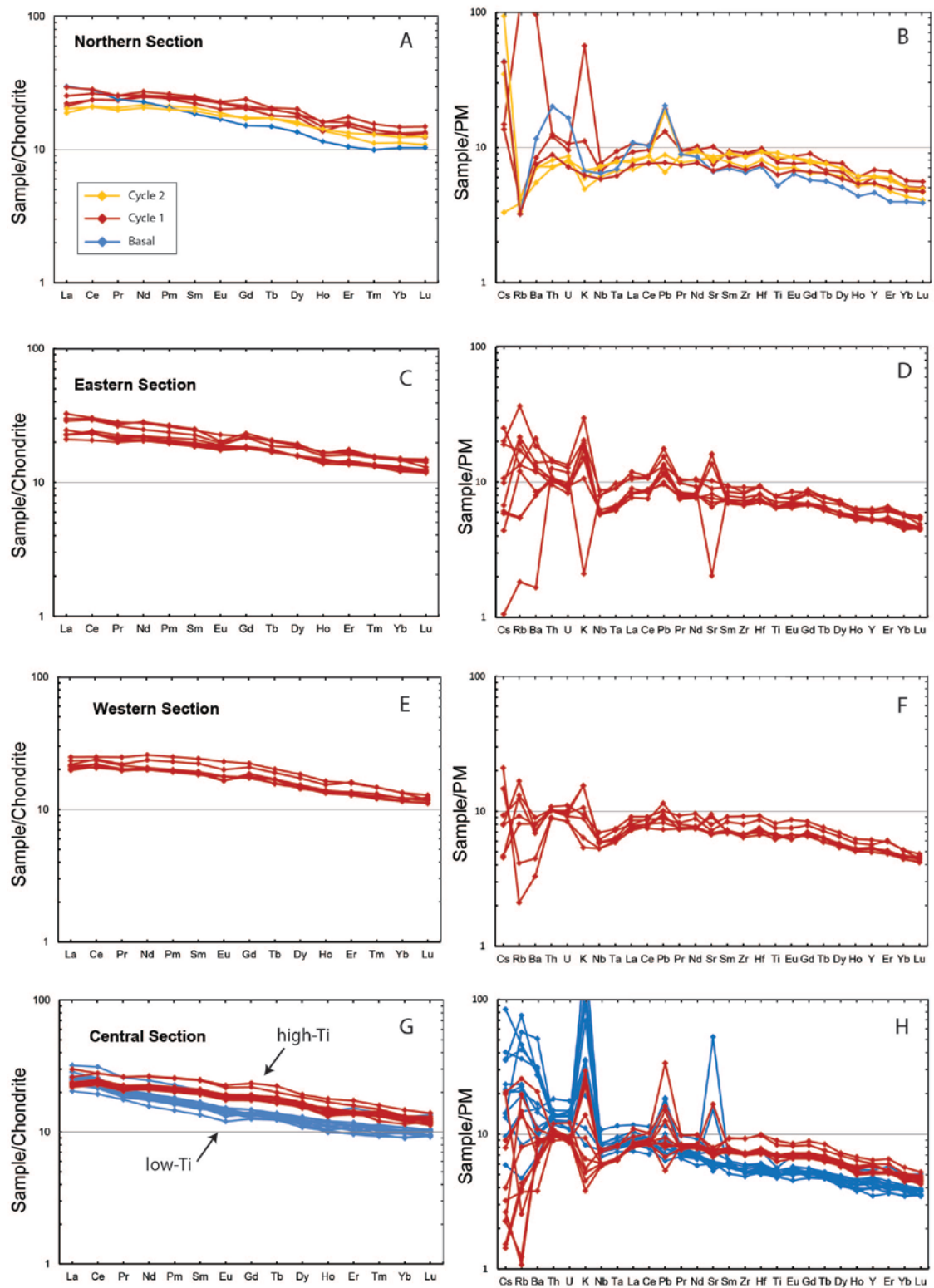
Figure 2.7 (continued)

Figure 2.8 C1 chondrite-normalized rare earth element diagrams and primitive mantle-normalized extended trace element of the Natkusiak basalts. Basal basalts show higher fractionation of LREE to HREE than the cycle 1 or cycle 2 basalts. Cycle 1 basalts show higher overall REE concentrations than the basal basalts in the central section. Cycle 2 basalts in the northern section show lower overall REE concentrations and similar slopes to samples of cycle 1. Normalizing values are from McDonough & Sun (1995).

2.3-2.4) basalts. Total REE concentrations approach the highest values in cycle 1 and show a

marked overall decrease in cycle 2 (Fig. 2.8). The distinctively more fractionated pattern of the

low-Ti basalts compared to the high-Ti basalts is also observed in mantle-normalized extended

trace element diagrams (Fig. 2.8).

2.5.2 Alteration and element mobilization

The Natkusiak basalts were erupted at approximately 723 Ma (Heaman et al., 1992) and

were subsequently buried beneath a thick Paleozoic marine sedimentary cover (MacDonald et

al., 2010). Consequently, seawater interaction and hydrothermal alteration of the Natkusiak

basalts have mobilized some major and trace elements. Chlorite- and calcite-filled amygdules are

present in large volumes (up to 35 vol.%) in the most altered samples (Table 2.3). Prominent Pb,

Sr, Rb, and Ba anomalies are observed in extended trace element diagrams in both high- and

low-Ti basalts (Fig. 2.8), reflecting variable degrees of alteration. Significant variation exists in

the highly mobile alkali and alkaline earth elements (e.g., K, Cs, Rb, and Ba) (Fig. 2.5 and Fig.

2.7) due to their soluble behavior in aqueous solution as illustrated in plots of select mobile

elements vs. immobile trace elements (Zr and La) (Fig. 2.7). Zr and La, normally considered

immobile during alteration, show positive correlations with other relatively immobile elements

(e.g., Zr vs. Sm and Zr vs. Hf). In contrast, mobile trace elements (e.g., Sr, Pb, and Rb) yield

scattered relationships with respect to Zr or La and indicate mobility during alteration. The

extent of mobility and addition of Sr is especially important to this study as many of these

samples were analyzed for Sr isotope ratios. In light of these results, acid leaching was

performed prior to Sr-Nd-Hf-Pb isotope measurements.

2.5.3 Sr-Nd-Hf-Pb Isotopes

The measured and initial (calculated at 723 Ma) isotope ratios are reported in Table 2.4 and plotted in (Fig. 2.9) along with published results from Dupuy et al. (1995) and the Franklin intrusive rocks from Beard (2012). The Natkusiak basalts are characterized by a relatively large range of initial Sr, Nd, and Hf isotopic compositions ($^{87}Sr/^{86}Sr_i$ = 0.70250 -0.70791; ε_{Ndi} = -1.3 to +11.8, $^{143}Nd/^{144}Nd_i$ = 0.51164-0.51231; ε_{Hfi} = +0.3 to +11.1, $^{176}Hf/^{177}Hf_i$ = 0.28231-0.28276), along with a moderate range of initial Pb isotopic compositions ($^{206}Pb/^{204}Pb_i$ = 16.147-18.978; $^{207}Pb/^{204}Pb_i$ = 15.383-15.686; $^{208}Pb/^{204}Pb_i$ = 36.19- 39.14). Basalt samples with initial $^{87}Sr/^{86}Sr_i$ values above 0.705 (Table 2.3) reflect extensive alteration that has not been removed by leaching (e.g., samples contain abundant secondary alterations phases).

The central section of the southern lobe represents the most complete and well-preserved sequence of Natkusiak basalts sampled during this study (Fig. 2.4). The chemostratigraphy of the central section demonstrates an isotopic separation that correlates with the stratigraphic units of the basalts (Fig. 2.10). Chemostratigraphic sections of select major, trace elements, and isotopes show a shift between a height of 40 and 70 m above the Kuujjua sandstone that is most prominently illustrated by TiO_2 contents and Sr-Nd-Hf-Pb isotopes. In the basal unit, the $^{207}Pb/^{204}Pb_i$ and $^{87}Sr/^{86}Sr_i$ ratios are more radiogenic: $^{207}Pb/^{204}Pb_i$ = 15.517-15.686 and $^{87}Sr/^{86}Sr_i$ = 0.70251-0.70661. The isotopic signature shifts to less radiogenic values in the overlying cycle 1 basalts, above the volcaniclastic rocks, to $^{207}Pb/^{204}Pb_i$ = 15.383-15.605 and $^{87}Sr/^{86}Sr_i$ = 0.70333-0.70792. In contrast, ε_{Hfi} and ε_{Ndi} values shift to more radiogenic values up-section: ε_{Hfi} in the basal basalts range from (+0.3 to +6.7) and increases (+4.1 to +9.7) in cycle 1, and ε_{Ndi} increases from (+4.0 to +8.1) in the basal basalts and shift to (+7.7 to +9.6) in cycle 1.The basal basalts (low-Ti) exhibit the widest range of initial Sr and Pb isotope ratios and variation decreases up-section into cycle 1 (high-Ti).

Table 2.4: Measured and initial (calculated to 723 Ma) Sr-Nd-Hf-Pb isotopic ratios of the Natkusiak basalts

Sample	10RATTD15A2	10RATTD16A1	10RATTD16A3	Rep-16A3	10RATTD17B1	10RATTD17B2	10RATTD18A1	10RATTD18A2	10RATTD19A1	Dup-19A1
Measured										
$^{87}Sr/^{86}Sr$	0.705379	0.712673	0.711209		0.703801	0.703846	0.712353	0.709335	0.703846	0.703838
2SE	0.000008	0.000008	0.000008		0.000008	0.000008	0.000008	0.000008	0.000008	0.000007
$^{176}Hf/^{177}Hf$	0.282840	0.282672	0.282648		0.283109	0.283009	0.282696	0.282692	0.282882	0.282785
2SE	0.000008	0.000006	0.000006		0.000005	0.000006	0.000005	0.000007	0.000008	0.000006
$^{143}Nd/^{144}Nd$	0.512941	0.512823	0.512805	0.512805	0.513082	0.513066	0.512732	0.512689	0.513084	0.513094
2SE	0.000008	0.000009	0.000005	0.000008	0.000006	0.000008	0.000007	0.000008	0.000007	0.000008
$^{208}Pb/^{204}Pb$	38.9555	40.0372	38.6970		37.7371	37.8842	38.8769	38.9728	38.7817	38.8047
2SE	0.0146	0.0030	0.0012		0.0043	0.0066	0.0019	0.0010	0.0016	0.0020
$^{207}Pb/^{204}Pb$	15.6669	15.7324	15.6330		15.4580	15.4904	15.6497	15.6674	15.5194	15.5208
2SE	0.0058	0.0011	0.0005		0.0016	0.0025	0.0007	0.0004	0.0010	0.0007
$^{206}Pb/^{204}Pb$	18.7763	19.7116	18.6213		17.3270	17.4061	18.7613	18.9047	18.2078	18.2260
2SE	0.0064	0.0013	0.0006		0.0017	0.0029	0.0008	0.0004	0.0007	0.0008
Initial										
$^{87}Sr/^{86}Sr_i$	0.70416	0.70706	0.70508		0.70367	0.70370	0.70628	0.70636	0.70354	
$^{176}Hf/^{177}Hf_i$	0.28252	0.28234	0.28235				0.28240	0.28242	0.28260	
ε_{Hfi}	6.7	0.3	0.8				2.4	3.1	9.5	
$^{143}Nd/^{144}Nd_i$	0.51212	0.51197	0.51199		0.51220	0.51217	0.51193	0.51191	0.51219	
ε_{Ndi}	8.1	5.2	5.5		9.6	9.2	4.4	4.0	9.4	
$^{208}Pb/^{204}Pb_i$	36.64	39.14	37.61		36.20	36.31	38.00	38.00	36.48	
$^{207}Pb/^{204}Pb_i$	15.550	15.686	15.579		15.383	15.416	15.607	15.614	15.408	
$^{206}Pb/^{204}Pb_i$	16.937	18.979	17.773		16.147	16.239	18.084	18.064	16.448	

All isotopic analyses were carried out at the PCIGR UBC. The 2SE is the absolute error of an individual sample analyses based on counting statistics and applies to the last decimal place. (Dup-) indicates complete chemistry duplicate of the sample. (Rep-) indicates a chemistry replicate of a sample. BL- samples are from Baragar, 1976. SRM897 is a strontium isotope standard, ULB-JMC is a Hf isotope standard, Rennes and LaJolla are Nd isotope standards, and NBS981 is a Pb isotope standard. Standard values shown here are the absolute averages of all runs during data collection. Published values for reference materials BCR-2 and BHVO-2 are from Weis et al. (2005).

Table 2.4 continued

Sample	10RATTD20A1	10RATTD21A1	10RATTD55A1	10RATTD55A3	10RATTD55A4	10RATTD55A5	10RATTD55A6	Dup-55A6	10RATTD55A7	10RATTD56A1
Measured										
^{87}Sr/^{86}Sr	0.704644	0.703984	0.706832	0.705220	0.706079	0.709210	0.709855	0.709790	0.706992	0.707659
2SE	0.000008	0.000009	0.000009	0.000009	0.000009	0.000008	0.000008	0.000009	0.000007	0.000008
^{176}Hf/^{177}Hf	0.282848	0.282725	0.282760	0.282717	0.282737	0.282732	0.282760	0.282769	0.282729	0.282763
2SE	0.000009	0.000018	0.000017	0.000012	0.000007	0.000007	0.000006	0.000005	0.000009	0.000036
^{143}Nd/^{144}Nd	0.513086	0.513004		0.512810	0.512779	0.512888	0.512779	0.512451	0.512788	0.512740
2SE	0.000008	0.000007		0.000006	0.000007	0.000007	0.000006	0.000008	0.000006	0.000009
^{208}Pb/^{204}Pb	38.1422	38.3143	38.7384	38.5582	38.9888	38.7736	39.3151	39.2646	39.7843	38.9796
2SE	0.0017	0.0048	0.0071	0.0024	0.0011	0.0010	0.0025	0.0008	0.0013	0.0080
^{207}Pb/^{204}Pb	15.4794	15.5237	15.6449	15.6170	15.6346	15.6281	15.6471	15.6479	15.6865	15.6827
2SE	0.0007	0.0019	0.0028	0.0009	0.0004	0.0004	0.0010	0.0007	0.0004	0.0031
^{206}Pb/^{204}Pb	17.6362	17.8522	18.5185	18.6131	18.8300	18.6724	18.9822	18.9722	19.3823	18.9696
2SE	0.0007	0.0022	0.0033	0.0008	0.0004	0.0004	0.0014	0.0020	0.0006	0.0034
Initial										
^{87}Sr/^{86}Sr$_i$	0.70360	0.70349	0.70374	0.70454	0.70424	0.70791	0.70648		0.70333	0.70453
^{176}Hf/^{177}Hf$_i$	0.28257	0.28244	0.28245	0.28242	0.28243	0.28237	0.28246		0.28244	0.28246
ε_{Hfi}	8.5	4.1	4.5	3.1	3.6	1.5	4.6		3.9	4.6
^{143}Nd/^{144}Nd$_i$	0.51220	0.51213		0.51202	0.51199	0.51206	0.51197		0.51201	0.51194
ε_{Ndi}	9.6	8.3		6.1	5.5	7.0	5.1		5.9	4.5
^{208}Pb/^{204}Pb$_i$	36.60	36.99	36.79	36.49	36.95	37.06	36.77		37.03	36.77
^{207}Pb/^{204}Pb$_i$	15.406	15.458	15.545	15.517	15.534	15.543	15.534		15.547	15.559
^{206}Pb/^{204}Pb$_i$	16.478	16.822	16.939	17.034	17.242	17.335	17.192		17.180	17.028

64

Table 2.4 continued

Sample	Rep-56A1	10RATTD57A1	10RATTD60B1	10RATTD60B3	10RATTD60B4	10RATTD60B5	10RATTD61A1	10RATTD61A2	11RATTD72B	11RATTD72C
Measured										
^{87}Sr/^{86}Sr		0.707342	0.706265	0.706148	0.707441	0.704233	0.704164	0.703503	0.707562	0.707013
2SE		0.000010	0.000008	0.000007	0.000007	0.000009	0.000008	0.000007	0.000009	0.000008
^{176}Hf/^{177}Hf		0.282794	0.282782	0.282726	0.282786	0.282734	0.282841	0.282835	0.282848	0.282826
2SE		0.000013	0.000007	0.000010	0.000006	0.000007	0.000017	0.000018	0.000023	0.000006
^{143}Nd/^{144}Nd			0.513004	0.512968		0.513037		0.513076	0.512862	0.512767
2SE			0.000010	0.000007		0.000008		0.000006	0.000006	0.000008
^{208}Pb/^{204}Pb	38.9616	38.4430	38.2121	38.2154	38.0427	38.3121	38.1509	38.0677	38.1941	38.0573
2SE	0.0064	0.0072	0.0011	0.0069	0.0010	0.0061	0.0078	0.0062	0.0038	0.0015
^{207}Pb/^{204}Pb	15.6820	15.6552	15.5135	15.5347	15.5122	15.5458	15.6000	15.6285	15.5366	15.5343
2SE	0.0025	0.0032	0.0004	0.0027	0.0004	0.0025	0.0033	0.0026	0.0015	0.0006
^{206}Pb/^{204}Pb	18.9497	18.4109	17.8547	17.8116	17.7502	17.7850	18.2119	18.1516	17.8432	17.7807
2SE	0.0033	0.0032	0.0005	0.0031	0.0004	0.0026	0.0036	0.0029	0.0016	0.0006
Initial										
^{87}Sr/^{86}Sr$_i$		0.70403	0.70376	0.70431	0.70605	0.70370	0.70251	0.70306	0.70661	0.70627
^{176}Hf/^{177}Hf$_i$		0.28248	0.28249	0.28245	0.28249	0.28247	0.28260	0.28260	0.28257	0.28254
ε_{Hfi}		5.5	5.8	4.2	5.8	5.0	9.6	9.7	8.4	7.6
^{143}Nd/^{144}Nd$_i$			0.51214	0.51210		0.51214		0.51220	0.51202	0.51191
ε_{Ndi}			8.5	7.7		8.4		9.6	6.1	4.0
^{208}Pb/^{204}Pb$_i$		36.96	37.40	36.80	37.09	36.32	37.45	37.62	37.17	37.04
^{207}Pb/^{204}Pb$_i$		15.585	15.477	15.469	15.466	15.455	15.563	15.605	15.490	15.487
^{206}Pb/^{204}Pb$_i$		17.310	17.275	16.770	17.014	16.357	17.636	17.788	17.109	17.034

Table 2.4 continued

Sample	Dup-72C	11RATTD72D	11RATTD72G	11RATTD129A	11RATTD129B	11RATTD129E	Rep-129E	11RATTD129G	08 JB 01	Dup-08 JB 01
Measured										
$^{87}Sr/^{86}Sr$	0.707002	0.706620	0.704921	0.704806	0.704263	0.705482		0.704658	0.703306	0.703304
2SE	0.000009	0.000009	0.000009	0.000010	0.000009	0.000009		0.000008	0.000009	0.000008
$^{176}Hf/^{177}Hf$	0.282822	0.282773	0.282839	0.282840	0.282874	0.282872		0.282782	0.282869	0.282869
2SE	0.000003	0.000024	0.000004	0.000007	0.000025	0.000025		0.000006	0.000005	0.000004
$^{143}Nd/^{144}Nd$	0.512764	0.512859	0.513021	0.513051	0.513189	0.512924		0.512989	0.512878	0.512882
2SE	0.000006	0.000007	0.000007	0.000007	0.000008	0.000009		0.000007	0.000008	0.000007
$^{208}Pb/^{204}Pb$	38.0134	38.6005	38.5575	38.4971	38.3390	38.2250	38.2203	38.2808	38.8471	38.8479
2SE	0.0027	0.0018	0.0016	0.0028	0.0034	0.0031	0.0024	0.0017	0.0027	0.0033
$^{207}Pb/^{204}Pb$	15.5312	15.5540	15.5642	15.5836	15.5676	15.5260	15.5241	15.5352	15.5589	15.5590
2SE	0.0010	0.0006	0.0006	0.0011	0.0014	0.0010	0.0009	0.0009	0.0012	0.0008
$^{206}Pb/^{204}Pb$	17.7505	18.0206	18.0438	18.4704	18.3296	17.7444	17.7423	17.8089	18.7726	18.7737
2SE	0.0009	0.0007	0.0006	0.0012	0.0016	0.0012	0.0009	0.0009	0.0018	0.0008
Initial										
$^{87}Sr/^{86}Sr_i$		0.70445	0.70327	0.70271	0.70286	0.70377		0.70357	0.70287	
$^{176}Hf/^{177}Hf_i$		0.28251	0.28256	0.28260	0.28264	0.28262		0.28249	0.28262	
ε_{Hfi}		6.3	8.2	9.5	11.1	10.3		5.7	10.5	
$^{143}Nd/^{144}Nd_i$		0.51203	0.51213	0.51217	0.51231	0.51205		0.51213	0.51199	
ε_{Ndi}		6.3	8.3	9.0	11.8	6.7		8.3	5.5	
$^{208}Pb/^{204}Pb_i$		37.24	37.47	37.03	36.99	37.10		36.71	37.46	
$^{207}Pb/^{204}Pb_i$		15.492	15.513	15.509	15.497	15.473		15.459	15.480	
$^{206}Pb/^{204}Pb_i$		17.042	17.233	17.291	17.216	16.910		16.615	17.535	

Table 2.4 continued

Sample	08 JB 02	08 JB 03	08 JB 04C-1	08 JB 06	08 JB 07	BL136	Rep-BL136	BL144	SRM987	ULB-JMC
Measured										
$^{87}Sr/^{86}Sr$	0.703592	0.703874	0.706130	0.704010	0.704733	0.714454		0.704154	0.710253	
2SE	0.000009	0.000009	0.000008	0.000008	0.000008	0.000009		0.000009	0.000018	
$^{176}Hf/^{177}Hf$	0.282853	0.282838	0.282695	0.282835	0.282867	0.282752	0.282762	0.282830		0.282170
2SE	0.000005	0.000005	0.000005	0.000004	0.000004	0.000005	0.000003	0.000024		0.000005
$^{143}Nd/^{144}Nd$	0.512881	0.512828	0.512401	0.512731	0.512816	0.512810		0.513017		
2SE	0.000010	0.000008	0.000006	0.000007	0.000009	0.000007		0.000007		
$^{208}Pb/^{204}Pb$	38.5140	38.8334	38.8839	38.9902	38.9412	39.0957		38.5073		
2SE	0.0035	0.0028	0.0028	0.0035	0.0034	0.0016		0.0017		
$^{207}Pb/^{204}Pb$	15.5452	15.5913	15.5865	15.5649	15.5705	15.5786		15.5868		
2SE	0.0011	0.0011	0.0011	0.0013	0.0012	0.0006		0.0006		
$^{206}Pb/^{204}Pb$	18.3504	18.6897	18.3063	18.1590	18.4153	18.4842		18.3384		
2SE	0.0012	0.0013	0.0012	0.0012	0.0014	0.0007		0.0006		
Initial										
$^{87}Sr/^{86}Sr_i$	0.70315	0.70351	0.70569	0.70358	0.70294	0.70447		0.70366		
$^{176}Hf/^{177}Hf_i$	0.28262	0.28260	0.28245	0.28255	0.28276	0.28251		0.282571		
ε_{Hfi}	10.4	9.8	4.2	7.7	15.1	6.3		8.6		
$^{143}Nd/^{144}Nd_i$	0.51198	0.51193	0.51164	0.51184	0.51196	0.51200		0.512155		
ε_{Ndi}	5.4	4.4	-1.3	2.7	4.9	5.8		8.8		
$^{208}Pb/^{204}Pb_i$	38.02	37.67	37.62	37.53	35.99	37.92		37.68		
$^{207}Pb/^{204}Pb_i$	15.517	15.528	15.534	15.505	15.507	15.531		15.551		
$^{206}Pb/^{204}Pb_i$	17.909	17.684	17.476	17.208	17.420	17.735		17.775		

Table 2.4 continued

Sample	La Jolla	Rennes	NBS981	BHVO-2-Leached	BCR-2	BHVO-2-Leached	BCR-2
Measured						Published	Published
$^{87}Sr/^{86}Sr$					0.705013	0.703481	0.705009
2SE					0.000009	0.000008	0.000007
$^{176}Hf/^{177}Hf$					0.282861	0.283105	0.282870
2SE					0.000009	0.000011	0.000008
$^{143}Nd/^{144}Nd$	0.511856	0.511980			0.512655	0.512984	0.512627
2SE	0.000011	0.000006			0.000006	0.000011	0.000007
$^{208}Pb/^{204}Pb$			36.0834	38.2045	38.8304	38.2055	38.7237
2SE			0.0028	0.0018	0.0035	0.0034	0.0023
$^{207}Pb/^{204}Pb$			15.2363	15.4892	15.6244	15.4892	15.6249
2SE			0.0010	0.0007	0.0014	0.0011	0.0012
$^{206}Pb/^{204}Pb$			16.6555	18.6480	18.8022	18.6455	18.7529
2SE			0.0010	0.0008	0.0017	0.0009	0.0010
Initial							
$^{87}Sr/^{86}Sr_i$							
$^{176}Hf/^{177}Hf_i$							
ε_{Hfi}							
$^{143}Nd/^{144}Nd_i$							
ε_{Ndi}							
$^{208}Pb/^{204}Pb_i$							
$^{207}Pb/^{204}Pb_i$							
$^{206}Pb/^{204}Pb_i$							
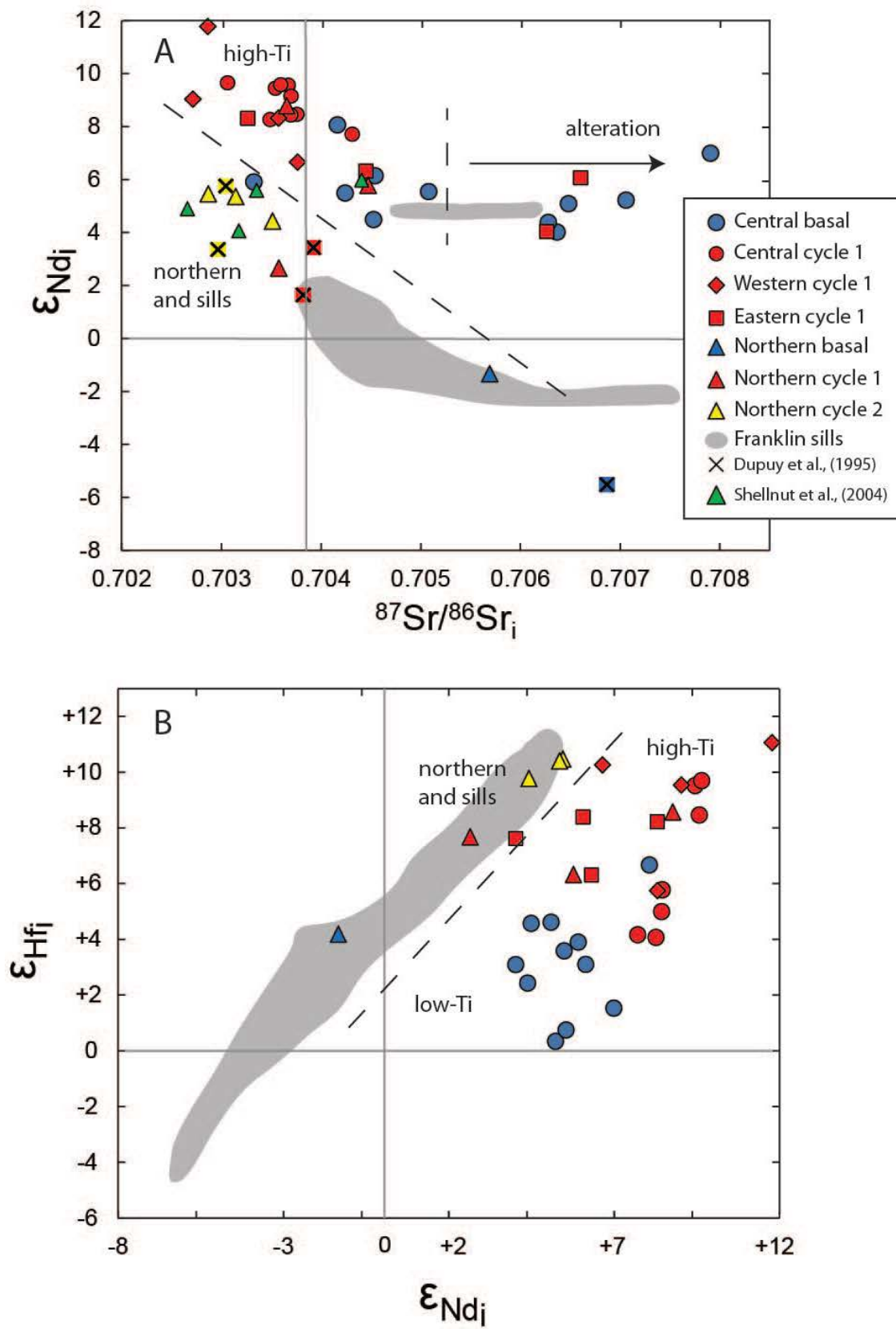
Figure 2.9
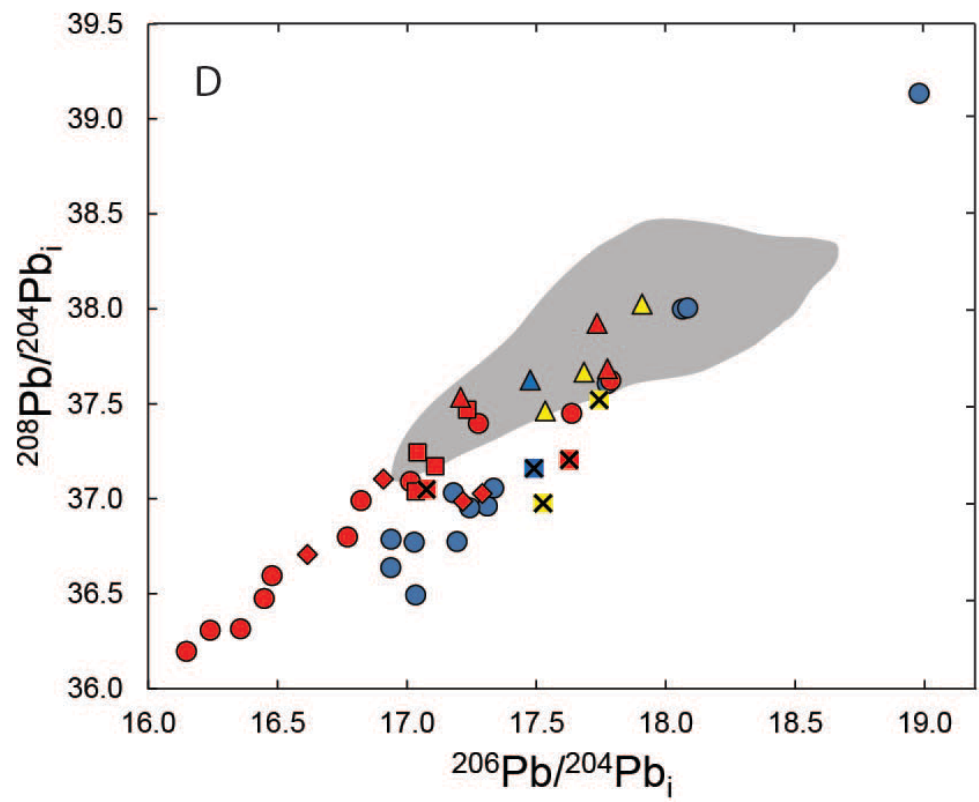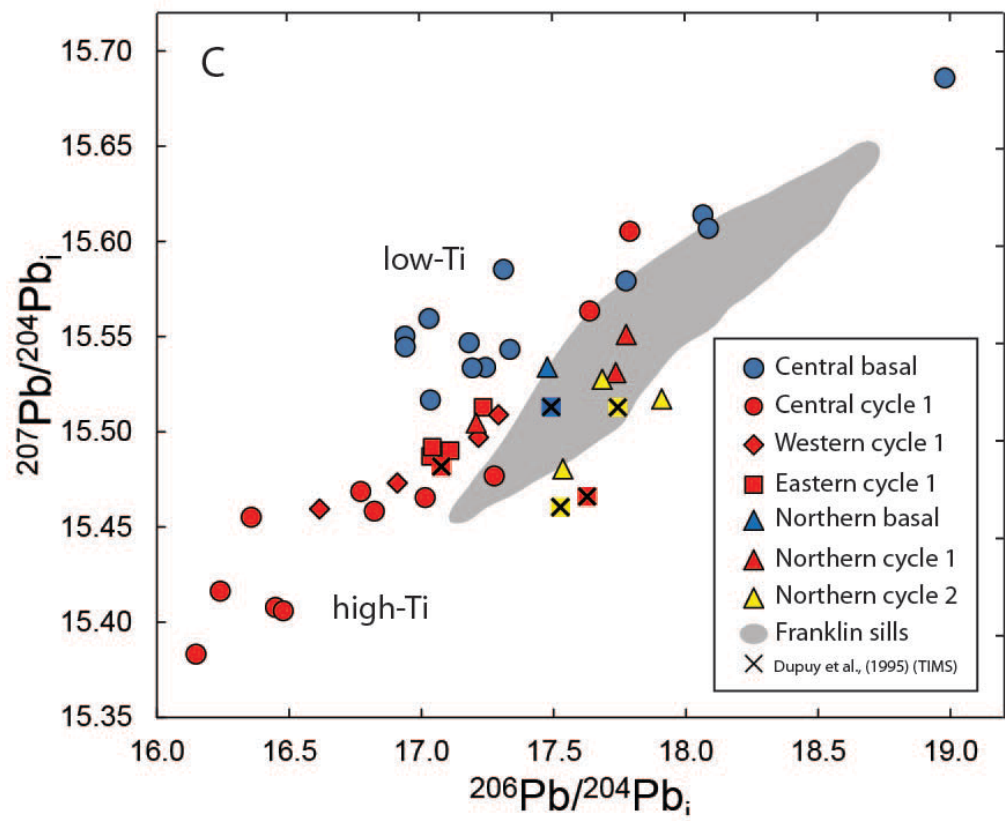
Figure 2.9 (continued)

Figure 2.9 (Preceding pages) Initial Sr-Nd-Hf-Pb isotope diagrams (calculated to 723 Ma) of the Natkusiak basalts and Franklin intrusive rocks on Victoria Island. The Franklin intrusive rock results are from Beard (2012). Previous basalt analyses of the northern lobe by Dupuy et al. (1995) are included for comparison and color-coded according to their location in the volcanic stratigraphy. Results from the Coronation sills by Shellnut et al. (2004) are included for comparison. Grey lines indicate Bulk Earth compositions. **A)** ε_{Ndi} versus $^{87}Sr/^{86}Sr_i$. Two correlations correspond to the northern basalts and to the southern basalt sections (i.e., central, eastern, western sections). Samples with high Sr isotope ratios (≥ 0.705 $^{87}Sr/^{86}Sr_i$) have resulted from alteration. **B)** ε_{Hfi} versus ε_{Ndi}. The northern basalts and sills form a distinct group from the southern section basalts. **C)** $^{207}Pb/^{204}Pb_i$ versus $^{206}Pb/^{204}Pb_i$. Three geochemical groups correspond to the southern high-Ti basalts, the southern low-Ti basalts, and to the northern basalts and sills. **D)** $^{208}Pb/^{204}Pb_i$ versus $^{206}Pb/^{204}Pb_i$. The three geochemical groups described above are evident here as well.
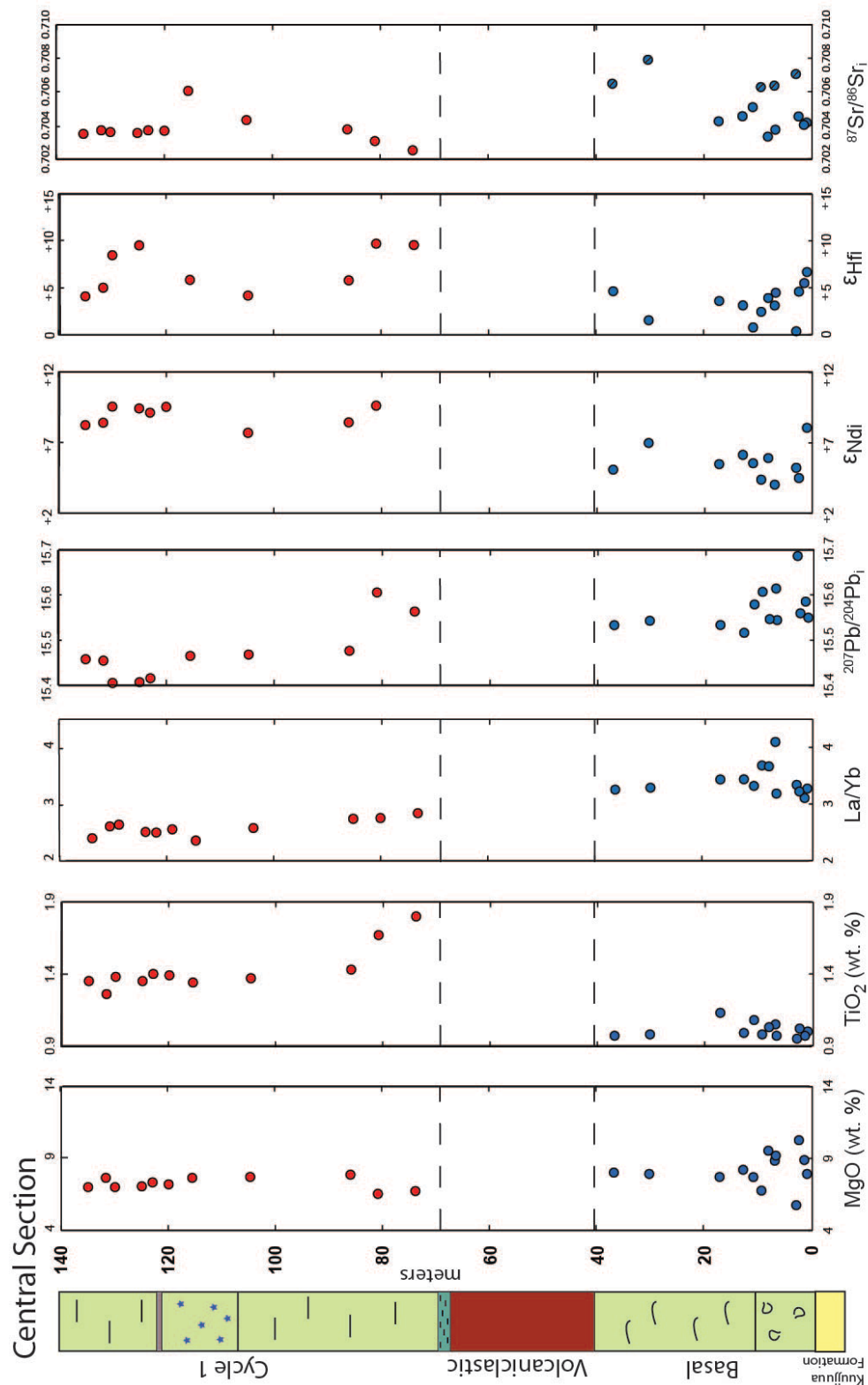
Figure 2.10 Chemostratigraphy of the central section, Natkusiak basalts. Initial isotope values are calculated to 723 Ma. A geochemical shift is observed between 40 and 70 m in height above the Kuujjua sandstone contact, from the basal unit low-Ti basalts to the cycle 1 unit high-Ti basalts. Basalt samples with $^{87}Sr/^{86}Sr_i$ values over 0.705 are excessively altered and marked with a cross-line through the symbol.

72

The western and eastern sections are geochemically indistinguishable from the cycle 1 high-Ti basalts of the central section. Cycle 1 is the only stratigraphic unit exposed in either the western or eastern sections and both sections have Sr-Nd-Hf-Pb isotopic compositions that overlap with the central cycle 1 basalts (Fig. 2.9). Collectively, the results for samples from these three sections form isotopic correlations that are distinct from the northern section basalts. There is no geochemical gradation between the southern sections (i.e., western, central, eastern) and the northern section (Fig. 2.9). The northern section (including samples from Dupuy et al., 1995) and Franklin intrusive rocks are shown to form an isotopically separate group from the more southern sections (i.e., central, eastern, western sections) in Sr-Nd-Hf-Pb isotopic diagrams. The northern basalts have overall lower ε_{Ndi} (-1.3 to +8.8) compared to the southern basalts (+4.0 to +11.8); this isotopic distinction is well-defined in diagrams of $^{87}Sr/^{86}Sr_i$ vs. ε_{Ndi} and ε_{Hfi} vs. ε_{Ndi} (Fig. 2.9). The basal (low-Ti) basalts of the northern section are characteristically more enriched with high $^{87}Sr/^{86}Sr_i$ (e.g., 0.7057) and isotopic Pb ratios, along with lower ε_{Ndi} (-1.3) and ε_{Hfi} (+4.2) than the overlying cycles 1 and 2 (high-Ti) basalts from the same section.

2.6 DISCUSSION

2.6.1 Geochemical groups in the Natkusiak basalts

Sr-Nd-Hf-Pb isotope and incompatible trace element compositions are used to identify distinct geochemical groups and assess the source components involved in the genesis of flood basalt provinces (White, 1985; Kempton et al., 2000; Pik et al., 2006; Escuder-Viruete et al., 2007; Jackson & Dasgupta, 2008). Multiple source components are identified within individual continental flood basalt provinces such as Central Atlantic Magmatic Province (CAMP) and the Ethiopian Plateau basalts, and result in distinct isotopic correlations and groups in Sr-Nd-Hf-Pb isotopic space (Melluso et al., 2006; Kieffer et al., 2004; Deckart et al., 2005; Pik et al., 2006). In

the Natkusiak basalts of Victoria, Island, four distinct geochemical groups are defined (Table 2.5).

The first group, most strongly defined in the cycle 1 (high-Ti) basalts of the southernmost sections (i.e., central, eastern and western), is less enriched in incompatible trace elements ((La/Yb): 2.2-3.1) and characterized by less radiogenic Sr and Pb isotopic ratios and more radiogenic Nd and Hf isotopic ratios than the other samples. The high-Ti basalts have less fractionated REE patterns (Fig. 2.8), narrow ranges of $^{87}Sr/^{86}Sr_i$ (0.7027-0.7045), high ε_{Ndi} (+4.0 to +11.8) and ε_{Hfi} (+4.1 to +11.1), and low $^{206}Pb/^{204}Pb_i$ (16.147-17.788), $^{207}Pb/^{204}Pb_i$ (15.383-15.605), and $^{208}Pb/^{204}Pb_i$ (36.20-38.03) compared to the basal (low-Ti) group (Fig. 2.9). The second geochemical group is defined by the low-Ti basalts in the southern sections. This group is characterized by relative LREE-enrichment, higher $^{87}Sr/^{86}Sr_i$ (0.7033-0.7051), $^{206}Pb/^{204}Pb_i$ (16.939-18.979), $^{207}Pb/^{204}Pb_i$ (15.517-15.686), and $^{208}Pb/^{204}Pb_i$ (36.49-39.14), along with lower ε_{Ndi} (+4.5 to +8.1) and ε_{Hfi} (+0.3 to +6.7). Cycle 1 (high-Ti) basalts show higher values of $^{208}Pb/^{204}Pb_i$ for a given $^{206}Pb/^{204}Pb_i$ value compared to the basal basalts, whereas the basal (low-Ti) group shows higher $^{207}Pb/^{204}Pb_i$ values for a given $^{206}Pb/^{204}Pb_i$ value in Pb-Pb isotopic diagrams. Those samples with significantly high $^{87}Sr/^{86}Sr_i$ (e.g., > 0.705) have been extensively altered and are not considered in the following discussion (Table 2.3).

Two additional geochemical groups are recorded primarily in the northern basalt section of the northern lobe. Similar to the southern samples, the basalts in the north may be divided into groups based on titanium contents, trace element enrichment (Fig. 2.11) and isotopic compositions (Fig. 2.9). The high-Ti basalts (cycle 1 and 2) in the north are characterized by low $^{87}Sr/^{86}Sr_i$ (0.7029-0.7036), moderate $^{206}Pb/^{204}Pb_i$ (17.131-17.909), $^{207}Pb/^{204}Pb_i$ (15.480-17.814), and $^{208}Pb/^{204}Pb_i$ (37.46-38.02), along with high ε_{Ndi} (+2.7 to +5.5) and ε_{Hfi} (+7.7 to +10.5). In contrast, the northern basal (low-Ti) basalts are characterized by higher $^{87}Sr/^{86}Sr_i$ (e.g., 0.7057)

Table 2.5: The four geochemical groups defined in the Natkusiak basalts

Group Unit(s)	Northern High-Ti Cycle 1 & 2	Northern Low-Ti Basal	Southern High-Ti Cycle 1	Southern Low-Ti Basal
TiO_2 wt.%	1.26-1.83	1.05	1.24-1.81	1.00-1.18
$^{87}Sr/^{86}Sr_i$	0.7029-0.7036	0.7057	0.7027-0.7045	0.7033-0.7051
εNdi	+2.7 to +5.5	-1.3	+4.0 to +11.8	+4.5 to +8.1
εHfi	+7.7 to +10.5	+4.2	+4.1 to +11.1	+0.3 to +6.7
$^{208}Pb/^{204}Pb_i$	37.46-38.02	37.62	36.20-38.03	36.49-39.14
$^{207}Pb/^{204}Pb_i$	15.480-17.814	15.534	15.383-15.605	15.517-15.686
$^{206}Pb/^{204}Pb_i$	17.131-17.909	17.477	16.147-17.788	16.939-18.979
La/Yb	2.2-3.1	4.0	2.2-3.1	3.1-4.1

and Pb isotopic ratios, along with lower ε_{Ndi} (-1.3) and ε_{Hfi} (+4.2). Despite the distinct isotopic correlations of the northern and southern sections (Fig. 2.9), the low- and high-Ti groups found in either region (north or south) share some strikingly similar geochemical characteristics. Both high-Ti groups (north and south) have relatively flat REE patterns, similar HREE enrichment compared to the low-Ti basalts, elevated ε_{Ndi} and ε_{Hfi}, and relatively lower $^{87}Sr/^{86}Sr_i$. The low-Ti basalts in both regions are similarly enriched in radiogenic Sr and Pb, contain lower ε_{Ndi} and ε_{Hfi} values, and show noticeable depletion in the HREE.

2.6.2 Isotopic correlation between Franklin volcanic and intrusive rocks

The isotopic composition of the Franklin intrusive rocks (Beard, 2012) and northern basalts from Dupuy et al. (1995) are plotted for comparison with the Natkusiak basalts from this study in Fig. 2.9. Overall, the northern basalts and Franklin intrusions have lower ε_{Ndi} values for a given ε_{Hfi} value than the southern basalts, which results in two distinct parallel correlations in Sr-Nd and Nd-Hf isotopic diagrams (Fig. 2.9). The geochemical distinction between the northern and southern groups is also apparent in $^{206}Pb/^{204}Pb_i$ versus $^{208}Pb/^{204}Pb_i$ and $^{206}Pb/^{204}Pb_i$ versus $^{207}Pb/^{204}Pb_i$ diagrams; the northern basalts (and intrusive rocks) have a lower $^{207}Pb/^{204}Pb_i$ value for a given $^{206}Pb/^{204}Pb_i$ value and a higher $^{206}Pb/^{204}Pb_i$ value for a given $^{208}Pb/^{204}Pb_i$ compared to the southern basalts. The Franklin intrusions mainly overlap with the northern section of Dupuy et al. (1995) and that of the current study (Fig. 2.9). This indicates that the southern (i.e., central, eastern, and western sections) basalts are not the extrusive equivalents to most of the exposed feeder system of sills and that the basalts in the north originate from a different source than the southern basalts.

The coeval Franklin sills on Victoria Island occur directly below the northern and southern lobe basalts, in some cases within tens of meters in stratigraphy. These intrusive rocks
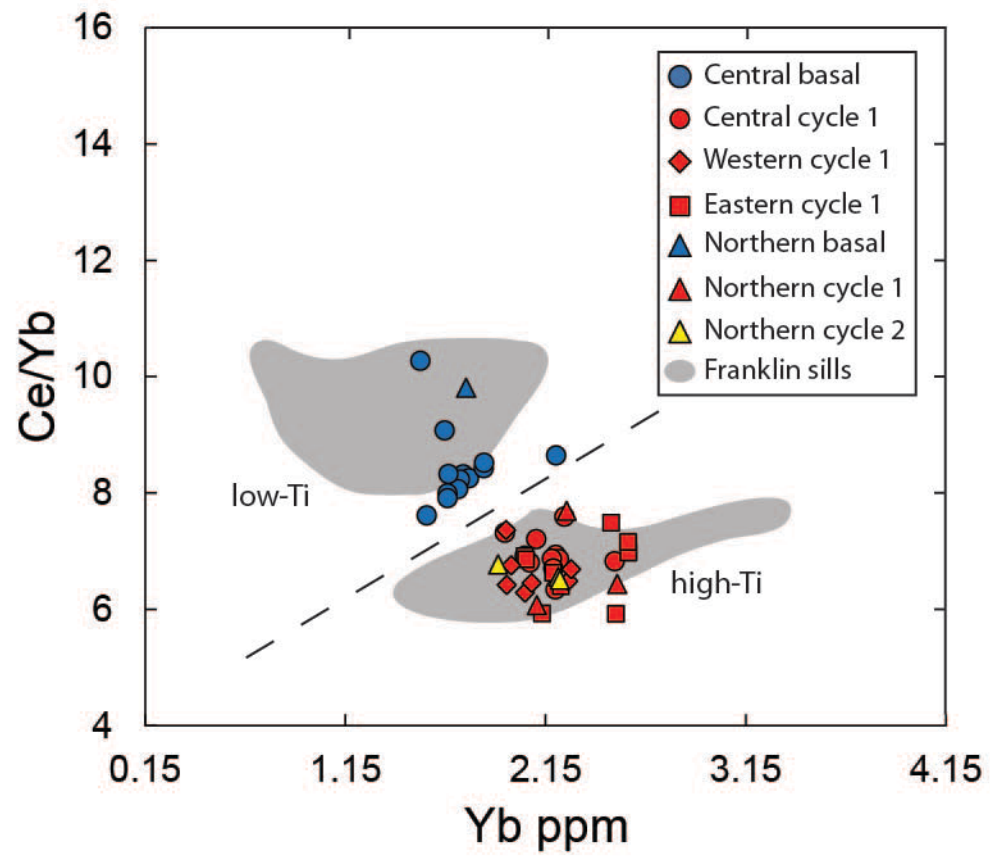
Figure 2.11 Diagram of Ce/Yb versus Yb concentration in ppm. The low-Ti and high-Ti basalt groups correlate well with the LREE-enriched and REE-unfractionated intrusive groups, respectively, from Beard (2012).

may be divided into similar geochemical groups to the overlying Natkusiak basalts on the basis of TiO_2 contents and HREE depletion (Fig. 2.11). According to Beard (2012), the sills found lowest in the stratigraphy of the Shaler Supergroup show negative Ti anomalies and have more radiogenic Pb and Sr isotopic compositions ($^{206}Pb/^{204}Pb_i$ = 16.975-18.662; $^{207}Pb/^{204}Pb_i$ = 15.494-15.644; $^{87}Sr/^{86}Sr_i$ = 0.7050-0.7068), characteristics similar to the basal (low-Ti) basalts in the north; these sills and basalts are proposed to be directly related. The northern cycle 1 (high-Ti) basalts have intrusive equivalents throughout the Shaler Supergroup; these sills are characterized by less radiogenic Sr and Pb isotope ratios ($^{87}Sr/^{86}Sr_i$ < 0.7055; $^{206}Pb/^{204}Pb_i$ < 17.814; $^{207}Pb/^{204}Pb_i$ < 15.575) than the deepest (low-Ti) sills, and moderately radiogenic Hf and Nd isotope ratios (i.e., ε_{Hfi} = +2.0 to +7.9; ε_{Ndi} = -2.0 to +2.0) (Beard, 2012). The sills found highest in the stratigraphy correlate with the cycle 2 (high-Ti) basalts in the north. These sills have high ε_{Hfi} (> +9.0) and ε_{Ndi} (> +4.7), moderate $^{206}Pb/^{204}Pb_i$ (17.925-18.229) and $^{207}Pb/^{204}Pb_i$ (15.554-15.570), and low $^{87}Sr/^{86}Sr_i$ (0.7041-0.7043) (Beard, 2012). The north-south isotopic divide observed in the Natkusiak Formation and the discrete correlations with the underlying intrusions are fundamental characteristics of the architecture of the Franklin LIP. The Coronation sills, located along the shore and on islands of the Coronation Gulf in Nunavut, Arctic Canada, are also isotopically distinct from the southern basalts and show more overlap with the northern basalts (Fig. 2.9). Flood basalts have the potential to flow 100s of km from their point of eruption by continuous lava injection and inflationary flow mechanisms (Walker, 1991; Hon et al., 1994; Self et al., 1997; Thordarson & Self, 1998; Anderson et al., 1999). Thus, the southern basalts were fed from a separate intrusive system from the one exposed in the Minto Inlier on Victoria Island, or from the sills exposed along the Coronation Gulf.

2.6.3 Extent of crustal contamination in basalts of the Natkusiak Formation

Flood basalts associated with LIP are found in both oceanic and continental plate settings, however, continental flood basalt provinces are commonly characterized by distinctive geochemical features such as highly radiogenic $^{87}Sr/^{86}Sr$ accompanied by relatively unradiogenic Nd and Hf isotopic ratios. This distinctive geochemical signature may result from contamination of parent magmas with lithospheric mantle or crust (DePaolo, 1981; Perry et al., 1987; Carlson, 1991; Wooden et al., 1993; Meyer et al., 2009; Jackson & Carlson, 2011). The incorporation of lithospheric material and crust likely occurs due to thermal erosion of the base of the lithosphere after plume impact and during the transit of melt through the continental crust, respectively (Arndt & Christensen, 1992; Pik et al., 1999; Frey et al., 2002; Ridley & Richards, 2010). The low-Ti basalts of the Natkusiak Formation (northern and three southern sections) include a component characterized by incompatible element-enrichment ((La/Yb): 3.1-4.1), high $^{87}Sr/^{86}Sr_i$ (0.7033-0.7079), relatively high $^{206}Pb/^{204}Pb_i$ (16.937-18.979), $^{207}Pb/^{204}Pb_i$ (15.517-15.686), and $^{208}Pb/^{204}Pb_i$ (36.49-39.14), along with low ε_{Ndi} (i.e., -1.3 to +8.1) and ε_{Hfi} (+0.3 to +6.7) (Fig. 2.9). In contrast to the low-Ti basalts, the overlying high-Ti basalts are characterized by high ε_{Ndi} (+2.7 to +11.8) and ε_{Hfi} (+4.1 to +11.1) and low $^{87}Sr/^{86}Sr_i$ (0.7027-0.7045) values.

Contamination of plume-derived magmas with subcontinental lithospheric mantle (SCLM)-derived melts may be a common process in LIP emplacement (e.g., Hergt et al., 1991; Gallagher & Hawkesworth, 1992; Lightfoot et al., 1993; Marques et al., 1999; Greene et al., 2008; Qi et al., 2010). LREE depletion and low titanium abundances have been attributed to partial melting of SCLM and to the formation of low-Ti basalts found in the Ferrar, Parana-Etendeka, and Wrangellia provinces (e.g., Hergt et al., 1991; Marques et al., 1999; Hawkesworth et al., 2000; Greene et al., 2009). Lithospheric melting may be triggered by transfer of heat from a mantle plume to a metasomatized lithospheric mantle (Emeishan and Wrangellia, e.g., Xiao et al., 2004; Greene et al., 2008) or by extension and decompression of the lithosphere combined

with heat transfer from a plume (Siberia, e.g., Saunders et al., 2005; Reichow et al., 2005). Crustal contamination of magmas during ascent to the surface may also explain some of these geochemical characteristics (Arndt & Christensen, 1992; Arndt et al., 1993; Wooden et al., 1993; Griselin et al., 1997, Keays & Lightfoot, 2010). Crustal contamination will result in comparable geochemical characteristics to that of SCLM component, such as elevated $^{87}Sr/^{86}Sr$, decreased $^{176}Hf/^{177}Hf$ and $^{143}Nd/^{144}Nd$, and depletion in Nb, Ta, and Ti contents (Pik et al., 1999; Reichow et al., 2005; Peate et al., 2008). Some contamination may be possible in the northern section based on the lower ε_{Ndi} and ε_{Hfi} values observed in the basal basalt samples.

Based on a more limited dataset (i.e., 10 samples), Dupuy et al. (1995) suggest that crustal contamination links the two types of basalts and propose that the combined effects of plume-related uplift and lithospheric insulation in addition to the thermal perturbation of mafic sills emplaced in the crust may have provided the conditions necessary for early crustal contamination in the Natkusiak basalts. The results presented in this study suggest that the two geochemical groups of basalts (low- and high-Ti) are distinct with no mixing trends between them and that the enriched low-Ti group was not derived from the isotopically depleted high-Ti end-member through crustal contamination.

Incompatible trace element ratios can be used to assess mixing between different geochemical components in pre-eruptive magmas. Trace element ratios, such as Ba/Ti, Ce/Hf, U/Y, and Pr/Lu, are used to monitor the involvement of various geochemical components in the Natkusiak basalts (Fig. 2.12). These ratios are measurements of the relative enrichment of the incompatible elements that characteristically distinguish the low-Ti basalts from the high-Ti basalts (northern and southern) in this study. The high-Ti basalts have lower Ba/Ti, Ce/Hf, U/Y, and Pr/Lu values than the low-Ti basalts. This might imply that the low-Ti basalts assimilated more crustal material than the high-Ti basalts prior to emplacement. However, if the low-Ti basalts were entirely derived from crustal contamination of the high-Ti basalts, a continuous and
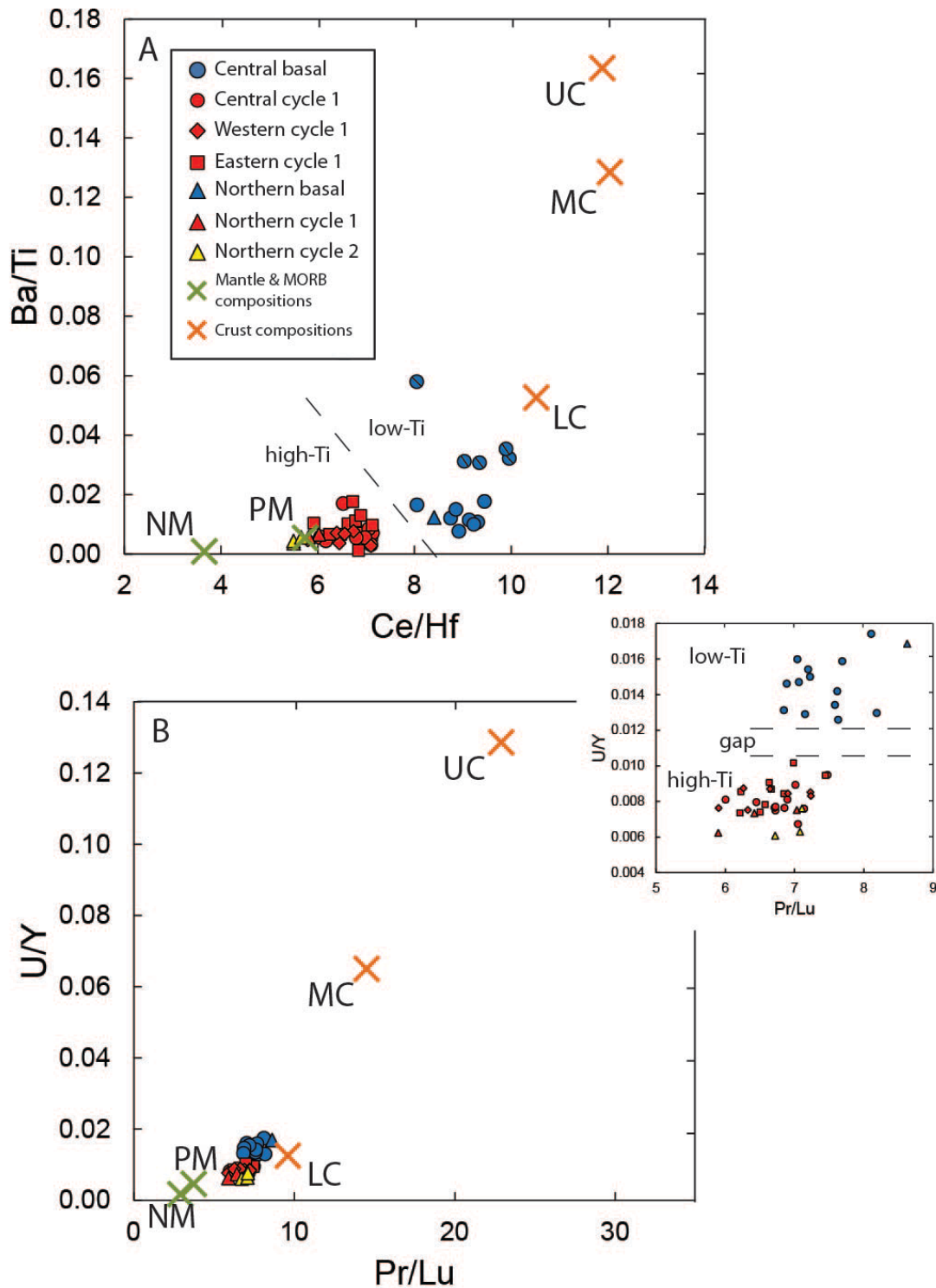
Figure 2.12 Incompatible trace element ratio-ratio diagrams for the Natkusiak basalts. A geochemical gap between the two groups (low and high-Ti) indicates that they were derived from distinct sources. LC = lower crust; MC = middle crust; UC = upper crust; PM = primitive mantle; NM = N-MORB. Average lower, middle, and upper crust values from Rudnick & Gao (2003), primitive mantle and N-MORB values from Sun & McDonough (1989). Altered samples with elevated Ba concentrations are marked with a cross-line through the symbol.

systematic relationship between the low-Ti and the high-Ti samples should be apparent. This is not the case as indicated by the geochemical gap found between the two groups in many trace element diagrams (Fig. 2.7, Fig. 2.11, and Fig. 2.12) and by the isotopic shift observed up-section (Fig.2.10). Collectively, these results indicate that a chnage in the source region occurred between the emplacement of the low-Ti basalts and the high-Ti basalts.

2.6.4 Origin of the high- and low-Ti basalts in the Natkusiak Formation

There are sufficient differences in the major, trace element, and isotope compositions between the low- and high-Ti basalts to indicate that different mechanisms and mantle source regions were involved in their formation. The low-Ti basalts have higher $^{87}Sr/^{86}Sr_i$ and radiogenic Pb values, lower ε_{Ndi} and ε_{Hfi} values, along with higher LREE/HREE than the high-Ti basalts. Both groups follow distinct correlations in isotopic diagrams (Fig. 2.9) and form distinct groups in trace element ratio-ratio diagrams (Fig. 2.12). In addition, most of the differentiation trends based on major and trace elements (Fig. 2.6 and 2.7) also allow for distinct correlation of the low- and high-Ti groups.

A key difference between the low- and high-Ti basalts is the contrast in trace and rare earth element patterns (Fig. 2.8), best illustrated by the LREE/HREE systematics (Fig. 2.11). The low-Ti basalts are more depleted in HREE relative to the high-Ti basalts, whereas the two groups overlap in LREE concentrations. These characteristics cannot be explained by fractional crystallization or crustal contamination processes (DePaolo, 1981), however, they may reflect different depths of melting. The low-Ti basalts require greater amounts of garnet in their source to account for the depletion in HREE relative to the high-Ti basalts. The REE systematics of the high-Ti group excludes the presence of garnet and suggests partial melting in a shallower spinel-bearing peridotite (e.g., Griselin et al., 1997; Jourdan et al., 2007).

Structural and stratigraphic evidence suggests that the Franklin LIP is associated with plume-related uplift and rifting that led to the breakup of the Laurentian Supercontinent and the opening of the Neoproterozoic Palaeo-Asian Ocean (Rainbird, 1993; Pelechaty, 1996; Rainbird & Freitas, 1997; Li et al., 2008; Pisarevsky et al., 2008). The presence of NW-trending normal faults and associated down-faulted blocks infilled with volcanic debris flows in the northeastern domain suggest that some NE-SW extension occurred *after* the initial eruptive phase of volcanism (Rainbird, 1993). Additionally, NW-trending dikes (also found in the northeastern domain) have intruded the entire preserved Natkusiak Formation and support the occurrence of syn-volcanic extension (Heaman et al., 1992; Rainbird, 1993). The thermal evolution of the continental lithosphere and the melt region of the plume are interrelated by three competing factors: the thermal influence of the underlying plume, the decompression as a result of thinning lithosphere, and the cooling as a consequence of extension (Arndt & Christensen, 1992; Herzberg, 2011). Syn-volcanic extension may have resulted in a shift in the melting region of the plume with time, as evidenced by the distinct geochemical characteristics of the low-Ti and high-Ti basalts. This geochemical shift may have resulted from decompression associated with continuous rifting as the depth and extent of melting is critically dependent on several parameters, including internal plume temperature, thickness of the overlying lithosphere, and the mantle potential temperature (Herzberg, 1995; Herzberg & O'Hara, 2002; Herzberg & Gazel, 2009; Herzberg, 2011). As the Franklin mantle plume continued to rise, in conjunction with lithospheric extension and rifting, the source region that was melting would have shifted from a deeper garnet-bearing to a shallower spinel-bearing peridotite, which led to the later emplacement of the high-Ti basalts.

Overall, the high-Ti basalts from the Natkusiak Formation display a more isotopically depleted signature in comparison to the underlying low-Ti basalts, illustrated by a noticeable shift in Sr, Nd, Hf, and Pb isotopic values up-section (Fig. 2.10). The high-Ti basalts from both

the southern and northern sections represent the most radiogenic samples in terms of Nd and Hf isotopes and the least radiogenic with respect to Sr and Pb isotopes, whereas the low-Ti basalts from both the northern and the southern sections are characterized by higher $^{206}Pb/^{204}Pb_i$, $^{207}Pb/^{204}Pb_i$, $^{208}Pb/^{204}Pb_i$, and $^{87}Sr/^{86}Sr_i$ along with relatively lower ε_{Ndi} and ε_{Hfi} values. The REE and extended trace element patterns of the high-Ti basalts indicate derivation from a trace element-enriched OIB-type source, not depleted MORB mantle (Fig. 2.8). These geochemical features imply that the high-Ti basalts of the Natkusiak Formation are derived from an asthenospheric mantle source, intrinsic to the Franklin mantle plume. The low-Ti basalts sample a more isotopically enriched component. The tectonic evolution (i.e., syn-volcanic rifting) of the magmatic province resulted in a shift in the region of partial melting to a different source (more asthenospheric) after the emplacement of the basal (low-Ti) basalts.

2.6.5 Comparison to global isotopic variations in continental flood basalts

A global comparison of flood basalt provinces (e.g., Deccan, Emeishan, Ethiopia, Etendeka) reveal Sr-Nd-Pb isotopic systematics that show complex mixing relationships between various mantle (e.g., FOZO, EM I, EM II) and crustal (e.g., lower or upper crust) geochemical reservoirs (Fig. 2.13 A & B). Flood basalts are the product of partial melt from mantle plumes that originate from a thermal boundary layer (i.e., core-mantle boundary) in the Earth (Morgan, 1971; Morgan, 1972; Richards et al., 1989; Campbell & Griffiths, 1990; Carlson, 1991; Morgan et al., 1999; Jellinek & Manga, 2004; Montelli et al., 2004; Ernst et al., 2005; Campbell, 2005, Weis et al., 2011). Evidence that suggests LIP are the result of mantle plume-related magmatism includes the primitive to slightly depleted isotopic signatures (i.e., low $^{87}Sr/^{86}Sr$ and high ε_{Hf} and ε_{Nd} values) found in many flood basalt provinces worldwide, such as in the Ethiopian basalts in Africa or the Emeishan flood basalt province in China (Fig. 2.13 A) (Kieffer et al., 2004; Xiao et al., 2004; White, 2010).

The incorporation of crustal material in to LIP parental magmas will result in higher and more variable $^{87}Sr/^{86}Sr$ (Rb/Sr is elevated in the crust) and less radiogenic Nd isotopic compositions in contaminated basalts (Fig. 2.13 A) (Devey & Cox, 1987; Baker et al., 1996; Melluso et al., 2006; Keays & Lightfoot, 2010). Phanerozoic continental flood basalt provinces such as Deccan, Siberia and NAP show large isotopic variations and evidence for extensive crustal contamination in the earliest erupted basalts (Lightfoot et al., 1990; Peng et al., 1994; Meyer et al., 2009), which decreases up-section as the feeder system establishes itself. The least contaminated basalts are commonly found in the latter stages of continental flood basalt volcanism (before the transition to persistent or hotspot volcanism), similar to the observed geochemical evolution of the Central Atlantic Magmatic Province (CAMP), Siberian, and Deccan provinces (Devey & Cox, 1987; Lightfoot et al., 1990; Sharma et al., 1992; Wooden et al., 1993, Peng et al., 1994; Deckart et al., 2005; Melluso et al., 2006).

Although a limited crustal contaminant signature is apparent in the Natkusiak basalts, the samples from this study show significantly less crustal contamination than the Deccan, Siberian, or the North Atlantic flood basalt provinces (Fig. 2.13 A). The extensive Sr and Nd isotopic variability of the Deccan ($^{87}Sr/^{86}Sr_i$ 0.7014-0.7122 and $^{143}Nd/^{144}Nd_i$ 0.5111-0.5123) and North Atlantic igneous province ($^{87}Sr/^{86}Sr_i$ 0.7010-0.7098 and $^{143}Nd/^{144}Nd_i$ 0.5111-0.5123) testifies to the extensive crustal contamination introduced into some parent magmas to continental flood basalt provinces as they ascended through the crust. The Natkusiak basalts show much less isotopic variation, mainly evident only in the lowermost flows (Fig. 2.13 A).
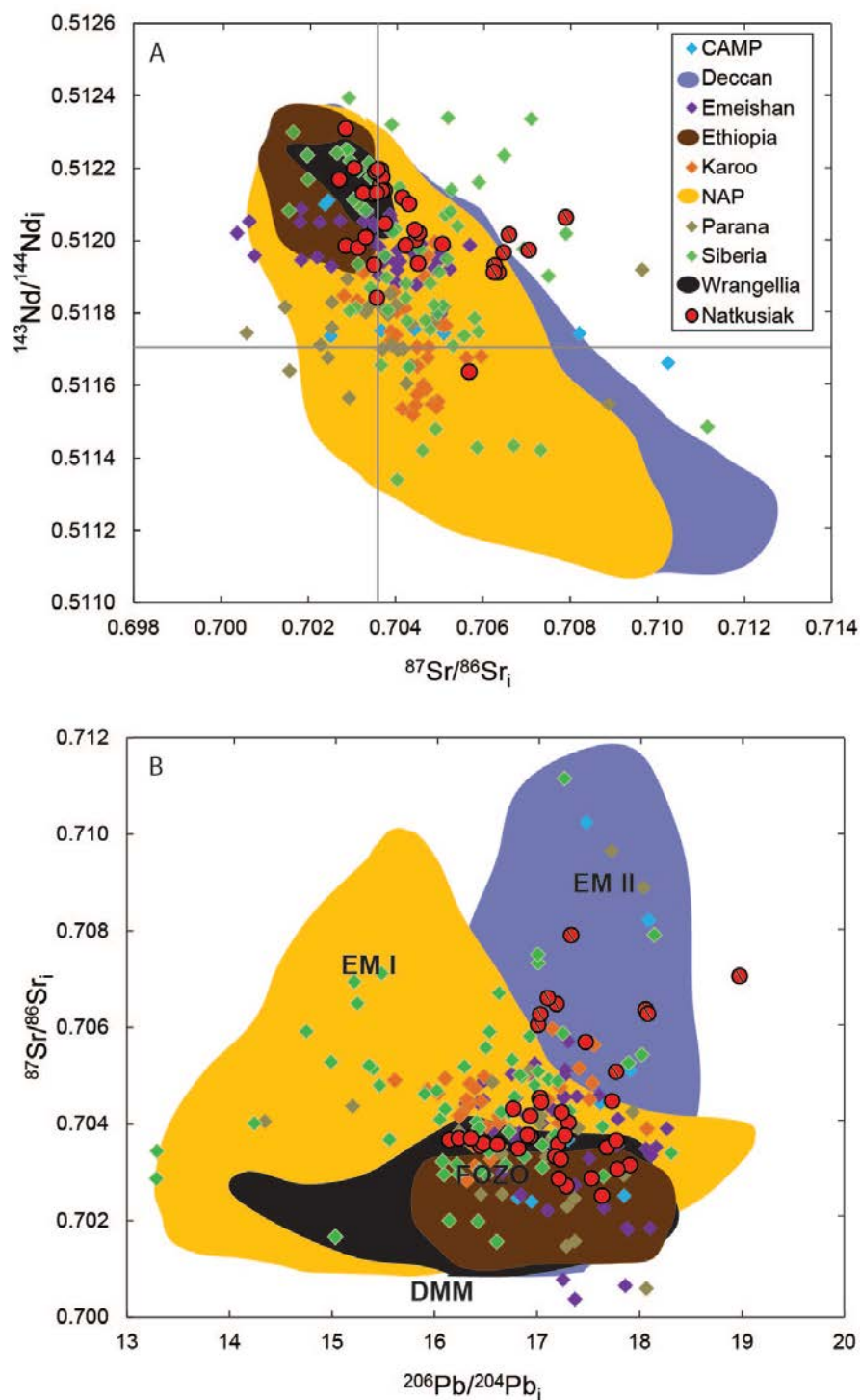
Figure 2.13 Diagrams of $^{143}Nd/^{144}Nd_i$ versus $^{87}Sr/^{86}Sr_i$ and $^{87}Sr/^{86}Sr_i$ versus $^{206}Pb/^{204}Pb_i$ for continental flood basalts worldwide. Calculated to 723 Ma. Grey lines indicate bulk Earth compositions. End-member compositions (DMM = Depleted MORB mantle; EMI = enriched mantle 1; EMII = enriched mantle 2; FOZO = FOcus ZOne) are from Zindler & Hart (1986) and Hart et al. (1992). The Natkusiak basalt samples with $^{87}Sr/^{86}Sr$ values over 0.705 are excessively altered (as described in the results section and Table 2.3) are marked with a cross-line through the symbol. Data from the GEOROC database compilation (http://www.georoc.mpch-mainz.gwdg.de).

The Sr-Nd isotopic compositions of continental flood basalt provinces (e.g., Deccan, NAP, Karoo, Siberia, and Natkusiak) converge at positive $^{143}Nd/^{144}Nd_i$ and less radiogenic $^{87}Sr/^{86}Sr_i$ values, which suggests that many continental flood basalts originate from a common mantle component (Fig. 2.13 A). The large variation in $^{143}Nd/^{144}Nd$ and high $^{87}Sr/^{86}Sr$ values are a consequence of the addition of crustal material (Fig. 2.13 A). Oceanic plateau basalts, such as Wrangellia, have not passed through continental crust prior to emplacement and show depleted and a relatively restricted range in $^{87}Sr/^{86}Sr$ and $^{143}Nd/^{144}Nd$ (Greene et al., 2008; Greene et al., 2009) (Fig. 2.13 A). The Ethiopian basalts encountered a limited crustal or lithospheric component prior to eruption and have a similarly restricted and depleted range in isotopic values (Pik et al., 1999; Kieffer et al., 2004). The Natkusiak basalts overlap with Ethiopia and Wrangellia basalts in Sr-Nd isotopic space.

The Sr-Nd-Pb isotopic variability observed among large igneous provinces and ocean island basalts (OIB) is explained by the existence of several discrete mantle components (i.e., EM I, EM II, HIMU, FOZO, and DMM) (White, 1985; Zindler & Hart, 1986; Sun & McDonough, 1989; Hart et al., 1992; Hofmann, 1997; Stracke et al., 2005; Tatsumi, 2005; Zhu, 2007; Willbold & Stracke, 2010; White, 2010). The FOZO has an intermediate composition and is common among continental flood basalt provinces, whereas the EM I and EM II components are present in only a few settings (Fig. 2.13 B) (Hart et al., 1992; Willbold & Stracke, 2010). Compositions from the Natkusiak basalts are mostly near FOZO, similar to the Ethiopia and Wrangellia provinces. These comparisons suggest that the Franklin mantle plume did not incorporate a significant amount of enriched-mantle or EM material. One reason for this may be that the EM components sampled by Phanerozoic LIP were not present in the lower mantle prior to initiation of the Franklin mantle plume.

2.7 CONCLUSIONS

High-precision trace element concentrations and Sr, Nd, Hf, and Pb isotopic compositions of the Natkusiak Formation continental flood basalts, part of the Franklin large igneous province on Victoria Island, allow for the assignment of four geochemical groups. Two groups (low- and high-Ti basalts) are found in the southernmost sections (i.e., central, eastern, and western) and two additional low- and high-Ti basalt groups are found in the northernmost section. The distinct isotopic composition of the northern basalts requires a geochemical division between the northern and southern sections. A shift in isotopic and trace element composition is observed up-section (i.e., from low-Ti to high-Ti basalt) in both the north and south. Crustal contamination is significantly less pronounced in the Natkusiak Formation than in other continental flood basalt provinces worldwide (e.g., NAP, Deccan, and Siberia) The two major magma types, low- and high-Ti basalts, are not related to each other by crustal contamination. These geochemical differences are attributed to the syn-volcanic tectonic evolution of the Franklin magmatic province, which may have resulted in a shift in the source region with time from a deeper garnet-bearing mantle source (low-Ti basalts) to a shallower spinel-bearing source prior to the formation of the high-Ti basalts. The Natkusiak basalts mainly overlap with the Focus Zone (FOZO) mantle component and show only minor enriched mantle (EM) signature in the basal low-Ti basalts.

CHAPTER 3

SUMMARY AND CONCLUSIONS

3.1 SUMMARY, CONCLUSIONS, AND DIRECTIONS FOR FUTURE RESEARCH

The Neoproterozoic (ca. 723 Ma) Franklin large igneous province located on Victoria Island, Canada, is characterized by continental flood basalts of the Natkusiak Formation and a sill-dominated feeder system exposed in the Minto Inlier. The Natkusiak basalts were successfully mapped and sampled for geochemical study during two field seasons (summer 2010 and 2011) with the Geological Survey of Canada (GSC) as part of a Geo-mapping for Energy and Minerals (GEM) project. The Sr-Nd-Hf-Pb isotope and trace element results of this study provide new insight into the geochemical evolution of the Natkusiak basalts. Contributions from this study include: (1) field work on Victoria Island, including field mapping and sample collection of the Neoproterozoic bedrock exposure in the Minto Inlier and the Natkusiak Formation flood basalts; (2) a petrographic catalogue of 47 basalt samples; (3) major and trace element analysis of 47 samples from the Natkusiak basalts; (4) 39 samples analyzed for combined Sr-Nd-Hf-Pb isotopic compositions; (5) geochemical characterization of the Natkusiak basalts; (6) assessment of the relative involvement of crustal contaminant in the Natkusiak basalts; (7) comparison with the underlying Franklin intrusions on Victoria Island; (8) isotopic comparison of the Natkusiak basalts to other flood basalt provinces worldwide; (9) archival of the samples; and (10) co-authorship on three geoscience conference abstracts (i.e., Bédard et al., 2011a, 2011b, 2012b).

The Natkusiak basalts are preserved in two lobes (northern and southern) on Victoria Island, Canada, and are divided into three volcanological units: *basal, cycle 1, and cycle 2*. Over 1100 meters are preserved in the center of the northern lobe and a maximum of 140 meters are preserved in the southern lobe. Basal, cycle 1, and cycle 2 units outcrop in the northern lobe, whereas only basal and cycle 1 units are preserved in the south. The heterogeneous basal unit is characterized by interbedded basalt and sandstone within the first two meters from the conformable contact with sandstones of the Kuujjua Formation in the south; hyaloclastites and

pillow basalts occur locally. Subophitic-textured clinopyroxene is common, and amygdules

constitute a high volume (up to 35 vol. %) in samples from the basal unit. A maroon-colored

volcaniclastic unit lies in between the basal and cycle 1 unit and is characterized by unsorted

matrix with no systematic size grading. The overlying cycle 1 unit is characterized by fine-

grained basalt (~0.5 mm plagioclase and clinopyroxene) with lower amygdule contents (~5 vol.

% on average). Cycle 2 basalts were not observed in the field during this study, however,

previous work by Jefferson et al. (1985) describe this unit as texturally and compositionally

similar to cycle 1 basalts.

Alteration is prevalent in the Natkusiak Formation and is recognized through elevated

large ion lithophile (LILE) concentrations, high loss-on-ignition (LOI), and the presence of

secondary minerals (see Table 2.3, Appendix A and B). LOI is overall higher in the samples

from the basal unit, whereas LILE mobilization is evident throughout the formation. Chlorite,

calcite, and quartz are the dominant secondary phases that precipitated during hydrothermal

alteration to form the prominent amygdules. All samples were acid-leached prior to dissolution

to minimize the chemical signature from alteration.

Trace element and Sr-Nd-Hf-Pb isotopic geochemistry of the Natkusiak Formation reveal

four geochemical groups of basalt found in geographic and stratigraphic context. The basalts in

the north and south are distinguished geochemically on the basis of TiO_2 contents (low- and

high-Ti basalts). The northern basalts and Franklin sills have lower $^{207}Pb/^{204}Pb_i$ values for given

$^{206}Pb/^{204}Pb_i$ values and higher $^{206}Pb/^{204}Pb_i$ values for given $^{208}Pb/^{204}Pb_i$ compared to the basalts

found in the southern region. The isotopic compositions of basalts from the northern section

overlap with those from the Franklin sills (Beard, 2012), whereas the southern basalts show only

a limited geochemical link to the underlying feeder system exposed in the Minto Inlier. This

geochemical division also corresponds with their stratigraphic position in the Natkusiak

Formation. The early erupted low-Ti basalts (basal unit) are characterized by depletion in HREE,

higher $^{87}Sr/^{86}Sr_i$ values, relatively higher $^{206}Pb/^{204}Pb_i$, $^{207}Pb/^{204}Pb_i$, and $^{208}Pb/^{204}Pb_i$, along with lower ε_{Ndi} and ε_{Hfi} values compared to the high-Ti basalts.

The tectonic evolution of the Franklin magmatic province in conjunction with the continued ascent of the Franklin mantle plume resulted in a shift to a shallower spinel-bearing source region after the emplacement of the low-Ti basalts that were derived from a garnet-bearing source. Overall, a signature of crustal contamination is significantly less pronounced in the Natkusiak basalts than in other continental flood basalt provinces worldwide. Unlike many Phanerozoic LIP, the Natkusiak basalts mainly overlap with the FOZO (FOcal ZOne) mantle component (Stracke et al., 2005). The lack of substantial variation in the Natkusiak basalts also indicates minimal contribution from enriched mantle reservoirs (i.e., EM I, EM II) or crust, which are found to be prominent in other continental flood basalt provinces such as Deccan and North Atlantic igneous province (Kempton et al., 2000; Melluso et al., 2006).

The Franklin large igneous province is one of the more understudied large igneous provinces in the world due to its remote location in the Arctic of Canada. There is much more to learn and discover concerning the development of the Franklin LIP and its geological role in the Neoproterozoic era, especially concerning the break-up of Laurentia and its involvement with the Snowball Earth event, the greatest ice age to ever occur on Earth. The youngest magmatic intrusions associated with the Franklin LIP are dated at 716.33 ± 0.54 Ma, and Sturtian glacial deposits in the Oglivie Mountains, Canada, have been dated at 716.5 ± 0.24 Ma (interbedded volcanic tuff) (MacDonald et al., 2010). The Franklin LIP may have expelled large quantities of SO_2, and aided in the drawdown of atmospheric CO_2 and sequestration in the oceans via chemical weathering. In conjunction with the high albedo of the Earth due to the equatorially placed Supercontinent Rodinia, the Franklin LIP, if involved at all, may have initiated or facilitated the cooling that lead to the Snowball Earth event. Stratigraphic evidence suggests pre-eruptive uplift occurred prior to the emplacement of the Franklin LIP and is interpreted as

thermal doming due to the impingent of a mantle plume at the base of the lithosphere (Rainbird et al., 1993). The differential force exerted upwards in conjunction with thermomechanical erosion of the lithosphere in response to the ascending mantle plume may have weakened the crust and resulted in late Proterozoic or early Cambrian rifting of Laurentia from Siberia (Pelechaty, 1996; Li et al., 2008; Pisarevsky et al., 2008). The geochemical study presented here constitutes a stepping stone to future research and studies on the Natkusiak Formation continental flood basalts and the Franklin large igneous province.

REFERENCES

R1. REFERENCES CITED

Albarède, F. (1992) How deep do common basaltic magmas form and differentiate. *Journal of Geophysical Research* **97**(B7), 10,997-11,009.

Albarède, F. (2009) Geochemistry: An introduction. 2nd Edition, *Cambridge University Press*. ISBN: 978-0-521-70693-3.

Anderson, S. W., Stofan, E. R., Smrekar, S. E., Guest, J. E. & Wood, B. (1999) Pulsed inflation of pahoehoe lava flows: implications for flood basalt emplacement. *Earth and Planetary Science Letters* **168**, 7-18.

Arndt, N., Kerr, A. & Tarney, J. (1997) Dynamic melting in plume heads: the formation of Gorgona komatiites and basalts. *Earth and Planetary Science Letters* **146**, 289-301.

Arndt, N. & Christensen, U. (1992) The role of lithospheric mantle in the continental flood volcanism: thermal and geochemical constraints. *Journal of Geophysical Research* **97**(B7), 10,967-10,981.

Arndt, N., Czamanske, G., Wooden, J. & Fedorenko, V. (1993) Mantle and crustal contributions to continental flood volcanism. *Tectonophysics* **223**, 39-52.

Baker, J. A., Thirlwall, M. F. & Menzies, M. A. (1996) Sr-Nd-Pb isotopic and trace element evidence for crustal contamination of plume-derived flood basalts: Oligocene flood volcanism in western Yemen. *Geochimica et Cosmochimica Acta* **60**(14), 2559-2581.

Ballmer, M. D., Ito, G., Wolfe, C. J., Cadio, C. & Solomon, S. C. (2012) Double layering of a thermochemical plume in the upper mantle beneath Hawaii. *EGU General Assembly 2012*, 22-27 April, 2012 in Vienna, Austria., p. 3262.

Bank, C. -G., Bostok, M. G., Ellis, R. M. & Cassidy, J. F. (2000) A reconnaissance teleseismic study of the upper mantle and transition zone beneath the Archean Slave craton in NW Canada. *Tectonophysics* **319**, 151-166.

Baragar, W. R. A. (1976) The Natkusiak Basalts, Victoria Island, District of Franklin. *GSC Current Research*, Paper 76-1A, p. 347-352.

Baragar, W. A. R. & Loveridge, W. D. (1986) A Rb-Sr study of the Natkusiak basalts, Victoria Island, District of Franklin. Report 5 in: *Current Research*, Part C, Geological Survey of Canada, Paper 82-1C, p. 167-168.

Beard, C. (2012) Magmatic plumbing and melt source characterisation: A Hf-Pb-Sr-Nd isotopic study of the sill-dominated intrusive complex of the Franklin Large Igneous Province, Victoria Island, Arctic Canada. Unpublished M.Sc. thesis, University of Bristol, United Kingdom. p. 1-53.

Beccaluva, L., Biachini, G., Natali, C. & Siena, F. (2009) Continental flood basalts and mantle plumes: a case study of the northern Ethiopian Plateau. *Journal of Petrology* **50**(7), 1377-1403.

Bédard, J. H., Rainbird, R. H., Dewing, K., Hadlari, T., Hayes, B., Naslund, H. R., Steigerwaldt, K., Macdonald, W., Carpenter, J., Hryciuk, M., Prince, J., Wing, B., Dell'Oro, T., Weis, D., Scoates, J., Williamson, N., Cousens, B., Nabelek, P., Winpenny, A., Beard, C., Ootes, L., Thomson, D., Mathieu, J., Durbano, A., Turner, E., Krapez, B., Pratt, B., Currie, L., Williamson, M.-C. & Girard, É. (2011a) Evolution of a Neoproterozoic platform and continental flood basalt province - The Franklin sills and Natkusiak lavas of Victoria Island, implications for Ni-PGE mineralization, In: *39th Annual Yellowknife Geoscience Forum,* November 15-17, 2011. pp. 21-22.

Bédard, J. H., Williamson, N., Dell'Oro, T. A., Hayes, B., Hryciuk, M., Winpenny, A., Scoates, J. S., Weis, D. A., Nabelek, P. I., Naslund, H. R. & MacDonald, W. D. (2011b) Emplacement and eruption style in the Franklin large igneous province, Victoria Island, Arctic Canada, *American Geophysical Union*, Fall Meeting 2011, December 5-9, San Francisco, abstract #V21F-02.

Bédard, J. H., Naslund, H. R., Nabelek, P., Winpenny, A., Hryciuk, M., Macdonald, W., Hayes, B., Steigerwaldt, K., Hadlari, T., Rainbird, R., Dewing, K. & Girard, E. (2012a) Fault-mediated melt ascent in a Neoproterozoic continental flood basalt province, the Franklin sills, Victoria Island, Canada. *Geological Society of America Bulletin* **124**, 723-736.

Bédard, J. H., Dell'Oro, T., Weis, D., Scoates, J. S., Williamson, N., Cousens, C., Naslund, H. R., Hayes, B., Hryciuk, M., Wing, B. & Beard, C. (2012b) The Neoproterozoic Franklin large igneous province, geochemical and isotopic evidence for changing sources, and linkages between intrusive and extrusive components. *22nd V. M. Goldschmidt Conference*, June 24-29, Montreal, Canada, abstract, session 4g p282.

Bettison-Varga, L. & Mackinnon, I.D. (1997) The role of randomly mixed chlorite/smectite in the transformation of smectite to chlorite. *Clays and Clay Minerals* **45**, 506-516

Bevins, R., Robinson, D. & Rowbotham, G. (1991) Compositional variations in mafic phyllosilicates from regional low-grade metabasites and application of the chlorite geothermometer. *Journal of Metamorphic Geology* **9**, 711-727.

Bryan, S. E. & Ernst, R. (2008) Revised definition of Large Igneous Provinces (LIPs). *Earth-Science Reviews* **86**, 175-202.

Buchan, K. L., Ernst, R. E., Bleeker, W., Davis, W.J., Villeneuve, M., van Breemen, O., Hamilton, M. A. & Söderlund, U. (2010) Proterozoic Magmatic Events of the Slave Craton, Wopmay Orogen and environs; *Geological Survey of Canada*, Open File 5985, 1 poster + 25p. report.

Camp, V. & Ross, M. (2004) Mantle dynamics and genesis of mafic magmatism in the intermontane Pacific Northwest. *Journal of Geophysical Research* **109**, doi: 10.1029/2003JB002838

Campbell, I. H. & Griffiths, R. W. (1990) Implications of mantle plume structure for the evolution of flood basalts. *Earth and Planetary Science Letters* **99**, 79-93.

Campbell, I. H. (2005) Large igneous provinces and the mantle plume hypothesis. *Elements* **1**, 265-269.

Carlson, R. W. (1991) Physical and chemical evidence on the cause and source characteristics of flood basalt volcanism. *Australian Journal of Earth Sciences* **38**, 525-544.

Cathelineau, M. & Nieva, D. (1985) A chlorite solid solution geothermometer: The Los Azufres (Mexico) geothermal system. *Contributions to Mineralogy and Petrology* **91**, 235-234.

Chakrabarti, R., Basu, A., Santo, A., Tedescco, D. & Vaselli, O. (2009) Isotopic and geochemical evidence for a heterogeneous mantle plume origin of the Virunga volcanics, Western rift, East African Rift system. *Chemical Geology* **259**, 273-289.

Coffin, M. F., Duncan, R., Eldholm, O., Fitton, J. G., Frey, F., Larson, H. C., Mahoney, J., Saunders, A., Schlich, R. & Wallace, P. (2006) Large igneous provinces and scientific ocean drilling. *Oceanography* **19**(4), 150-160.

Coffin, M. F. & Eldholm, O. (1994) Large igneous provinces: crustal structure, dimensions, and external consequences. *Reviews of Geophysics* **32**, 1-36.

Courtillot, V., Besse, J., Vandamme, D., Montigny, R., Jaeger, J. & Cappetta, H. (1986) Deccan flood basalts at the Cretaceous/Tertiary boundary? *Earth and Planetary Science Letters* **80**, 361-374.

Courtillot, V., Fluteau, F., Chenet, A. & Moulin, M. (2010) Environmental impact of subaerial large igneous provinces: the latest on the case of the Deccan and Karoo traps. *EGU General Assembly 2010*, 2-7 May 2010, Vienna, Austria, p. 4027.

Cox, K.G. & Hawkesworth, C. J., (1984) Relative contribution of crust and mantle to flood basalt magmatism, Mahabaleshwar area, Deccan Traps. *Philosophical Transactions of the Royal Society of London* **310**, 627-641.

Dalziel, I. W., Lawver, L. A. & Murphy, J. B. (2000) Plumes, orogenesis, and supercontinental fragmentation. *Earth and Planetary Science Letters* **178**, 1-11.

Davis, W. J., Jones, A. G., Bleeker, W. & Grutter, H. (2003) Lithosphere development in the Slave craton: a linked crustal and mantle perspective. *Lithos* **71**, 575-589.

Deenen, M. H. L., Ruhl, M., Bonis, N. R., Krijgsman, W., Kuerschner, W. M., Reitsma, M. & Bergen, M. J. (2010) A new chronology for the end-Triassic mass extinction. *Earth and Planetary Science Letters* **291**, 113-125.

Deer, W. A., Howie, R. A., & Zussman, J. (1992) An Introduction to the Rock-Forming Minerals. 2nd edition. *Pearson Education Limited*. Harlow, England. p. 332-343.

DePaolo, D. & Weis, D. (2007) Hotspot volcanoes and large igneous provinces, In: Harms, U., C. Koeberl, and M. Zoback (eds.), *Continental Scientific Drilling: A Decade of Progress, and Challenges for the Future*, Berlin Heidelberg: Springer, 259-288.

DePaolo, D. J. (1981) Trace element and isotopic effects of combined wallrock assimilation and fractional crystallization. *Earth and Planetary Science Letters* **53**, 189-202.

Devey, C. W. & Cox, K. G. (1987) Relationships between crustal contamination and crystallization in continental flood basalt magmas with special reference to the Deccan Traps of the Western Ghats, India. *Earth and Planetary Science Letters* **84**, 59-68.

Dostal, J., Baragar, W. R. & Dupuy, C. (1986) Petrogenesis of the Natkusiak continental basalts, Victoria Island, Northwest Territories, Canada. *Canadian Journal of Earth Sciences* **23**, 622-632.

Duncan, R. A. & Richards, M. A. (1991) Hotspots, mantle plumes, flood basalts, and true polar wander. *Reviews of Geophysics* **29**, 31-50.

Dupuy, C., Michard, A., Dostal, J., Dautel, D., & Baragar, W. R. (1995) Isotope and trace-element geochemistry of Proterozoic Natkusiak flood basalts from the northwestern Canadian Shield. *Chemical Geology* **120**, 15-25.

Durbano, A., Pratt, B., Hadlari, T. & Dewing, K., 2010. Sedimentology and stratigraphy of the Lower Clastic Unit of the Cambrian, Northwest Victoria Island, *38th Annual Yellowknife Geoscience Forum*, November 16-18, 2010. pp. 73-74.

Egger, H. & Brückl, E. (2006) Gigantic volcanic eruptions and climatic change in the early Eocene. *International Journal of Earth Science* **95**, 1065-1070.

Ernst, R. E., Buchan, K. L. & Campbell, I. H. (2005) Frontiers in large igneous province research. *Lithos* **79**, 271-297.

Escuder-Virueta, J., Perez-Estaun, A., Contreras, F., Joubert, M., Weis, D., Ullrich, T. & Spadea, P. (2007) Plume mantle source heterogeneity through time: Insights from the Duarte Complex, Hispaniola, northeastern Caribbean. *Journal of Geophysical Research* **112**, doi:10.1029/2006JB004323.

Fahrig, W. F., Irving, E. & Jackson, G. D. (1971) Paleomagnetism of the Franklin diabases. *Canadian Journal of Earth Sciences* **8**, 455-467.

Farmer, G. L. (2003) Continental basaltic rocks, In: *Treatise on Geochemistry, Volume 3: The Crust*, edited by Holland, H. & Turekian, K., pp. 85-121, Elsevier Ltd.

Foulger, G. R. (2007) The "plate" model for the genesis of melting anomalies, In: Foulger, G. R., & Jurdy, D. M., eds., Plates, Plumes, and Planetary processes: *Geological Society of America Special Paper* **430**, p. 1-28, doi: 10.1130/2007.2430(01).

Frey, F.A., Weis, D., Borisova, A.Y. & Xu, G. (2002) Involvement of continental crust in the formation of the Cretaceous Kerguelan Plateau: New perspectives from ODP Leg 120 sites. *Journal of Petrology* **43**(7), 1207-1239.

Galer, S. J. G. & Abouchami, W. (1998) Practical application of lead triple spiking for correction of instrumental mass discrimination. *Mineralogical Magazine* **62A**, 491-492. doi:10.1180/minmag.1998.62A.1.260.

Gallagher, K. & Hawkesworth, C. (1992) Dehydration melting and the generation of continental flood basalts. *Nature* **358**, 57-59.

Garfunkel, Z. (2008) Formation of continental flood volcanism – The perspective of setting of melting. *Lithos* **100**, 49-65.

Greene, A. R., Scoates, J. S. & Weis, D. (2008) Wrangellia flood basalts in Alaska: A record of plume-lithosphere interaction in a Late Triassic accreted oceanic plateau. *Geochemistry Geophysics Geosystems* **9**(12) Q12004, doi:10.1029/2008GC002092.

Greene, A. R., Scoates, J. S., Weis, D. & Israel, S. (2009) Geochemistry of Triassic flood basalts from the Yukon (Canada) segment of the accreted Wrangellia oceanic plateau. *Lithos* **110**, 1-19.

Griselin, M., Arndt, N. & Baragar, W. R. (1997) Plume-lithosphere interaction and crustal contamination during formation of Coppermine River basalts, Northwest Territories, Canada. *Canadian Journal of Earth Sciences* **34**, 958-975.

Hanano, D., Scoates, J. & Weis, D. (2009) Alteration mineralogy and the effect of acid-leaching on the Pb-isotope systematics of ocean-island basalts. *American Mineralogist* **94**, 17-26.

Hart, S. R., Erlank, A. J. & Kable, E. J. D. (1974) Sea floor basalt alteration: some chemical and Sr isotopic effects. *Contributions to Mineralogy and Petrology* **44**, 219-230.

Hart, S. R., Hauri, E. H., Oschmann, L. A. & Whitehead, J. A. (1992) Mantle plumes and entrainment: isotopic evidence. *Science* **256**, 517-520.

Hawkesworth, C. J. & Morrison, M. A. (1978) A reduction in $^{87}Sr/^{86}Sr$ during basalt alteration. *Nature* **276**, 381-383.

Hawkesworth, C. J., Gallagher, K., Kirstein, L., Mantovani, M., Peate, D. W. & Turner, S. P. (2000) Tectonic controls on magmatism associated with continental break-up: an example from the Parana-Etendeka Province. *Earth and Planetary Science Letters* **179**, 335-349.

Hawkesworth, C. J. & Schersten, A. (2007) Mantle plumes and geochemistry. *Chemical Geology* **241**, 319-331.

Head, J. W. & Coffin, M. F. (1997) Large igneous provinces: a planetary perspective, In: Mahoney, J.J. & Coffin, M.F. (eds.) (1997) *Large Igneous Provinces: Continental, Oceanic, and Planetary Flood Volcanism*. AGU Geophysical Monograph 100, pp. 411-438.

Heaman, L. M, LeCheminant, A. N. & Rainbird, R. H. (1992) Nature and timing of Franklin igneous events, Canada, implications for a late Proterozoic mantle plume and the break-up of Laurentia. *Earth and Planetary Science Letters* **109**, 117-131.

Hergt, J .M., Peate, D. W. & Hawkesworth, C. J. (1991) The petrogenesis of Mesozoic Gondwana low-Ti flood basalts. *Earth and Planetary Science Letters* **105**, 134-148.

Herzberg, C. & O'Hara, M. J. (2002) Plume-associated ultramafic magmas of Phanerozoic age. *Journal of Petrology* **43**(10), 1857-1883.

Herzberg, C. (1995) Generation of plume magmas through time: an experimental perspective. *Chemical Geology* **126**, 1-16.

Herzberg, C. & Gazel, E. (2009) Petrological evidence for secular cooling in mantle plumes. *Nature* **458**, 619-622.

Herzberg, C. (2011) Basalts as temperature probes of Earth's mantle. *Geology* **39**(12), 1179-1180.

Higgins, M. D. (2000) Measurements of crystal size distributions. *American Mineralogist* **85**, 1105-1116.

Higgins, M. D. (2011) CSDCorrections$^{©}$ software, version 1.3.9.5.

Hoernle, K., Hauff, F. & Bogaard, P. (2004) 70 m.y. history (139–69 Ma) for the Caribbean large igneous province. *Geology* **32**, 697-700.

Hoffman, P. F. & Schrag, D. P. (2002) The snowball earth hypothesis: testing the limits of global change. *Terra Nova* **14**, 129-155.

Hoffman, P. F., Kaufman, A. J., Halverson, G. P. & Schrag, D. (1998) A Neoproterozoic snowball earth. *Science* **281**, 1342-1346.

Hofmann, A. W. (1988) Chemical differentiation of the Earth: the relationship between, continental crust, and oceanic crust. *Earth and Planetary Science Letters* **90**, 297-314.

Hofmann, A. W. (1997) Mantle geochemistry: the message from oceanic volcanism. *Nature* **385**, 219-229.

Hofmann, A. W. (2003) Sampling mantle heterogeneity through oceanic basalts: isotopes and trace elements, In: *Treatise on Geochemistry, Volume 2: The Mantle and Core*, edited by Holland, H. & Turekian, K., pp. 61-101, Elsevier Ltd.

Hofmann, A. W. & Rainbird, R. (1994) Carbonaceous megafossils from the Neoproterozoic Shaler Supergroup of Arctic Canada. *Paleontology* **37**, 721-731.

Hon, K., Kauahikaua, J., Denlinger, R. & MacKay, K. (1994) Emplacement and inflation of pahoehoe sheet flows: Observations and measurements of active lava flows on Kilauea Volcano, Hawaii. *Geological Society of America Bulletin* **106**, 351-370.

Hulbert, L. T., Rainbird, R. W., Jefferson, C. W. & Friske, P. (2005) Map of mafic and ultramafic bodies related to the Franklin magmatic event, Minto Inlier, Victoria Island. *Geological Survey of Canada* Open-File Map 4928, map sheet scale 1:100,000 + CD-ROM.

Hyde, W. T., Crowley, T. J., Baum, S. K. & Petler, W. R. (2000) Neoproterozoic 'snowball Earth' simulations with a coupled climate/ice-sheet model. *Nature* **405**, 425-429.

Jackson, M. & Carlson, R. W. (2011) An ancient recipe for flood-basalt genesis. *Nature* **476**, 316-320.

Jackson, M. & Dasgupta, R. (2008) Compositions of HIMU, EM1, and EM2 from global trends between radiogenic isotopes and major elements in ocean island basalts. *Earth and Planetary Science Letters* **276**, 175-186.

Jay, A. & Widdowson, M. (2008) Stratigraphy, structure and volcanology of the SE Deccan continental flood basalt province: implications for eruptive extent and volumes. *Journal of the Geological Society of London* **165**, 177-188.

Jefferson, C. (1985) Uppermost Shaler Group and its contact with the Natkusiak Basalts, Victoria Island, District of Franklin, in: *Current Research*, Part A: Geological Survey of Canada Paper **85-1A**, 103-110.

Jefferson, C., Nelson, W., Kirkham, R., Reedman, J. & Scoates, R. (1985) Geology and copper occurrences of the Natkusiak basalts, Victoria Island, District of Franklin, in: *Current Research*, Part A: Geological Survey of Canada Paper **85-1A**, 203-214.

Jefferson, C., Hulbert, L. & Rainbird, R. (1994) Mineral resource assessment of the Neoproterozoic Franklin igneous events of Arctic Canada: Comparison with the Permo-Triassic Noril'sk-Talnakh Ni-Cu-PGE deposits of Russia. *Open File* **2789** Geological Survey of Canada.

Jellinek, A. M. & Manga, M. (2004) Links between long-lived hot spots, mantle plumes, D", and plate tectonics. *Reviews of Geophysics* **42**(3), RG3002, doi: 10.1029/2003RG000144.

Jerram, D. A., Mountney, N. P., Howell, J. A., Long, D. & Stollhofen, H. (2000) Death of a sand sea: an active aeolian erg systematically buried by the Etendeka flood basalts of NW Namibia. *Journal of the Geological Society, London* **157**, 513-516.

Jerram, D. & Widdowson, M. (2005) The anatomy of continental flood basalt provinces: geological constraints on the processes and products of flood volcanism. *Lithos* **79**, 385-405.

Jolley, D. & Widdowson, M. (2005) Did Paleogene North Atlantic rift-related eruptions drive early Eocene climate cooling? *Lithos* **79**, 355-366.

Jones, D. S., Maloof, A. C., Hurtgen, M. T., Rainbird, R. H. & Schrag, D. P. (2010) Regional and global chemostratigraphic correlation of the early Neoproterozoic Shaler Supergroup, Victoria Island, Northwestern Canada. *Precambrian Research* **181**, 43-63.

Jourdan, F., Bertrand, H., Scharer, U., Blichert-Toft, J., Feraud, G. & Kampunzu, A. B. (2007) Major and trace element and Sr, Nd, Hf, and Pb isotope compositions of the Karoo large igneous province, Botswana-Zimbabwe: lithosphere vs mantle plume contribution. *Journal of Petrology* **48**(6) 1043-1077.

Kawahata, H., Kusakabe, M. & Kikuchi, Y. (1987) Strontium, oxygen, and hydrogen isotope geochemistry of hydrothermally altered and weathered rocks in DSDP Hole 504B, Costa Rica Rift. *Earth and Planetary Science Letters* **85**(4), 343-355.

Keays, R. & Lightfoot, P. C. (2010) Crustal sulfur is required to form magmatic Ni–Cu sulfide deposits: evidence from chalcophile element signatures of Siberian and Deccan Trap basalts. *Mineralium Deposita* **45**, 241-257.

Kerr, A, Saunders, A., Tarney, J., Berry, N. & Hards, V. (1995) Depleted mantle-plume geochemical signatures: No paradox for plume theories. *Geology* **23**, 843-846.

Keir, D., Belachew, M., Ebinger, C.J., Kendall, J.-M., Hammond, J.O.S., Stuart, G.W., Ayele, A. & Rowland, J.V. (2011) Mapping the evolving strain field during continental breakup from crustal anisotropy in the Afar depression. *Nature Communications* **2:285**, DOI: 10.1038/ncomms1287.

Kempton, P. D., Fitton, J. G., Saunders, A. D., Nowell, G. M., Taylor, R. N., Hardarson, B. S. & Pearson, G. (2000) The Iceland plume in space and time: a Sr-Nd-Pb-Hf study of the North Atlantic rifted margin. *Earth and Planetary Science Letters* **177**, 255-271.

Kieffer, B., Arndt, N., Lapierre, H., Bastien, F., Bosch, D., Pecher, A., Yirgu, G., Ayalew, D., Weis, D., Jerram, D., Keller, F. & Meugniot, C. (2004) Flood and shield basalts from Ethiopia: Magmas from the African Superswell. *Journal of Petrology* **45**(4), 793-834.

Kolebaba, M., Read, G., Kahlert, B. & Kelsch, D. (2003) Diamondiferous kimberlites on Victoria Island, Canada: A northern extension of the Slave Craton, in: *8th International Kimberlite Conference*, 2003, Fort á la Corne, Sasketchewan, Canada. pp. 1-4.

Le Bas, M. J., Le Maitre, R. W., Streckeisen, A. & Zanettin, B. (1986) A chemical classification of volcanic rocks based on the total alkali-silica diagram. *Journal of Petrology* **27**, 745-750.

Le Bas, M. J. (2000) IUGS Reclassification of the high-Mg and picritic volcanic rocks. *Journal of Petrology* **41**(10), 1467-1470.

Lightfoot, P. C., Naldrett, A. J., Gorbachev, N. S., Doherty, W. & Fedorenko, V. A. (1990) Geochemistry of the Siberian Trap of the Noril'sk area, USSR, with implications for the relative contributions of crust and mantle to flood basalt magmatism. *Contributions to Mineralogy and Petrology* **104**, 631-644.

Lin, S. -C. & Keken, P. (2005) Multiple volcanic episodes of flood basalts caused by thermochemical mantle plumes. *Nature* **436**, 250-252.

Liou, J. (1979) Zeolite facies metamorphism of basaltic rocks from the East Taiwan Ophiolite. *American Mineralogist* **64**, 1-14.

Liou, J., Maruyama, S. & Cho, M. (1987) Very low-grade metamorphism of volcanic and volcaniclastic rocks- mineral assemblages and facies. *Low Temperature Metamorphism* **1987**, 59-113.

Li, Z. X., Bogdanova, S. V., Collins, A. S., Davidson, A., De Waele, B., Ernst, R.E., Fitzsimons, I. C. W., Fuck, R. A., Gladkochub, D. P., Jacobs, J., Karlstrom, K. E., Lu, S., Natapov, L. M.,

Pease, V., Pisarevsky, S. A., Thrane, K. & Vernikovsky, V. (2008) Assembly, configuration, and break-up history of Rodinia: A synthesis. *Precambrian Research* **160**, 179-210.

Lyubetskaya, T. & Korenaga, J. (2007) Chemical composition of Earth's primitive mantle and its variance: 2. Implications for global geodynamics. *Journal of Geophysical Research* **112**, doi:10.1029/2005JB004224.

MacDonald, F., Schmitz, M. D., Crowley, J. L., Roots, C. F., Jones, D. S., Maloof, A. C., Strauss, J. V., Cohen, P. A., Johnston, D. T. & Schrag, D. P. (2010) Calibrating the Cryogenian. *Science* **327**, 1241-1243.

Mahoney, J. J. & Coffin, M. F. (eds.) (1997) Large Igneous Provinces: Continental, Oceanic, and Planetary Flood Volcanism. *AGU Geophysical Monograph* **100**. 438 pp.

Marsh, J. S., Ewart, A., Milner, S. C., Duncan, A. R. & Miller, R. (2001) The Etendeka igneous province: magma types and their stratigraphic distribution with implications for the evolution of the Parana-Etendeka flood basalt province. *Bulletin of Volcanology* **62**, 464-486.

Marques, L. S., Dupre, B. & Piccirillo, E. M. (1999) Mantle source compositions of the Parana Magmatic Province (southern Brazil): evidence from trace element and Sr-Nd-Pb isotope geochemistry. *Journal of Geodynamics* **28**, 439-458.

McClintock, M. & White, J. (2006) Large phreatomagmatic vent complex at Coombs Hills, Antarctica: Wet, explosive initiation of flood basalt volcanism in the Ferrar-Karoo LIP. *Bulletin of Volcanology* **68**, 215-239.

McDonough, W. F. & Sun., S. S. (1995) The composition of the Earth. *Chemical Geology* **120**, 223-253.

Melluso, L., Mahoney, J. & Dallai, L. (2006) Mantle sources and crustal input as recorded in high-Mg Deccan Traps basalts of Gujarat (India). *Lithos* **89**, 259-274.

Meyer, R., Hertogen, J., Pedersen, R. B., Viereck-Gotte, L. & Abratis, M. (2009) Interaction of mantle derived melts with crust during the emplacement of the Vøring Plateau, N.E. Atlantic. *Marine Geology* **261**, 3-16.

Millet, M., Doucelance, R., Schiano, P., David, K. & Bosq, C. (2008) Mantle plume heterogeneity versus shallow-level interactions: A case study, the Sao Nicolau Island, Cape Verde archipelago. *Journal of Volcanology and Geothermal Research* **176**, 265-276.

Montelli, R., Nolet, G., Dahlen, F. A., Masters, G., Engdahl, E. R. & Hung, S. (2004) Finite-frequency tomography reveals a variety of plumes in the mantle. *Science* **303**, 338-343.

Morgan, J. P. & Morgan, W. J. (1999) Two-stage melting and the geochemical evolution of the mantle: a recipe for mantle plum-pudding. *Earth and Planetary Science Letters* **170**, 215-239.

Morgan, W. J. (1971) Convection plumes in the lower mantle. *Nature* **230**, 42-43.

Morgan W. J. (1972) Deep mantle convection plumes and plate motions. *American Association of Petroleum Geologists Bulletin* **56**(2), 203-213.

Neal, C. R., Mahoney, J. J. & Chazey, W. J. (2002) Mantle sources and the highly variable role of continental lithosphere in basalt petrogenesis of the Kerguelen Plateau and Broken Ridge LIP: results from ODP Leg 183. *Journal of Petrology* **43**(7), 1177-1205.

Neuhoff, P., Rogers, K., Stannius, L., Bird, D. & Pedersen, A. (2006) Regional very low-grade metamorphism of basaltic lavas, Disko–Nuussuaq region, West Greenland. *Lithos* **92**, 33-54.

Nobre Silva, I. G., Weis, D., Barling, J. & Scoates, J. S. (2009) Leaching systematics and matrix elimination for the determination of high-precision Pb isotope compositions of ocean island basalts. *Geochemistry Geophysics Geosystems* **10**(8), Q08012, doi:10.1029/2009GC002537.

Nobre Silva, I.G., Weis, D. & Scoates, J. S. (2010) Effects of acid leaching on the Sr-Nd-Hf isotopic compositions of ocean island basalts: *Geochemistry Geophysics Geosystems* **11**(9) Q09011, doi:10.1029/2010GC003176.

Patchett, P. J. & Tatsumoto, M. (1981) A routine high-precision method for Lu-Hf isotope geochemistry and chronology. *Contributions to Mineralogy and Petrology* **75**, 263-267.

Peate, D., Barker, A., Riishuus, M. & Andreasen, R. (2008) Temporal variations in crustal assimilation of magma suites in the East Greenland flood basalt province: Tracking the evolution of magmatic plumbing systems. *Lithos* **102**, 179-197.

Peate, D. W. (1997) The Parana-Etendeka Province, In: Mahoney, J.J. & Coffin, M.F. (eds.) (1997) *Large Igneous Provinces: Continental, Oceanic, and Planetary Flood Volcanism.* AGU Geophysical Monograph 100, pp. 217-245.

Pehrsson, S. & Buchan, K., (1999) Borden dykes of Baffin Island, Northwest Territories: a Franklin U–Pb baddeleyite age and a paleomagnetic reinterpretation. *Canadian Journal of Earth Sciences* **36**, 65-73.

Pelechaty, S. M. (1996) Stratigraphic evidence for the Siberia-Laurentia connection and Early Cambrian rifting. *Geology* **24**, 719-722.

Peng, Z. X., Mahoney, J., Hooper, P., Harris, C. & Beane, J. (1994) A role for lower continental crust in flood basalt genesis? Isotopic and incompatible element study of the lower six formations of the western Deccan Traps. *Geochimica et Cosmochimica Acta* **58**, 267-288.

Perry, F. Baldridge, W. S. & DePaolo, D. (1987) Role of asthenosphere and lithosphere in the genesis of late Cenozoic basaltic rocks from the Rio Grande rift and adjacent regions of the southwestern United States. *Journal of Geophysical Research* **92**, 9193-9213.

Pik, R., Deneil, C., Coulin, C., Yirgu, G. & Marty, B. (1999) Isotopic and trace element signatures of Ethiopian flood basalts: evidence for plume-lithosphere interactions. *Geochimica et Cosmochimica Acta* **63**(15), 2263-2279.

Pik, R., Marty, B. & Hilton, D. R. (2006) How many mantle plumes in Africa? The geochemical point of view. *Chemical Geology* **226**, 100-114.

Pisarevsky, S. A., Natapov, L. M., Donskaya, T. V., Gladkochub, D. P. & Vernikovsky, V. A. (2008) Proterozoic Siberia: A promontory of Rodinia. *Precambrian Research* **160**, 66-76.

Pollack, J., Toon, O., Sagan, C., Summers, A., Baldwin, B. & Camp, W. (1976) Volcanic explosions and climatic change: a theoretical assessment. *Journal of Geophysical Research* **81**(6), 1071-1083.

Rainbird, R. H. (1993) The sedimentary record of mantle plume uplift preceding eruption of the Neoproterozoic Natkusiak flood basalt. *The Journal of Geology* **101**, 305-318.

Rainbird, R. H., Jefferson, C. W. & Young, G. M. (1996) The early Neoproterozoic sedimentary Succession B of northwestern Laurentia: correlations and paleogeographic significance. *Geological Society of America Bulletin* **108**, 454-470.

Rainbird, R. H. & de Freitas, T. A. (1997) Stratigraphic evidence for the Siberia–Laurentia connection and Early Cambrian rifting. Comment, *Geology* **25**, 569–570.

Raczek, I., Stoll, B., Hofmann, A. W. & Jochum, K. P. (2001) High-precision trace element data for the USGS reference materials BCR-1, BCR-2, BHVO-1, BHVO-2, AGV-1, AGV-2, DTS-1, DTS-2, GSP-1 and GSP-2 by ID-TIMS and MIC-SSMS. *Geostandards Newsletter* **25**, 77-86.

Rasband, W. (2012) ImageJ[©] software, version 1.45s.

Rampone, E. & Hofmann, A. (2012) A global overview of isotopic heterogeneities in the oceanic mantle. *Lithos* **148**, 247-261.

Reichow, M., Saunders, A. D., White, R. V., Mukhamedov, A. I. & Medvedev, A. (2005) Geochemistry and petrogenesis of basalts from the West Siberian Basin: an extension of the Permo-Triassic Siberian Traps, Russia. *Lithos* **79**, 425-452.

Renac, C., Kyser, K., Bowden, P., Moine, B. & Cottin, J. (2009) Hydrothermal fluid interaction in basaltic lava units, Kerguelen Archipelago (SW Indian Ocean). *European Journal of Mineralogy* **22**, 215-234.

Richards, M. A., Duncan, R. A. & Courtillot, V. E. (1989) Flood basalts and hot-spot tracks: Plume heads and tails. *Science* **246**, 103-107.

Ridley, V. A. & Richards, M. A. (2010) Deep crustal structure beneath large igneous provinces and the petrologic evolution of flood basalts. *Geochemistry Geophysics Geosystems* **11**(9), Q09006, doi:10.1029/2009GC002935

Rudnick, R. L. & Gao, S. (2003) Composition of the continental crust, in: The Crust, Vol. 3, *Treatise on Geochemistry*, edited by Holland, H. & Turekian, K.,, pp. 1-64, Elsevier Ltd.

Said, N. & Kerrich, R. (2009) Geochemistry of coexisting depleted and enriched Paringa Basalts, in the 2.7 Ga Kalgoorlie Terrane, Yilgarn Craton, Western Australia: Evidence for a heterogeneous mantle plume event. *Precambrian Research* **174**, 287-309.

Salters, V. & Stracke, A. (2004) Composition of the depleted mantle. *Geochemistry Geophysics Geosystems* **5**(5), Q05004, doi:10.1029/2003GC000597.

Saunders, A., Fitton, J. G., Kerr, A. C., Norry, M. J. & Kent, R. W. (1997) The North Atlantic Igneous Province, In: Mahoney, J.J. & Coffin, M.F. (eds.) (1997) *Large Igneous Provinces: Continental, Oceanic, and Planetary Flood Volcanism*. AGU Geophysical Monograph 100, pp. 45-93.

Saunders, A. (2005) Large igneous provinces: origin and environmental consequences. *Elements* **1**, 259-263.

Schiffman, P. & Fridleifsson, G. (1991) The smectite-chlorite transition in drillhole N 1-15, Nesjavellir geothermal field, Iceland: XRD, BSE and electron microprobe investigations. *Journal of Metamorphic Geology* **9**, 679-676.

Schlische, R. W., Withjack, M. O. & Olsen, P. E. (2002) Relative timing of CAMP, rifting, continental breakup, and basin inversion: Tectonic significance, in: Hames, W. E., McHone, G. C., Renne, R .P., & Ruppel, C. R. (eds.), The Central Atlantic Magmatic Province: Insights from Fragments of Pangea, *American Geophysical Union Monograph*, **136**, 33-59.

Schmidt, S. (1993) Regional and local patterns of low grade metamorphism in the North Shore Volcanic group, Minnesota, USA. *Journal of Metamorphic Geology* **11**, 401-414.

Schulte, P., Alegret, L., Arenillas, I., Arz, J., Barton, P. R., Bown, P., Brawlower, T. J., Christeson, G. L., Claeys, P., Cockell, C. S., Collins, G. S., Deutsch, A., Goldin, T. J., Goto, K., Grajales-Nishimura, J. M., Grieve, R. A. F., Gulick, S. P. S., Johnson, K. R., Kiessling, W., Koeberl, C., Kring, D., MacLeod, K., Matsui, T., Melosh, J., Montanari, A., Morgan, J. V., Neal, C.R., Nichols, D. J., Norris, R. D., Pierazzo, E., Ravizza, G., Rebolledo-Vieyra, M., Reimold, W.U., Robin, E., Salge, T., Speijer, R. P., Sweet, A. R., Urrutia-Fucugauchi, J., Vajda, V., Whalen, M. & Willumsen, P. S. (2010) The Chicxulub asteroid impact and mass extinction at the Cretaceous-Paleogene boundary. *Science* **327**, 1214-1218.

Self, S., Thordarson, T. & Widdowson, M. (2005) Gas fluxes from flood basalt eruptions. *Elements* **1**, 283-287.

Self, S., Keszthelyi, L. & Thordarson, T. (1998) The importance of pahoehoe. *Annual Review of Earth and Planetary Science* **26**, 81-110.

Self, S., Thordarson, T. & Keszthelyi, L. (1997) Emplacement of continental flood basalt lava flows, In: Mahoney, J. J. & Coffin, M. F. (eds.) (1997) *Large Igneous Provinces: Continental, Oceanic, and Planetary Flood Volcanism*. AGU Geophysical Monograph 100, pp. 381-410.

Sevigny, J., Whitechurch, H., Storey, M. & Salters, V. (1992) Zeolite-facies metamorphism of central Kerguelen Plateau Basalts. *Proceedings of the Ocean Drilling Program, Scientific Results* **120**, 63-69.

Sharma, M., Basu, A. & Nesterenko, G. V. (1992) Temporal Sr-, Nd- and Pb-isotopic variations in the Siberian flood basalts: Implications for the plume-source characteristics. *Earth and Planetary Science Letters* **113**, 365-381.

Sharma, M. (1997) Siberian Traps, In: Mahoney, J. J. & Coffin, M. F. (eds.) (1997) *Large Igneous Provinces: Continental, Oceanic, and Planetary Flood Volcanism.* American Geophysical Union Geophysical Monograph 100, pp. 273-295.

Shea, T. Houghton, B., Gurioli, L., Cashman, K., Hammer, J. & Hobden, B. (2010) Textural studies of vesicles in volcanic rocks: An integrated methodology. *Journal of Volcanology and Geothermal Research* **190**, 271-289.

Shellnut J., Dostal, J. & Keppie, J. (2004) Petrogenesis of the 723 Ma Coronation sills, Amundsen basin, Arctic Canada, implications for the break-up of Rodinia. *Precambrian Research* **129**, 309-324.

Shellnut, J. & Jahn, B. (2011) Origin of Late Permian Emeishan basaltic rocks from the Panxi region (SW China): Implications for the Ti-classification and spatial-compositional distribution of the Emeishan flood basalts. *Journal of Volcanology and Geothermal Research* **199**, 85-95.

Sheth, H. (2007) 'Large Igneous Provinces (LIPs)': Definition, recommended terminology, and a hierarchical classification. *Earth-Science Reviews* **85**, 117-124.

Søager, N. & Holm, P. (2011) Changing compositions in the Iceland plume: Isotopic and elemental constraints from the Paleogene Faroe flood basalts. *Chemical Geology* **280**, 297-313.

Sobolev, S., Sobolev, A., Kuzmin, D., Krivolutskaya, N., Petrunin, A., Arndt, N., Radko, V. & Vasiliev, Y. (2011) Linking mantle plumes, large igneous provinces and environmental catastrophes. *Nature* **477**, 312-316

Stracke, A. & Hofmann, A. W. (2005) FOZO, HIMU, and the rest of the mantle zoo. *Geochemistry Geophysics Geosystem* **6**(5), Q05007, doi:10.1029/2004GC000824.

Sun, S. -s. & McDonough, W. F. (1989) Chemical and isotopic systematics of oceanic basalts: implications for mantle composition and processes, from: Saunders, A. D. & Norry, M. J. (eds), 1989, Magmatism in the Ocean Basins, *Geological Society Special Publication* **42**, 313-354.

Tatsumi, Y. (2005) The subduction factory: How it operates in the evolving Earth. *GSA Today* **15**(7), 4-10.

Tejada, M. L. G., Mahoney, J. J., Castillo, P. R., Ingle, S. P., Sheth, H. C. & Weis, D. (2004) Mahoney, J. J., Wallace, P. J., & Saunders, A. D., (eds.) 2004. Origin and evolution of the Ontong Java Plateau. *Geological Society of London, Special Publications* **229**, 133-150.

Thordarson, T. & Self, S. (1998) The Roza Member, Columbia River Basalt Group: A gigantic pahoehoe lava flow field formed by endogenous processes? *Journal of Geophysical Research* **103**, 27,411-27,445.

Thorsteinsson, R. & Tozer, E. T. (1962) Banks, Victoria and Stefansson Islands, Arctic Archipelago. *Geological Survey of Canada Memoir* **85p**.

Verma, S. (1992) Seawater alteration effects on REE, K, Rb, Cs, Sr, U, Th, Pb, and Sr-Nd-Pb isotope systematics of Mid-Ocean-Ridge-Basalt. *Geochemical Journal* **26**, 159-177.

Walker, G. (1960) Zeolite zones and dike distribution in relation to the structure of the basalts of Eastern Iceland. *Journal of Geology* **68**(5), 515-527.

Walker, G. (1991) Structure, and origin by injection of lava under surface crust, of tumuli, "lava rises", "lava-rise pits", and "lava-inflation clefts" in Hawaii. *Bulletin of Volcanology* **53**, 546-558.

Weis, D., Kieffer, B., Maerschalk, C., Pretorius, W. & Barling, J. (2005) High-precision Pb-Sr-Nd-Hf isotopic characterization of USGS BHVO-1 and BHVO-2 reference materials. *Geochemistry Geophysics Geosystems* **6**, Q02002, DOI: 10.1029/2004GC000852.

Weis, D., Keiffer, B., Maerschalk, C., Barling, J., de Jong, J., Williams, G. A., Hanano, D., Mattielli, N., Scoates, J. S., Goolaerts, A., Friedman, R. A. & Mahoney, J. B. (2006) High precision isotopic characterization of USGS reference materials by TIMS and MC-ICP-MS. *Geochemistry Geophysics Geosystems* **7**(8), Q08006, DOI: 10.1029/2006GC001473.

Weis, D., Kieffer, B., Hanano, D., Nobre Silva, I., Barling, J. & Pretorius, W. (2007) Hf isotope compositions of U.S. Geological Survey reference materials. *Geochemistry Geophysics Geosystems* **8**(6), Q06006, doi:10.1029/2006GC001473.

Weis, D. Garcia, M. O., Rhodes, M., Jellinek, M. & Scoates, J. S. (2011) Role of the deep mantle in generating the compositional asymmetry of the Hawaiian mantle plume. *Nature Geoscience* **4**(12), 831-838. doi:10.1038/ngeo1328

Whiteside, J., Olsen, P., Eglinton, T., Brookfield, M. & Sambrotto, R. (2010) Compound-specific carbon isotopes from Earth's largest flood basalt eruptions directly linked to the end-Triassic mass extinction. *Proceedings of the National Academy of Sciences* **107**(15), 6721-6725.

White, R. S. & McKenzie, D. M. (1995) Mantle plumes and flood basalts. *Journal of Geophysical Research* **100**(B9), 17,543-17,585.

White, W. M. (1985) Sources of oceanic basalts: Radiogenic isotopic evidence. *Geology* **13**, 115-118.

White, R. W., Powell, R. & Phillips, G. N. (2003) A mineral equilibria study of the hydrothermal alteration in mafic greenschist facies rocks at Kalgoorlie, Western Australia. *Journal of Metamorphic Geology* **21**, 455-468.

White, W. M. (2010) Oceanic island basalts and mantle plumes: the geochemical perspective. *Annual Review of Earth and Planetary Sciences* **38**, 133-160.

Wignall, P. (2005) The link between large igneous province eruptions and mass extinctions. *Elements 1*, 293-297.

Willbold, M. & Stracke, A. (2010) Formation of enriched mantle components by recycling of upper and lower continental crust. *Chemical Geology* **276**, 188-197.

Williamson, N., Cousens, B., Ootes, L., Bédard, J., Rainbird, R. & Dell'Oro, T., (2012) Volcano-stratigraphy and major element geochemistry of the Southern Lobe of the Natkusiak Formation Flood Basalts of Victoria Island: Insights into the initiation of the Neoproterozoic Franklin Magmatic Event, Abstract, Geological Association of Canada - *Mineralogical Association of Canada*, May 27-29, 2012, Meetings and Activities, St. Johns, Newfoundland, 1p.

Wooden, J., Czamanske, G., Fedorenko, V., Arndt, N., Chauvel, C., Bouse, R., King, B., Knight, R. & Siems, D. (1993) Isotopic and trace-element constraints on mantle and crustal contributions to Siberian continental flood basalts, Noril'sk area, Siberia. *Geochimica et Cosmochimica Acta* **57**, 3677-3704.

Xiao, L., Xu, Y. G., Mei, H. J., Zheng, Y. F., He, B. & Pirajno, F. (2004) Distinct mantle sources of low-Ti and high-Ti basalts from the western Emeishan large igneous province, SW China: implications for plume–lithosphere interaction. *Earth and Planetary Science Letters* **228**, 525-546.

Zartman, R. E. & Doe, B. R. (1981) Plumbotectonics - The model. *Tectonophysics* **75**, 135-162.

Zindler, A., Jagoutz, E. & Goldstein, S. (1982) Nd, Sr, and Pb isotopic systematics in a three-component mantle: a new perspective. *Nature* **298**, 519-523.

Zindler, A. & Hart, S. (1986) Chemical geodynamics. *Annual Reviews in Earth and Planetary Sciences* **14**, 493-571.

Zhang, D. Zhou, T., Yuan, F., Jowitt, S., Fan, Y. & Liu, S. (2012) Source, evolution and emplacement of Permian Tarim Basalts: Evidence from U-Pb dating, Sr-Nd-Pb-Hf isotope systematics and whole rock geochemistry of basalts from the Keping area, Xinjiang Uygur Autonomous region, northwest China. *Journal of Asian Earth Sciences* **49**, 175-190.

Zhu, B. (2007) Pb-Sr-Nd isotopic systematics of mantle derived rocks in the world. *Earth Science Frontiers* **14**, 24-36.

R2. REFERENCE LIST FOR GEOROC COMPILATION

Ayalew, D., Yirgu, G. & Pik, R. (1989) Geochemical and isotopic (Sr, Nd and Pb) characteristics of volcanic rocks from southwestern Ethiopia. *The Journal of African Earth Sciences* **29**, 381-391.

Bogatikov, O. A., Kononova, V. A., Golubeva, Y. Y., Zinchuk, N. N., Ilupin, I. P., Rotman, A. Y., Levsky, L. K., Ovchinnikova, G. V. & Kondrashov, I. A. (2004) Variations in chemical and isotopic compositions of the Yakutian kimberlites and their causes. *Geochemistry International* **42**, 799-821.

Carlson, R. W., Czamanske, G. K., Fedorenko, V. A. & Ilupin, I. P. (2006) A comparison of Siberian meimechites and kimberlites: implications for the source of high-Mg alkalic magmas and flood basalts. *Geochemistry Geophysics Geosystems* **7**, doi:10.1029/2006GC001342.

Chakrabarti, R. & Basu, A. R. (2006) Trace element and isotopic evidence for Archean basement in the Lonar crater impact breccia, Deccan volcanic province. *Earth and Planetary Science Letters* **247**, 197-211.

Czamanske, G. K., Wooden, J. L., Walker, R. J., Fedorenko, V. A., Simonov, O. N., Budahn J. R. & Siems, D. F. (2000) Geochemical, isotopic, and SHRIMP age data for Precambrian basement rocks, Permian volcanic rocks, and sedimentary host rocks to the ore-bearing intrusions, Norilsk-Talnakh district, Siberian Russia. *International Geology Review* **42** 895-927.

Fan, W. -M., Zhang, C., Wang, Y., Guo F. & Peng, T. (2008) Geochronology and geochemistry of Permian basalts in western Guangxi province, southwest China: evidence for plume-lithosphere interaction. *Lithos* **102**, 218-236.

Greene, A. R., Scoates, J. S. & Weis, D. (2008) Wrangellia flood basalts in Alaska: A record of plume-lithosphere interaction in a Late Triassic accreted oceanic plateau. *Geochemistry Geophysics Geosystems* **9**(12) Q12004, doi:10.1029/2008GC002092.

Greene, A. R., Scoates, J. S., Weis, D., Nixon, G. T. & Kieffer, B. (2009) Melting history and magmatic evolution of basalts and picrites from the accreted Wrangellia oceanic plateau, Vancouver Island, Canada. *Journal of Petrology* **50**, 467-505.

Hanghoj, K., Storey, M. & Stecher, O. (2003) An isotope and trace element study of the East Greenland Tertiary dyke swarm: constraints on temporal and spatial evolution during continental rifting. *Journal of Petrology* **44**, 2081-2112.

Hansen, H. & Nielsen, T. F. D. (1999) Crustal contamination in Paleogene East Greenland flood basalts: plumbing system evolution during continental rifting. *Chemical Geology* **157,** 89-118.

Harmer, R. E., Lee, C. A. & Eglington, B. M. (1998) A deep mantle source for carbonatite magmatism: evidence from the nephelinites and carbonatites of the Buhera district, SE Zimbabwe. *Earth and Planetary Science Letters* **158**, 131-142.

Heatherington, A. L. & Mueller, P. A. (1999) Lithospheric sources of north Florida, USA tholeiites and implications for the origin of the Suwannee Terrane. *Lithos* **46**, 215-233.

Jourdan, F., Bertrand, H., Scharer, U., Blichert-Toft, J., Feraud, G. & Kampunzu, A. B. (2007) Major and trace element and Sr, Nd, Hf, and Pb isotope compositions of the Karoo large igneous province, Botswana-Zimbabwe: lithosphere vs mantle plume contribution. *Journal of Petrology* **48**(6) 1043-1077.

Kerr, A. C., Kempton, P. D. & Thompson, R. N. (1995) Crustal assimilation during turbulent magma ascent: new isotopic evidence from the mull tertiary lava succession, NW Scotland. *Contributions to Mineralogy and Petrology* **119**, 142-154.

Kieffer, B., Arndt, N., Lapierre, H., Bastien, F., Bosch, D., Pecher, A., Yirgu, G., Ayalew, D., Weis, D., Jerram, D., Keller, F. & Meugniot, C. (2004) Flood and shield basalts from Ethiopia: Magmas from the African Superswell. *Journal of Petrology* **45**(4), 793-834.

Krivolutskaya, N. A., Sobolev, A. V., Mikhailov, V. N., Plechova, A. A., Kostitsyn, Y. A., Roschina, I. A. & Fekiacova, Z. (2012) Parental melt of the Nadezhdinsky Formation: geochemistry, petrology and connection with Cu-Ni deposits (Noril'sk area, Russia). *Chemical Geology* **87,** 302-303.

Lai, S., Qin, J., Li, Y., Li, S. & Santosh, M. (2012) Permian high Ti/Y basalts from the eastern part of the Emeishan large igneous province, southwestern China: petrogenesis and tectonic implications. *The Journal of Asian Earth Sciences* **47**, 216-230.

Larsen, L. M., Pedersen, A. K., Sundvoll, B. & Frei, R. (2003) Alkali picrites formed by melting of old metasomatized lithospheric mantle: Manitdlat member, Vaigat Formation, Palaeocene of West Greenland. *Journal of Petrology* **44**, 3-38.

Lassiter, J. C., DePaolo, D. J. & Mahoney J. J. (1995) Geochemistry of the Wrangellia flood basalt province: implications for the role of continental and oceanic lithosphere in flood basalt genesis. *Journal of Petrology* **36**, 983-1009.

Lightfoot, P. C., Hawkesworth, C. J., Olshefsky, K., Green, T., Doherty W. & Keays, R. R. (1997) Geochemistry of tertiary tholeiites and picrites from Qeqertarssuaq (Disko Island) and Nuusuaq, West Greenland, with implications for the mineral potential of comagmatic intrusions. *Contributions to Mineralogy and Petrology* **128**, 139-163.

Maas R., Kamenetsky, M. B., Sobolev, A. V., Kamenetsky, V. S. & Sobolev, N. V. (2005) Sr, Nd, and Pb isotope evidence for a mantle origin of alkali chlorides and carbonates in the Udachnaya kimberlite, Siberia. *Geology* **33**, 549-552.

Melluso, L., Mahoney, J. J. & Dallai, L. (2006) Mantle sources and crustal input as recorded in high-Mg Deccan Traps basalts of Gujarat (India). *Lithos* **89**, 259-274.

Merle, R., Marzoli, A., Bertrand, H., Reisberg L., Verati, C., Zimmermann, C., Chiaradia, M., Bellieni, G. & Ernesto, M. (2011) ^{40}Ar/^{39}Ar ages and Sr-Nd-Pb-Os geochemistry of CAMP tholeiites from western Maranhao basin (NE Brazil). *Lithos* **122**, 137-151.

Peate, D. W. & Hawkesworth, C. J. (1996) Lithospheric to asthenospheric transition in low-Ti flood basalts from southern Parana, Brazil. *Chemical Geology* **127**, 1-24.

Peate, D. W., Hawkesworth, C. J., Mantovani, M. S. M., Rogers N. W. & Turner, S. P. (1999) Petrogenesis and stratigraphy of the high-Ti/Y Urubici magma type in the Paraná flood basalt province and implications for the nature of Dupal-type mantle in the south Atlantic region. *Journal of Petrology* **40**, 451-473.

Peate, D. W., Baker, J. A., Blichert-Toft, J., Hilton, D. R., Storey, M., Kent, A. J. R., Brooks, C. K., Hansen, H., Pedersen, A. K. & Duncan, R. A. (2003) The Prinsen of Wales Bjerge Formation lavas, East Greenland: the transition from tholeiitic to alkalic magmatism during Paleogene continental breakup. *Journal of Petrology* **44**, 279-304.

Peng, Z. X. & Mahoney, J. J. (1995) Drillhole lavas from the northwestern Deccan Traps, and the evolution of Reunion hotspot mantle. *Earth and Planetary Science Letters* **134**, 169-185.

Pik, R., Deneil, C., Coulin, C., Yirgu, G. & Marty, B. (1999) Isotopic and trace element signatures of Ethiopian flood basalts: evidence for plume-lithosphere interactions. *Geochimica et Cosmochimica Acta* **63**(15), 2263-2279.

Sen, G., Bizimis, M., Das, R., Dalim, K., Arijita, R. & Biswas, S. K. (2009) Deccan plume, lithosphere rifting, and volcanism in Kutch, India. *Earth and Planetary Science Letters* **277**, 101-111.

Sheth, H. C., Ray, J. S., Ray, R., Vanderkluysen, L., Mahoney, J. J., Kumar, A., Das, P., Adhikari, S. & Jana, B. (2009) Geology and geochemistry of Pachmarhi dykes and sills, Satpura Gondwana basin, central India: problems of dyke-sill-flow correlations in the Deccan Traps. *Contributions to Mineralogy and Petrology* **158**, 357-380.

Simonetti, A., Goldstein, S. L., Schmidberger, S. S. & Viladkar, S. G. (1998) Geochemical and Nd, Pb, and Sr isotope data from Deccan alkaline complexes: inferences for mantle sources and plume lithosphere interaction. *Journal of Petrology* **39**, 1847-1864.

Turner, S. P., Kirstein, L. A., Hawkesworth, C. J., Peate, D. W., Hallinan, S. & Mantovani, M. S. M. (1999) Petrogenesis of an 800 m lava sequence in eastern Uruguay: insights into magma chamber processes beneath the Paraná flood basalt province. *Journal of Geodynamics* **28**, 471-487.

Vanderkluysen, L., Mahoney, J. J., Hooper, P. R., Sheth, H. C. & Ray, R. (2011) The feeder system of the Deccan Traps (India): insights from dike geochemistry. *Journal of Petrology* **52**, 315-343.

Wooden, J., Czamanske, G., Fedorenko, V., Arndt, N., Chauvel, C., Bouse, R., King, B., Knight, R. & Siems, D. F. (1993) Isotopic and trace-element constraints on mantle and crustal contributions to Siberian continental flood basalts, Noril'sk area, Siberia. *Geochimica et Cosmochimica Acta* **57**, 3677-3704.

Zhang, Z., Mahoney, J. J., Mao, J. & Wang, F. (2006) Geochemistry of picritic and associated basalt flows of the western Emeishan flood basalt province, China. *Journal of Petrology* **47**, 1997-2019.

Zhang, Z., Zhi, X., Chen, L., Saunders, A. D. & Reichow, M. K. (2008) Re-Os isotopic compositions of picrites from the Emeishan flood basalt, province. *Earth and Planetary Science Letters* **276**, 30-39.

APPENDICES

APPENDIX A

PETROGRAPHIC CHARACTERISTICS AND ATLAS OF THE NATKUSIAK BASALTS

Background information

The following section is a petrographic catalogue of the Natkusiak basalt samples collected on Victoria Island during fieldwork in the summers of 2008, 2010, and 2011. The catalogue includes textural descriptions and mineralogy with modal abundances (visual estimates) in volume percent (totals 100% and do not include amygdules). Secondary alteration phases are listed separately from primary phases (phenocrysts and groundmass). Amygdule abundance is also estimated for each sample (up to ~35 vol. % in some extreme cases) and loss-on-ignition (LOI) values in wt. % are given for those samples that have been analyzed for whole rock geochemistry. A Nikon Eclipse E600 Pol microscope was used for petrographic analyses. Representative photomicrographs are included with the field of view (FOV) indicated (e.g., 2x, 5x, 10x, 20x objectives), along with scanned images of entire thin sections in both transmitted (TL) and crossed-polarized (XPL) light. Scanned images were collected with an EPSON Perfection 4490 PHOTO image scanner using 2400 dpi; all scanned thin sections are 45 x 25 mm. A summary table (Table 2.1) of the petrographic catalogue is provided in Chapter 2 and includes: sample, section, and group name for each sample as well as volume percent phenocrysts, igneous textures, extent of alteration, and pertinent petrographic notes. Opaque minerals are titanomagnetite and, to a lesser extent, pyrrhotite, based on energy-dispersive spectral analyses during the hydrothermal alteration study (Appendix B). Plag = plagioclase; cpx = clinopyroxene; ol = olivine; qtz = quartz; FOV = field of view; XPL = cross-polarized light; PPL = plane polarized light.

Sample: 08JB01

Rock type: Basalt
Location: Northern Section, cycle 2
Collected by: Jean Bédard, 2008 season

Fine-grained cpx, plag, and opaques with interspersed secondary chlorite. Photo 1244, XPL 2x magnification, FOV = 7 mm.

Primary phases (vol. %)
Plagioclase – 38%
Clinopyroxene – 32%
Opaque minerals – 12%

Secondary phases (vol. %)
Chlorite – 13%
Quartz – 5%

Amygdules 10 vol. %

LOI: 1.42 wt. %

Description
Intergranular basalt with tabular plagioclase (0.5 mm) and equant clinopyroxene (0.3 mm) groundmass. Green chlorite and microcrystalline quartz in amygdules. Rare clinopyroxene microphenocrysts (~1 mm).

Scan: TL

Scan: XPL

Sample: 08JB02

Rock type: Basalt
Location: Northern Section, cycle 2
Collected by: Jean Bédard, 2008 season

Coarse-grained plag and cpx with green chlorite-filled amygdules. Photo 1247, XPL 2x magnification, FOV = 7 mm.

Primary phases (vol. %)
Plagioclase – 35%
Clinopyroxene – 33%
Opaque minerals – 11%

Secondary phases (vol. %)
Chlorite – 15%
Quartz – 6%

Amygdules 13 vol. %

LOI: 2.37 wt. %

Description
Amygdaloidal, intergranular, coarse-grained basalt with tabular plagioclase (1-2 mm) and equant clinopyroxene (0.5-1 mm) in groundmass. Plagioclase grains are partially altered. Green chlorite and microcrystalline quartz in amygdules. Quartz tends to rim amygdules with chlorite centers.

Scan: TL
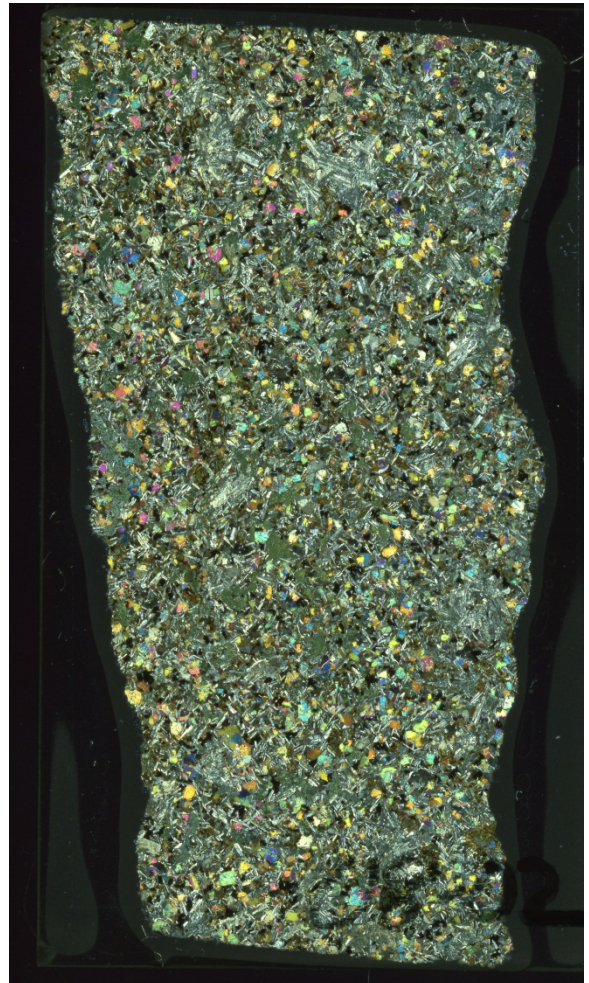
Scan: XP

Sample: 08JB03

Rock type: Basalt
Location: Northern Section, cycle 2
Collected by: Jean Bédard, 2008 season
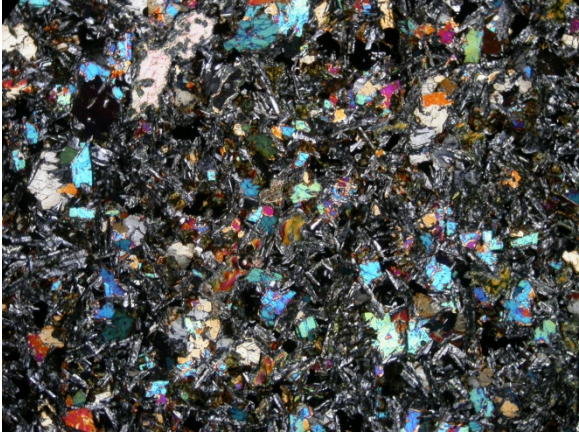
Subophitic cpx grains and tabular plag. Photo 1248, XPL 2x magnification, FOV = 7 mm.

Primary phases (vol. %)
Plagioclase – 37%
Clinopyroxene – 33%
Opaque minerals – 11%

Secondary phases (vol. %)
Chlorite – 8%
Calcite – 5%
Serpentine – 4%

Amygdules 14 vol. %

LOI: 2.63 wt. %

Description
Basalt with tabular plagioclase (0.5-1mm) and subophitic clinopyroxene (0.2-0.5 mm) in groundmass with intergranular opaque minerals. Rare relict olivine replaced by serpentine. Plagioclase is altered.

Scan: TL
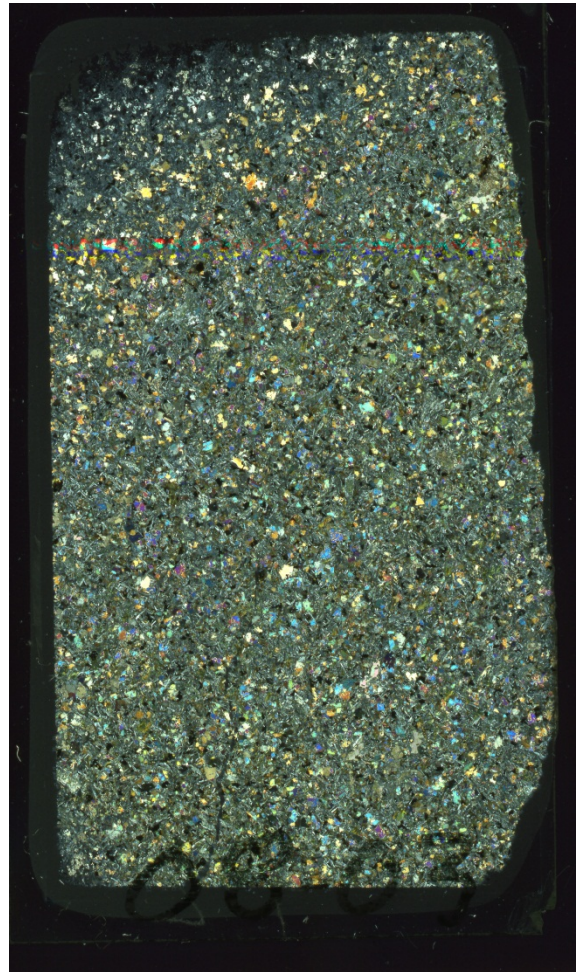
Scan: XPL

Sample: 08JB04C

Rock type: Basalt
Location: Northern Section, basal group
Collected by: Jean Bédard, 2008 season

Fine-grained plag and cpx with interspersed relict ol grains. Photo 1249, XPL 2x magnification, FOV = 7 mm.

Primary phases (vol. %)
Plagioclase – 35%
Clinopyroxene – 32%
Opaque minerals – 10%

Secondary phases (vol. %)
Chlorite – 8%
Calcite – 6%
Quartz – 4%
Serpentine – 4%

Amygdules 16 vol. %

LOI: 2.70 wt. %

Description
Fine-grained intergranular basalt with plagioclase (~0.2 mm) and clinopyroxene (~0.1 mm) in groundmass. Green chlorite rims calcite/quartz-filled amygdules. Relict olivine is replaced by serpentine.

Scan: TL
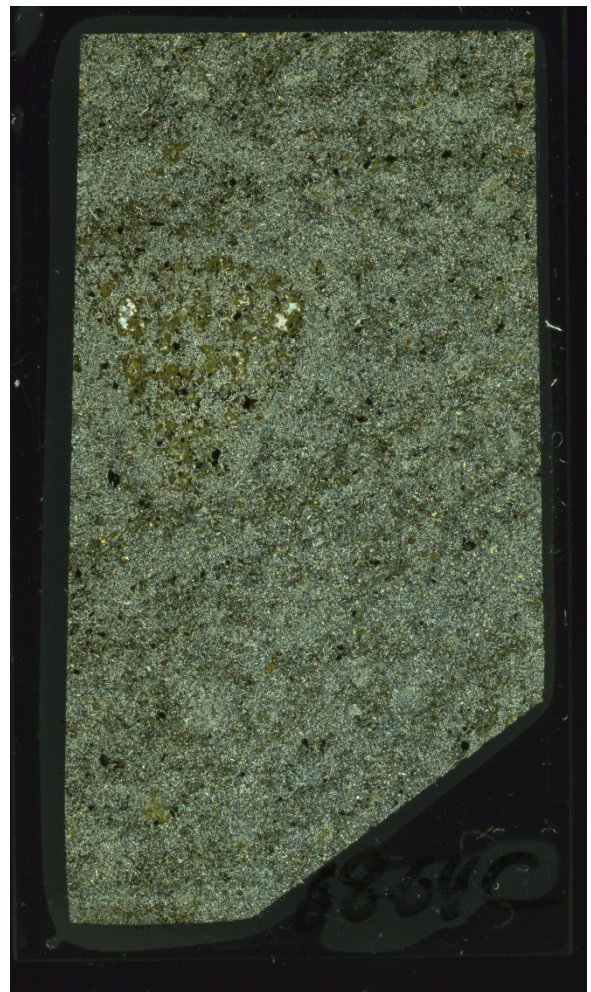
Scan: XPL

Sample: 08JB06

Rock type: Basalt
Location: Northern Section, cycle 1
Collected by: Jean Bédard, 2008 season

Fresh, unaltered groundmass of plag, cpx, and opaque minerals. Photo 1251, XPL 2x magnification, FOV = 7 mm.

Primary phases (vol. %)
Plagioclase – 46%
Clinopyroxene – 35%
Opaque minerals – 14%

Secondary phases (vol. %)
Chlorite – 5%

Amygdules 2 vol. %

LOI: 1.20 wt. %

Description
Fine-grained intergranular basalt with acicular plagioclase (0.1 mm) and equant clinopyroxene (0.07 mm) in groundmass. Minor alteration and secondary chlorite.

Scan: TL

Scan: XPL

Sample: 10RAT TD15A2

Rock type: Basalt
Location: Central Section, basal group
Collected by: Trent Dell'Oro, 2010 season
1 m from Kuujjua Formation contact

Ophitic cpx intergrown around plag, with green-brown chlorite-filled amygdules. Photo 9151, XPL 2x magnification, FOV = 7 mm.

Primary phases (vol. %)
Plagioclase – 36%
Clinopyroxene – 32%
Opaque minerals – <1%

Secondary phases (vol. %)
Calcite – 7%
Chlorite – 20%
Quartz – 5%

Amygdules 17 vol. %

LOI: 4.8 wt. %

Description
Subhedral plagioclase (0.5 mm) forms an irregular mesh around subophitic pyroxene (0.5-3 mm). Pyroxenes are zoned with some twinning. Chlorite rims the margins of quartz- and calcite-filled amygdules. Plagioclase and pyroxene are only minimally altered. Sparse glomerocryts of plagioclase are present (3 mm diameter).

Scan: TL
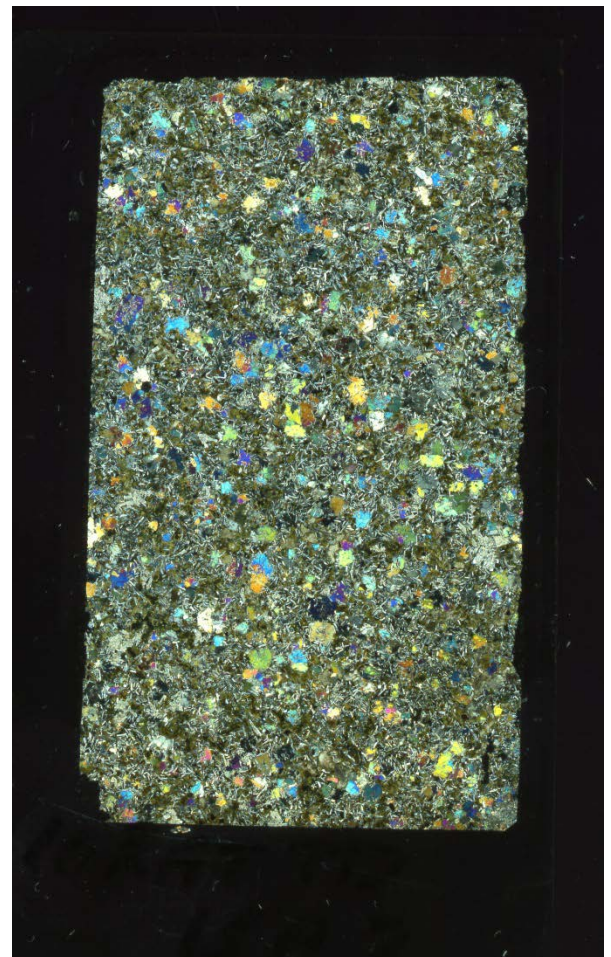
Scan: XP

Sample: 10RAT TD16A1

Rock type: Basalt
Location: Central Section, basal group
Collected by: Trent Dell'Oro, 2010 season
3 m from Kuujjua Formation contact

Altered basalt with calcite-filled amygdules, cpx is mostly altered. Photo 1192, XPL 2x magnification, FOV = 7 mm.

Primary phases (vol. %)
Plagioclase – 30%
Clinopyroxene – 28%
Opaque minerals – 2%

Secondary phases (vol. %)
Chlorite – 22%
Calcite – 18%
Quartz – 3%

Amygdules 28 vol. %

LOI: 13.7 wt. %

Description
Altered basalt, primary groundmass consists of tabular plagioclase grains (0.5 mm). Clinopyroxene mostly replaced by secondary phases and plagioclase by sericite. Calcite-filled amygdules are abundant. Primary accessory minerals include titanomagnetite.

Scan: TL

Scan: XPL

Sample: 10RAT TD16A2

Rock type: Basalt
Location: Central Section, basal group
Collected by: Trent Dell'Oro, 2010 season
3rd flow above Kuujjua Formation

Altered basalt with chlorite- and calcite-filled amygdules, primary plag and cpx groundmass. Photo 9158, XPL 2x magnification, FOV = 7 mm.

Primary phases (vol. %)
Plagioclase – 30%
Clinopyroxene – 28%

Secondary phases (vol. %)
Calcite – 18%
Chlorite – 15%
Quartz – 10%
Zeolite – 2%

Amygdules 35 vol. %

LOI: (Sample not analyzed)

Description
Amygdaloidal basalt with acicular plagioclase and clinopyroxene in groundmass, rare pyroxene phenocrysts and sericitized plagioclase. Amygdules are filled with radially zoned blue chlorite, calcite, and quartz. Amygdules are typically rimmed with microcrystalline quartz.

Scan: TL
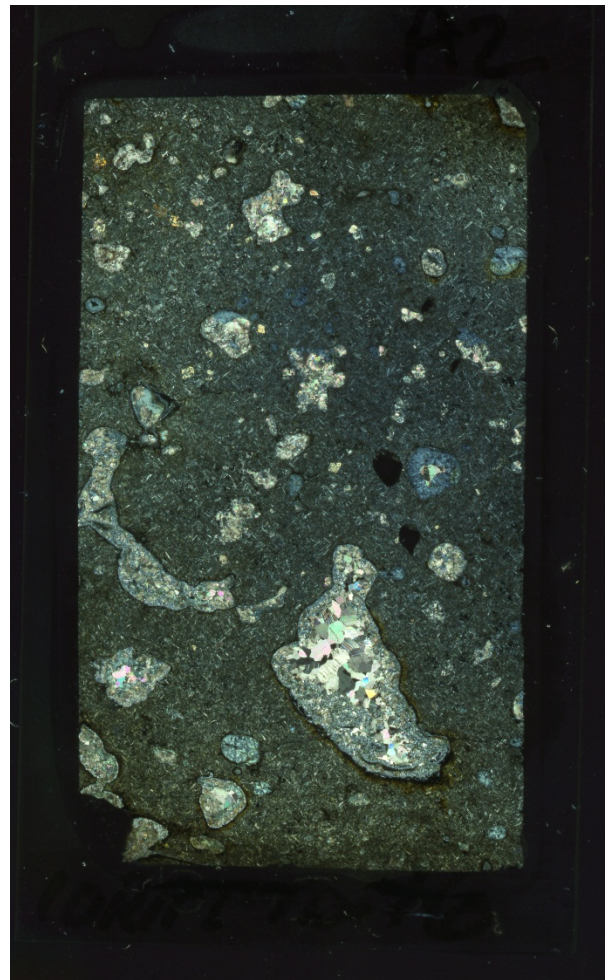
Scan: XPL

Sample: 10RAT TD16A3

Rock type: Basalt
Location: Central Section, basal group
Collected by: Trent Dell'Oro, 2010 season
3rd flow above Kuujjua Formation

Calcite- and quartz-filled amygdule with plag and cpx in groundmass. Photo 9160, XPL 2x magnification, FOV = 7 mm.

Primary phases (vol. %)
Plagioclase – 35%
Clinopyroxene – 30%

Secondary phases (vol. %)
Chlorite – 10%
Calcite – 13%
Quartz – 12%

Amygdules 25 vol. %

LOI: 6.7 wt. %

Description
Amygdaloidal, intergranular basalt with plagioclase and clinopyroxene in groundmass and minor pyroxene phenocrysts. Significant chlorite alteration. Abundant large (up to 1 mm) amygdules contain calcite, chlorite, and quartz and typically rimmed with chlorite.
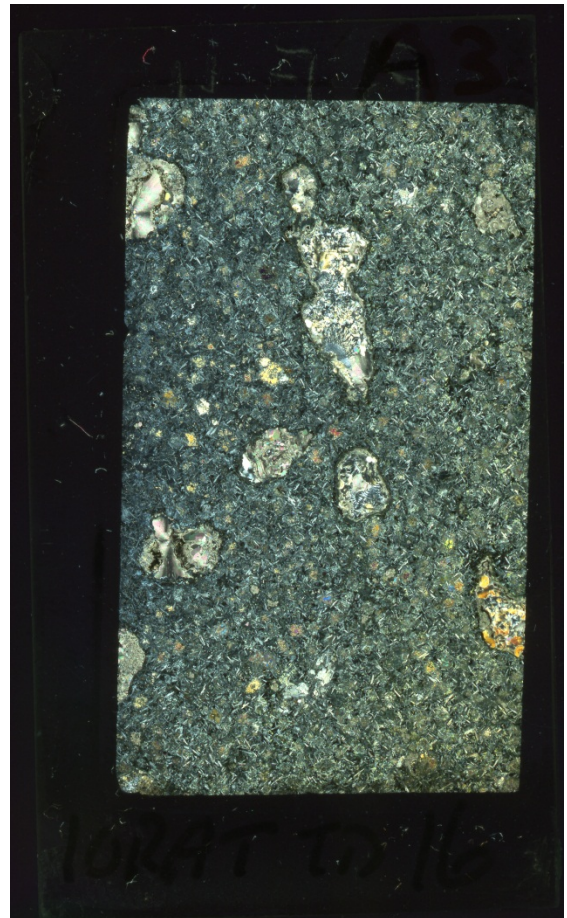
Scan: TL

Scan: XPL

Sample: 10RAT TD17B1

Rock type: Basalt
Location: Central Section, cycle 1
Collected by: Trent Dell'Oro, 2010 season
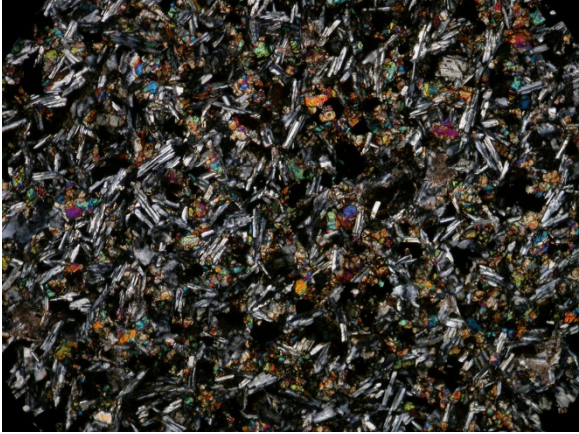
Homogeneous groundmass of cpx, plag, and opaque minerals. Photo 9162, XPL 5x magnification, FOV = 3 mm.

Primary phases (vol. %)
Plagioclase – 40%
Clinopyroxene – 35%
Opaque minerals – 15%

Secondary phases (vol. %)
Oxidized opaque minerals – 5%

Amygdules <1 vol. %

LOI: 1.5 wt.%

Description
Relatively unaltered fine-grained intergranular basalt with tabular plagioclase and equant clinopyroxene in the groundmass (0.2-0.5 mm).

Scan: TL

Scan: XPL

Sample: 10RAT TD17B2

Rock type: Basalt
Location: Central Section, cycle 1
Collected by: Trent Dell'Oro, 2010 season

Homogeneous groundmass of cpx, plag, and opaque minerals. Photo 9164, XPL 5x magnification, FOV = 3 mm.

Primary phases (vol. %)
Plagioclase – 45%
Clinopyroxene – 40%
Opaque minerals – 7%

Secondary phases (vol. %)
Chlorite – 5%

Amygdules <1 vol. %

LOI: 1.3 wt.%

Description
Relatively unaltered fine-grained intergranular basalt with groundmass of tabular plagioclase and equant clinopyroxene (0.2-0.5 mm). Some oxidation and chlorite alteration throughout.

Scan: TL

Scan: XPL

Sample: 10RAT TD18A1

Rock type: Basalt
Location: Central Section, basal group
Collected by: Trent Dell'Oro, 2010 season

Calcite-filled amygdules and groundmass of plag and cpx. Photo 9214, XPL 2x magnification, FOV = 7 mm.

Primary phases (vol. %)
Plagioclase – 34%
Clinopyroxene – 26%
Opaque minerals – 5%

Secondary phases (vol. %)
Calcite – 16%
Chlorite – 14%
Quartz – 7%

Amygdules 25 vol. %

LOI: 9.1 wt.%

Description

Amygdaloidal and strongly altered basalt with acicular plagioclase and clinopyroxene in groundmass. Minor clinopyroxene phenocrysts throughout. Amygdules (up to 4 mm) are rimmed with microcrystalline quartz. Calcite in amygdules displays concentric growth rings.

.

Scan: TL
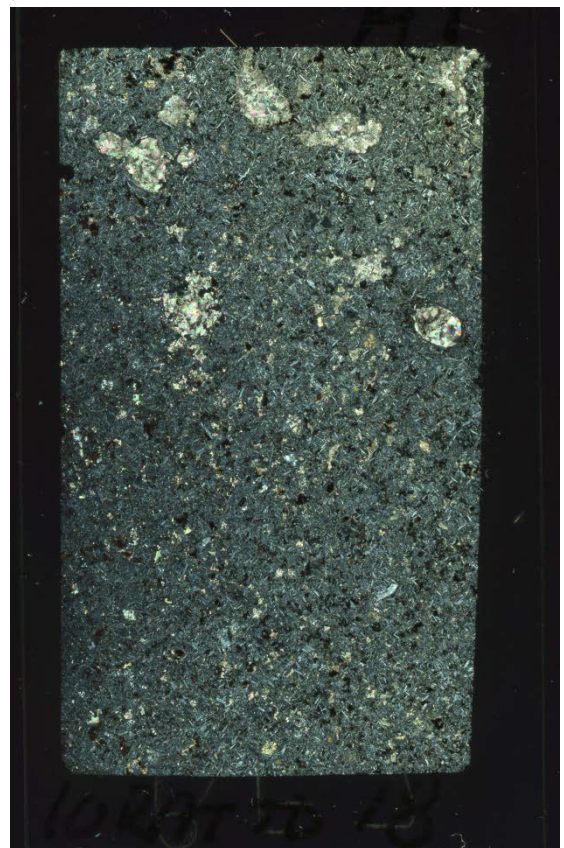
Scan: XPL

Sample: 10RAT TD18A2

Rock type: Basalt
Location: Central Section
Collected by: Trent Dell'Oro, 2010 season
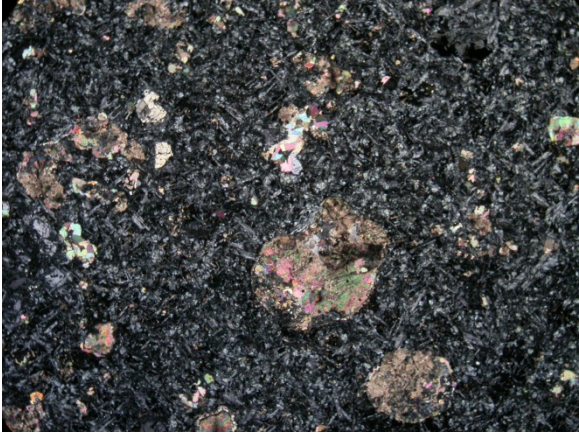
Calcite-filled amygdules surrounded by fine-grained plag and cpx groundmass. Photo 1188, XPL 2x magnification, FOV = 7 mm.

Primary phases (vol. %)
Plagioclase – 35%
Clinopyroxene – 25%
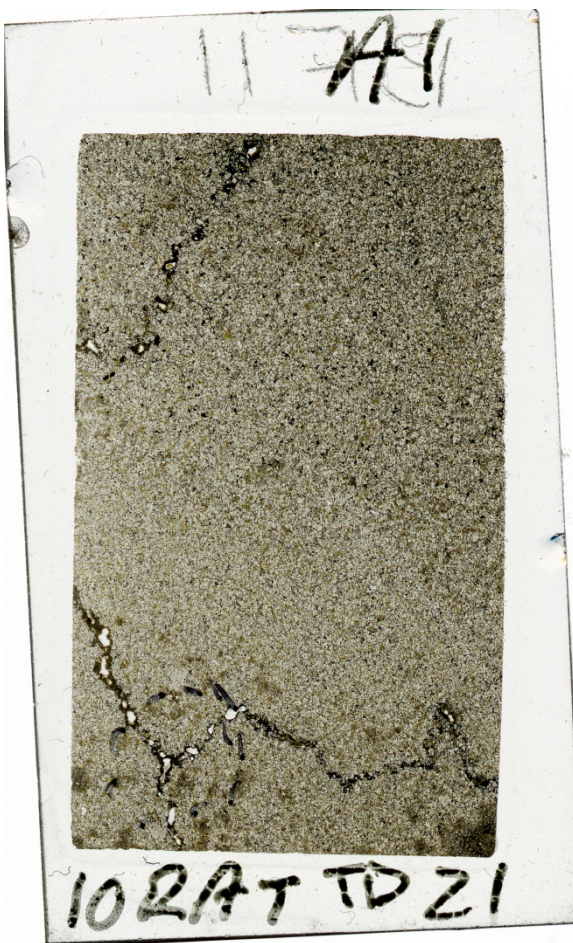Opaque minerals – <1%

Secondary phases (vol. %)
Calcite – 20%
Chlorite – 15%
Quartz – 5%

Amygdules 24 vol. %

LOI: 8.2 wt.%

Description

Amygdaloidal, fine-grained basalt with plagioclase and clinopyroxene grains (0.1-0.5 mm) in the groundmass. Clinopyroxene phenocrysts (0.5-1.5 mm). Chlorite alteration throughout. Amygdules (0.5-2 mm) are predominantly composed of calcite. Accessory minerals include minor sulfides and titanomagnetite.

Scan: TL

Scan: XPL

Sample: 10RAT TD19A1

Rock type: Basalt
Location: Central Section, cycle 1
Collected by: Trent Dell'Oro, 2010 season

Unaltered groundmass of plag and cpx with minor secondary chlorite. Photo 9167, XPL 5x magnification, FOV = 3 mm.

Primary phases (vol. %)
Plagioclase – 40%
Clinopyroxene – 35%
Opaque minerals – 5%

Secondary phases (vol. %)
Chlorite – 10%

Amygdules <1 vol. %

LOI: 2.3 wt.%

Description
Relatively unaltered, fine-grained, intergranular basalt with a groundmass of tabular plagioclase and equant clinopyroxene (0.1-0.4 mm).

Scan: TL

Scan: XPL

Sample: 10RAT TD20A1

Rock type: Basalt
Location: Central Section, cycle 1
Collected by: Trent Dell'Oro, 2010 season
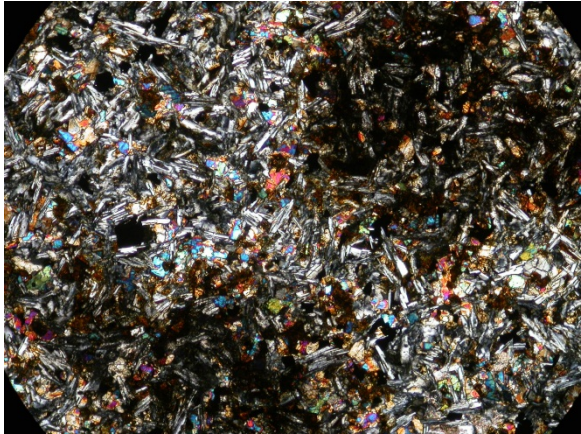
Cpx and plag groundmass with chlorite alteration. Photo 9165, XPL 5x magnification, FOV = 3 mm.

Primary phases (vol. %)
Plagioclase – 40%
Clinopyroxene – 35%
Opaque minerals – <1%

Secondary phases (vol. %)
Chlorite – 20%

Amygdules <1 vol.%

LOI: 2.4 wt. %

Description
Fine-grained intergranular basalt with a groundmass of plagioclase and clinopyroxene grains (0.01-0.4 mm). Patchy chlorite alteration throughout.

Scan: TL
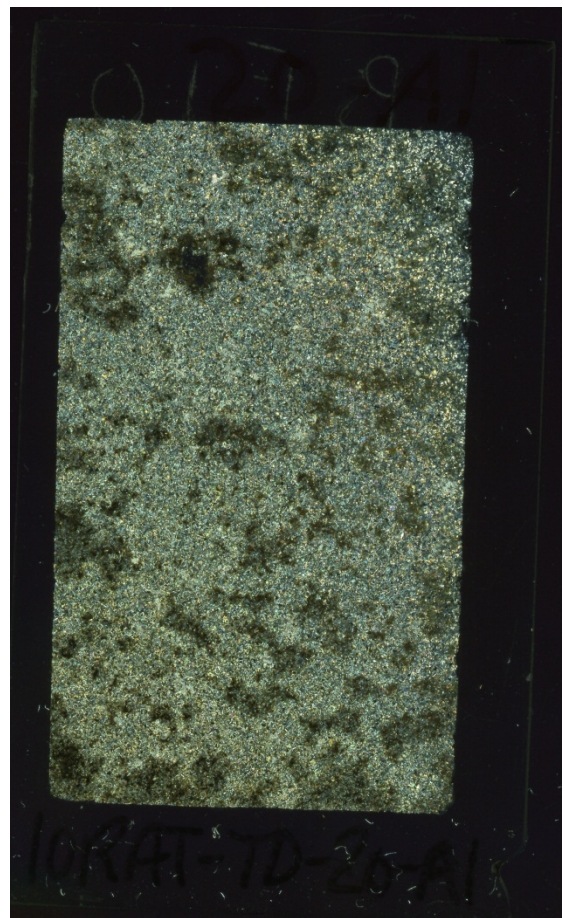
Scan: XP

Sample: 10RAT TD21A1

Rock type: Basalt
Location: Central Section, cycle 1
Collected by: Trent Dell'Oro, 2010 season

Cpx and plag in groundmass with minor chlorite alteration. Photo 9168, XPL 5x magnification, FOV = 3 mm.

Primary phases (vol. %)
Plagioclase – 42%
Clinopyroxene – 38%
Opaque minerals – <1%

Secondary phases (vol. %)
Chlorite – 9%
Calcite – 7%
Quartz – 4%

Amygdules <1 vol. %

LOI: 3.3 wt. %

Description
Fine-grained basalt with a groundmass of plagioclase and clinopyroxene (0.1-0.4 mm). Chlorite alteration throughout. Secondary calcite and quartz in fractures and veins.
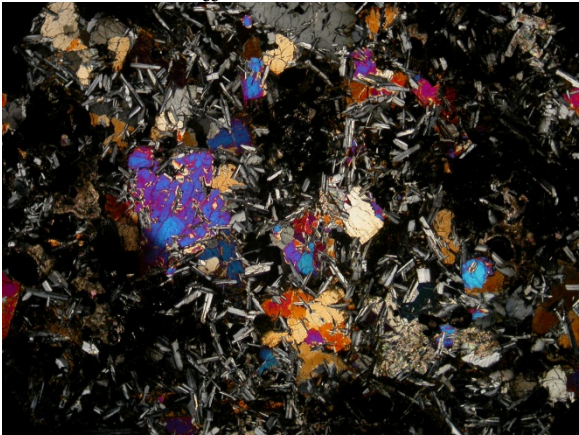

Scan: TL
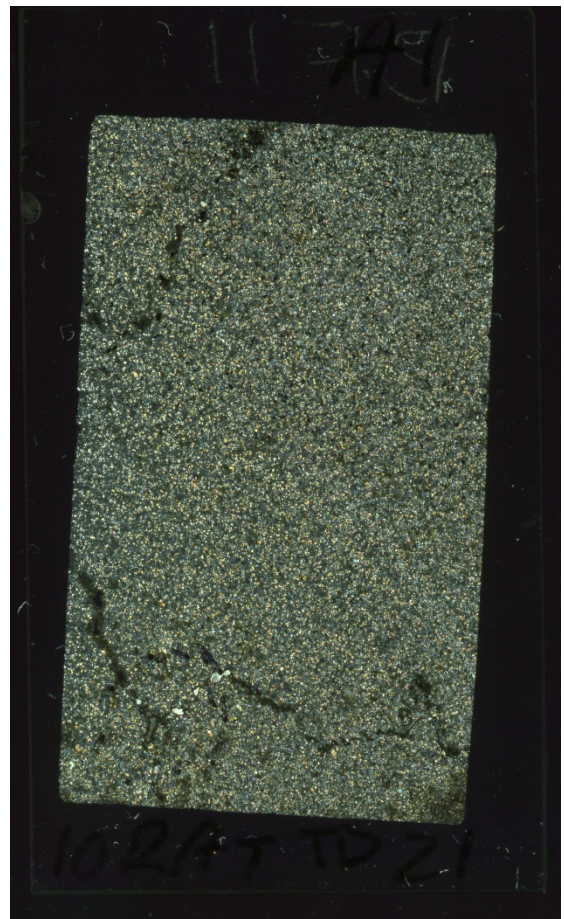
Scan: XPL

Sample: 10RAT TD55A1

Rock type: Basalt
Location: Central Section, basal group
Collected by: Trent Dell'Oro, 2010 season
6.8 m up from Kuujjua Formation contact
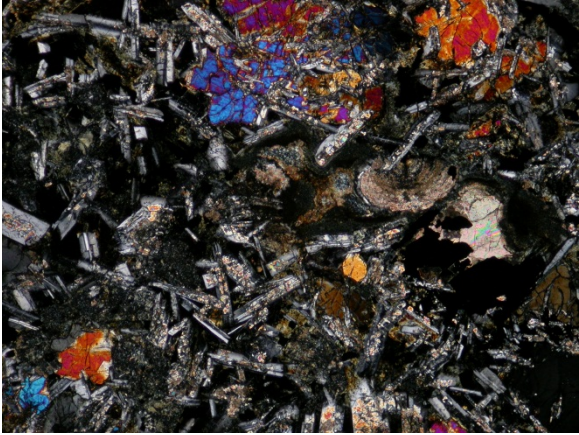
Ophitic cpx and plag in groundmass with calcite-filled amygdules. Photo 9325, XPL 5x magnification, FOV = 3 mm.

Primary phases (vol. %)
Plagioclase – 32%
Clinopyroxene – 25%
Opaque minerals – 4%

Secondary phases (vol. %)
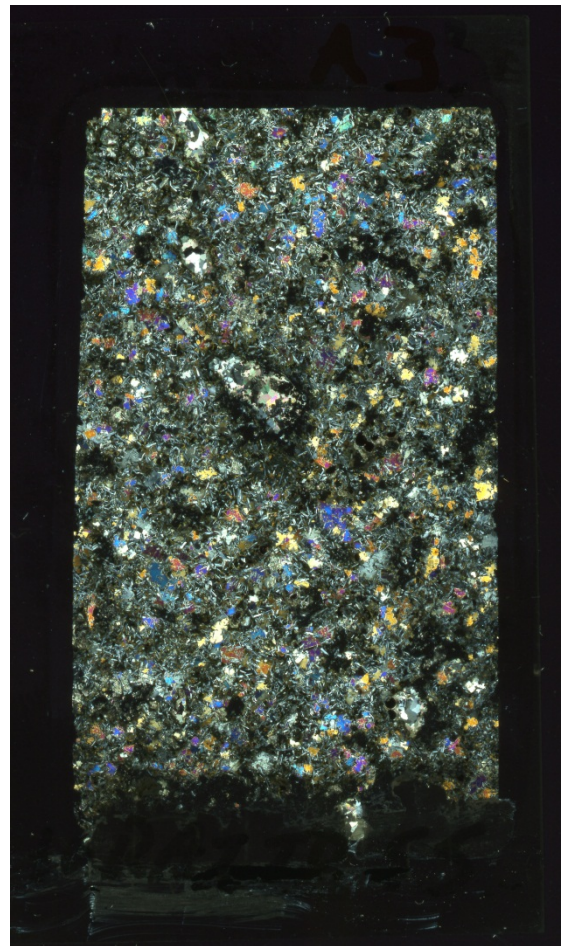Calcite - 17%
Chlorite – 15%
Quartz - 5%

Amygdules 22 vol. %

LOI: 5.7 wt. %

Description
Amygdaloidal, medium-grained basalt with ophitic clinopyroxene (0.5-1.5 mm) and plagioclase (0.5-1 mm). Plagioclase partially replaced by sericite. Amygdules contain calcite with radial extinction.
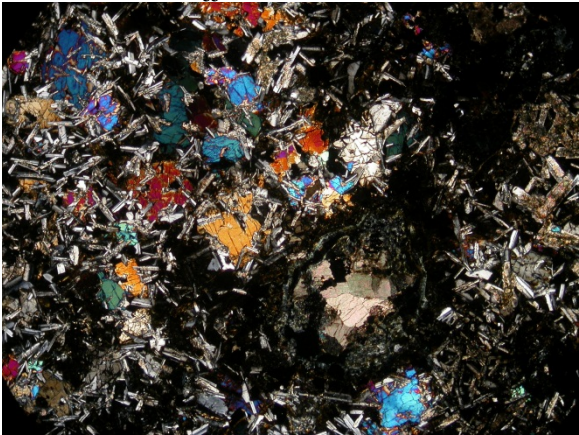

Scan: TL

Scan: XPL

Sample: 10RAT TD55A2

Rock type: Basalt
Location: Central Section, basal group
Collected by: Trent Dell'Oro, 2010 season
9.8 m from Kuujjua Formation contact

Large calcite-filled amygdule within altered cpx and plag in groundmass. Photo 9328, XPL 2x magnification, FOV = 7 mm.

Primary phases (vol. %)
Plagioclase – 31%
Clinopyroxene – 20%
Opaque minerals – 8%

Secondary phases (vol. %)
Calcite – 19%
Chlorite – 17%
Quartz – 5%

Amygdules 32 vol. %

LOI: (sample not analyzed)

Description
Amygdaloidal basalt with plagioclase (0.5-1 mm) and clinopyroxene groundmass. Pervasive chlorite alteration throughout. Amygdules predominantly filled with calcite.

Scan: TL
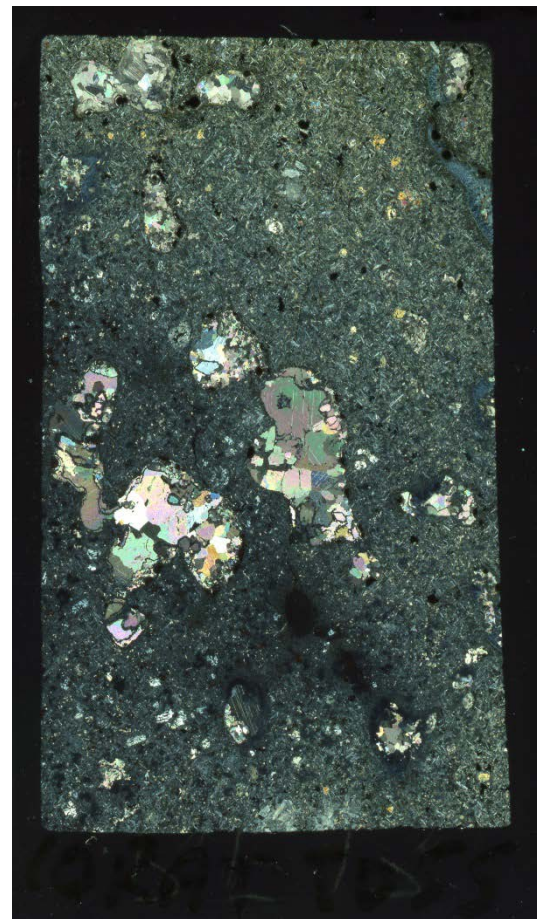
Scan: XPL

Sample: 10RAT TD55A3

Rock type: Basalt
Location: Central Section, basal group
Collected by: Trent Dell'Oro, 2010 season
12.9 m from Kuujjua Formation contact

Ophitic cpx and plag in groundmass with secondary phases interspersed. Photo 9171, XPL 2x magnification, FOV = 7 mm.

Primary phases (vol. %)
Plagioclase – 30%
Clinopyroxene – 25%
Opaque minerals – 5%

Secondary phases (vol. %)
Chlorite – 16%
Calcite – 12%
Quartz – 9%

Amygdules 15 vol. %

LOI: 4.1 wt. %

Description
Amygdaloidal basalt with plagioclase (~1 mm) and ophitic clinopyroxene (1-2 mm) in groundmass. Pervasive alteration. Amygdules filled with calcite and quartz, many rimmed with chlorite.
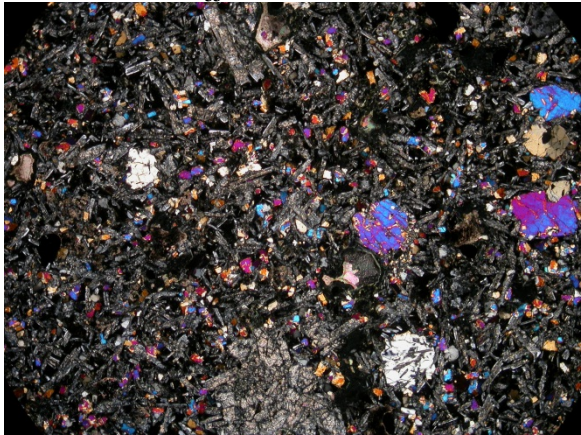

Scan: TL

Scan: XPL

Sample: 10RAT TD55A4

Rock type: Basalt
Location: Central Section, basal group
Collected by: Trent Dell'Oro, 2010 season
17.3 m from Kuujjua Formation contact

Ophitic cpx and plag groundmass with calcite-filled amygdule and pervasive alteration. Photo 9173, XPL 2x magnification, FOV = 7 mm.

Primary phases (vol. %)
Plagioclase – 31%
Clinopyroxene – 24%
Opaque minerals – 3%

Secondary phases (vol. %)
Chlorite – 20%
Calcite – 8%
Quartz – 4%

Amygdules 10 vol. %

LOI: 4.2 wt. %

Description
Amygdaloidal basalt with plagioclase (~1 mm) and ophitic clinopyroxene (1-2 mm) in groundmass. Extensive chlorite alteration. Amygdules filled with calcite and quartz, many rimmed with chlorite.

Scan: TL
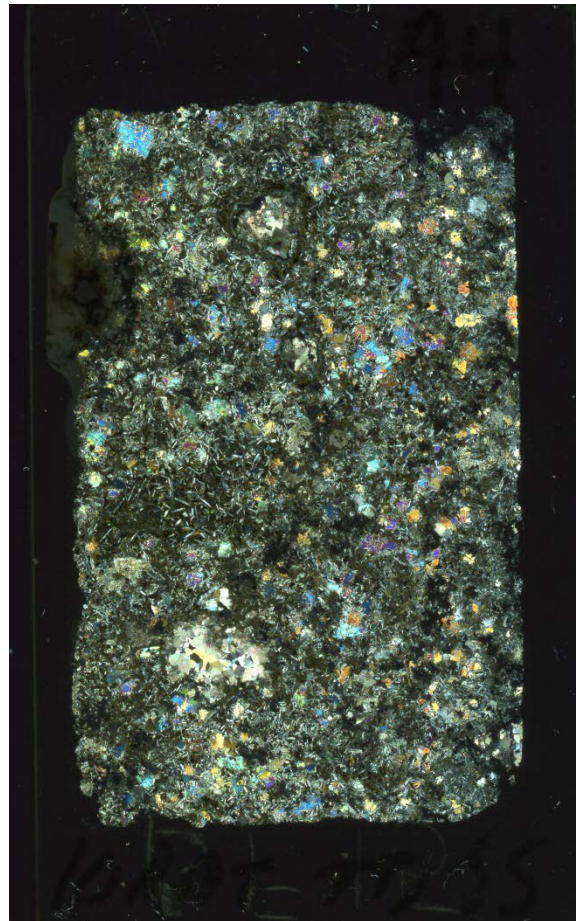
Scan: XPL

Sample: 10RAT TD55A5

Rock type: Basalt
Location: Central Section, basal group
Collected by: Trent Dell'Oro, 2010 season
30.4 m from Kuujjua Formation contact

Cpx phenocrysts amongst fine-grained cpx and plag. Photo 9174, XPL 2x magnification, FOV = 7 mm.

Primary phases (vol. %)
Plagioclase – 35%
Clinopyroxene – 30%
Opaque minerals – 5%
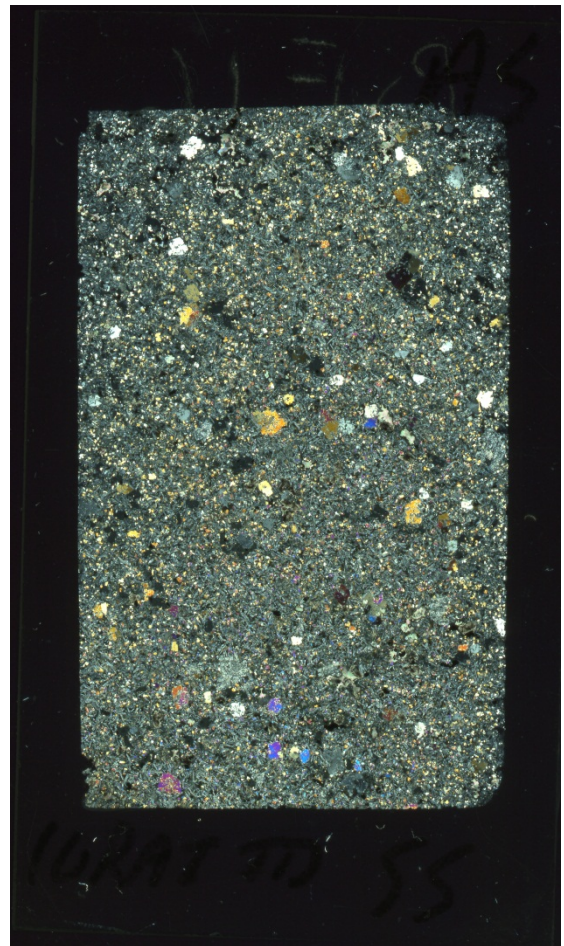
Secondary phases (vol. %)
Chlorite – 17%
Quartz – 4%
Calcite – 8%

Amygdules 10 vol. %

LOI: 4.3 wt. %

Description

Porphyritic basalt with plagioclase and clinopyroxene (0.2-0.5 mm) in the groundmass. Clinopyroxene phenocrysts (0.5-1.5 mm) are common. Chlorite, calcite, and quartz fill amygdules. Most plagioclase is partially altered, and clinopyroxene is unaltered.

Scan: TL

Scan: XPL

Sample: 10RAT TD55A6

Rock type: Basalt
Location: Central Section, basal group
Collected by: Trent Dell'Oro, 2010 season
37 m up from Kuujjua formation contact

Plag and cpx in the groundmass with calcite-filled amygdules. Photo 1191, XPL 2x magnification, FOV = 7 mm.

Scan: TL
Primary phases (vol. %)

Plagioclase – 41%
Clinopyroxene –34%
Opaque minerals – 11%
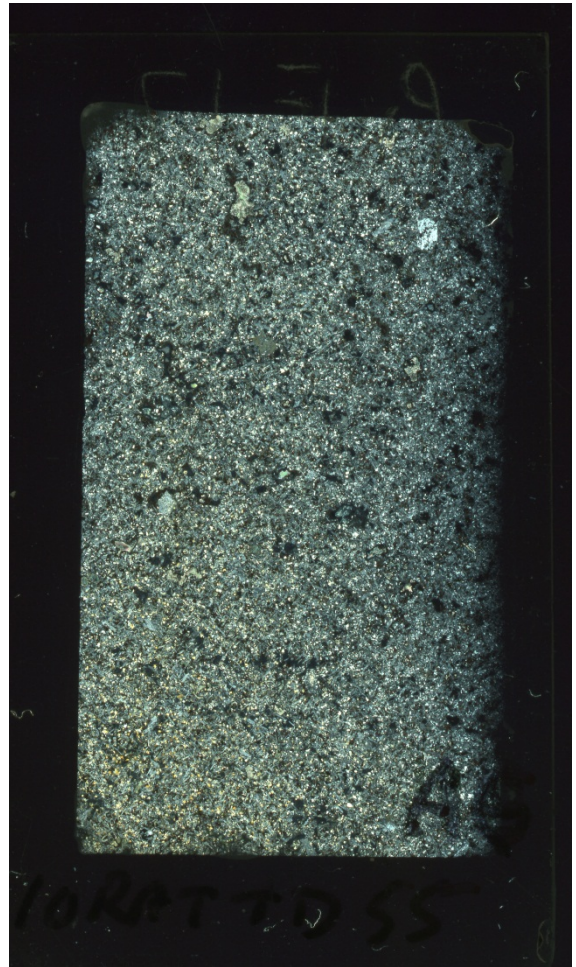
Secondary phases (vol. %)
Quartz – 6%
Calcite – 8%

Amygdules 15 vol. %

LOI: 3.8 wt. %

Description
Medium-grained intergranular basalt with plagioclase (0.3-0.6 mm) and clinopyroxene (0.1-0.2 mm) in the groundmass, minor clinopyroxene phenocrysts (0.5 to 1.2 mm). Amygdules (1-2 mm) contain calcite and quartz.

Scan: XPL

Sample: 10RAT TD56A1

Rock type: Basalt
Location: Central Section, basal group
Collected by: Trent Dell'Oro
2.5 m up from Kuujjua Formation contact

Partially altered subophitic cpx with calcite- and qtz-filled amygdules. Photo 9354, XPL 2x magnification, FOV = 7 mm.

Primary phases (vol. %)
Plagioclase – 33%
Clinopyroxene – 29%
Opaque minerals – 6%

Secondary phases (vol. %)
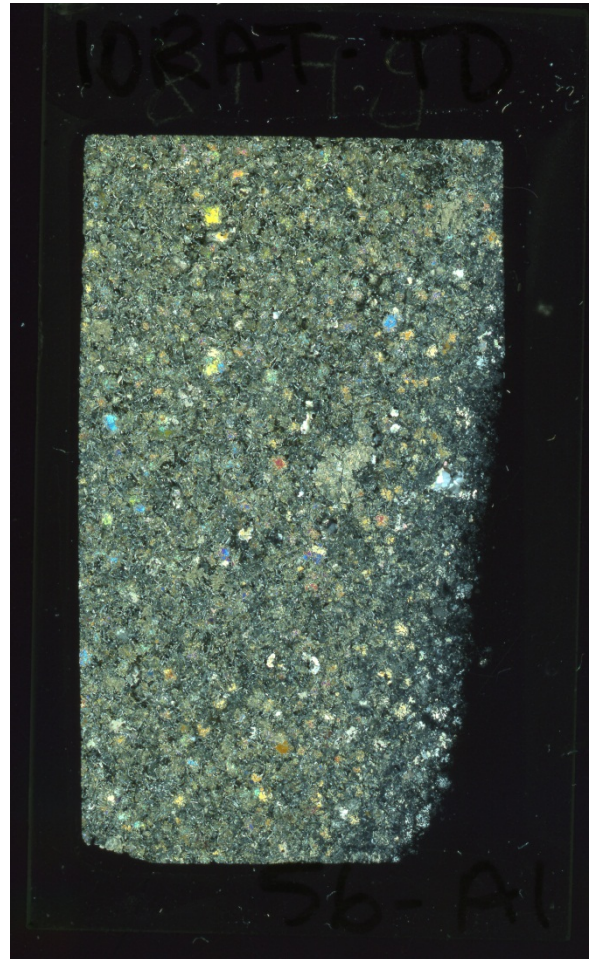Chlorite – 16%
Quartz – 5%
Calcite – 10%

Amygdules 15 vol. %

LOI: 6.0 wt. %

Description
Medium-grained subophitic basalt with plagioclase and clinopyroxene in the groundmass (0.2-0.5 mm). Amygdules filled with quartz and calcite. Opaque minerals include titanomagnetite.

Scan: TL

Scan: XPL

Sample: 10RAT TD57A1

Rock type: Basalt
Location: Central Section, basal group
Collected by: Trent Dell'Oro, 2010 season
1.5 m up from Kuujjua Formation contact

Subophitic cpx with plag and cpx in the groundmass. Photo 9178, XPL 2x magnification, FOV = 7 mm.

Scan: TL

Primary phases (vol. %)

Plagioclase – 34%
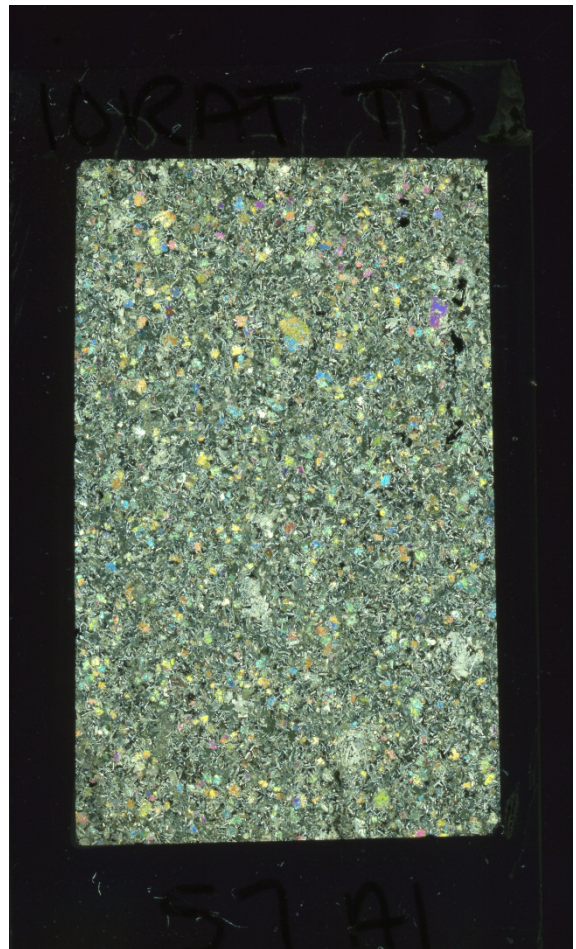Clinopyroxene – 30%
Opaque minerals – 8%

Secondary phases (vol. %)
Chlorite – 13%
Quartz – 5%
Calcite – 10%

Amygdules 13 vol. %

LOI: 5.0 wt. %

Description
Fine-grained subophitic basalt with plagioclase (0.5 mm) and clinopyroxene (0.5-1 mm) in the groundmass. Calcite and quartz amygdules (0.5-1 mm) with chlorite rims.
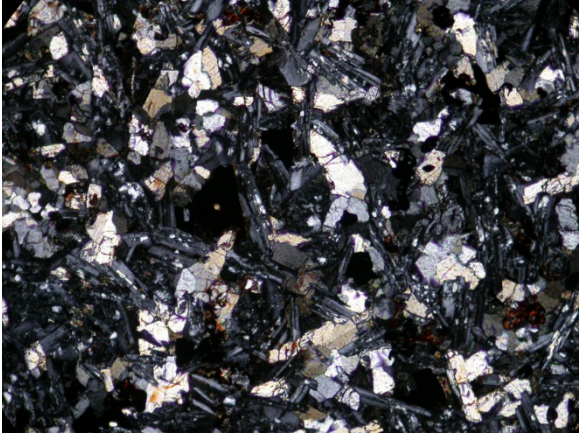

Scan: XPL

Sample: 10RAT TD60B1

Rock type: Basalt
Location: Central Section, cycle 1
Collected by: Trent Dell'Oro, 2010 season
86.1 m up from Kuujjua Formation contact

Cpx and plag with opaque minerals in
groundmass. Photo 9357, XPL 10x
magnification, FOV = 1.5 mm.

Primary phases (vol. %)
Plagioclase – 40%
Clinopyroxene – 37%
Opaque minerals – 12%

Secondary phases (vol. %)
Chlorite – 7%
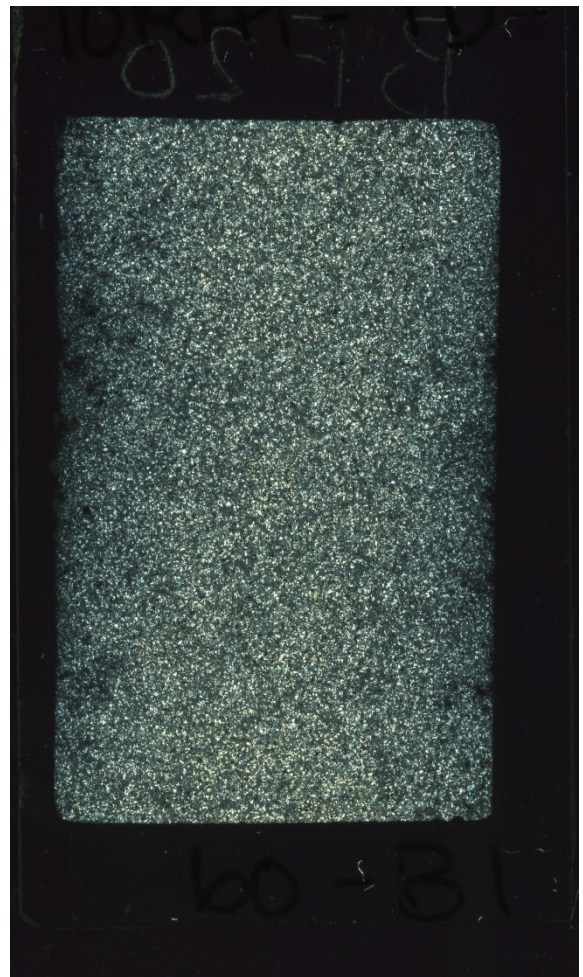Epidote – 4%

Amygdules <1 vol. %

LOI: 1.6 wt. %

Description
Fine-grained basalt with clinopyroxene (0.1-0.2 mm)
and plagioclase (0.1-0.3 mm) in the groundmass.
Rare amygdules throughout.

Scan: TL

Scan: XPL

Sample: 10RAT TD60B3

Rock type: Basalt
Location: Central Section, cycle 1
Collected by: Trent Dell'Oro, 2010 season
104.8 m up from Kuujjua Formation

Cpx and plag in the groundmass with minor opaque minerals. Photo 9362, XPL 10x magnification, FOV = 1.5 mm.

Primary phases (vol. %)
Plagioclase –42%
Clinopyroxene – 38%
Opaque minerals –8%

Secondary phases (vol. %)
Chlorite – 9%
Epidote – 3%

Amygdules <1 vol. %

LOI: 2.9%

Description
Very fine-grained basalt with plagioclase (0.1-0.3 mm) and clinopyroxene (0.08-0.2 mm) in the groundmass. Alteration phases include chlorite and epidote.
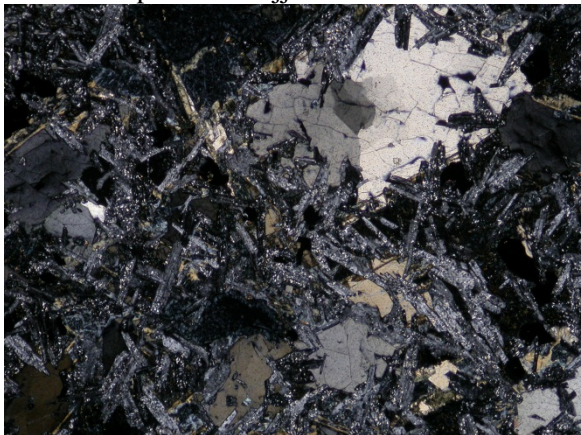

Scan: TL

Scan: XPL

142

Sample: 10RAT TD60B4

Rock type: Basalt
Location: Central Section, cycle 1
Collected by: Trent Dell'Oro, 2010 season
115.56 m up from Kuujjua Formation contact

Ophitic cpx and partially sericitized plag. Photo 9365, XPL 5x magnification, FOV = 3 mm.

Primary phases (vol. %)
Plagioclase – 36%
Clinopyroxene – 35%
Opaque minerals – 8%

Secondary phases (vol. %)
Chlorite – 10%
Calcite – 7%
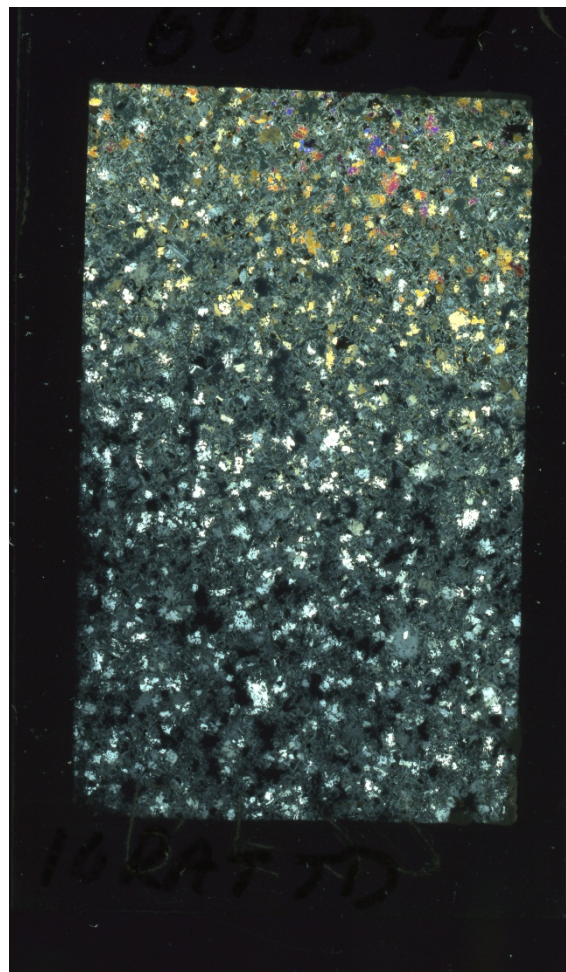Epidote – 3%

Amygdules 15 vol. %

LOI: 3.0 wt. %

Description
Basalt with ophitic clinopyroxene (0.5-1 mm) and plagioclase (0.3-0.8 mm) in the groundmass. Plagioclase is partially replaced by sericite. Chlorite- and calcite-filled amygdules throughout.

Scan: TL

Scan: XPL

Sample: 10RAT TD60B5

Rock type: Basalt
Location: Central Section, cycle 1
Collected by: Trent Dell'Oro, 2010 season
131.7 m up from Kuujjua Formation contact

Cpx, plag, and opaque minerals in the groundmass. Photo 9380, XPL 5x magnification, FOV = 3 mm.

Primary phases (vol. %)
Plagioclase – 42%
Clinopyroxene – 38%
Opaque minerals – 12%

Secondary phases (vol. %)
Chlorite – 7%

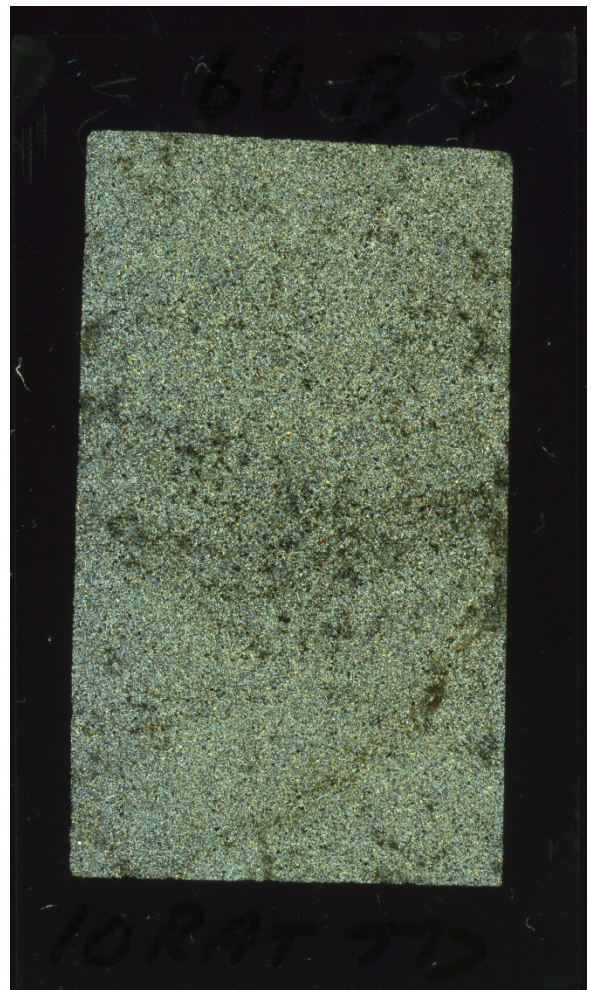**Amygdules** <1 vol. %

LOI: 1.2 wt. %

Description
Relatively unaltered, fine-grained basalt with subhedral plagioclase (0.1-0.3 mm) and anhedral clinopyroxene (0.5-0.1 mm) in the groundmass. Patchy chlorite alteration.

Scan: TL

Scan: XPL

Sample: 10RAT TD61A1

Rock type: Basalt
Location: Central Section, cycle 1
Collected by: Trent Dell'Oro, 2010 season
74 m up from Kuujjua Formation

Green chlorite-filled amygdules, unaltered plag and cpx in the groundmass. Photo 9384, XPL 2x magnification, 7 mm.

Primary phases (vol. %)
Plagioclase – 42%
Clinopyroxene – 37%
Opaque minerals – 8%

Secondary phases (vol. %)
Chlorite – 12%
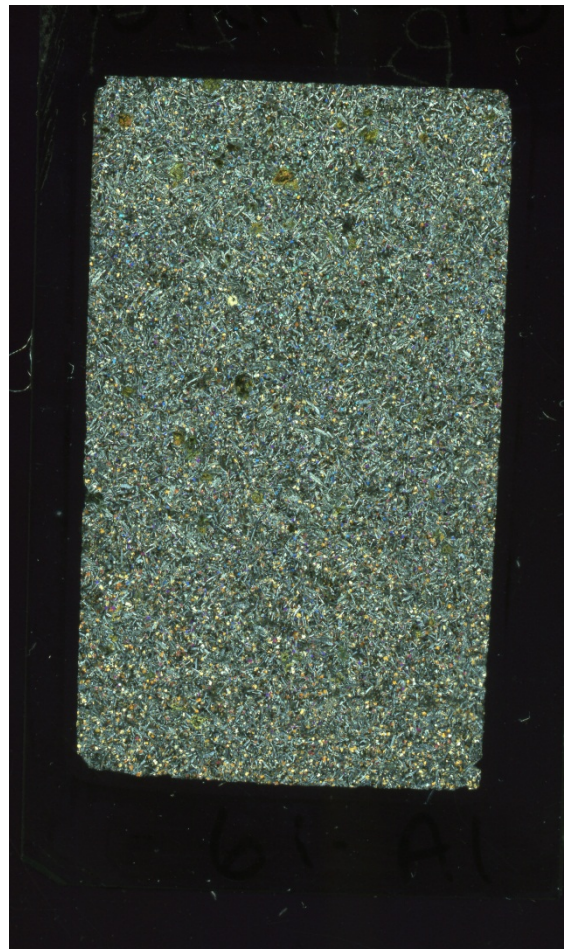Epidote – 4%

Amygdules <1 vol. %

LOI: 1.6 wt. %

Description
Fine-grained basalt with tabular plagioclase (0.3-0.6 mm) and equant clinopyroxene (0.2 mm) in the groundmass. Patchy green chlorite alteration and chlorite-filled amygdules.

Scan: TL

Scan: XPL

Sample: 10RAT TD61A2

Rock type: Basalt
Location: Central Section, cycle 1
Collected by: Trent Dell'Oro, 2010 season
81 m up from Kuujjua Formation contact

Chalcedony nodule with chlorite rim amongst plag and cpx in the groundmass. Photo 9392, XPL 5x magnification, FOV = 3 mm.

Primary phases (vol. %)
Plagioclase – 38%
Clinopyroxene – 34%
Opaque minerals – 8%
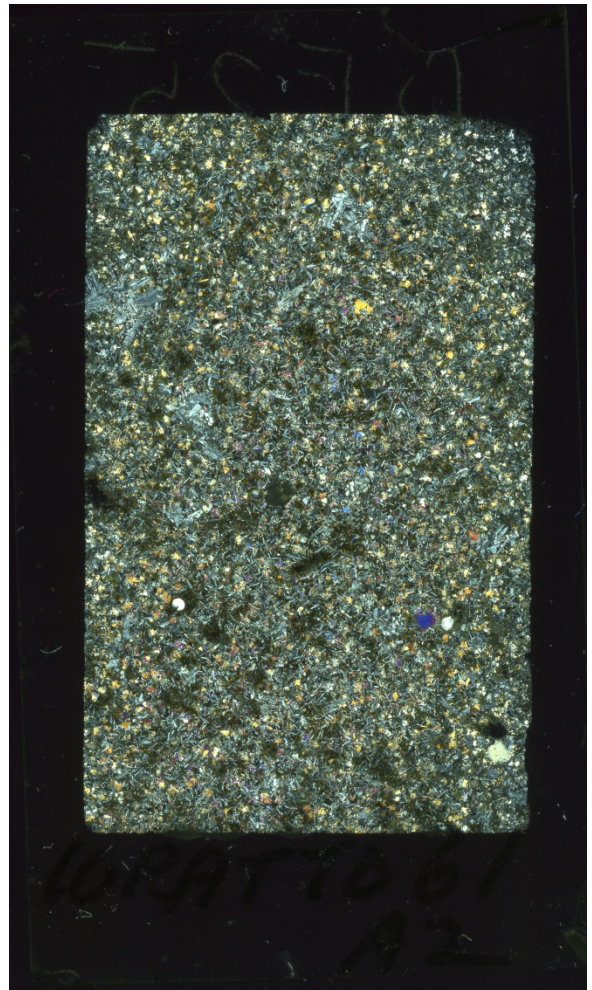
Secondary phases (vol. %)
Chlorite – 15%
Chalcedony – 5%

Amygdules 7 vol. %

LOI: 2.6 wt. %

Description

Medium-grained basalt with tabular plagioclase and clinopyroxene in the groundmass (0.4-0.8 mm), Clinopyroxene phenocrysts up to 1.5 mm across. Glomerocrysts (4 mm) of plagioclase (1-1.3 mm) are rare. Circular amygdules are filled with chalcedony and rimmed with dark green chlorite.

Scan: XPL

Scan: TL

Sample: 11RAT TD43B

Rock type: Basalt
Location: Eastern Section, cycle 1
Collected by: Trent Dell'Oro, 2011 season

Plag and cpx in the groundmass with chlorite alteration. Photo 0359, XPL 2x magnification, FOV = 7 mm.

Primary phases (vol. %)
Plagioclase – 40%
Clinopyroxene – 34%
Opaque minerals – 10%

Secondary phases (vol. %)
Chlorite – 15%

Amygdules 10 vol. %

LOI: 3.1 wt. %

Description
Fine-grained basalt, with anhedral to subhedral fine-grained plagioclase (0.2-0.4 mm) and clinopyroxene (0.1-0.3 mm) in the groundmass. Small secondary chlorite-filled amygdules range from 0.2-0.5 mm in diameter.

Scan: TL

Scan: XPL

Sample: 11RAT TD43C

Rock type: Basalt
Location: Eastern Section, cycle 1
Collected by: Trent Dell'Oro, 2011 season

Fine-grained plag, cpx, and opaque minerals in the groundmass. Photo 0367, XPL 2x magnification, FOV = 7 mm.

Primary phases (vol. %)
Plagioclase – 41%
Clinopyroxene – 36%
Opaque minerals – 12%

Secondary phases (vol. %)
Chlorite – 10%

Amygdules 8 vol. %

LOI: 2.6 wt. %

Description
Fine-grained basalt with subhedral plagioclase (0.3-0.5 mm) and clinopyroxene (0.1-0.4 mm) in the groundmass. Plagioclase partially replaced by sericite. Small chlorite-filled amygdules throughout.

Scan: TL

Scan: XPL

Sample: 11RAT TD72B

Rock type: Basalt
Location: Eastern Section, cycle 1
Collected by: Trent Dell'Oro, 2011 season

Fine-grained plag, cpx, and opaque minerals in the groundmass. Photo 0358, XPL 2x magnification, FOV = 7 mm.

Primary phases (vol. %)
Plagioclase – 38%
Clinopyroxene – 34%
Opaque minerals – 8%

Secondary phases (vol. %)
Chlorite – 13%
Calcite – 7%

Amygdules 18 vol. %

LOI: 2.5 wt. %

Description
Fine-grained basalt with subhedral plagioclase (0.2-0.4 mm) and clinopyroxene (0.1-0.3 mm) in the groundmass. Plagioclase is partially altered to sericite. Chlorite-filled and calcite-filled amygdules throughout.
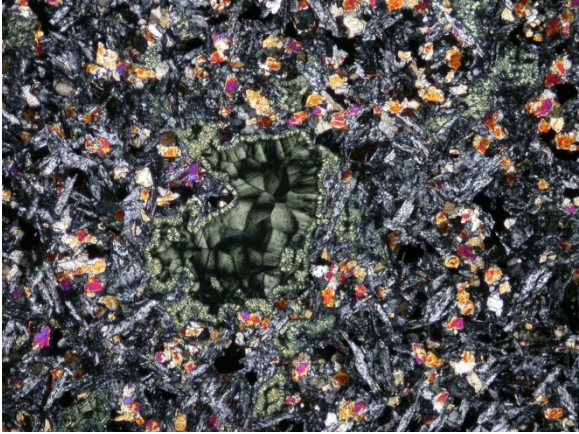

Scan: TL

Scan: XPL

Sample: 11RAT TD72C

Rock type: Basalt
Location: Eastern Section, cycle 1
Collected by: Trent Dell'Oro, 2011 season

Chlorite-filled amygdule, with cpx and plag in the groundmass. Photo 0335, XPL 5x magnification, FOV = 3 mm.

Primary phases (vol. %)
Plagioclase – 38%
Clinopyroxene – 31%
Opaque minerals – 10%

Secondary phases (vol. %)
Chlorite – 15%
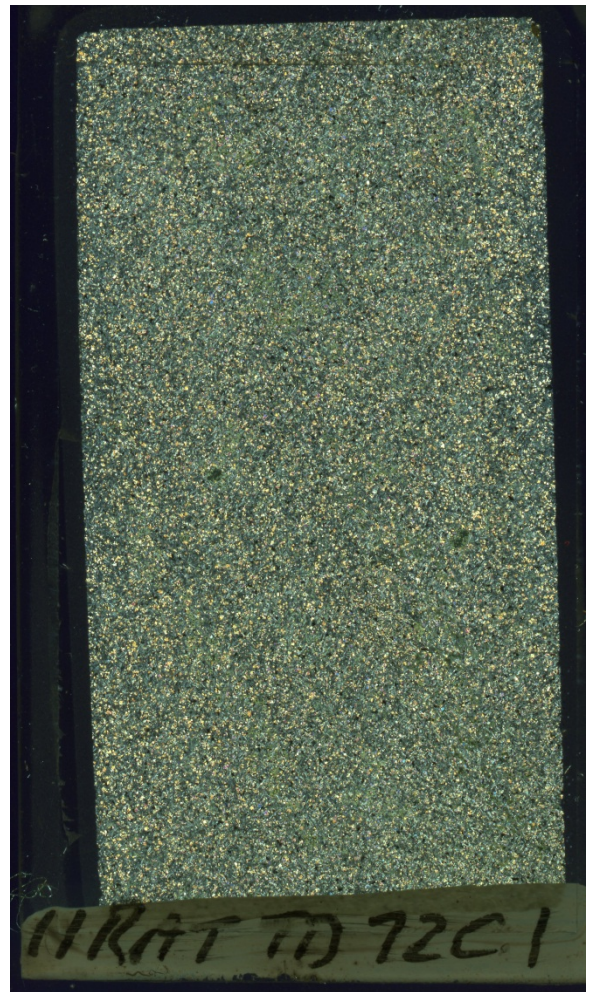Calcite – 6%

Amygdules 21%

LOI: 2.6 wt. %

Description
Fine-grained intergranular basalt with anhedral to subhedral plagioclase (0.4 mm) and clinopyroxene (0.1-0.2 mm) in the groundmass. Partially sericitized plagioclase. Amygdules (0.1-0.5 mm) consist of chlorite with radial extinction.

Scan: TL

Scan: XPL

Sample: 11RAT TD72D

Rock type: Basalt
Location: Eastern Section, cycle 1
Collected by: Trent Dell'Oro, 2011 season

Cpx and plag in the groundmass with interspersed chlorite alteration. Photo 0368, XPL 2x magnification, FOV = 7 mm.

Primary phases
Plagioclase – 41%
Clinopyroxene – 34%
Opaque minerals – 11%

Secondary phases
Chlorite – 13%

Amygdules 7 vol. %

LOI: 1.9 wt. %

Description
Fine-grained intergranular basalt with anhedral to subhedral plagioclase (0.2-0.5 mm) and clinopyroxene (0.1-0.4 mm) in the groundmass. Plagioclase is partially replaced by sericite. Chlorite-filled amygdules throughout.
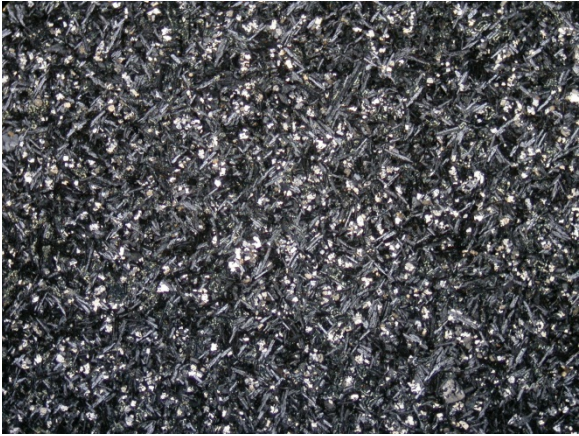

Scan: TL

Scan: XPL

Sample: 11RAT TD72E

Rock type: Basalt
Location: Eastern Section, cycle 1
Collected by: Trent Dell'Oro, 2011 season

Cpx and plag in the groundmass. Photo 0373, XPL 2x magnification, FOV = 7 mm.

Primary phases (vol. %)
Plagioclase – 39%
Clinopyroxene – 32%
Opaque minerals – 5%

Secondary phases (vol. %)
Chlorite – 14%
Calcite – 7%
Quartz – 5%

Amygdules 14 vol. %

LOI: 4.3 wt. %

Description
Fine-grained intergranular basalt with subhedral plagioclase (0.3-0.7 mm) and clinopyroxene (0.1-0.2 mm) in the groundmass. Plagiolcase is partially replaced by sericite. Chlorite dominates much of the small size fraction of amygdules (0.2-0.5 mm); quartz and calcite fill the larger amygdules (2-3 mm).

Scan: TL

Scan: XPL

Sample: 11RAT TD72F

Rock type: Basalt
Location: Eastern Section, cycle 1
Collected by: Trent Dell'Oro, 2011 season

Plag and cpx in the groundmass with cpx phenocrysts. Photo 0572, XPL 2x magnification, FOV = 7 mm.

Primary phases (vol. %)
Plagioclase – 40 %
Clinopyroxene – 35%
Opaque minerals – 10%

Secondary phases (vol. %)
Chlorite – 15%
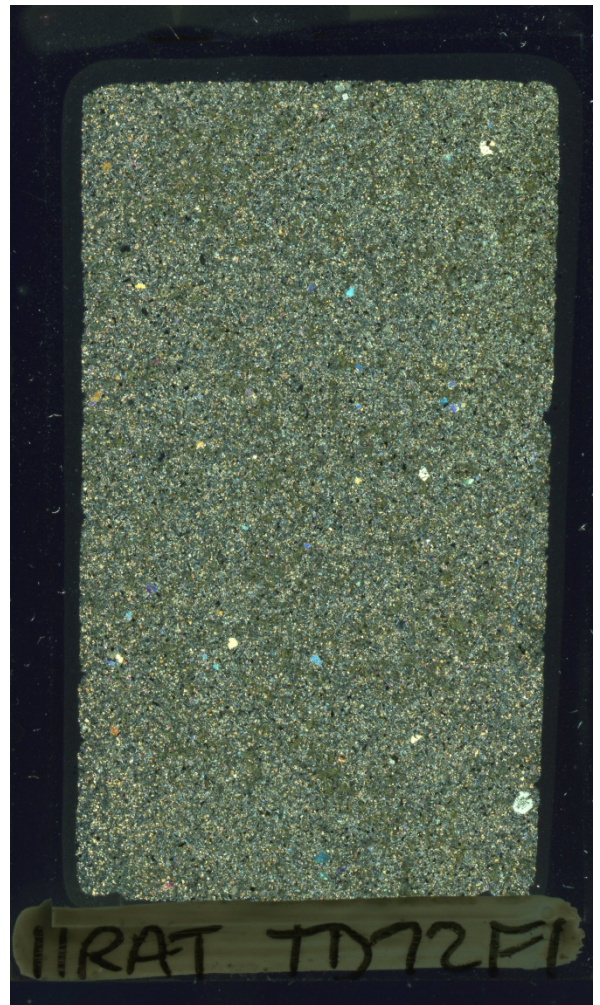
Amygdules 7 vol. %

LOI: 2.20 wt. %

Description
Fine-grained intergranular basalt with subhedral plagioclase (0.2-0.4 mm) and clinopyroxene (0.1-0.4 mm) in the groundmass. Rare clinopyroxene phenocrysts. Plagioclase partially replaced sericite. Chlorite-filled amygdules present throughout.

Scan: TL

Scan: XPL

Sample: 11RAT TD72G

Rock type: Basalt
Location: Eastern Section, cycle 1
Collected by: Trent Dell'Oro, 2011 season

Clot of coarse-grained cpx/plag amongst groundmass. Photo 0575, XPL 2x magnification, FOV = 7mm.

Primary phases (vol. %)
Plagioclase – 43%
Clinopyroxene – 35%
Opaque minerals –11%

Secondary phases (vol. %)
Chlorite – 4%
Apatite – 2%

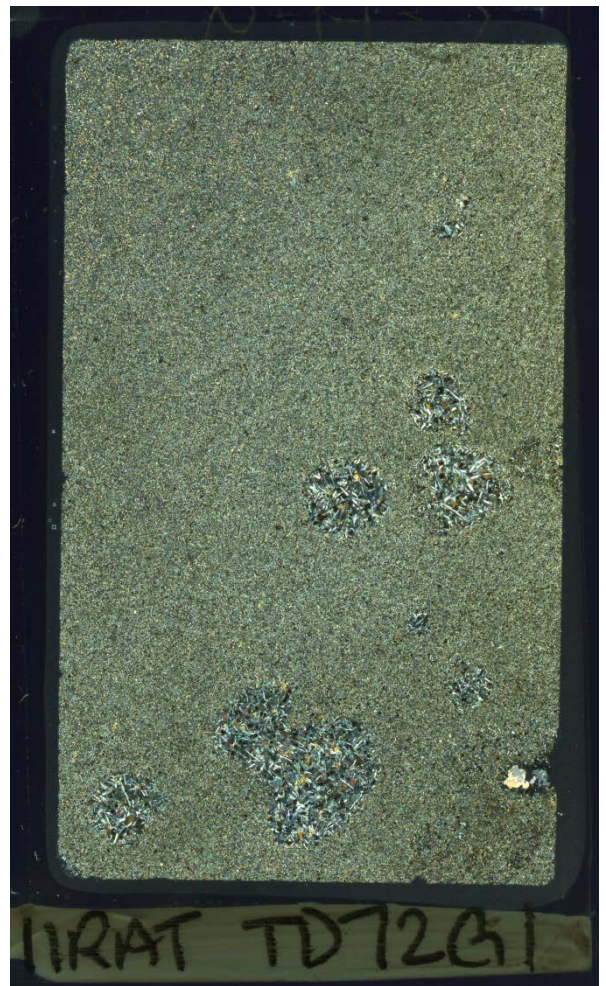**Amygdules** <1 vol. %

LOI: 0.5 wt. %

Description
Basalt with clinopyroxene and plagioclase groundmass (0.1-0.2 mm). Clots of coarse-grained clinopyroxene/plagioclase aggregates present throughout sample. The clots are up to 5 mm across.

Scan: XPL

Scan: TL

Sample: 11RAT TD73A

Rock type: Basalt
Location: Eastern Section, cycle 1
Collected by: Trent Dell'Oro, 2011 season

Cpx and plag in the groundmass with interspersed chlorite alteration. Photo 0584, XPL 2x magnification, FOV = 7 mm.

Primary phases (vol. %)
Plagioclase – 43%
Clinopyroxene – 34%
Opaque minerals –7%

Secondary phases (vol. %)
Chlorite – 15%

Amygdules 15 vol. %

LOI: 3.0 wt. %

Description
Fine-grained basalt with subhedral plagioclase (0.4-0.7 mm) and clinopyroxene (0.1-0.2 mm) in the groundmass. Rare plagioclase (~1.5 mm) and clinopyroxene (0.8 mm) phenocrysts. Green chlorite-filled amygdules throughout.

Scan: TL

Scan: XPL

Sample: 11RAT TD129A

Rock type: Basalt
Location: Western Section, cycle 1
Collected by: Trent Dell'Oro, 2011 season

Coarse-grained cpx and plag in the groundmass. Photo 1235, XPL 2x magnification, FOV = 7 mm.

Primary phases (vol. %)
Plagioclase – 40%
Clinopyroxene – 35%
Opaque minerals – 7%

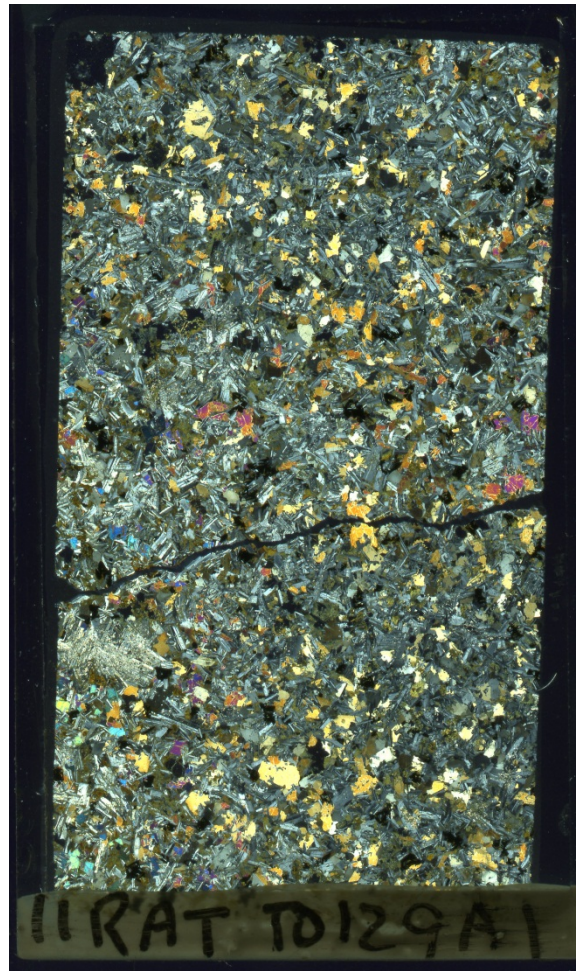**Secondary phases** (vol. %)
Chlorite – 15%
Calcite – 2%

Amygdules 10 vol. %

LOI: 1.8 wt. %

Description
Coarse-grained basalt with plagioclase (1-2 mm) and clinopyroxene (0.5-2 mm) in the groundmass. Secondary chlorite in amygdules. Minor calcite along veins and fractures.

Scan: TL

Scan: XPL

Sample: 11RAT TD129B

Rock type: Basalt
Location: Western Section, cycle 1
Collected by: Trent Dell'Oro, 2011 season
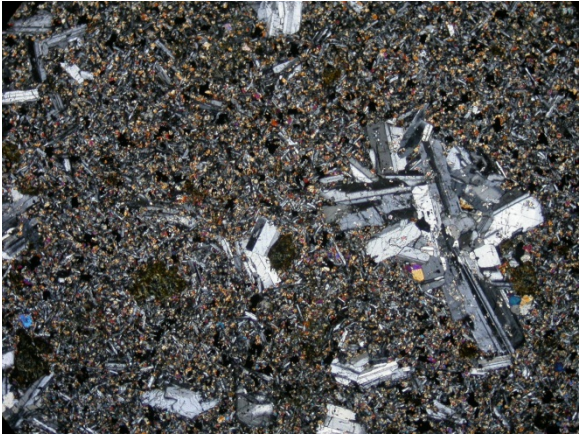
Plag glomerocrysts amongst fine-grained groundmass. Photo 1236, XPL 2x magnification, FOV = 7 mm.

Primary phases (vol. %)
Plagioclase – 40%
Clinopyroxene – 35%
Opaque minerals – 10%

Secondary phases (vol. %)
Chlorite – 10 %

Amygdules 5 vol. %

LOI: 0.8 wt. %

Description
Fine-grained glomeroporphyritic basalt with plagioclase (0.1-0.5 mm) and clinopyroxene (0.05-0.2 mm) in the groundmass. Plagioclase phenocrysts (1-2 mm) present as dispersed glomerocrysts (~2-4 mm) throughout the sample; clinopyroxene phenocrysts are rare. Relatively unaltered with minor amygdules.

Scan: TL
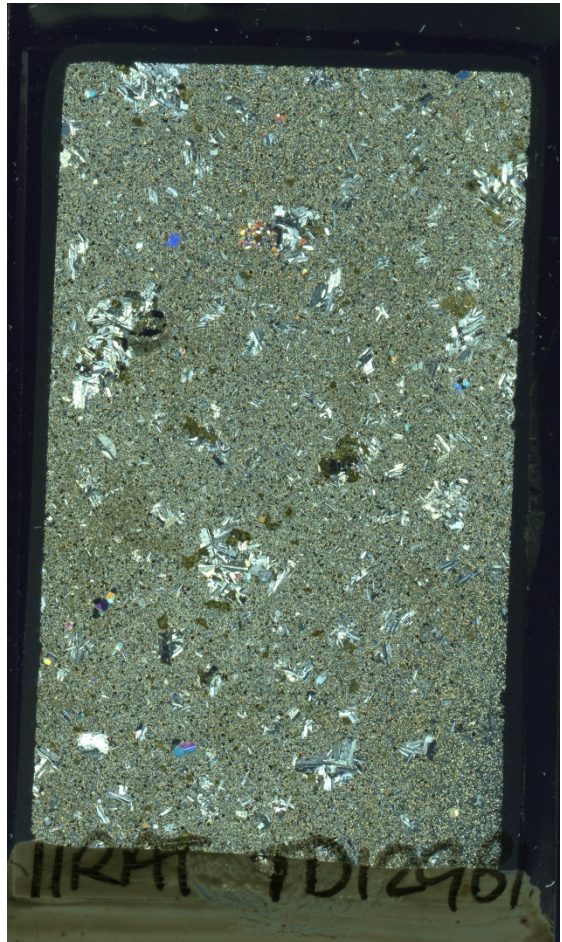
**Scan: XPL**

Sample: 11RAT TD129C

Rock type: Basalt
Location: Western Section, cycle 1
Collected by: Trent Dell'Oro, 2011 season

Ophitic cpx with plag in the groundmass and minor chlorite alteration. Photo 1237, 2x magnification, FOV = 7 mm.

Primary phases (vol. %)
Plagioclase – 32%
Clinopyroxene – 35%
Opaque minerals – 12%

Secondary phases (vol. %)
Chlorite – 18%
Calcite – 3%

Amygdules 20 vol. %

LOI: 3.2 wt. %

Description
Medium-grained basalt with distinctive subophitic clinopyroxene (1-1.5 mm) and plagioclase (0.5 mm) in the groundmass. Amygdules are filled with chlorite and calcite.

Scan: TL
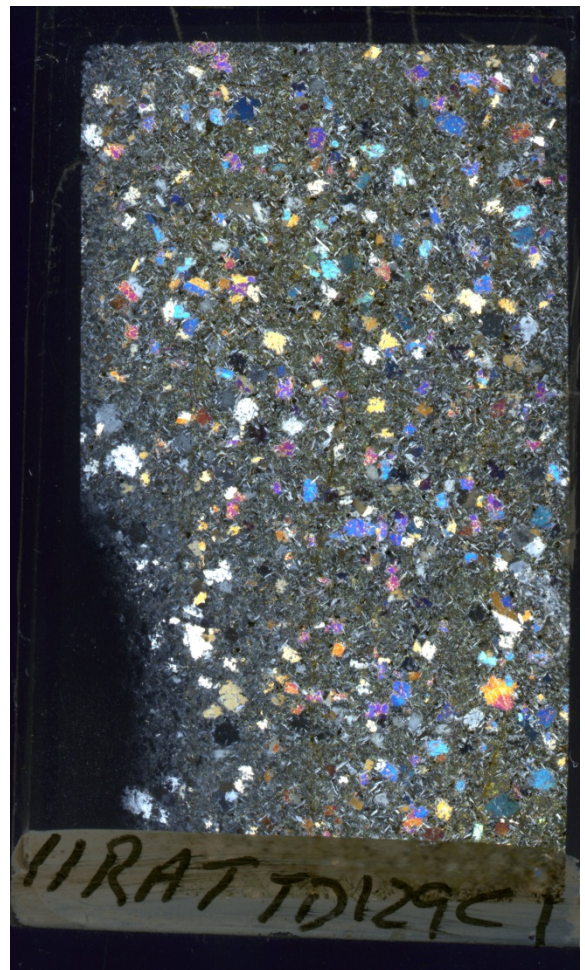
Scan: XPL

Sample: 11RAT TD129D

Rock type: Basalt
Location: Western Section, cycle 1
Collected by: Trent Dell'Oro, 2011 season

Ophitic cpx with plag in the groundmass and interspersed chlorite amygdules. Photo 0339, XPL 2x magnification, FOV = 7 mm.

Primary phases (vol. %)
Plagioclase – 30%
Clinopyroxene – 50%

Secondary phases (vol. %)
Chlorite – 20%

Amygdules 20 vol. %

LOI: 3.8 wt. %

Description
Basalt with ophitic clinopyroxene (0.5-1 mm) and plagioclase (1-3 mm) in the groundmass. Chlorite in amygdules (0.5-2 mm) and along grain boundaries.

Scan: TL
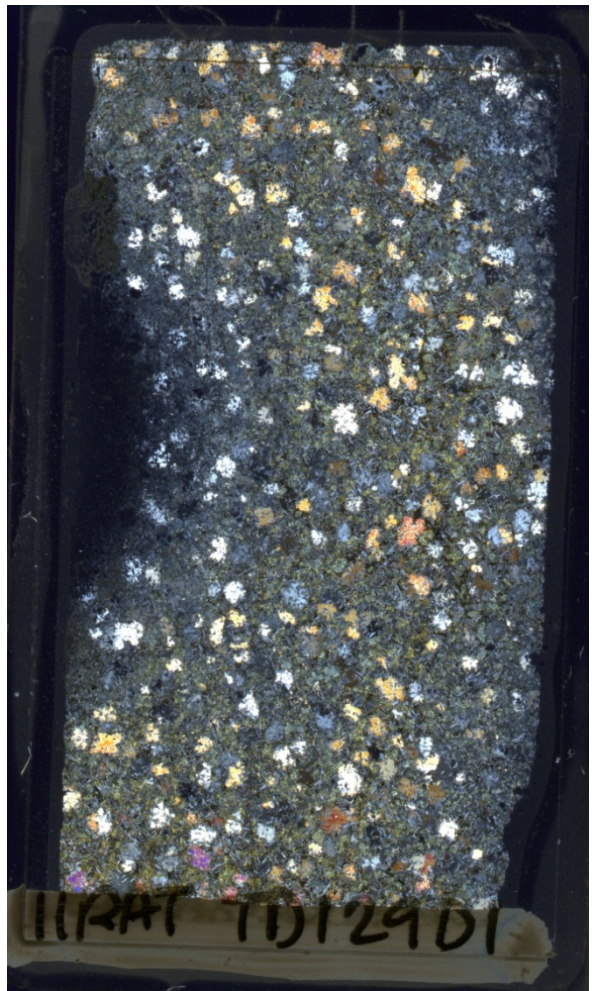
Scan: XPL

Sample: 11RAT TD129E

Rock type: Basalt
Location: Western Section, cycle 1
Collected by: Trent Dell'Oro, 2011 season

Cpx, plag, and opaque minerals in the groundmass. Photo 1240, XPL 2x magnification, FOV = 7 mm.

Primary phases (vol. %)
Plagioclase – 43%
Clinopyroxene – 38%
Opaque minerals – 15%

**Secondary phases** (vol. %)
Chlorite 3%

Amygdules <1 vol. %

LOI: 0.8 wt. %

Description
Relatively unaltered fine-grained basalt with plagioclase (0.1-0.5 mm) and clinopyroxene (0.05-0.1 mm) in the groundmass. Minor patches of chlorite alteration.
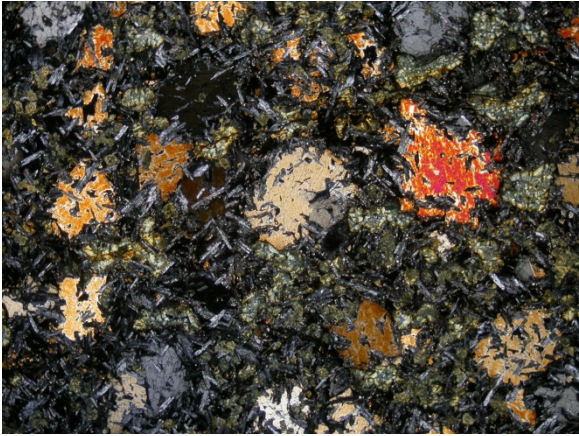

Scan: TL

Scan: XPL

Sample: 11RAT TD129F

Rock type: Basalt
Location: Western Section, cycle 1
Collected by: Trent Dell'Oro, 2011 season
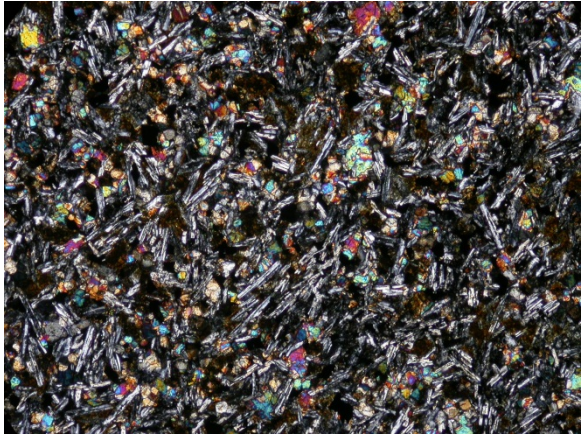
Cpx and plag in the groundmass with pervasive chlorite alteration. Photo 1241, XPL 5x magnification, FOV = 3 mm.

Primary phases (vol. %)
Plagioclase – 38%
Clinopyroxene – 32%
Opaque minerals – 14%

Secondary phases (vol. %)
Chlorite – 15%

Amygdules 12 vol. %

LOI: 4.2 wt. %

Description
Fine-grained basalt with plagioclase (0.1-0.5 mm) and clinopyroxene (0.05-0.2 mm) in the groundmass. Pervasive alteration, especially along fractures. Abundant small amygdules (~0.2 mm) of chlorite.

Scan: TL

Scan: XPL

Sample: 11RAT TD129G

Rock type: Basalt
Location: Western Section, cycle 1
Collected by: Trent Dell'Oro, 2011 season

Cpx and plag in the groundmass with minor chlorite alteration. Photo 1242, XPL 5x magnification, FOV = 3 mm.

Primary phases (vol. %)
Plagioclase – 40%
Clinopyroxene – 37%
Opaque minerals – 12%

Secondary phases (vol. %)
Chlorite – 10%

Amygdules 8 vol. %

LOI: 2.2 wt. %

Description
Fine-grained basalt with plagioclase (~0.3 mm) and clinopyroxene (0.2-0.4 mm) in the groundmass. Chlorite fills amygdules and void spaces.

Scan: TL

Scan: XPL

APPENDIX B

CHARACTERIZATION OF HYDROTHERMAL ALTERATION AND SECONDARY CHLORITE IN THE NATKUSIAK BASALTS

B1. Background

The most common secondary phases in hydrothermally altered basalt include mafic phyllosilicates, calcite, zeolites, and quartz. Secondary alteration of basaltic rocks has been extensively studied, including locations such as the Kerguelen Archipelago, Hawaiian Islands and the Emperor Seamount chain, basalts of eastern Iceland, the East Taiwan Ophiolite, western Greenland, and Keweenawan basalts (e.g., Walker 1960; Liou 1979; Sevigny et al., 1992; Schmidt 1993; Neuhoff et al., 2006; Hanano et al., 2009; Renac et al., 2009).

Secondary hydrothermal alteration is pervasive throughout the basalts of the Natkusiak Formation (see Table 2.3 and Appendix A) on Victoria Island, Canada. The basalts contain a variety of secondary minerals mostly precipitated within the former vesicles of the rock in the form of amygdules that range in diameter from a few fractions of a millimeter to centimeters. The secondary minerals include chlorite ($(Mg,Fe^{2+},Fe^{3+},Mn,Al)_{12}[(Si,Al)_8O_{20}](OH)_{16}$) (Deer et al., 1992), quartz, calcite, and rare zeolites. This study focused on assessing the alteration assemblages in the Natkusiak Formation, and estimates the relative temperature of the hydrothermal fluids during precipitation of secondary minerals. Relative fluid temperatures are based on the smectite-chlorite reaction series (trioctahedral smectite $\rightarrow$ mixed chlorite-smectite $\rightarrow$ chlorite). This mineralogical transition is largely a result of increasing temperature in a hydrothermal system (Cathelineau et al., 1985; Schiffman et al., 1991; Bevins et al., 1991; Bettison-Varga et al., 1997; Schmidt et al., 1997; Neuhoff et al., 2006;).

Chlorite composition is used to estimate the relative fluid temperatures based on the Schiffman et al. (1991) study of drillhole Nj-15 in Iceland's Nesjavellir geothermal field. They report on a complete smectite to chlorite transition within an active hydrothermal system that ranges in temperature from 60 to 300 ºC. The hydrothermal temperatures and mineralogical compositions determined in Schiffman et al. (1991) provide a modern-day example of a system

undergoing hydrothermal alteration through the smectite-chlorite transition and allow for the assignment of relative hydrothermal fluid temperatures in the Natkusiak basalts by comparison.

B2. Methods

Alteration phases were initially identified based on morphology and optical properties in polished thin sections using a conventional optical microscope. Further alteration characterization and mineral identification were carried out on a scanning electron microscope (SEM). Backscattered electron images (BSE), digital multi-element maps, and qualitative energy dispersive spectra (EDS) were collected on carbon-coated polished petrographic thin sections using a Phillips XL-30 scanning electron microscope equipped with a Princeton-Gamma-Tech energy dispersive spectrometer in the electron microbeam/ X-ray diffraction facility at UBC. Operating parameters of the SEM were set to 15 kV with a spot diameter of 6 µm and a peak count time of 30 seconds for EDS. Electronprobe microanalysis (EPMA) was carried out on four samples (10RAT TD15A2, 10RAT TD16A2, 10RAT TD55A3, and 10RAT TD61A1) selected based on SEM analysis where chlorite was positively identified (initially identified by optical microscopy). The analyses were done on a CAMECA SX100 electron-probe micro-analyzer with a beam current of 10 nA and 10 µm beam size over a series of 40 analyses. Elements analyzed included Si, Ti, Al, Fe, Mn, Ca, K, Mg, and Na; corrections for calibration were made with biotite standard S453. Data are shown in Table B1; all microprobe results for chlorite were recalculated on a 28 oxygen basis.

B3. Results

The basal unit of the Natkusiak Formation, located within the first 70 m of section measured from the contact with the Kuujjua sandstone, contains the highest volume of amygdules (up to 32 vol.%). Basal basalts are pervasively altered throughout; up to 30% of

Table B1: Electron microprobe analyses of chlorite from the Natkusiak basalts

Sample*	55A3-1	55A3-2	55A3-3	55A3-4	61A1-1	61A1-2	61A1-3	61A1-4	61A1-5	61A1-6	61A1-7	61A1-8	61A1-9	61A1-10
Section	Central	Central	Central	Central	Central	Central	Central	Central	Central	Central	Central	Central	Central	Central
Group	Basal	Basal	Basal	Basal	Cycle 1	Cycle 1	Cycle 1	Cycle 1	Cycle 1	Cycle 1	Cycle 1	Cycle 1	Cycle 1	Cycle 1
Oxides														
SiO_2	31.36	30.38	32.12	30.78	27.90	32.59	33.56	31.54	32.13	33.01	32.03	31.60	34.16	31.14
TiO_2	0.06	0.06	0.04	0.02	0.05	0.59	0.00	0.03	0.00	0.06	0.02	0.00	0.03	0.01
Al_2O_3	12.58	12.52	11.67	12.79	9.79	11.33	12.00	11.57	12.21	12.01	11.30	11.52	12.02	11.07
Fe_2O_3	28.31	27.56	27.08	28.46	20.81	24.28	25.45	26.41	27.97	27.73	29.81	25.28	25.28	24.90
MnO	0.15	0.11	0.16	0.21	0.04	0.19	0.18	0.28	0.26	0.24	0.16	0.16	0.24	0.24
MgO	15.97	16.11	16.21	16.00	13.52	17.68	15.85	16.48	14.70	14.87	13.64	15.77	15.82	14.22
CaO	0.21	0.22	0.37	0.21	0.63	0.66	0.82	0.36	0.59	0.64	0.61	0.46	0.85	0.86
Na_2O	0.05	0.05	0.05	0.08	0.12	0.08	0.13	0.06	0.10	0.12	0.16	0.08	0.09	0.24
K_2O	0.01	0.01	0.05	0.05	0.07	0.07	0.10	0.04	0.05	0.06	0.07	0.08	0.06	0.11
Total	88.71	87.01	87.75	88.61	72.91	87.47	88.09	86.78	88.01	88.74	87.82	84.95	88.54	82.79
Cations														
Si	6.60	6.52	6.80	6.51	7.00	6.82	6.99	6.74	6.81	6.91	6.88	6.86	7.06	6.96
Ti	0.01	0.01	0.01	0.00	0.01	0.09	0.00	0.00	0.00	0.01	0.00	0.00	0.00	0.00
Al	3.12	3.17	2.91	3.19	2.89	2.80	2.95	2.92	3.05	2.96	2.86	2.95	2.93	2.91
Fe^{+2}	4.99	4.95	4.79	5.03	4.37	4.25	4.43	4.72	4.96	4.85	5.36	4.59	4.37	4.65
Mn	0.03	0.02	0.03	0.04	0.01	0.03	0.03	0.05	0.05	0.04	0.03	0.03	0.04	0.05
Mg	5.02	5.16	5.11	5.05	5.06	5.52	4.92	5.25	4.64	4.64	4.37	5.10	4.87	4.74
Ca	0.05	0.05	0.08	0.05	0.17	0.15	0.18	0.08	0.13	0.14	0.14	0.11	0.19	0.21
Na	0.02	0.02	0.02	0.03	0.06	0.03	0.05	0.03	0.04	0.05	0.07	0.03	0.03	0.10
K	0.00	0.00	0.01	0.01	0.02	0.02	0.03	0.01	0.01	0.02	0.02	0.02	0.01	0.03
Total	19.84	19.90	19.76	19.92	19.58	19.71	19.58	19.81	19.70	19.63	19.73	19.69	19.50	19.65
Si+Al+Fe+Mg	19.73	19.79	19.61	19.78	19.32	19.39	19.29	19.64	19.46	19.37	19.47	19.50	19.22	19.26
Na+Ca+K	0.07	0.07	0.12	0.10	0.25	0.20	0.26	0.12	0.19	0.21	0.23	0.16	0.24	0.34

*Samples analyzed are 10RAT TD15A2, 1RAT TD16A2, 10RAT TD55A3, and 10RAT TD61A1.

Table B1 continued

Sample	16a2-1	16a2-2	16a2-3	16a2-4	16a2-5	16a2-6	16a2-7	16a2-8	16a2-9	16a2-10	15A2-11	15A2-12	15A2-13	15A2-14
Section	Central	Central	Central	Central	Central	Central	Central	Central	Central	Central	Central	Central	Central	Central
Group	Basal	Basal	Basal	Basal	Basal	Basal	Basal	Basal	Basal	Basal	Basal	Basal	Basal	Basal
Oxides														
SiO_2	32.02	31.47	32.07	32.82	32.52	32.27	31.98	31.72	32.01	31.88	41.44	42.70	42.93	39.54
TiO_2	0.01	0.00	0.02	0.00	0.02	0.01	0.00	0.04	0.00	0.00	0.00	0.01	0.05	0.00
Al_2O_3	12.76	12.69	12.57	12.69	12.76	12.20	12.79	12.98	12.59	12.70	8.15	7.34	7.42	7.40
Fe_2O_3	23.90	22.57	23.93	20.48	22.58	19.46	23.00	24.93	24.17	23.93	21.59	18.62	19.02	20.13
MnO	0.17	0.11	0.09	0.18	0.19	0.11	0.13	0.17	0.16	0.12	0.05	0.00	0.06	0.00
MgO	18.88	18.71	19.03	20.51	19.88	20.04	18.55	18.91	18.69	18.50	17.36	18.39	18.27	16.27
CaO	0.17	0.22	0.18	0.31	0.20	0.41	0.24	0.18	0.13	0.21	1.46	1.12	1.24	4.47
Na_2O	0.06	0.02	0.05	0.06	0.08	0.08	0.04	0.05	0.06	0.07	0.12	0.21	0.23	0.10
K_2O	0.04	0.06	0.03	0.11	0.10	0.17	0.06	0.03	0.07	0.07	0.11	0.22	0.17	0.10
Total	88.02	85.84	87.98	87.17	88.34	84.76	86.79	89.01	87.89	87.49	90.28	88.63	89.39	88.01
Cations														
Si	6.63	6.65	6.65	6.74	6.66	6.79	6.69	6.54	6.65	6.65	8.11	8.36	8.35	8.01
Ti	0.00	0.00	0.00	0.00	0.00	0.00	0.00	0.01	0.00	0.00	0.00	0.00	0.01	0.00
Al	3.12	3.16	3.07	3.07	3.08	3.03	3.15	3.15	3.08	3.12	1.88	1.69	1.70	1.77
Fe^{+2}	4.14	3.99	4.15	3.52	3.87	3.43	4.02	4.30	4.20	4.17	3.53	3.05	3.10	3.41
Mn	0.03	0.02	0.02	0.03	0.03	0.02	0.02	0.03	0.03	0.02	0.01	0.00	0.01	0.00
Mg	5.83	5.89	5.88	6.28	6.07	6.29	5.78	5.81	5.79	5.75	5.07	5.37	5.30	4.91
Ca	0.04	0.05	0.04	0.07	0.04	0.09	0.05	0.04	0.03	0.05	0.31	0.24	0.26	0.97
Na	0.02	0.01	0.02	0.02	0.03	0.03	0.02	0.02	0.03	0.03	0.05	0.08	0.09	0.04
K	0.01	0.02	0.01	0.03	0.03	0.05	0.02	0.01	0.02	0.02	0.03	0.06	0.04	0.02
Total	19.82	19.78	19.83	19.75	19.82	19.73	19.75	19.90	19.83	19.81	18.98	18.85	18.85	19.14
Si+Al+Fe+Mg	19.72	19.69	19.74	19.60	19.68	19.54	19.64	19.79	19.73	19.70	18.59	18.48	18.45	18.10
Na+Ca+K	0.07	0.07	0.07	0.12	0.10	0.17	0.09	0.07	0.07	0.09	0.38	0.37	0.39	1.03

Table B1 continued

Sample	15A2-15	15A2-16	15A2-17	15A2-18	15A2-19	15A2-20	15A2-21	15A2-22	15A2-23	15A2-24	15A2-25	15A2-26
Section	Central	Central	Central	Central	Central	Central	Central	Central	Central	Central	Central	Central
Group	Basal	Basal	Basal	Basal	Basal	Basal	Basal	Basal	Basal	Basal	Basal	Basal
Oxides												
SiO_2	37.48	41.64	40.30	37.07	47.98	46.50	38.50	47.13	37.46	42.52	47.24	40.42
TiO_2	0.00	0.08	0.04	0.01	0.01	0.01	0.04	0.01	0.00	0.00	0.01	0.03
Al_2O_3	9.36	7.34	8.15	8.78	5.77	5.98	8.65	5.86	8.69	7.05	5.77	8.35
Fe_2O_3	25.08	19.52	20.72	24.11	16.75	16.62	22.80	16.26	22.71	18.40	16.40	21.25
MnO	0.00	0.08	0.03	0.01	0.03	0.02	0.05	0.00	0.02	0.00	0.08	0.05
MgO	16.52	18.25	17.80	16.56	16.58	16.86	17.55	16.79	16.96	18.38	16.12	18.08
CaO	0.90	1.00	1.05	1.29	2.17	1.89	0.70	1.75	0.76	0.99	2.04	0.89
Na_2O	0.07	0.21	0.14	0.12	0.27	0.23	0.18	0.29	0.16	0.21	0.28	0.10
K_2O	0.05	0.15	0.17	0.08	0.16	0.19	0.15	0.22	0.12	0.18	0.25	0.15
Total	89.45	88.27	88.40	88.01	89.73	88.30	88.62	88.31	86.89	87.73	88.19	89.32
Cations												
Si	7.60	8.25	8.04	7.63	9.10	8.98	7.78	9.07	7.73	8.40	9.11	8.00
Ti	0.00	0.01	0.01	0.00	0.00	0.00	0.01	0.00	0.00	0.00	0.00	0.00
Al	2.23	1.71	1.92	2.13	1.29	1.36	2.06	1.33	2.11	1.64	1.31	1.95
Fe^{+2}	4.25	3.23	3.46	4.15	2.66	2.68	3.85	2.62	3.92	3.04	2.65	3.52
Mn	0.00	0.01	0.01	0.00	0.00	0.00	0.01	0.00	0.00	0.00	0.01	0.01
Mg	4.99	5.39	5.29	5.08	4.69	4.85	5.28	4.82	5.22	5.42	4.64	5.33
Ca	0.20	0.21	0.23	0.28	0.44	0.39	0.15	0.36	0.17	0.21	0.42	0.19
Na	0.03	0.08	0.06	0.05	0.10	0.09	0.07	0.11	0.06	0.08	0.11	0.04
K	0.01	0.04	0.04	0.02	0.04	0.05	0.04	0.05	0.03	0.05	0.06	0.04
Total	19.31	18.94	19.05	19.34	18.32	18.41	19.24	18.35	19.26	18.84	18.31	19.07
Si+Al+Fe+Mg	19.07	18.59	18.71	18.99	17.74	17.88	18.97	17.83	18.99	18.50	17.71	18.79
Na+Ca+K	0.24	0.33	0.33	0.35	0.58	0.52	0.26	0.52	0.26	0.34	0.59	0.26

primary plagioclase is altered to secondary minerals in some samples. Clinopyroxene was

relatively resistant to secondary alteration and phenocrysts are fresh and intact. The infilling

quartz, chlorite, and calcite is not entirely uniform or concentric in many specimens (Fig.B1 A).

Only a few amygdules are dominated by a single phase, and when this occurs it is most

commonly chlorite or calcite (Fig. B1 B and C). In many cases, amygdules are uniformly

distributed throughout the sample and appear in both discrete and interconnected patches (Fig.

B1 D).

Secondary chlorite is texturally variable. In basalts closer to the Kuujjua sandstone

contact, chlorite amygdules are rimmed with radially textured chlorite, whereas the chloritic

cores of these amygdules are quite featureless with no radiating texture. A few meters upsection,

radiating chlorite is the dominant texture in amygdules with no distinction between the rims and

core (Fig. B1 B). Further up the sampled section, secondary chlorite becomes deeper green in

plane-polarized light (PPL) with a distinct foliated texture (Fig. B1 E).

BSE images and multi-element maps highlight the complex mineral distribution in the

amygdules (Fig. B2 A), as several phases are typically intergrown making optical identification

difficult. A multi-element map of an amygdule from Fig. B1 A and B is shown in a multi-

element image where several chemically distinct phases of secondary minerals are evident (Fig.

B2 A, B, C and D). In some cases, amygdules show sequential precipitation of secondary

minerals with well-formed rims of chlorite and calcite cores (Fig. B2 B).

Chlorite minerals were identified by EDS in a number of amygdules (Fig. B3). The

chemical variation between chlorite and smectite is discernible through microanalysis and reveal

the presence of multi-layered smectite mixed with pure chlorite layers in the Natkusiak basalts.

When recalculated, chlorites that contain more than 6.25 Si cations per formula unit invariably

contain some smectite clay layers (Fig. B4 A) (e.g., Schiffman et al. 1991). Silica content is

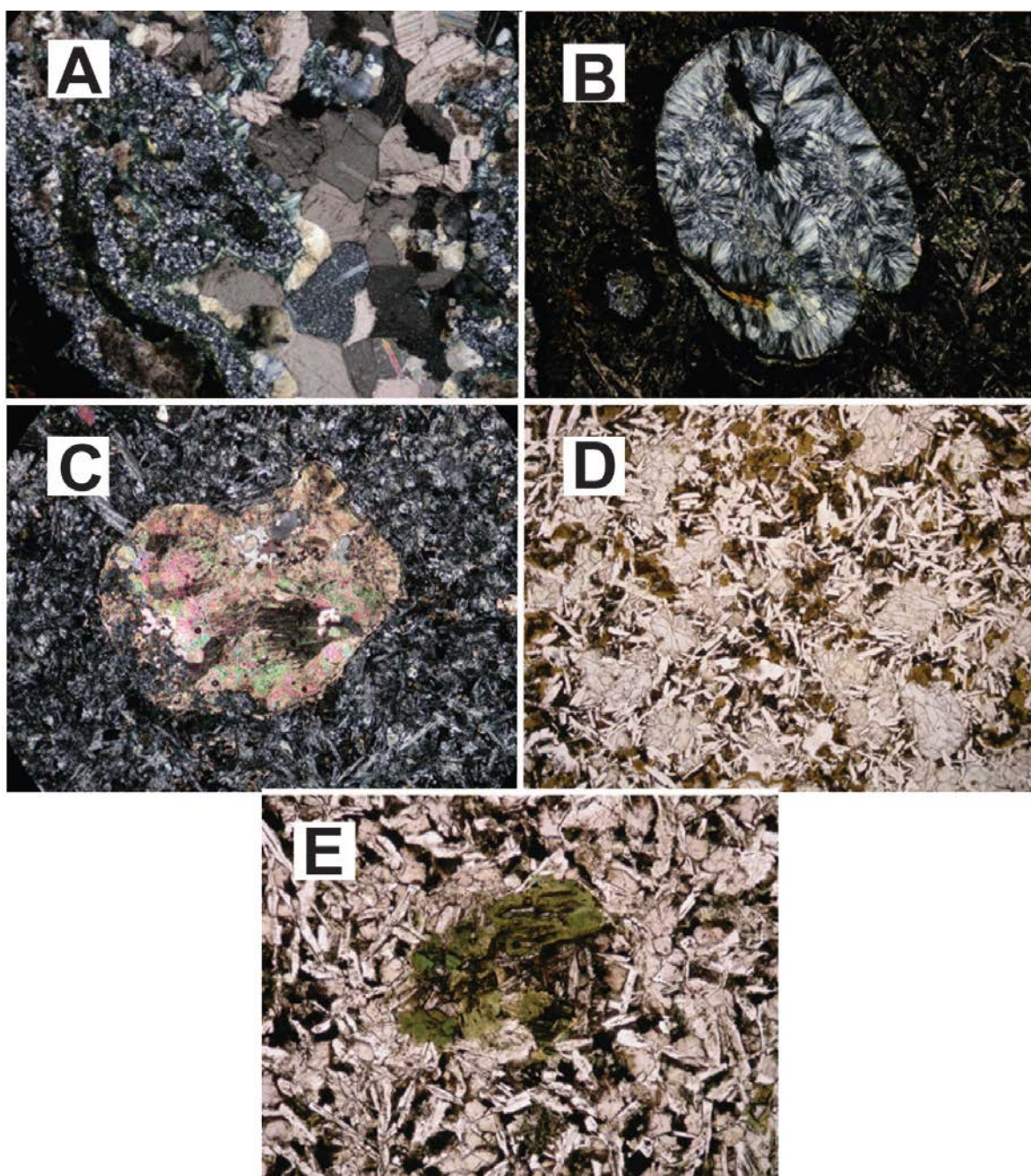strongly correlated to the alkali and alkaline earth elements (Na, K, and Ca), because smectite

Figure B1 Photomicrographs of alteration minerals in the Natkusiak basalts. **A)** Sample 16A2, FOV = 1.5 mm XPL. Several phases including hydrothermal calcite, quartz, and chlorite in a single amygdule. **B)** Sample 16A2, FOV = 3mm, XPL. Amygdule filled with radiating chlorite. **C)** Sample 18A2, FOV = 3mm field of view, XPL. Calcite-filled amygdule with minor quartz. **D)** Sample 15A2, FOV = 7 mm field of view, PPL. Discrete and interconnected patches of greenish-brown chlorite-filled amygdules. **E)** Sample 61A1, FOV = 1.5 mm, PPL. Secondary chlorite with foliated texture and deep green color in PPL.
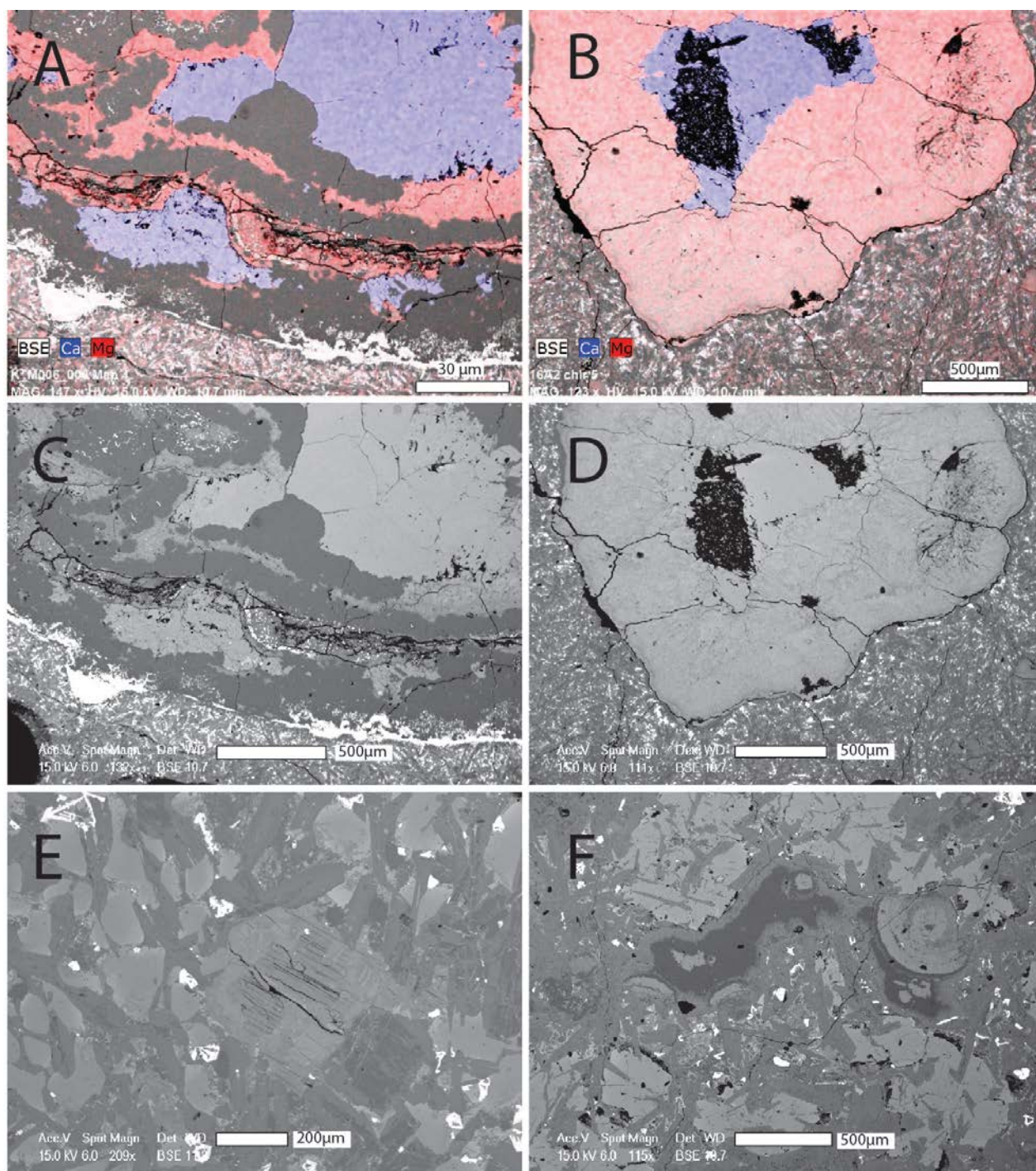
Figure B2 Backscatter electron images and multi-element maps of basalt samples. **A)** Multi-element map of amygdule shown in Figure 1 A. Calcium and magnesium are highlighted to visually distinguish calcite and chlorite. **B)** Multi-element map of amygdule, calcium and magnesium are highlighted to visually distinguish calcite and chlorite. **C)** BSE image of the same amygdule shown in Figure 2 A. **D)** BSE image of the same amygdule shown in Figure B2 B. **E)** BSE image of foliated chlorite shown in Figure 1 E. **F)** BSE image of an amygdule with chlorite core and radial chlorite rim from sample 15A2. Scales as indicated on pictures.
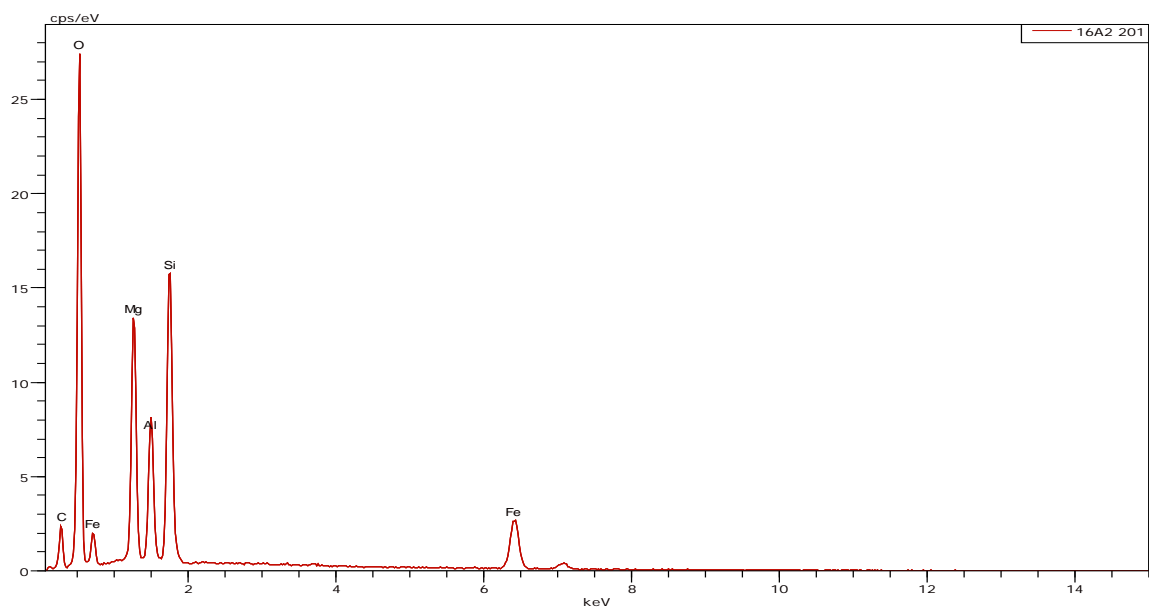
Figure B3 Energy dispersive spectra (EDS) collected on chlorite in amygdule in sample 16A2.
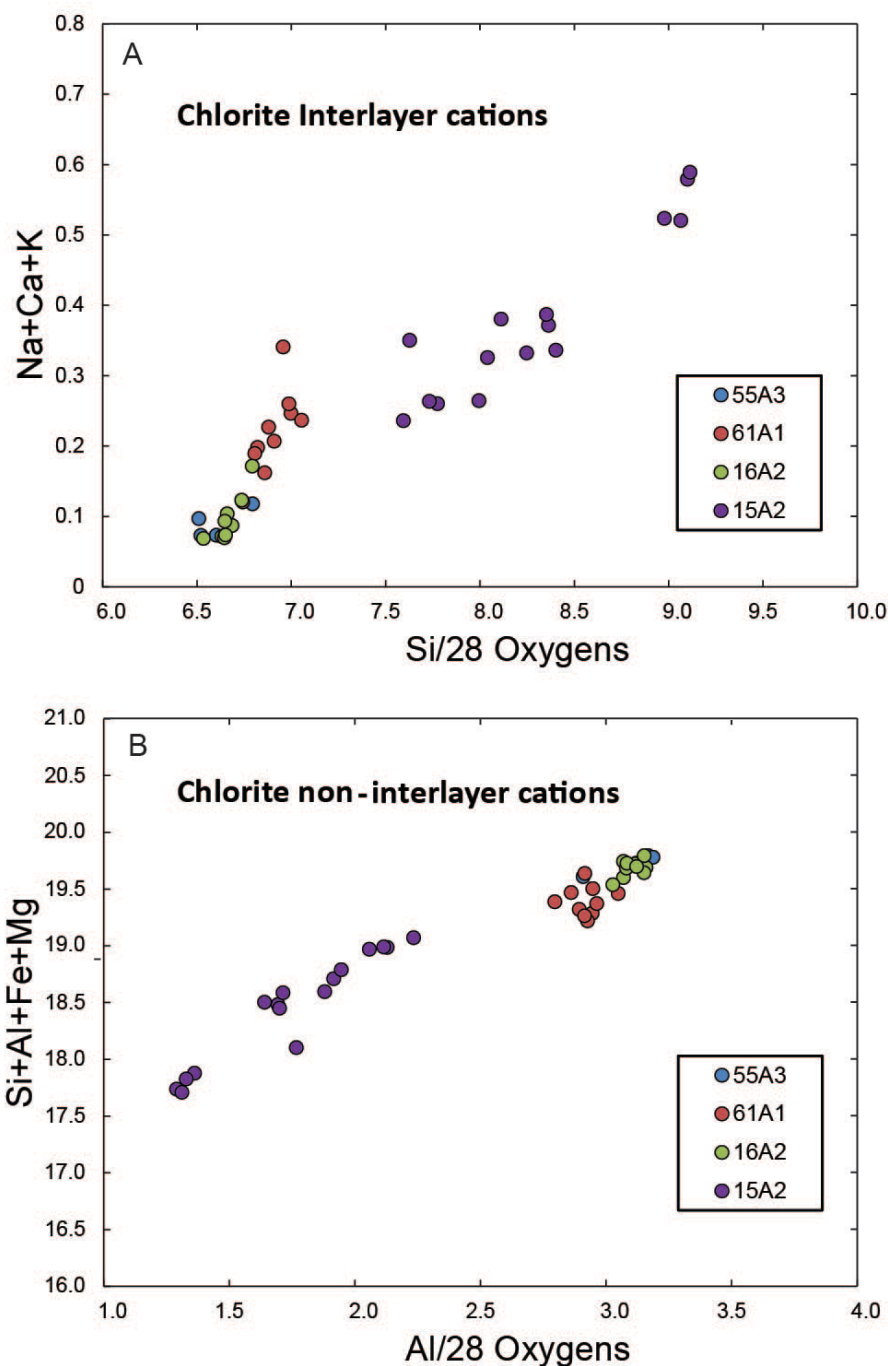
Figure B4 Chlorite compositions on binary variation diagrams. All microprobe analyses have been recalculated to a 28 oxygen basis. **A)** The positive correlation of Si and interlayer cations (Na+Ca+Ca) indicates smectite-chlorite interlayers; analyses exceeding 6.25 Si cations contain some smectite interlayers. Sample 15A2 has the largest variation in terms of both Si content and interlayer cations. Samples 61A1 and 16A2 plot beyond the 6.25 Si point and 55A3 is near 7 Si with slightly higher interlayer cation contents than samples 61A1 and 16A2. **B)** Chlorite non-interlayer cations (Si+Al+Fe+Mg) plotted against total Al in chlorite. Sample 15A2 shows the lowest contents of non-interlayer cations per Al and the largest variation in the diagram. Samples 16A2, 55A3, and 61A1 plot very near to pure chlorite.

173

contains a larger proportion of interlayers stratified amongst the pure chlorite non-interlayers. Chlorite will always contain a higher proportion of non-interlayers per Al in its crystal structure than smectite. A plot of non-interlayers versus total Al also effectively distinguishes between pure chlorite and specimens mixed with smectite (Fig. B4 B).

B4. Interpretation

Mafic phyllosilicates exhibit changes in crystal structure and chemistry as a result of ambient hydrothermal conditions. The smectite-chlorite transition is strongly temperature dependent, which makes chlorite microanalysis a valuable tool for estimating relative temperature in hydrothermally altered mafic rocks (Cathelineau et al., 1985; Schiffman et al., 1991; Bevins et al., 1991; Bettison-Varga et al., 1997; Schmidt et al., 1997; Neuhoff et al., 2006). Dioctahedral smectite clays are stable in fluid temperatures up to around 200°C, and are transformed into mixed-layer clay minerals (e.g., illite) and swelling chlorite in the temperature range of 200-230°C. Finally, at temperatures above 240°C, trioctahedral smectite is transformed into chlorite, which becomes the prominent mafic phyllosilicate phase (Bevins et al., 1991, Neuhoff et al., 2006).

The lowermost basalt sample (15A2), collected 1 m from the Kuujjua contact, contains the largest variation in non-interlayer cations (Fig. B4 B), which is likely related to variable hydrothermal fluid temperatures recorded in the smectite-chlorite transition sequence. Sample 15A2 also defines a trend apart from the basalts found up-section (Fig. B4 B). This suggests that the hydrothermal fluid that chlorite was precipitating from in the lowermost basalts was geochemically distinct from the fluid in the upper basalts. Chlorite from the three samples analyzed up-section are nearly pure chlinochlore $(Mg_5Al)(AlSi_3)O_{10}(OH)_8$ – chamosite $(Fe_5Al)(AlSi_3)O_{10}(OH)_8$ solid solution and provide evidence for a steep hydrothermal temperature gradient within the Natkusiak basalts. Sample 16A2 is located just 12 m above the

Kuujjua contact, and is nearly pure chlorite, and samples 55A3 (14 m) and 61A1 (74 m) have compositions similar to 16A2. Thus, at least two zones of alteration are apparent within the first 70 m of stratigraphy of the Natkusiak basalts. Zone 1 contains a variety of smectite-chlorite mixtures and occurs from the base of the Natkusiak Formation up to no more than 12 m and likely records hydrothermal temperatures between 200 and 240ºC. Zone 2 is defined by nearly pure chlorite and appears to have experienced hydrothermal fluids to at least 270ºC or higher. Zone 1 may be an interface zone between the overlying high temperature zone 2 and the underlying cooler wet sediments below. The chlorite-smectite compositions recorded in sample 15A2 may be explained by an influx of cooler fluids derived from the underlying unconsolidated sediments. The Kuujjua sandstone was an active fluvial system during initial eruption of the Natkusiak basalts (Rainbird et al., 1996); pillow basalts and thin inter-beds of sandstone and basalt occur within the first few meters of the section.

APPENDIX C

A RECONNAISSANCE STUDY OF PLAGIOCLASE CRYSTAL SIZE DISTRIBUTION (CSD) IN THE NATKUSIAK BASALTS

C1. Background

Quantitative petrographic analysis of igneous rocks includes crystal size distribution (CSD) (Higgins et al., 2000). In a CSD study, measured grain sizes are plotted against the population densities of grain sizes and the resulting curves are related to the igneous processes involved in the crystallization of the rock. In this study, the systematics of plagioclase crystals in select basalts from the Natkusiak Formation, Victoria Island, are examined.

C2. Methods

Four samples were selected from the western section (see Fig. 1.8) of the Natkusiak Formation flood basalts in the southern lobe. Sample 129A is the lowermost sample in the measured section, followed by 129B, 129C, and 129D; each of the samples is approximately spaced 5-10 meters in the section. Both samples 129A and 129B are plagioclase-phyric basalts, whereas samples 129C and 129D are aphyric basalts with prominent subophitic clinopyroxene. Plagioclase crystal size distributions were measured two-dimensionally on scanned thin section images. The thin sections were scanned at 3200 dpi to capture the fine-grained groundmass of the basalt rocks. Plagioclase grains were outlined manually over the scanned images in Adobe Illustrator to produce black polygon outlines of the grains (Figs. C1-4). A total of 1,847 grains were outlined for sample 129A, 1,332 grains for 129B, 1,701 grains for 129C, and 912 grains for 129D. The images produced in Adobe Illustrator were converted to binary black and white images for automatic analysis of the polygons. The black and white images were then processed with ImageJ software (Rasband, 2012), which automatically measures lengths, widths, and area of the polygons. Data produced from the ImageJ software was then processed in CSDCorrections[©] software (Higgins, 2011) to calculate the frequency distribution of the area number densities.

C3. Results

The results utilize the measured lengths, widths, and areas of plagioclase crystals to calculate the sizes and population densities of varying grain sizes in the samples (Shea et al., 2010). CSD data typically have a logarithmic-normal distribution when ln (population density) vs. grain size is plotted. Sample 129A displays a near linear relationship (Fig. C5 A); a slight decrease in the population of the smallest grains may be an artifact due to sampling bias. Sample 129B shows a similar relationship (Fig. C5 A), but with a drop-off at the smallest grain sizes. Samples 129C and 129D show similar relationships, but with concave down curves at the smallest grain sizes, suggesting that smaller grains are less abundant. Sample 129C has a kinked concave-up line at the largest grain sizes.

C4. Interpretation

Interpretation of the CSD graphs of ln(population density) versus grain size suggest a single stage of nucleation and crystallization occurred in the lower basalts. Basalts for samples 129A and 129B show simple log-linear results that suggest a single nucleation event and steady growth occurred uninterrupted during cooling (Shea et al., 2010). The results for sample 129C show a kink that corresponds to a larger population of plagioclase grains (0.4 to 0.6 mm) (Fig. C5 B). This kink may indicate a second stage of nucleation and growth of plagioclase that may be related to the growth of clinopyroxene in the groundmass. Clinopyroxene was not outlined for CSD calculations, however, microscope observation reveal strongly subophitic clinopyroxene. Sample 129D appears textually comparable to 129C in thin section and the CSD results are similar (Fig. C5 B), although without the largest grains. The apparent loss of the smallest plagioclase crystals in these two samples may also reflect growth of the subophitic clinopyroxene and resorption of the smallest plagioclase grains as they were the most energetically unstable.
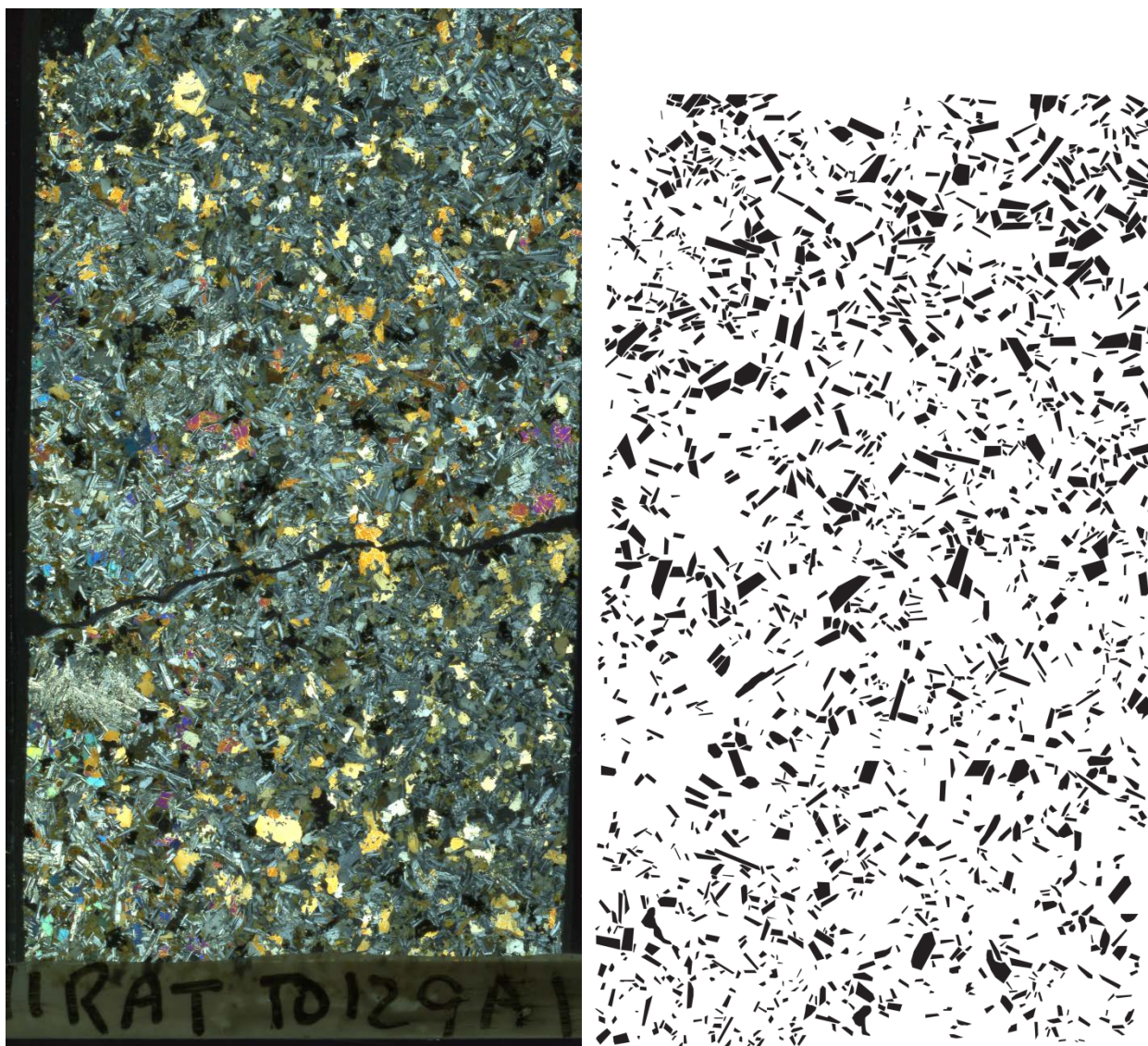
Figure C1 Thin section scan and polygon outlines of plagioclase in sample 11RAT TD129A. **Left)** Thin section scan of sample in crossed-polarized light (26 x 46 mm). **Right)** Binary (black and white images) of 1,847 polygon outlines of plagioclase crystals.
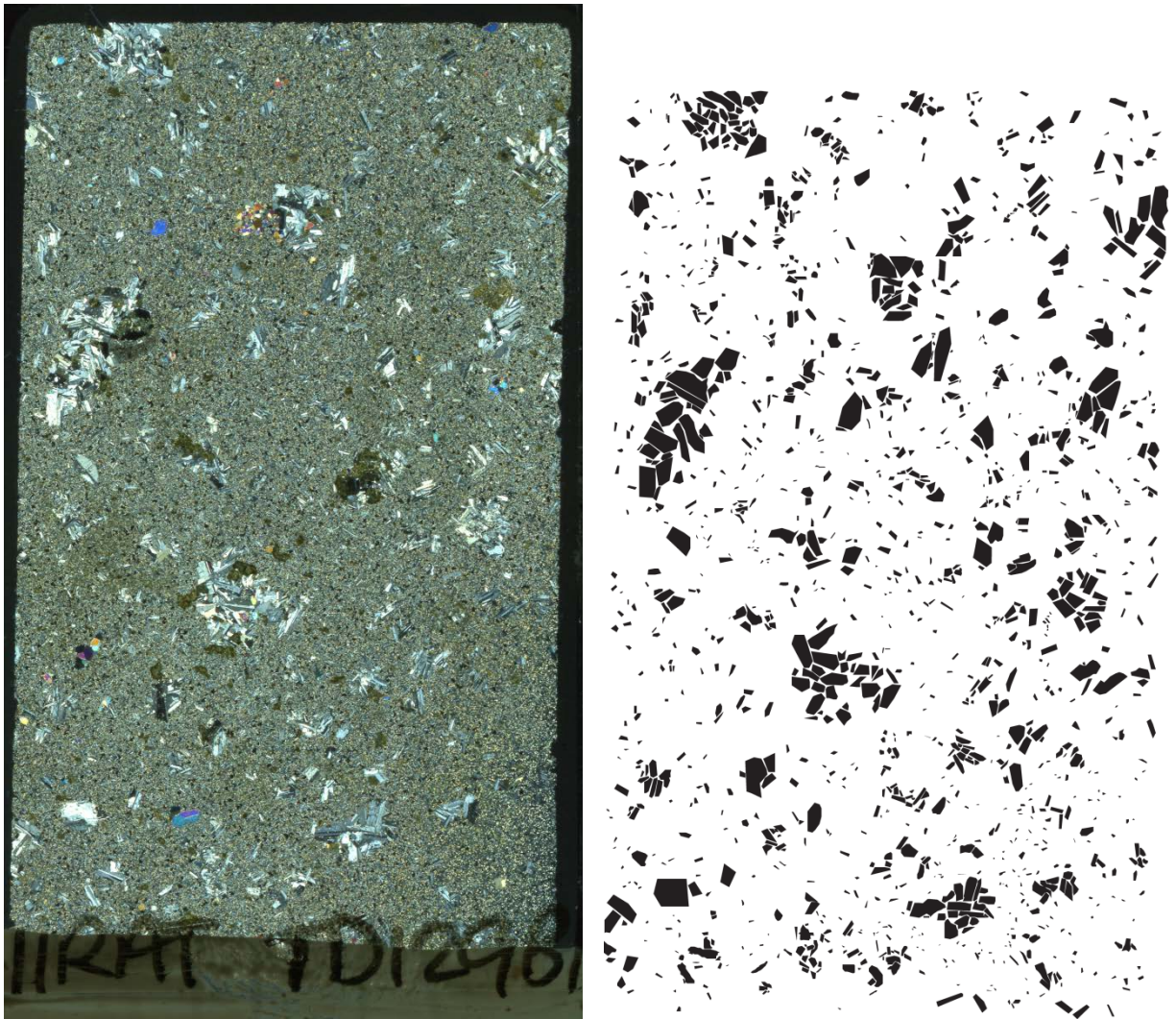
Figure C2 Thin section scan and polygon outlines of plagioclase in sample 11RAT TD129B. **Left)** Thin section scan of sample in crossed-polarized light (26 x 46 mm). **Right)** Binary (black and white images) of 1,332 polygon outlines of plagioclase crystals.

Figure C3 Thin section scan and polygon outlines of plagioclase in sample 11RAT TD129C. **Left)** Thin section scan of sample in crossed-polarized light (26 x 46 mm). **Right)** Binary (black and white images) of 1,701 polygon outlines of plagioclase crystals.
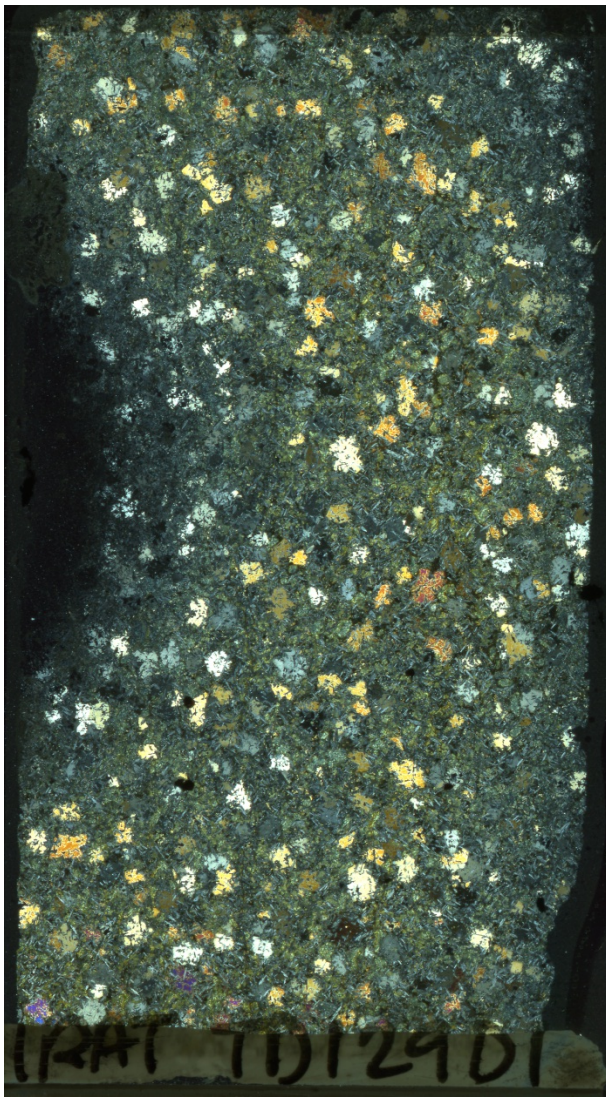
Figure C4 Thin section scan and polygon outlines of plagioclase in sample 11RAT TD129D. **Left)** Thin section scan of sample in crossed-polarized light (26 x 46 mm). **Right)** Binary (black and white images) of 912 polygon outlines of plagioclase crystals.
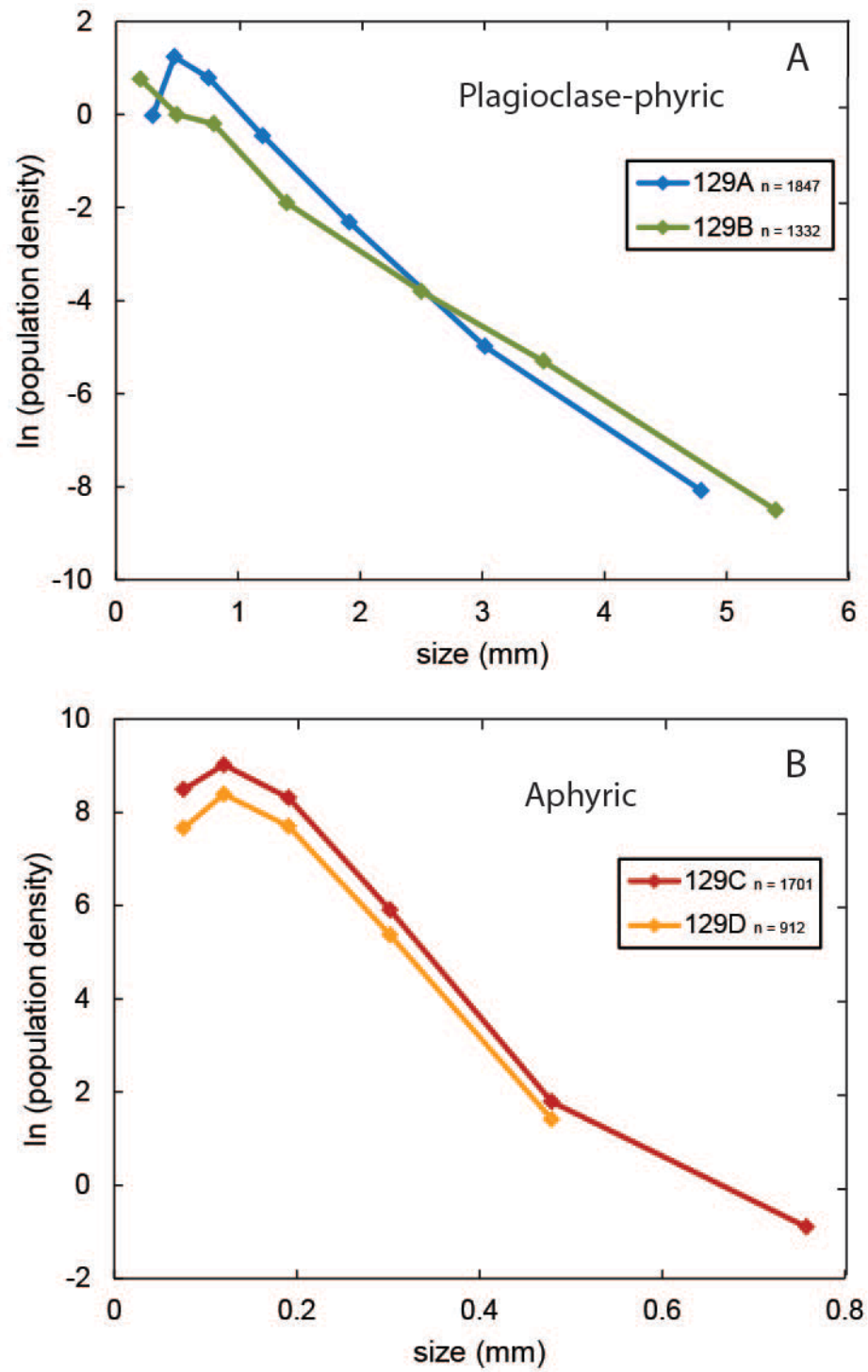
Figure C5 CSD diagrams with ln(population density) on the y-axis and grain size on the x-axis. **A)** Samples 129 A and 129B – plagioclase-phyric basalts. **B)** Samples 129C and 129D – aphyric basalts with prominent subophitic pyroxene.